

# **New Methods for Structural Health Monitoring and Damage Localization**

By

**Xueyan Zhao**



**A thesis submitted for the degree of**

**Doctor of Philosophy**

in the

Department of Automatic Control and Systems Engineering,

Faculty of Engineering, University of Sheffield

February 2015

## Abstract

Structural Health Monitoring (SHM) is traditionally concerned with fitting sensors inside structural systems and analyzing the features of signals from the sensor measurements using appropriate signal processing techniques in order to reveal the systems' health status. A significant change of signal features is often considered to be an indication of damage. However, generally speaking, these techniques often cannot distinguish normal structural changes due to variations in system environmental or operating conditions from the changes which are induced by damage. For example, transmissibility analysis is a widely used signal analysis method for SHM. But traditional transmissibility is determined by the ratio of the spectra of two different system outputs, which generally depends on the location of loadings on the system and is, consequently, affected by system environmental conditions. In order to solve this challenge, a series of studies are conducted in this PhD project. The objectives are to develop new SHM and damage localization methods, which can effectively address the effects of changing system environmental or operational conditions and have potential to be applied in practice to more effectively solve practical SHM and damage localization problems.

First, a general baseline model based SHM method is developed in this thesis. This method can be used to address a wide class of SHM problems via a baseline modelling and baseline model based analysis. The method can systematically take the effects of system's operating or environmental conditions such as, e.g., environmental temperature etc. on signal analysis into account, and can therefore solve relevant challenges. Both simulation studies and field data analyses have been conducted to demonstrate the performance of the proposed new technique.

Moreover, new transmissibility analysis methods are proposed for the detection and

location of damage with nonlinear features in Multi-Degree-Of-Freedom (MDOF) structural systems. These methods extend the traditional transmissibility analysis to the nonlinear case. More importantly, the methods are independent from the locations of loading inputs to the systems and, to a great extent, provide effective solutions to the above mentioned problems with traditional transmissibility analysis. Again both numerical simulation studies and experimental data analysis have been conducted to verify the effectiveness and demonstrate potential practical applications of the new methods.

Based on the results of nonlinearity detection and localization, new guidelines are proposed for the application of transmissibility analysis based modal identification method to nonlinear structural systems, which have potential to be further developed into a new approach to transmissibility based nonlinear modal analysis.

In summary, the present study has addressed a series of fundamental problems with SHM, especially, problems associated with how to deal with the effects of changing system environmental or operational conditions on SHM results. Experimental studies have demonstrated the potential and significance of these results in practical engineering applications.

## Acknowledgements

First and foremost, I would like to express my deepest gratitude to Professor Zi-Qiang Lang, my supervisor, for his excellent supervision, persistent support, and valuable advice in my research and writing within the last four years. Professor Zi-Qiang Lang is very knowledgeable and patient, and always encourages me wherever and whenever I face challenges and difficulties.

Many thanks also go to my colleagues who have provided useful discussions and advices which are really helpful in my general research studies: Dr. Peng-Fei Guo, Dr. Yu-Zhu Guo, Dr. Ling-Zhong Guo, Dr. Fei He, Dr. Long Zhang, Dr. Rui Wang, Dr. Shu Wang, Dr. Da-Zhi Jiang, Dr. Liang Zhao, Dr. Jing-Jing Luo, Dr. Krishnanathan Kirubhakaran, Dr. Carmen Ho, Dr. Adrian Alecu, Xi-Liang Zhang, Xiao-Kai Nie, You-Chen Wang, Jia Zhao. Thanks are extended particularly to Dr. Andrew Hills who helped me a lot in my first year study.

I also would like to thank my friends: Yu Liu, Dr. Qian Wang, Dr. Vivian Yang, Dr. Fang Yang, Dr. Wen Qiu, Tzu-Pei Yeh, Tzu-Ling Tseng, Man-Lu Wang and Mo-Ran Wang for their companionship and comfort since I am living in Sheffield.

In addition, very special thanks go to Department of Automatic Control and Systems Engineering for providing full departmental scholarship. This thesis would not have been conducted without this financial support.

Finally, I wish to thank my parents, sisters and brother for their support and encouragement throughout my study.

# Contents

Abstract.....	i
Acknowledgements .....	iii
Acronyms .....	xi
Nomenclature .....	xiii
List of Figures.....	xx
List of Tables.....	xxiii
Chapter 1 .....	1
Introduction .....	1
1.1    Backgrounds .....	1
1.2    Research motivation and contributions .....	5
1.3    Layout of this thesis .....	8
Chapter 2 .....	11
Structural health monitoring and damage localization: literature review .....	11
2.1    Time domain analysis .....	12
2.1.1    Time-waveform analysis .....	12
2.1.2    Time-waveform indices.....	12
2.1.3    Orbits .....	14
2.1.4    Probability density function .....	14
2.1.5    Probability density moments.....	14

## Contents

---

2.2	Frequency domain analysis.....	15
2.2.1	Envelope spectrum .....	16
2.2.2	Cepstrum.....	18
2.2.3	High-order spectrum .....	21
2.3	Time-frequency domain analysis.....	22
2.3.1	Short time Fourier transform.....	22
2.3.2	Wavelet analysis .....	23
2.3.3	Hilbert-Huang Transform .....	25
2.3.4	Others .....	26
2.4	Modal analysis .....	27
2.4.1	Natural frequency .....	27
2.4.2	Mode shape .....	28
2.4.3	Modal strain energy.....	29
2.5	Frequency response analysis .....	30
2.5.1	Coherence function .....	30
2.5.2	GFRFs .....	31
2.5.3	NOFRFs.....	33
2.5.4	Transmissibility based damage detection and localization .....	34
2.6	SHM under changing environmental and operational conditions .....	36
2.6.1	The effect of Environmental and operational conditions.....	36
2.6.2	SHM under changing environmental and operational conditions ....	40

## Contents

---

2.7	Damage localization under changing environmental and operational conditions .....	45
2.7.1	Alternative transmissibility analysis based on nonlinear features .....	46
Chapter 3	.....	48
A novel health probability based structural health monitoring method .....		48
3.1	Methodology .....	49
3.1.1	B-spline baseline model.....	49
3.1.2	Modelling error tolerance range and bins for environmental and operating parameters .....	51
3.1.3	Health probability .....	53
3.2	Simulation case study .....	54
3.2.1	Simulation model.....	54
3.2.2	Simulation data analysis .....	55
3.3	Experimental case study.....	58
3.3.1	Experimental measurements.....	59
3.3.2	Experimental data analyses .....	60
3.4	Conclusions.....	66
Chapter 4	.....	68
Transmissibility analysis method for detection and localization of damage via nonlinear features in MDOF structural systems .....		68
4.1	MDOF nonlinear structural systems and associated engineering backgrounds.....	69

## Contents

---

4.2	The NOFRFs of Single-Input Multi-Output nonlinear systems .....	74
4.3	The NOFRF transmissibility of MDOF nonlinear structural systems.....	76
4.4	Transmissibility at super-harmonics .....	79
4.5	Detection and location of damage via nonlinear features using a new transmissibility analysis method.....	83
4.5.1	Basic ideas.....	83
4.5.2	The method.....	84
4.5.3	Remarks .....	87
4.6	Simulation studies.....	89
4.6.1	Simulation study: case 1 .....	89
4.6.2	Simulation study: case 2 .....	91
4.7	Experimental studies .....	93
4.7.1	Experimental setup.....	93
4.7.2	Experiments and experimental data analyses.....	94
4.8	Conclusions .....	99
Chapter 5	.....	100
Nonlinearity detection and location for MIMO nonlinear systems using transmissibility analysis.....		100
5.1	A class of MIMO dynamic systems .....	101
5.2	Description of MIMO nonlinear systems in the time and frequency domains .....	102



## Contents

---

5.3	The NOFRFs and NOFRF transmissibility of MIMO nonlinear systems....	104
5.4	Transmissibility at nonlinearity generated frequencies .....	109
5.5	Detection and location of damage via nonlinear features using a transmissibility analysis method for MIMO nonlinear systems .....	115
5.5.1	The method .....	115
5.5.2	Remarks .....	121
5.6	Simulation studies .....	122
5.6.1	Simulation study: case 1 .....	122
5.6.2	Simulation study: case 2 .....	125
5.6.3	Simulation study: case 3 .....	127
5.7	General case .....	130
5.7.1	Power cable systems.....	130
5.7.2	Application of proposed method on power cable system.....	133
5.8	Conclusions.....	136
Chapter 6	.....	137
Transmissibility analysis based nonlinearity localization and modal identification for nonlinear MDOF systems.....		137
6.1	Output frequencies of multi-input nonlinear systems .....	138
6.2	Transmissibility based nonlinearity detection and localization for MDOF nonlinear systems subject to band limited loading inputs.....	141
6.2.1	Simulation study: case 1 .....	142

## Contents

---

6.2.2	Simulation study: case 2 .....	145
6.3	Modal identification .....	149
6.3.1	Modal identification of linear MDOF systems using transmissibility analysis.....	150
6.3.2	Modal identification of nonlinear MDOF systems using transmissibility analysis .....	153
6.3.3	Remarks .....	158
6.3.4	Simulation study .....	159
6.4	Conclusions .....	162
Chapter 7	.....	163
Conclusions	.....	163
7.1	Main contributions of this thesis .....	164
7.2	Suggestions for further work .....	165
Publication list	.....	166
Appendix A	.....	167
Recursive forward-regression orthogonal estimator	.....	167
Appendix B	.....	170
Proof of Proposition 4.2	.....	170
Appendix C	.....	172
Proof of Proposition 4.3	.....	172
Appendix D	.....	175

## Contents

---

Proof of Proposition 5.1.....	175
Appendix E.....	188
Proof of Proposition 5.3.....	188
Appendix F.....	192
Mathematical model of the power cable system.....	192
References.....	197

## Acronyms

<b>AANN</b>	Auto-Associative Neural Network
<b>AE</b>	Acoustic Emission
<b>AR-ARX</b>	Auto-Regression and Auto-Regression with an eXogenous input
<b>ARX</b>	Autoregressive model with an eXogenous input
<b>BPNN</b>	Back-Propagation Neural Network
<b>COMAC</b>	Coordinate Modal Assurance Criterion
<b>CSD</b>	Cone-Shape Distribution
<b>CWD</b>	Choi-Williams Distribution
<b>CWT</b>	Continuous Wavelet Transform
<b>DOF</b>	Degree Of Freedom
<b>DRQ</b>	Detection and Relative Damage Quantification
<b>DWT</b>	Discrete Wavelet Transform
<b>EEQ</b>	Elemental Energy Quotient
<b>EMD</b>	Empirical Mode Decomposition
<b>ERR</b>	Error Reduction Ratio
<b>FA</b>	Factor Analysis
<b>FFT</b>	Fast Fourier Transform
<b>FRF</b>	Frequency Response Function
<b>FT</b>	Fourier Transform
<b>FWT</b>	Fast Wavelet Transform

## Acronyms

---

<b>GFRFs</b>	Generalized Frequency Response Functions
<b>HFRFs</b>	Higher-order Frequency Response Functions
<b>HHT</b>	Hilbert-Huang Transform
<b>IMFs</b>	Intrinsic Mode Functions
<b>MAC</b>	Modal Assurance Criterion
<b>MDOF</b>	Multi-Degree-Of-Freedom
<b>MIMO</b>	Multi-Input Multi-Output
<b>MSD</b>	Mahalanobis Squared Distance
<b>MSE</b>	Mean Square Error
<b>NOFRFs</b>	Nonlinear Output Frequency Response Functions
<b>PDF</b>	Probability Density Function
<b>PSD</b>	Power Spectrum Density
<b>RMS</b>	Root Mean Square
<b>SDOF</b>	Single Degree Of Freedom
<b>SHM</b>	Structural Health Monitoring
<b>SIMO</b>	Single-Input Multi-Output
<b>STFT</b>	Short-Time Fourier Transform
<b>SVD</b>	Singular Value Decomposition
<b>TDI</b>	Transmissibility Damage Indicator
<b>WT</b>	Wavelet Transform
<b>WVD</b>	Wigner-Ville Distribution

# Nomenclature

## Nomenclature in Chapter 3

$n$	Number of basis functions
$m$	Number of knots
$p$	Degree of basis functions
$\mathbf{u}$	Displacement vector
$\mathbf{x}$	Knot vector
$x$	Variable
$x^{(1)}, x^{(2)}, \dots, x^{(N)}$	Variables
$x_{\min}^{(i)}$	Minimum value of variable $x^{(i)}$
$y$	Variable
$z$	Feature extracted from a sensor measurement
$\hat{z}$	Feature predicted from baseline model
$B_{n_1, n_2, \dots, n_N}$	Bins
$C$	Damping matrix
$F$	Input vector
$F_{\text{rub}}$	Effects of rub-impact damage
$G$	Gyroscopic moment matrix
$K$	Stiffness matrix

## Nomenclature

---

$M_i$	Number of the segments for $i^{\text{th}}$ variable $x^{(i)}$
$M$	Mass matrix
$N$	Number of variables
$\bar{N}$	Number of $z$
$N_{in}$	Number of the values of $\varepsilon$ within the tolerance range
$N_{all}$	Total number of $\varepsilon$
$N_{i,p}(x)$	$i^{\text{th}}$ B-spline basis functions of degree $p$
$P$	Health probability
$S_{n_i}^{(i)}$	Length of $n_i^{\text{th}}$ segment for variable $x^{(i)}$
$\alpha_0, \alpha_1, \dots, \alpha_n$	Control parameters
$\alpha_{i_1, i_2, \dots, i_N}$	Control parameters
$\varepsilon$	Error between $z$ and $\tilde{z}$
$\mu$	Mean
$\sigma$	Standard deviation

### Nomenclature in Chapters 4, 5 and 6

$[a_i, b_i]$	$i^{\text{th}}$ frequency range
$c_i$	Damping of $i^{\text{th}}$ damper

## Nomenclature

---

$k_i$	Stiffness of $i^{\text{th}}$ spring
$f(t)$	Input of SIMO systems
$f_i(t)$	$i^{\text{th}}$ input of MIMO systems
$f^{(1)}(t)$	Input of SIMO systems under the 1 <sup>st</sup> loading condition
$f^{(2)}(t)$	Input of SIMO systems under the 2 <sup>nd</sup> loading condition
$f_{si}(t)$	Force due to $i^{\text{th}}$ nonlinear spring
$f_{di}(t)$	Force due to $i^{\text{th}}$ nonlinear damper
$h_{(i,\bar{n})}(\tau_1, \dots, \tau_{\bar{n}})$	$\bar{n}^{\text{th}}$ order Volterra kernel of the $i^{\text{th}}$ system output of SIMO systems
$h_{(i,p_1=n_1,p_2=n_2,\dots,p_m=n_m)}^{(\bar{n})}(\tau_1, \tau_2, \dots, \tau_{\bar{n}})$	One of $\bar{n}^{\text{th}}$ order Volterra kernels of $i^{\text{th}}$ output of MIMO systems
$i_i(t)$	Current of $i^{\text{th}}$ section in power cable system
$i_{wt}(t)$	Current of water tree degradation
$\bar{k}$	General order of harmonics
$\tilde{k}$	Selected order of harmonics
$m_i$	$i^{\text{th}}$ mass
$m$	Number of inputs
$n$	Number of DOFs
$\bar{n}$	Order of nonlinearity
$n_i^+, n_i^-, n_i$	Number of positive, negative and total $i^{\text{th}}$ input
$nf_i(t)$	Effects of $i^{\text{th}}$ nonlinear components



## Nomenclature

---

$r_{(J_i, \bar{n})}$	Nonlinear stiffness coefficient
$r$	Parameters in the water tree degradation
$u_i(t)$	Voltage of $i$ th section in power cable system
$u_{wt}(t)$	Voltage of water tree degradation
$w_{(J_i, \bar{n})}$	Nonlinear damping coefficient
$\mathbf{x}(t)$	System output vector
$x_i(t)$	$i^{\text{th}}$ system output
$x_i^{(\bar{n})}(t)$	$i^{\text{th}}$ system output with order $\bar{n}$
$\mathbf{x}^{\{\bar{n}\}}(t)$	$\bar{n}^{\text{th}}$ order derivative of $\mathbf{x}(t)$
<b><math>A_{\bar{N}}</math></b>	
$A_{\bar{N}}$	Coefficient matrix
$A_1, A_2$	Input amplitude
<b><math>C</math></b>	
$C_i$	Capacitance of $i^{\text{th}}$ section in power cable systems
<b><math>F_m(t), F(t)</math></b>	
$F_m(t), F(t)$	Force vector
<b><math>F(j\omega)</math></b>	
$F(j\omega)$	Spectra of the SIMO system input
<b><math>F_{\bar{n}}(j\omega)</math></b>	
$F_{\bar{n}}(j\omega)$	Fourier Transform of $f^{\bar{n}}(t)$
<b><math>F_{(i, p_1=n_1, \dots, p_m=n_m)}^{(\bar{n})}(j\omega)</math></b>	
$F_{(i, p_1=n_1, \dots, p_m=n_m)}^{(\bar{n})}(j\omega)$	One kind of integration about system inputs
<b><math>F_{S_p}(\omega)</math></b>	
$F_{S_p}(\omega)$	Spectrum of the $p^{\text{th}}$ system input
<b><math>G_i</math></b>	
$G_i$	Conductance of $i^{\text{th}}$ section in power cable system

## Nomenclature

---

$G_{(i,\bar{n})}(j\omega)$	$\bar{n}^{\text{th}}$ order NOFRF associated with the $i^{\text{th}}$ SIMO system output
$G_{(i,p_1=n_1,\dots,p_m=n_m)}^{(\bar{n})}(j\omega)$	One of the $\bar{n}^{\text{th}}$ NOFRFs with the $i^{\text{th}}$ MIMO system output
$H_{(i,\bar{n})}(j\omega_1, \dots, j\omega_{\bar{n}})$	$\bar{n}^{\text{th}}$ GFRF associated with the $i^{\text{th}}$ SIMO system output
$H_{(i,p_1=n_1,p_2=n_2,\dots,p_m=n_m)}^{(\bar{n})}(j\omega_1, j\omega_2, \dots, j\omega_{\bar{n}})$	One of the $\bar{n}^{\text{th}}$ GFRFs with the $i^{\text{th}}$ MIMO system output
$IND_1$	Index of strength of frequencies generated by nonlinearity
$\bar{J}$	Number of nonlinear components
$J_i$	Location of $i^{\text{th}}$ nonlinear components
<b>K</b>	System stiffness matrix
$L_j$	Inductance of $i^{\text{th}}$ section in power cable system
<b>M</b>	System mass matrix
$N$	Highest order of the nonlinearity
<b>NF(t)</b>	Effects of nonlinear components
$\bar{Q}_{i,k}(j\omega)$	Linear system parameters dependent function
$\bar{\bar{Q}}_{i,k}(j\omega)$	Linear system parameters dependent function
$Q_{i,k}(j\omega)$	Linear system parameters dependent function
$R_{wt}$	Parameters in the water tree degradation
$R_j$	Resistance of $i^{\text{th}}$ section in power cable system
$S$	Location of input of SIMO systems
$S_i$	Location of $i^{\text{th}}$ input of MIMO systems

## Nomenclature

---

$ST^{i,i+1}(j\omega)$	Transmissibility at frequency $\omega$ between $i^{\text{th}}$ and $(i + 1)^{\text{th}}$ outputs
$ST1^{i,i+1}(j\omega)$	$ST^{i,i+1}(j\omega)$ under the 1 <sup>st</sup> loading condition
$STI1^{i,i+1}$	Integration of $ST1^{i,i+1}(j\omega)$
$ST2^{i,i+1}(j\omega)$	$ST^{i,i+1}(j\omega)$ under the 2 <sup>nd</sup> loading condition
$STI2^{i,i+1}$	Integration of $ST2^{i,i+1}(j\omega)$
$STI^{i+1}$	Integration of $ST^{i,i+1}(j\omega)$
$S\delta^{i,i+1}(j\omega)$	Difference between $ST1^{i,i+1}(j\omega)$ and $ST2^{i,i+1}(j\omega)$
$SI\delta^{i,i+1}$	Difference between $ST1^{i,i+1}$ and $STI2^{i,i+1}$
$S\delta_{\max}(\tilde{k})$	Maximum $S\delta^{i,i+1}(j\tilde{k}\omega_F)$
$S\delta_{\max}(j\omega)$	Maximum $S\delta^{i,i+1}(j\omega)$
$\overline{S\delta}^{i,i+1}(j\omega)$	Normalized $S\delta^{i,i+1}(j\omega)$
$T_{i,k}^{NL}(j\omega)$	NOFRF transmissibility between the $i^{\text{th}}$ and $k^{\text{th}}$ outputs
$T_{i,k}^L(j\omega)$	Traditional transmissibility between the $i^{\text{th}}$ and $k^{\text{th}}$ outputs
$T_{i,k}^{S'}(\omega)$	Transmissibility between $i^{\text{th}}$ and $k^{\text{th}}$ outputs under the loading condition $S'$
$X_i(j\omega)$	Spectra of the $i^{\text{th}}$ system output
$X_i^1(j\bar{k}\omega_F), X_i^2(j\bar{k}\omega_F)$	Spectra of the $\bar{k}^{\text{th}}$ harmonic responses of the system to first and second loading conditions

## Nomenclature

---

$X_i^{(\bar{n})}(j\omega), X_{(i,\bar{n})}(j\omega)$	$\bar{n}^{\text{th}}$ order frequency response of the $i^{\text{th}}$ system output
$X_{(i,p_1=n_1,\dots,p_m=n_m)}^{(\bar{n})}(j\omega)$	$\bar{n}^{\text{th}}$ order frequency responses of the $i^{\text{th}}$ system output with $p_1 = n_1, \dots, p_m = n_m$
$\alpha_i$	Input amplitude
$\gamma_{(i,k,p_1=n_1,\dots,p_m=n_m)}^{(N)}(j\omega)$	A NOFRF transmissibility of MIMO nonlinear system
$\varepsilon_1, \varepsilon_2, \varepsilon_3, \varepsilon_4$	Threshold parameters
$\zeta_{\bar{m}}$	$\bar{m}^{\text{th}}$ order damping ratio
$\lambda_{\bar{m}}$	Pole of mode $\bar{m}$
$v_{\bar{m}}$	Modal participation factor of mode $\bar{m}$
$\phi_{\bar{m}}$	Modal shape of mode $\bar{m}$
$\omega_F, \omega_{f\bar{m}}, \omega_{f\bar{m}1}, \omega_{f\bar{m}2}$	Frequency of system input
$\omega_{\bar{m}}$	$\bar{m}^{\text{th}}$ order natural frequency
$\omega_{NL}$	General frequencies generated by nonlinearity
$\omega_{NL1}$	Selected frequencies generated by nonlinearity
$\Delta^{-1}T_{i,k}^{S',S''}(\omega)$	Inverse of $T_{i,k}^{S'}(\omega) - T_{i,k}^{S''}(\omega)$

## List of Figures

Fig. 1.1	Procedure of SHM.....	3
Fig. 2.1	Techniques in structural health monitoring.....	11
Fig. 2.2	Signal with modulated amplitude and its envelope signal.....	17
Fig. 2.3 (a)	Acceleration signal measured on a bearing suffering outer race damage .....	18
Fig. 2.3 (b)	Spectrum of the acceleration signal.....	18
Fig. 2.3 (c)	Envelope spectrum of the acceleration signal.....	18
Fig. 2.4	Vibration power spectra of health and damaged induction motors.....	20
Fig. 2.5	Vibration cepstrum of health and damaged induction motors.....	20
Fig. 2.6	Wavelet scalograms of the two signals.....	24
Fig. 3.1	Definition of bins.....	52
Fig. 3.2	Signal features.....	54
Fig. 3.3	A dual-disc rotor system and FE model.....	55
Fig. 3.4	Vibration levels of the rotor systems.....	57
Fig. 3.5	Basis functions for B-spline approximation model.....	57
Fig. 3.6	Validation of baseline model.....	58
Fig. 3.7	Errors and tolerance ranges.....	58
Fig. 3.8	Data acquisition schedule.....	60
Fig. 3.9	Basis functions for B-spline approximation model.....	61

## List of Figures

---

Fig. 3.10	Validation of each model.....	63
Fig. 3.11	Bins used to calculate error distribution.....	63
Fig. 3.12	The tolerance range of errors in each bin and errors between signal features of measurements in December 2010 and predicted features.....	65
Fig. 3.13	The tolerance range of errors in each bin and errors between signal features of measurements in February 2011 and predicted features.....	65
Fig. 4.1	An MDOF nonlinear structural system.....	69
Fig. 4.2	Modeling of a multi-storey building block.....	71
Fig. 4.3	Modeling of a simple-supported beam.....	71
Fig. 4.4	Modeling of a rotor-bearing system.....	72
Fig. 4.5	Flow chart of damage detection and localization method for SIMO systems.....	87
Fig. 4.6	Three-storey building structure used for the experimental studies.....	94
Fig. 4.7	4DOF system model of the three-storey building structure.....	94
Fig. 4.8	Output spectra on the 1 <sup>st</sup> floor in Experiments #1 - #6.....	95
Fig. 5.1	MIMO nonlinear structural system subject to $m$ inputs.....	101
Fig. 5.2	Flow chart of damage detection and localization method for MIMO systems.....	120
Fig. 5.3	Output responses of the 5 <sup>th</sup> mass when the system is subject to the 1 <sup>st</sup> loading conditions.....	123
Fig. 5.4	Output response of the 8 <sup>th</sup> mass when the system is subject to the 2 <sup>nd</sup>	

List of Figures

---

	loading conditions.....	128
Fig. 5.5	Equivalent circuit of power cable system.....	131
Fig. 5.6	Spectra of the 3 <sup>rd</sup> current when the system is subject to the 2 <sup>nd</sup> loading condition.....	134
Fig. 6.1	Output response of the 5 <sup>th</sup> mass when the system is subject to the 2 <sup>nd</sup> loading condition.....	143
Fig. 6.2	Output response of the 3 <sup>rd</sup> mass when the system is subject to the 2 <sup>nd</sup> loading condition.....	146
Fig. 6.3	Some transmissibility functions and associated $\Delta^{-1}T_{i,k}^{S',S''}(\omega)$ of linear system (4.1).....	152
Fig. 6.4	Some transmissibility functions and associated $\Delta^{-1}T_{i,k}^{S',S''}(\omega)$ of the nonlinear system (4.5) .....	154
Fig. 6.5	Some transmissibility functions and associated $\Delta^{-1}T_{i,k}^{S',S''}(\omega)$ of the nonlinear system (4.5).....	155
Fig. 6.6	Output response of the 7 <sup>th</sup> mass when the input is applied on the 2 <sup>nd</sup> mass.....	160
Fig. 6.7	$\Delta^{-1}T_{3,8}^{2,6}(\omega)$ and $\Delta^{-1}T_{3,8}^{2,9}(\omega)$ of the nonlinear system (4.5).....	162

## List of Tables

Table 2.1	Meaning of the first four order probability density moments.....	15
Table 2.2	Different terms employed in the spectral and cepstral analyses.....	19
Table 3.1	Calculation of health probability.....	54
Table 3.2	Selected terms and corresponding coefficients for B-spline approximation model.....	57
Table 3.3	Health probability for rotor system suffering rub-impact damage.....	58
Table 3.4	Location of each sensor.....	60
Table 3.5	Selected terms and corresponding coefficients for B-spline approximation model.....	62
Table 3.6	Health probability for measurements in December 2010.....	66
Table 3.7	Health probability for measurements in February 2011.....	66
Table 4.1	Threshold parameters used in the simulation studies.....	90
Table 4.2	The value of $\overline{S\delta}^{l,i+1}(j2\omega_F)$ when the 3rd, 5th and 6th springs are nonlinear .....	91
Table 4.3	The value of $\overline{S\delta}^{l,i+1}(j\omega_F)$ when the 8th spring is nonlinear.....	93
Table 4.4	Details of the experiments.....	95
Table 4.5	The threshold parameters used in the experimental data analysis.....	96
Table 4.6	The values of $IND_1$ evaluated using data for different tests where no nonlinear components were introduced.....	96



List of Tables

---

Table 4.7	Details of the experimental data analysis results.....	98
Table 5.1	Frequency components when $m = 2$ , $\omega_{f1} = 30$ , $\omega_{f2} = 40$ and $N=4$ .....	110
Table 5.2	The value of $\overline{S\delta}^{i,i+1}(j\omega_{NL1})$ when the 3 <sup>rd</sup> , 5 <sup>th</sup> and 6 <sup>th</sup> springs are nonlinear.....	125
Table 5.3	The value of $\overline{S\delta}^{i,i+1}(j\omega_{NL1})$ when the 3 <sup>rd</sup> , 5 <sup>th</sup> and 6 <sup>th</sup> springs are nonlinear.....	127
Table 5.4	The value of $\overline{S\delta}^{i,i+1}(j\omega_{f1})$ when the 6 <sup>th</sup> spring is nonlinear.....	129
Table 5.5	The value of $\overline{S\delta}^{i,i+1}(j\omega_{f2})$ when the 6 <sup>th</sup> spring is nonlinear.....	129
Table 5.6	Threshold parameters used in the simulation study on power cable system.....	134
Table 5.7	The value of $\overline{S\delta}^{i,i+1}(j\omega_{NL1})$ in the simulation study on power cable system.....	136
Table 6.1	Frequency components when $m = 1$ , $[a_1, b_1] = [90, 100]$ and $N=4$ .....	139
Table 6.2	Frequency components when $m = 2$ , $[a_1, b_1] = [90, 100]$ , $[a_2, b_2] = [30, 35]$ and $N = 2$ .....	140
Table 6.3	The value of $\overline{SI\delta}^{i,i+1}$ when the 5 <sup>th</sup> , 6 <sup>th</sup> and 7 <sup>th</sup> springs are nonlinear....	145
Table 6.4	The value of $\overline{SI\delta}_1^{i,i+1}$ when the 6 <sup>th</sup> spring is nonlinear.....	148
Table 6.5	The value of $\overline{SI\delta}_2^{i,i+1}$ when the 6 <sup>th</sup> spring is nonlinear.....	149
Table 6.6	The value of $\overline{SI\delta}^{i,i+1}$ when the 5 <sup>th</sup> , 6 <sup>th</sup> and 7 <sup>th</sup> springs are nonlinear....	161

# Chapter 1

## Introduction

This introduction addresses three topics: background of structural health monitoring and damage localization, research motivation and contributions, and the layout of the thesis.

### 1.1 Backgrounds

Engineering systems including, for example, mechanical, aerospace and civil systems and structures are prone to suffering damage including fatigue damage after long service time and damage due to improper use, hostile working environment or operational conditions. In most general terms, damage is defined as any changes to the material properties and/or geometric features of structural systems, including variation of system connectivity and boundary conditions, which affect the systems' current and future behaviours or characteristics adversely [1-3]. In terms of length scales, all damage stems from the defects or flaws in materials encompassing inclusions, voids and dislocations, which are inherent and present to some degree but will not cause changes of overall system behaviours. As the structural system keeps working under some loadings scenarios, such defects or flaws will grow, get serious and coalesce at different speed until they reach a point where the system cannot work in its ideal condition. This point is referred to as damage. Therefore, damage means the system is no longer operating optimally but it is still functioning. When damage grows continually, it may reach to another point where system functionality is no longer satisfactory. This point is referred to as failure. In terms of time scales, damage such as fatigue related damage, corrosion, erosion or even creep can be accumulated over long periods of time. Besides, damage can be the result of unscheduled events

such as earthquakes and wind loading and scheduled events such as aircraft landings [1, 3].

The structural health monitoring (SHM) refers to the process of implementing damage detection and identification technique for mechanical, aerospace and civil engineering structures [1]. SHM is becoming increasingly significant in life-safety and economic benefits during the service lifespan of these structural systems or components. First, the life-safety and reliability of the structural systems can be guaranteed [4] when SHM techniques are conducted to make sure that these systems are operating in a healthy condition. Then the structural systems can serve for a longer time than the designed lifespan if the results of SHM indicate that no damage arises at that moment. Besides, SHM can help to avoid unnecessary economic loss caused by unpredicted downtime. When damage is detected, the SHM system will raise alarm so that the maintenance or repair work can be scheduled in time and corresponding actions can be taken to avoid the consequences of failure. Finally, SHM allows time-based/preventive maintenance, which means that maintenance is carried out periodically, to evolve into condition-based/corrective maintenance, which means that maintenance will be taken only when SHM indicates that damage has arisen. Condition-based/corrective maintenance is more cost effective than time-based/preventive maintenance [1, 3, 5, 6].

SHM can be achieved by measuring various signals related to the structure health status (such as vibration, bearing temperature, oil pressure and oil debris), such that the change of the features extracted from measurements can indicate a developing structural damage. The main procedure of SHM is shown in Fig.1.1 [1, 3]. Obviously, SHM involves the process of operational evaluation, data acquisition and cleansing, feature selection and statistical model development [1, 3, 7].

**Operational evaluation:** This is to provide for possible damage to the system to be

monitored, to evaluate the operational and environmental conditions under which the system is working, and to understand the limitations on data measurements under these conditions.

**Data acquisition and cleansing:** Data acquisition is to select the type and number of sensors used in data acquisition and to determine the location of sensors to be placed and the hardware for data-acquisition/storage. In the process of data acquisition, in order to obtain a faithful reproduction of the signal, Nyquist Sampling Theorem must be met, which is the sampling frequency must be at least twice the highest analogue frequency component. Data cleansing is to choose data which are suitable for the feature selection process.

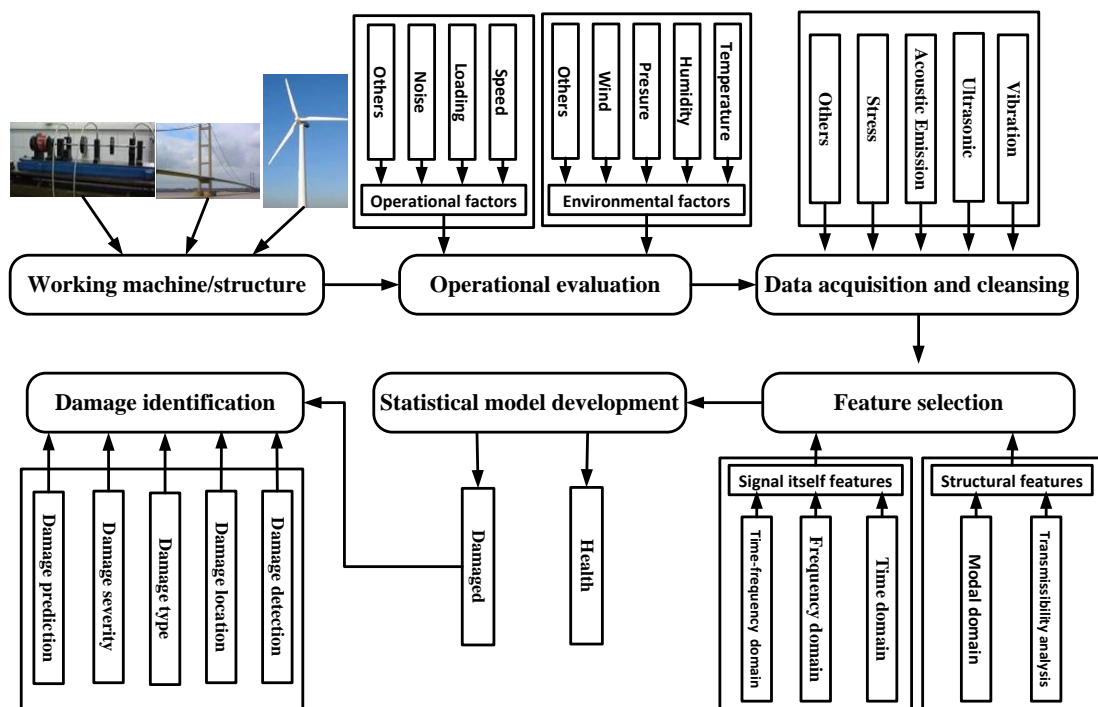


Fig. 1.1 Procedure of SHM [1, 3]

**Feature selection:** Large amounts of data are typically produced in the step of data acquisition. It is complicated and inconvenient to evaluate the difference among these data directly therefore, information condensation is necessary and advantageous. Feature selection is to identify data features that can indicate the difference between

damaged and undamaged systems. The features can be either the properties of the structural systems, such as natural frequencies and output frequency response, or the features of the signal itself, such as time-waveform. The features that depend on the presence and severity of damage are named as damage sensitive features. Damage sensitive features will change significantly when damage arises in structural systems, so they can help to distinguish damaged and undamaged structures. Feature selection is the part of SHM to which the researchers pay the most attention.

**Statistical model development:** This is to determine the current state of system health by implementing the statistical algorithms on the extracted features. There are different ways to summarise the different levels of damage identification. For example, Rytter proposed the following four levels of damage identification [8]:

Level 1: Determine whether the damage occurs in the structure.

Level 2: Determine where the damage happens geometrically.

Level 3: Quantify how serious the damage is.

Level 4: Predict how long the structure can serve in the future.

However, Farrar and Worden [1, 3, 9] pointed out that the type of damage should also be taken into account. Consequently, they have classified damage identification into five levels:

Level 1: Determine whether the damage occurs in the structure.

Level 2: Determine where the damage happens geometrically.

Level 3: Determine what the type of damage is.

Level 4: Quantify how serious the damage is.

Level 5: Predict how long the structure can serve in the future.

These are hierarchical structures; each level requires that all lower-level information is available. Obviously, the later levels of SHM provide more details of damage and thus are more appropriated. The process to determine the existence of the damage in the structure is defined as damage detection. The process involving the determination of location, type and severity of damage is defined as damage diagnosis[10], while the process to predict the remaining service life time of a structure is defined as damage prognosis [11]. The research in this thesis focuses primarily on the first two Levels, namely, damage detection and damage diagnosis.

## **1.2 Research motivation and contributions**

Extensive research studies on SHM have been conducted to solve one or more problems above. The effective features, which are sensitive to the existence of damage and are able to indicate the appearance and location of damage, are most important for SHM. Therefore, significant researches focus on signal analysis methods and extensive techniques are available to obtain useful features for SHM purpose.

Many researchers consider the characteristics of structural systems as damage sensitive features, including natural frequency, mode shape, modal strain energy, generalized frequency response functions (GFRFs) and transmissibility. Salawu [12] discussed the effect of structural damage on the natural frequency and reviewed the application of natural frequency on the SHM. Fan [13] and Fanning [14] reviewed comprehensively modal parameter-based damage identification methods including natural frequency-based methods, curvature mode shape-based methods, mode shape-based methods, and methods using both natural frequencies and mode shapes. Fan [13] also discussed the merits and drawbacks of each method.

Researchers have also investigated the variation of features extracted from measured signals to find the health states of structural systems. The corresponding techniques can be divided into three categories: time domain analysis, frequency domain analysis

and time-frequency domain analysis. The techniques in the time domain analysis are composed of time-waveform analysis, time-waveform indices, orbits, probability density function and probability density moments. Techniques in the frequency domain analysis include envelope spectrum, cepstrum, high-order spectrum, coherence function. A summary of damage identification methods in the time and frequency domains can be found in Ref. [15]. Time-frequency domain analysis is used to study non-stationary signals as the analysis can simultaneously reveal the signal features in both the time and frequency domains. The corresponding techniques include short time Fourier transform, wavelet analysis, Hilbert-Huang transform and Wigner-Ville distribution. Peng [16] discussed the advantages and disadvantages of these methods and reviewed the application of wavelet transform on SHM.

However, the problem with all these available techniques is that most of them cannot take the system operational and environmental conditions into account. But these factors often have a significant impact on the measurements and signal features. Environmental factors which can change the behaviors of the structural system include temperature, pressure, humidity [12, 17-19] and loading conditions such as traffic loading [20] and wind loading [21]. The operational parameters which have an impact on system responses include speed of operation [22, 23] and loading conditions. Sohn [24] reviewed the influence of the environmental and operational factors on the SHM.

For example, Farrar et al. [17] tested the vibration of a bridge in the USA for about 9 months when four different levels of damage severity were introduced intentionally in this bridge. The severer damage in the bridge is expected to reduce the bridge's stiffness more and so result in lowering the bridge's natural frequency. However, Farrar found that adversely the natural frequency of the bridge became larger at first and then dropped down when the damage became more and more serious. Further investigation explained that the environmental temperature contributed considerably to the change of the bridge's natural frequency. From the analysis of measurements

from another bridge carried on continuously over 24 hours, Farrar et al. observed that the first modal frequency of the bridge altered about 5% during a day circle [18].

It is obvious that neglecting environmental and operating conditions, which often have an impact on sensor measurements, will result in that sensor measurements cannot show what happens in an inspected structure correctly. But, all available techniques considering the effect of environmental and operating conditions are only effective in special cases. There is still no relatively general method which is able to deal with any number and type of sensor measurements and environmental parameters, and can also address this and related issues for a wide range of SHM problems.

If damage has been detected in a system, its location should be identified so that corresponding repair work can be scheduled intentionally. Transmissibility analysis is one class of the most popular techniques for damage detection and location [25-29]. Transmissibility is traditionally defined as the ratio of the spectra of two different system outputs. It has been comprehensively studied frequently, and is widely used for damage detection and localization. However, there are many problems when applying this approach in practice. Firstly, traditional transmissibility between two system responses depends on the location of loadings on the system. Namely, if a loading acts on the system at a different location, the transmissibility between the two responses will be different. Consequently, the position of loading on monitored systems has to be known a priori, which implies that traditional transmissibility based methods may not be able to be applied in many practical systems. In addition, because traditional transmissibility is basically a linear system concept, it cannot be used to propose a systematic approach to detecting and locating damage of nonlinear features.

In engineering structural systems, some damage often manifests itself as the introduction of nonlinearity into an otherwise linear system. Examples include post-buckled structures (Duffing non-linearity), rattling joints (impacting system with



discontinuities), or breathing cracks (bilinear stiffness), etc., and such damage has been referred to as damage with nonlinear features [30]. Recently, Lang developed a novel nonlinear frequency analysis method: Nonlinear Output Frequency Response Functions [31] (NOFRFs) and furthermore proposed a new transmissibility concept known as the transmissibility of NOFRFs [28]. The transmissibility of NOFRFs extends, for the first time, the concept of transmissibility to the nonlinear case. By using this new concept, important properties of system nonlinear responses can be revealed and exploited to identify the existence and the location of structural damage with nonlinear nature.

The research study in this thesis is motivated by the aforementioned practical needs for SHM, the recent development in nonlinear structural system transmissibility analysis, and the great potential of applying nonlinear transmissibility analysis in damage localization. A general structural health monitoring method is proposed in this thesis. This approach can be used to address a wide class of SHM problems via systematically taking the effects of operating conditions and environmental changes into account. Moreover, a new and more general transmissibility analysis methodology for the detection and location of damage with nonlinear features in structural systems is developed. The algorithms under the framework of this novel methodology can deal with an arbitrary number of nonlinearly damaged components in the system, does not need specific tests, and does not require that the loading on inspected structural systems is measurable. This methodology enables the basic principles of the NOFRF transmissibility based damage detection and localization to be literally applied in engineering practice to address many significant practical SHM problems.

### **1.3 Layout of this thesis**

This thesis consists of seven chapters. The first one is an introductory chapter which introduces the concept of SHM and damage localization, points out possible problems

during application of the methods in SHM and damage localization and covers the research motivation and contributions of this thesis. Chapter 2 reviews the available techniques in SHM and damage localization in detail. Chapters 3-6 are dedicated to the main research work of the present studies on SHM and damage localization. Finally, Chapter 7 summarizes the main results achieved by the studies presented in this thesis. A more detailed summary of Chapters 2-7 is provided as follows.

Chapter 2 reviews the commonly used damage sensitive features in SHM and damage localization firstly including features in time domain, frequency domain, time-frequency domain, modal domain and frequency response analysis, and then introduces the effect of environmental and operational conditions on these features such as temperature, humidity, operational speed, traffic loading and wind loading. Finally, the techniques in SHM and fault localization under changing environmental and operational conditions are reviewed.

Chapter 3 proposes a novel health probability based SHM method. In this method, the relationship between a signal feature and the normal changes in the system environmental and operating parameters, known as the baseline model, is first established. Then, a tolerance range of the signal feature's deviation from what is determined by the baseline model is evaluated via a data based training process. Furthermore, the health probability, which is defined as the proportion of the cases where the system's working status as represented by the signal feature is within the tolerance range, is used to determine whether a system is in a normal working condition or not so as to implement the system condition and health monitoring. Both simulation studies and experimental data analyses have been conducted to demonstrate the performance of the proposed new technique.

In Chapter 4, a new transmissibility analysis method is proposed for the detection and location of damage via nonlinear features in MDOF structural systems. The method is

derived based on the concept of the transmissibility of NOFRFs, a concept which extends the traditional transmissibility concept to the nonlinear system case [28]. The implementation of the method is only based on measured system output responses and by evaluating and analyzing the transmissibility of these system responses at super-harmonics. Both numerical simulation studies and experimental data analysis have been conducted to verify the effectiveness and demonstrate the potential practical applications of the new method.

In Chapter 5, the proposed method in Chapter 4 is extended to the nonlinearity detection and localization in multi-input multi-output (MIMO) nonlinear systems. In this chapter, after the description of the model and mathematical representation of a class of MIMO systems, the concept of NOFRFs of MIMO nonlinear systems is introduced and some important properties of the transmissibility of NOFRFs of MIMO nonlinear systems are derived. Then, the transmissibility at frequencies generated by system nonlinearities is studied. Finally, a transmissibility analysis based method is developed to detect and localize the nonlinearities in MIMO systems and the effectiveness of this method is verified by simulation case studies.

Based on the results in Chapters 4 and 5, Chapter 6 studies nonlinearity detection and localization when a system is subject to an arbitrary number and type of general loadings. The determination of the output frequency range of a nonlinear system subject to general loadings is investigated so that a procedure similar to that in Chapter 4 or Chapter 5 can be followed to find the location of nonlinearity in the system. Finally, based on the results of nonlinearity detection and localization, some guidelines are provided for how to apply the transmissibility analysis based modal identification to nonlinear structural systems.

Finally, in Chapter 7, the main conclusions of this thesis and suggestions for further studies are provided.

## Chapter 2

### Structural health monitoring and damage localization: literature review

Structural health monitoring can be achieved by measuring various signals related to the structure health status and then evaluating the changes in the features of signal measurements. Two different kinds of features are usually used in SHM. One is the features extracted from measurements by different signal analysis methods, including the time domain analysis, frequency domain analysis, and time-frequency domain analysis. The other one is the features which can represent the characteristics of the structural systems, including modal parameters such as natural frequency and mode shape and frequency response features such as coherence functions and transmissibility. These methods of SHM are summarized in Fig. 2.1 and will be discussed in the following sections [15, 32].

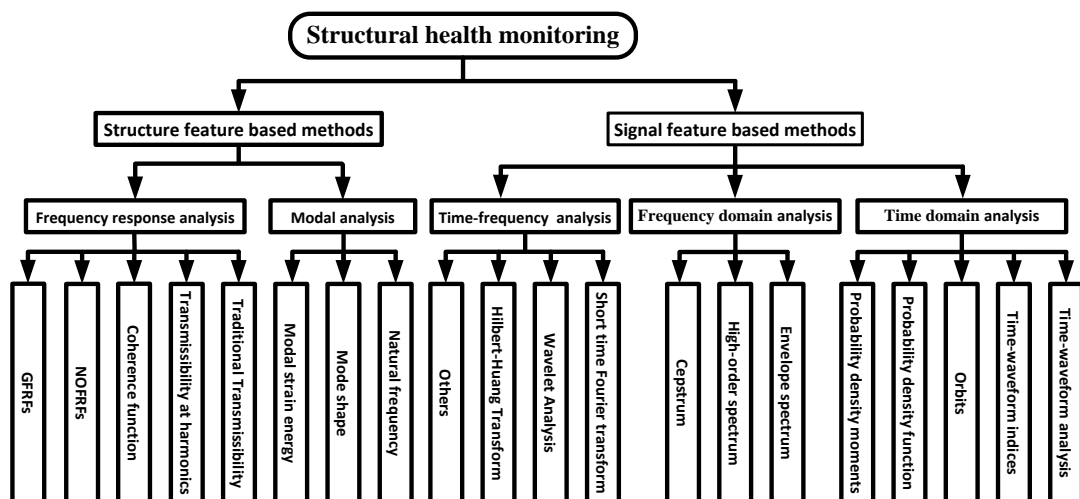


Fig. 2.1 Techniques in structural health monitoring [15, 32]

## 2.1 Time domain analysis

Traditionally, the approach of analyzing signals is to observe them in the time domain which means that the measured data are displayed and analyzed as a function of time. The signal analysis in the time domain is a direct technique for feature extraction because measured signals always are in the time domain. Therefore, the significant merit of this kind of analysis is that little or even no information is missing before processing. However, the drawback is that too much data will be involved. Main time-domain analysis methods are introduced as follows.

### 2.1.1 Time-waveform analysis

Time-waveform analysis is to observe visually the time-history of the data set. Different signals look different in time-waveform. Especially, distinctions among sinusoidal, random, repetitive, and transient events can be clearly seen [15]. In addition, some faults can be observed by the abnormal time-waveform. For example, in a rotor system with rub-impact fault, the waveform displays clipping characteristics. The more serious the fault is, the more abnormal the deformation in the waveform will appear [33].

### 2.1.2 Time-waveform indices

Numerous useful features obtained from time-waveform can be applied in SHM, but they are difficult to be used directly for trending and comparisons and there are always too many data to store. From this viewpoint, time-waveform indices, the separate numbers extracted from original measured data by some calculation, look like more applicable and convenient for SHM [34]. These indices include, for example,

**Peak level:** Largest value of amplitude within the data set.

$$P = \max\{x(n), n = 1, 2, \dots, N\} \quad (2.1)$$

where  $x(n)$  is data set in the time domain, and  $N$  is the length of the data. Tandon [35] reported that peak levels of both outer and inner races of a bearing increased obviously and became much greater than that of healthy bearings when the defect diameter became larger. So he concluded that peak level could serve as an indicator of defect bearing.

**Mean level:** Average amplitude.

$$\bar{x} = \frac{\sum_{n=1}^N x(n)}{N} \quad (2.2)$$

**RMS level:** Root-mean-square (RMS).

$$R = \sqrt{\frac{\sum_{n=1}^N x^2(n)}{N}} \quad (2.3)$$

The overall RMS of a signal is a representative of the energy. Williams [36] investigated the change of RMS of accelerometer signal when there was damage in inner race of ball bearing. He found that the variation of the signal RMS level reflected the development of the damage. The existence and growth of the damage on the surface induced the incipient rise of RMS level. When the bearing keeps working and rolling contact continues, the rough edges of a crack or small damage zone will become smoothed. Therefore, the signal RMS level tends to drop down. However, as cracks develop and extend to a large zone, the signal RMS increases again. The research in Ref. [35] found that the overall RMS increases when damage becomes serious. So the RMS can indicate not only the development of damage but also the severity of damage.

**Peak-to-peak amplitude:** The ratio of positive peak to negative peak of signal amplitudes.

$$P_p = \frac{P}{\max\{-x(n), n = 1, 2, \dots, N\}} \quad (2.4)$$

**Crest factor:** The ratio of maximum amplitude of the signal to its RMS level.

$$C = \frac{P}{R} \quad (2.5)$$

The incipient structural damage can be reflected by the crest factor. However, when damage becomes serious, the crest factor will generally drop down because the level of RMS goes up with a developing damage.

### 2.1.3 Orbits

Orbit is a diagram displaying vibration in horizontal vs vertical directions. An orbit can, for example, represent different characteristics of faults in rotating structures such as shaft unbalance [37], lubrication instabilities (whirl [38] and whip), and impact-rubs between rotor and stator [22], etc.

### 2.1.4 Probability density function

Probability density function (PDF) of a random variable is a function that represents the relative probability for this random variable to take a special value [39]. In engineering, the shape of the PDF of a health structure is similar to a Gaussian probability distribution. However, the damage will cause the change of the shape. For example, the impulse, which often indicates there is an abnormality in rolling-element-bearing systems, will lead to large probability at the average value with a wide spread of low probabilities [15].

### 2.1.5 Probability density moments

Like the time-waveform indices, probability density moments are separate-number indices based on the probability density function.

$$M_N = \int_a^b x^N f(x) dx \quad (2.6)$$

where  $N$  is the order of the moments,  $x$  is a time series,  $f(x)$  is the PDF of  $x$ , and  $[a, b]$  is the interval in which the moments are defined. Probability density moments

of the first four orders have special meaning as listed in Table 2.1 [3].

Table 2.1 Meaning of the first four order probability density moments

Probability density moments	Meaning
The first order: $M_1$	Mean
The second order: $M_2$	Variance
The third order: $M_3$	Skewness
The fourth order: $M_4$	Kurtosis

Odd moments (mean  $M_1$  and skewness  $M_3$ ) reflect the maximum location of PDF relative to the average value, while even moments (variance  $M_2$  and kurtosis  $M_4$ ) provide an extension of PDF [15]. Among these moments, the fourth one is most commonly used in SHM, because kurtosis is sensitive to the impulsiveness in a signal which can be the result of a damaged component, for example, a rolling-element-bearing in the early damage stage [15]. Dyer and Stewart [40], for the first time, applied kurtosis in damage diagnosis of bearings. They found that the value of kurtosis is approximately around 3 when a bearing suffers no defect. When impending failure happens, this value would be greater than 3. Other studies [41-43] also succeeded in the application of kurtosis in bearing damage detection. However, in some other cases [44, 45] kurtosis failed to detect impending bearing defects.

## 2.2 Frequency domain analysis

In the frequency domain, a signal is represented as a function of frequency. The frequency-domain representation of a signal can be obtained from Fourier transform (FT) of the signal, usually using the fast Fourier transform (FFT) algorithm. The signal can also be transferred back into the time-domain by the inverse Fourier transform (IFT). Although the process of Fourier transform will lead to the loss of some information, such as transients or non-repetitive signal components, its advantage is



also obvious. For example, the periodical information of the original signal in the time domain is distinctly represented by amplitude peaks in the frequency spectrum at the corresponding frequencies. Structural damage can induce specific periodical signals. If the frequency characteristics are exploited properly, such damage can be diagnosed early [15]. Therefore, various SHM techniques in the frequency domain have been developed.

The main procedure of the frequency domain analysis is firstly to look closely at either special interesting frequency components or the whole frequency spectrum and then extract features from the signal spectrum. Some commonly used techniques in the spectrum analysis are envelope analysis, cepstrum and high-order spectrum analysis.

### **2.2.1 Envelope spectrum**

Envelope spectrum can be obtained by taking the Fourier transform on the envelope signal of an original amplitude-modulated signal [46]. System response with modulated amplitude is a common phenomenon in damaged rotating systems, such as gearboxes, turbines and induction motors as well as rolling element bearings. For example, with rolling element bearings, if the surface of a ball is suffering damage, the impact between the damaged spot and other components will produce an impulse force. When such strike continues, impulse responses with modulated amplitude will be induced and the strike frequency can be observed on envelope spectrum [47]. So the analysis of envelope spectrum can be applied to detect the damage which can generate a signal with modulated amplitude at given frequencies.

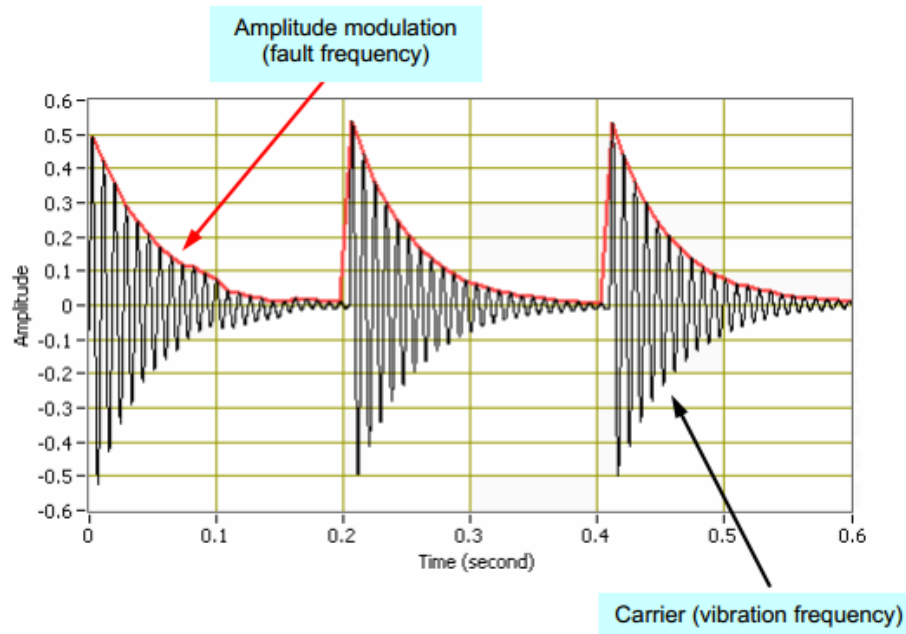


Fig. 2.2 Signal with modulated amplitude and its envelope signal [48]

Konstantin-Hansen [48] studied the application of envelope spectrum in damage detection of a rolling element bearing system. Fig. 2.2 shows a simulated amplitude-modulated signal, the red curve illustrates the envelope of the black curve. The Fourier transform of the red curve is referred to as the envelope spectrum of the black curve. Fig. 2.3 shows an acceleration signal measured on a bearing which has outer race damage, the corresponding spectrum and envelope spectrum. It can be observed from Fig. 2.3 (a) that an impulse is induced when a ball in the bearing system passes the local damaged area of the outer race about every 0.0095 second. So there are sideband frequencies around the carrier frequency. The frequency intervals among them is about 105 Hz ( $\approx 1/0.0095$  second) as shown in Fig. 2.3 (b). This is indicated by the envelope frequency at 105.45Hz and its second order harmonic at 210.9 Hz on the envelope spectrum in Fig. 2.3 (c).

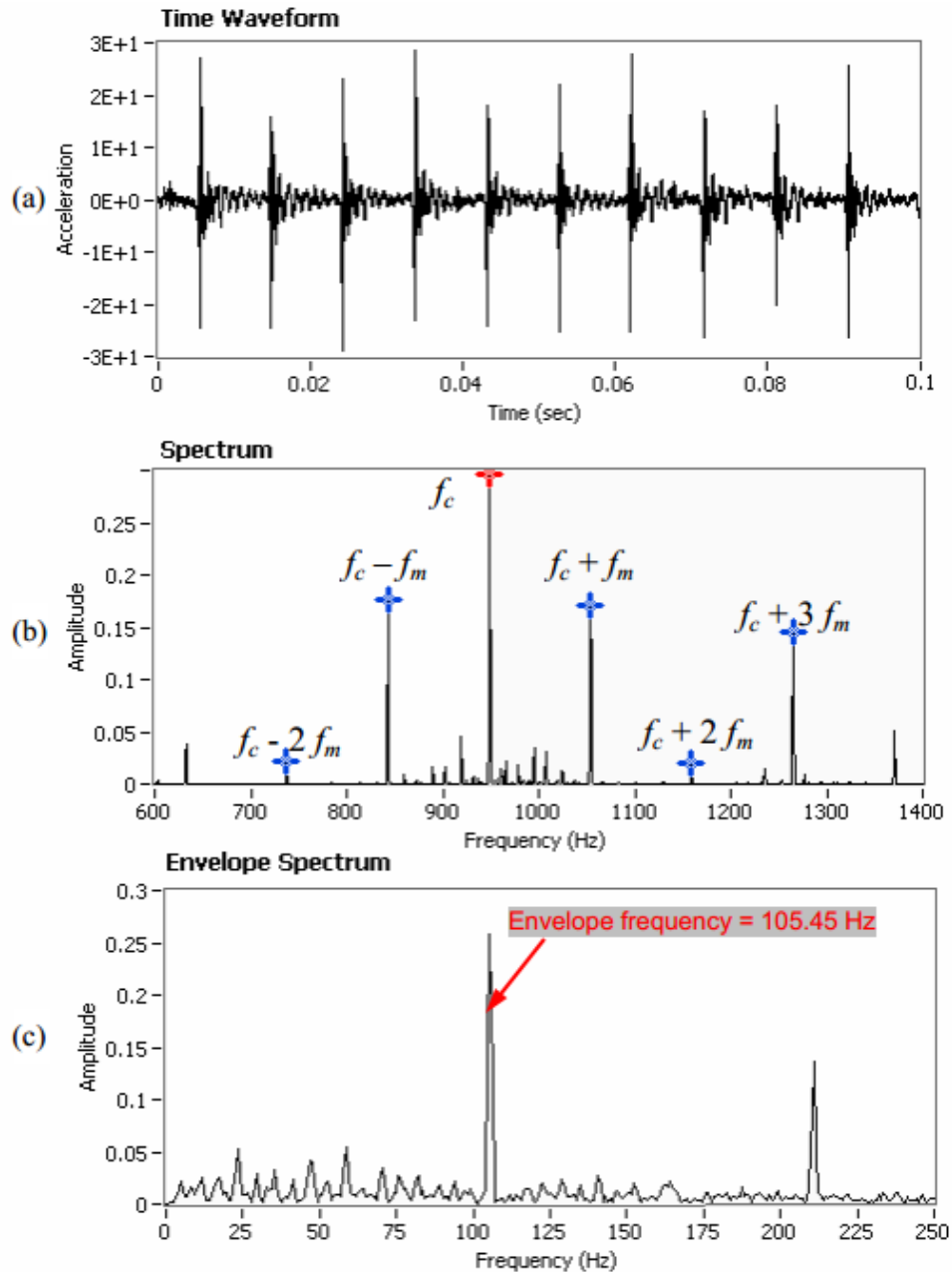


Fig. 2.3 (a) Acceleration signal measured on a bearing suffering outer race damage  
 (b) Spectrum of the acceleration signal  
 (c) Envelope spectrum of the acceleration signal [48]

Envelope spectrum based techniques have been used in SHM successfully [46, 48, 49], but it is only efficient for a modulated signal which sets an annoying limitation in its application.

## 2.2.2 Cepstrum

Literally, cepstrum is an anagram of spectrum. The calculation of cepstrum involves the

IFT of the natural logarithm of spectrum. Concrete definitions are not the same in different literatures. Given a discrete time signal  $x[n]$  and its corresponding Discrete Time Fourier Transform  $X(e^{j\omega})$ , there are three different forms of cepstrum [48, 49]:

$$\text{Complex cepstrum: } C_{\text{cplx}}[n] = \frac{1}{2\pi} \int_{-\pi}^{\pi} \log[X(e^{j\omega})] e^{j\omega n} d\omega \quad (2.7)$$

$$\text{Real cepstrum: } C_{\text{real}}[n] = \frac{1}{2\pi} \int_{-\pi}^{\pi} \log|X(e^{j\omega})| e^{j\omega n} d\omega \quad (2.8)$$

$$\text{Power cepstrum: } C_{\text{power}}[n] = \frac{1}{2\pi} \int_{-\pi}^{\pi} \log[XX^*] e^{j\omega n} d\omega \quad (2.9)$$

Different terms are used in the cepstral analysis and they are listed in Table 2.2.

Table 2.2 Different terms employed in the spectral and cepstral analyses [48, 49]

Spectral analysis	Cepstral analysis
Spectrum	Cepstrum
Frequency (unit: Hz)	Quefrequency ( unit: second)
Harmonic	Rahmonic
Filter	Lifter

The cepstrum reflects particular periodical information in the frequency spectrum, such as sidebands in gearbox vibration signals, and this is similar to frequency spectrum, which represents periodicities in the time domain.

Liang [50] stated that the damage in the circuit of an induction motor will cause a modulation effect in stator vibration. So he implemented cepstrum analysis to detect the harmonics and sidebands in the vibration spectra of a damaged induction motor so that the damage in the motor circuit can be found. Figs. 2.4 (a) and (b) show the vibration power spectra of health and damaged induction motors respectively when induction motors are under 50% loading. The motor speed 24.5 Hz, several harmonics and sidebands can be observed clearly from the vibration power spectrum of damaged induction motor in Fig. 2.4 (b). Figs. 2.5 (a) and (b) show the vibration cepstrum of

health and damaged induction motors respectively. Quefrequency components at 40.8ms and 20.4ms which are roughly equal to 24.5 Hz and its second order harmonic 49 Hz are obviously displayed in Fig. 2.5 (b). In addition, the sidebands in Fig. 2.4(b) are represented by the quefrequency components at 285.7 ms (1/3.5Hz) and 142.8 ms (1/7Hz) respectively. Therefore, cepstrum can detect the damage in induction motor correctly. Other applications of cepstrum can be found in Refs. [48, 49].

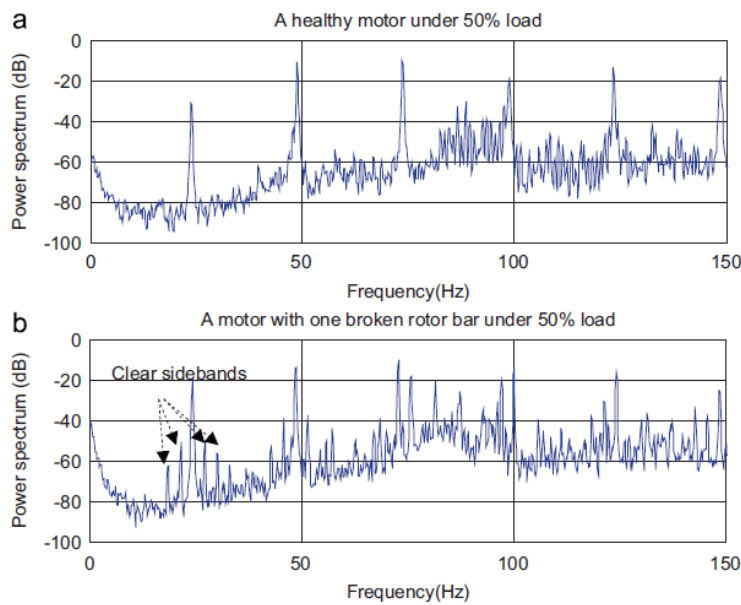


Fig. 2.4 Vibration power spectra of healthy and damaged induction motors [50]

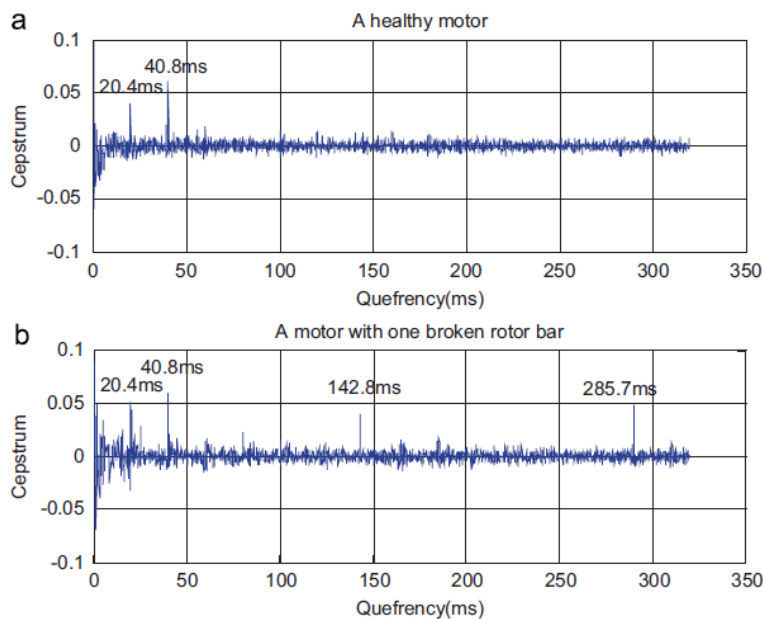


Fig. 2.5 Vibration cepstrum of healthy and damaged induction motors [50]

### 2.2.3 High-order spectrum

The definitions of the commonly used high-order spectrum, including bi-spectrum and tri-spectrum, as well as power spectrum density (PSD) are as follows [51]:

PSD:

$$S_{xx} = E[X(f_l)X^*(f_l)], \quad l = 1, 2, 3, \dots, N \quad (2.10)$$

bi-spectrum:

$$B_{xxx}(f_l, f_m) = E[X(f_l)X(f_m)X^*(f_{l+m})], \quad l + m \leq N \quad (2.11)$$

tri-spectrum:

$$T_{xxxx}(f_l, f_m, f_n) = E[X^*(f_l)X^*(f_m)X^*(f_k)X(f_l + f_m + f_k)], \quad l + m + k \leq N \quad (2.12)$$

where  $E[\ ]$  means expectation;  $X(\blacksquare)$  denotes the DFT of the original data series  $x[n]$ ;  $X^*(\blacksquare)$  is the complex conjugate of  $X(\blacksquare)$  and  $f_l, f_m, f_k$  and  $N$  are frequency variables and the number of their points, respectively.

Obviously, the second-order characteristic of a signal, such as energy, is provided by the conventional power spectrum density while the bi-spectrum and tri-spectrum can offer information on the signal's third- and fourth-order features. The traditional PSD only provides insight into different frequencies and their corresponding amplitudes in a signal. However, because high-order spectrum involves both amplitudes and phases in the frequency domain, it can give information about nonlinear coupling between frequencies of a signal so that high-order spectrum can be used to detect higher order harmonics and their phase relationship in the signal, and to detect nonlinear behavior in dynamic response of a structural system. Therefore, high-order spectrum analysis has been extensively used in SHM for different rotating related components and systems such as gears [52], bearings [53] and rotating machines [54]. McCormick et al in [55] discuss the application of both bi-spectrum and tri-spectrum in bearing fault diagnostics.

## 2.3 Time-frequency domain analysis

The above reviewed time and frequency domain methods are based on the stationary signals. However, in practical engineering, this is not always the case. Structures often experience some degree of unpredicted damage inevitably before they are out of service, and certain damage will induce some nonlinear or time-varying behaviours. Therefore, the properties of measurements on these structures are often time-variant [56, 57]. The above reviewed stationary signal based techniques may not be able to be used in these cases.

The time-frequency methods are especially appropriate to analyse such kind of signals because they can offer simultaneously both time and frequency properties of a signal. Therefore, time-frequency analysis based techniques have been extensively investigated in SHM in recent years. Three most popular methods will be reviewed below including the Short-time Fourier Transform (STFT) [58, 59] method, the Wavelet Transforms (WT) [60] method and the Hilbert–Huang Transform (HHT) [61, 62] respectively.

### 2.3.1 Short time Fourier transform

The traditional procedure of STFT is as follows. Firstly, the signal is sliced up into numerous suitable overlapping time segments by a windowing method. Then Fourier analysis is conducted for each segment to extract frequency information in it. Finally, these spectra are accumulated in the spectrogram which indicates how the frequency components are varying in time. The corresponding formula for continuous-time signals is :

$$STFT(f, t) = \int_{-\infty}^{\infty} x(\tau) \omega(\tau - t) e^{-j2\pi f\tau} d\tau \quad (2.13)$$

where  $\omega(\blacksquare)$  is a window, which can be chosen according to the characteristics of the signal.

Some applications of STFT in SHM can be found in [63-65]. However, STFT has inherent shortcomings. One is that resolution for all frequencies is the same because STFT employed the fixed window for the analysis of the entire signal. This means that good frequency resolution and excellent time resolution cannot be achieved at the same time. Another is that STFT has no orthogonal bases so that no fast and effective algorithm is available for the calculation of STFT [66].

### 2.3.2 Wavelet analysis

Unlike STFT, the window in wavelet transform (WT) is flexible by dilation and translation. Morlet proposed the wavelet firstly in 1984 and then defined continuous wavelet transform (CWT) as follows [16].

$$W_x(a, b, \psi) = a^{-\frac{1}{2}} \int x(t) \psi^*\left(\frac{t-b}{a}\right) dt \quad (2.14)$$

where  $W_x(a, b, \psi)$  is CWT of  $x(t)$ ,  $a$  is the scale or dilation parameter for changing the oscillating frequency,  $b$  is the time parameter,  $\psi(t)$  is an analysing wavelet, and  $\psi^*(t)$  is the complex conjugate of  $\psi(t)$ .

Compared with the STFT, whose window remains the same for the entire signal, the window of WT varies with the frequency of the signal so that both good time and frequency resolution can be achieved [66]. Therefore, wavelet analysis is competent to process non-stationary signal in SHM.

The wavelet transform can be classified into three categories: the continuous wavelet transform (CWT), the continuous wavelet transform with discrete coefficients, and the discrete wavelet transform (DWT). In order to improve computing effectiveness and efficiency, different wavelets have been developed, such as Haar Wavelet, Morlet Wavelet and Mexican Hat Wavelet.

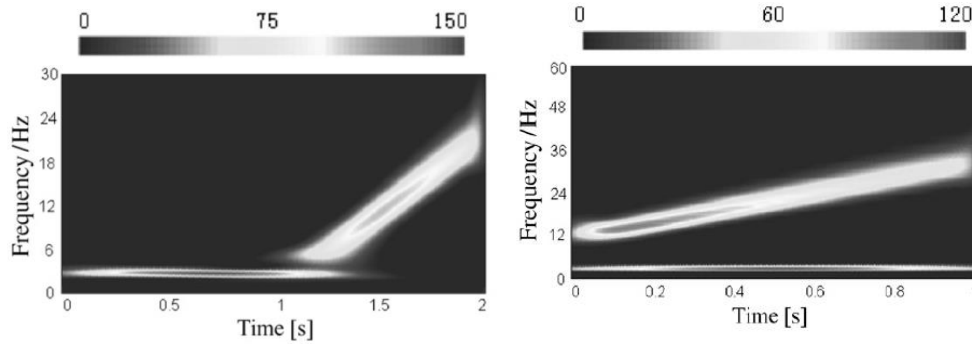
Peng [67] analysed two signals with changing frequency by wavelet transform. The representations of the two signals are given by Eqs. (2.15) and (2.16). The wavelet



scalograms are shown in Figs. 2.6 (a) and (b) respectively.

$$s_1 = \begin{cases} \sin(6\pi t), & 0 \leq t \leq 1 \\ 2 \sin(24\pi(t-1)^2), & 1 \leq t \leq 2 \end{cases} \quad (2.15)$$

$$s_2 = \sin(6\pi t) + \sin \sin(24\pi(t-1)^2), 0 \leq t \leq 1 \quad (2.16)$$



(a) Signal in Eq. (2.15)      (b) Signal in Eq. (2.16)

Fig. 2.6 Wavelet scalograms of the two signals [67]

Obviously, both the constant frequency component and time-varying frequency component in  $s_1$  and  $s_2$  can be recognized from the wavelet scalograms in Fig. 2.6. The two kinds of components are represented by different type of lines. One is straight line at  $f = 3\text{Hz}$  which means that the frequency does not vary with time; the other is skew line which means that the frequency changes with time linearly. The duration of each line indicates the existence time of the corresponding frequency components. It can be observed from Fig. 2.6 (a) that the constant frequency component exists between 0-1s and the time-varying frequency component appears from 1s to 2s. But interference terms make the frequency components between 1-1.3s not to be identified correctly. The duration of both frequency components in  $s_2$  is from 0s to 1s as shown in Fig. 2.6 (b). The above results are consistent with the properties of the signals in Eqs. (2.15) and (2.16). Therefore, the wavelet analysis can provide the time and frequency information in a signal simultaneously.

Currently, WT based techniques have been widely applied in SHM [68-75]. Sometimes, they are integral with the modern signal analysis method, such as fuzzy-logic inference [76], genetic algorithms [77] and artificial neural networks [78-82]. However,

compared with the FT, WT technique is still immature due to many factors.

Firstly, although some algorithms, such as fast wavelet transform (FWT) by Mallat [83], have been developed to improve computing efficiency of wavelet analysis, the algorithm of CWT is still too time consuming to analyze large data sets. Also, no criteria exist for the selection of wavelet basis of various signals [84]. Furthermore, the choice of range scales in the WT is very important. An inappropriate choice of range scales will produce interferential information that can confuse signal analysis [85].

### 2.3.3 Hilbert-Huang Transform

The Hilbert-Huang transform (HHT) is an empirical data-analysis method. It consists of two parts: a time adaptive decomposition operation named empirical mode decomposition (EMD) and Hilbert spectral analysis (HSA).

The goal of EMD is to decompose a signal  $x(t)$  into monocomponent 'intrinsic mode functions' (IMFs) which are the components to be used to conduct well-behaved HHT. The concrete procedure of EMD can be found in Ref. [61].

The original signal can be rewritten as follows:

$$x(t) = \sum_{j=1}^n c_j(t) + r_n(t) \quad (2.17)$$

where,  $c_j(t)$  ( $j = 1, 2, \dots, n$ ) is the IMFs of the original signal  $x(t)$ , and  $r_n(t)$  is residue.

For general signal  $y(t)$ , its Hilbert transform,  $\tilde{y}(t)$  is defined as:

$$\tilde{y}(t) = HT[y(x)] = \int_{-\infty}^{+\infty} \frac{y(\tau)}{\pi(t - \tau)} d\tau \quad (2.18)$$

The analytical signal  $Y(t)$  of  $y(t)$  is expressed as:

$$Y(t) = y(t) + i\tilde{y}(t) = A(t)e^{i\theta(t)} \quad (2.19)$$

where  $A(t)$  is the instantaneous amplitude and  $\theta(t)$  is the instantaneous phase angle. The instantaneous frequency  $\omega(t)$  is obtained as:

$$\omega(t) = \frac{d\theta}{dt} \quad (2.20)$$

For signal  $x(t)$  with  $n$  IMFs, analytical signal  $X(t)$  is:

$$X(t) = \sum_{j=1}^n A_j(t) e^{i \int \omega_j(t) dt} = \sum_{j=1}^n A_j(t, \omega_j) e^{i \int \omega_j(t) dt} \quad (2.21)$$

where the  $A_j(t, \omega_j)$  is the amplitude of the  $j$ th IMF  $c_j$  at time  $t$  with frequency  $\omega_j$ . Finally, the amplitude of the frequency-time decomposition of  $x(t)$  is given by:

$$A(t, \omega, x) = \sum_{j=1}^n A_j(t, \omega_j) \quad (2.22)$$

Definitely, the EMD operation is the most computation consuming step in the whole HHT procedure, but there is no time-consuming procedure, so the HHT can process large size signals. Moreover, although HHT is time-frequency analysis, it involves only the instantaneous frequency instead of the time and frequency resolution.

The HHT based techniques have their specific advantages in time efficiency and reliability when processing nonstationary data sets and have been applied in SHM successfully [86-93]. However, Bao [56] believed that the classic HHT still suffered some deficiencies, especially in the EMD process. Apart from numerous needless low amplitude IMFs and inseparable closely-spaced modes, the classic HHT method is sensitive to unpleasant noise. Moreover, the first IMF always covers too broad frequency range to become mono-component.

### 2.3.4 Others

Other time-frequency domain analysis methods include Wigner-Ville distribution (WVD), Choi-Williams distribution (CWD) and Cone-Shape distribution (CSD). They are

all capable of detecting faults [94-97]. Staszewski and Worden successfully detected a broken tooth in a spur gear by using Wigner-Ville distribution [96]. However, the disadvantage of WVD is the severe interference terms which can exist in the time-frequency domain results and may mislead the signal analysis[16]. So Li conducted the Empirical Mode Decomposition which is the first step of Hilbert-Huang Transform, then evaluated the Wigner-Ville distribution on the intrinsic modes function. In this case, WVD contained no interference terms because IMF is a mono-component function. Finally, this WVD based on the EMD method effectively diagnosed the fault in a ball bearing [97]. The CWD and CSD can overcome the shortcoming of the interference term, but bring the problem of the reduction of time-frequency concentration [16].

## **2.4 Modal analysis**

In the preceding sections signal analysis in the time, frequency and time-frequency domains are discussed. In this section, modal analysis will be investigated. This kind of signal processing method is especially suitable for analysing the vibration of mechanical and civil structures.

### **2.4.1 Natural frequency**

Natural frequency is the particular vibration frequency at which a system naturally oscillates. It is the inherent characteristics of a system, and one system can have one or more natural frequencies.

Salawu [12] reviewed the contribution of natural frequencies in SHM. For example, the crack in a beam would reduce its natural frequency by decreasing the local bending stiffness at corresponding cross-section. Therefore, the natural frequency based technique has been considered as one of the most useful damage detection methods. However, other findings [12, 98, 99] suggest that if the fault occurred at low stresses

region, the change of natural frequency might be unreliable for SHM. In addition, Chen et al. [100] argued that the information of the natural frequency variation was not sufficient enough to serve as an effective damage indicator because they found the variations of the first four natural frequencies were smaller than 10% even when the fault was serious enough to induce structural failure.

### **2.4.2 Mode shape**

Mode shape is defined as a particular vibrating pattern at a given natural frequency of mechanical/civil structures. It varies with the different natural frequencies. Generally, a unique modal shape is associated with one natural frequency, but symmetrical structure sometimes has two modal shapes at one frequency. The damage or abnormal behaviour in a structure can cause changes in modal shape.

Two approaches are frequently adopted to directly compare two mode shapes. One is Modal Assurance Criterion (MAC) [101, 102], the other is the Coordinate Modal Assurance Criterion (COMAC [102]). The MAC denotes the similarity between two sets of mode shapes. When two modal shapes are completely different, the value of MAC is 0, while when they match perfectly, the value of MAC is equal to 1. Therefore, the value of MAC can be considered as a fault indicator. The COMAC shows discordance between two mode shapes and its value also changes between 0 and 1. The value of COMAC at a damage region is greater than that at a normal spot, so the COMAC is able to reflect potential damage location[14].

Another indirect method is mode shape curvature, the change of which is more prominent than that of the mode shapes and is highly focused on the damage zone. Wahab and De Roeck [103] proposed 'curvature damage factor', which involved the difference of healthy and faulty curvatures, and successfully applied it to the Z24 Bridge in Switzerland. Some other examples of applications of modal shape in SHM can be found in Refs. [104-108].

SHM techniques based on mode shapes possess numerous merits that natural frequencies related methods cannot achieve. For example, mode shapes depend on local information, so they are susceptible to local damage and can be applied directly in the identification of damage location. Furthermore, the mode shapes are less prone to be affected by environments than natural frequencies [109]. However, such approaches are imperfect. The first disadvantage is that measurement of the mode shapes requires a series of sensors to measure displacements. The second one is that the measured mode shapes are more likely to be polluted by unwanted noise than natural frequencies [13].

### **2.4.3 Modal strain energy**

Similar to modal shape, modal strain energy is also sensitive to local damage so that it can be exploited to identify the location of damage. Kim and Stubbs [110] proposed a damage indicator according to the ratio of modal strain energy of a healthy structure to that of a damaged structure. Then a proper damage identification algorithm about locating and sizing the damage was verified by an experimental plate girder with a single crack and a simulated plate girder with up to two damage sites.

Law [111] defined the ratio of the modal strain energy of an element to its kinetic energy as elemental energy quotient (EEQ) and proposed a damage location indicator which is the deviation of the EEQ before and after damage normalized and averaged over numerous modes. Further simulation studies verified that such indicator could identify damage location successfully not only when 10% random noise was added but also when the experimental two-storey plane frame suffered two loosened joints.

Damage location and size identification method based on modal strain energy was compared with natural frequency analysis based method in Ref. [112]. It was found that the former could provide more precise information about fault location than the latter. In addition, modal strain energy based methods were considered as a special

case of modal based methods by some researchers [13, 112].

## 2.5 Frequency response analysis

### 2.5.1 Coherence function

Coherence function is used to inspect the relationship between two different signals,  $u(t)$  and  $x(t)$  in the frequency domain. It is mathematically defined as the cross-power spectrum normalized by spectral densities of the two signals as follows.

$$C_{xu}(f) = \frac{|P_{xu}(f)|^2}{P_{xx}(f)P_{uu}(f)} \quad (2.23)$$

where  $P_{xx}(f)$  and  $P_{uu}(f)$  represent spectral densities of  $u(t)$  and  $x(t)$  respectively; and  $P_{xu}(f)$  denotes cross-power spectrum of these two signals. Coherence function  $C_{xu}(f)$  can determine the linearity between  $x(t)$  and  $u(t)$ . For a linear system with output  $x(t)$ , input  $u(t)$ , and frequency response function  $H(f)$ ,  $X(f) = H(f)U(f)$ , where  $X(f)$  and  $U(f)$  are the spectrum of  $x(t)$  and  $u(t)$  respectively. Moreover, it is known that  $P_{xx}(f) = |H(f)|^2P_{uu}(f)$  and  $P_{xu}(f) = H(f)P_{uu}(f)$ , therefore, in this case, coherence function  $C_{xu}(f)$  becomes

$$C_{xu}(f) = \frac{|P_{xu}(f)|^2}{P_{xx}(f)P_{uu}(f)} = \frac{|H(f)P_{uu}(f)|^2}{|H(f)|^2P_{uu}(f)P_{uu}(f)} = 1 \quad (2.24)$$

When the output signal is mixed with white noise,  $X(f) = H(f)U(f) + N(f)$ , so  $P_{xx}(f) = |H(f)|^2P_{uu}(f) + P_{nn}(f)$  and  $P_{xu}(f) = H(f)P_{uu}(f)$ , where  $N(f)$  and  $P_{nn}(f)$  are spectrum and spectral density of noise, respectively. In this case, coherence function  $C_{xu}(f)$  becomes

$$C_{xu}(f) = \frac{|P_{xu}(f)|^2}{P_{xx}(f)P_{uu}(f)} = \frac{|H(f)P_{uu}(f)|^2}{P_{xx}(f)P_{uu}(f)} = \frac{|H(f)|^2P_{uu}(f)}{P_{xx}(f)} = 1 - \frac{P_{nn}(f)}{P_{xx}(f)} \quad (2.25)$$

Because  $P_{xu}(f)$ ,  $P_{xx}(f)$ ,  $P_{uu}(f)$  and  $P_{nn}(f)$  are all positive values, so the coherence function  $C_{xu}(f) \leq 1$  and

$$C_{xu}(f) \begin{cases} = 1 & \text{for linear system} \\ \approx 1 & \text{for linear system with little noise} \\ \ll 1 & \text{for nonlinear system} \end{cases} \quad (2.26)$$

In other words,  $C_{xu}(f) = 1$  indicates the system is linear; when  $C_{xu}(f) \approx 1$ , the system may still be linear but the measured signals are mixed with noise.  $C_{xu}(f) \ll 1$  means that the system behaves nonlinearly, which can, in many cases, be induced by a damage. Therefore, these characteristics are often employed to detect damage in different systems. For example, Bejger investigated the coherence function in the application of marine engine injection pump diagnosis, and concluded that the coherence function was sensitive to damage in the lower frequency range and this phenomenon corresponds to his previous research results [113]. Reddy found that coherence function could help to detect the damage in a power transformer by directly observing the coherence spectrum [114].

Although analysis of coherence function has detected damage successfully, it has inevitable limitations. For example, it is only effective to detect nonlinear fault. The level of coherence still keeps 1 in linear damage cases because the relationship between the input and output remains linear even though the linear relationship changes when a linear fault occurs.

### 2.5.2 GFRFs

The Volterra series can describe a class of nonlinear systems which are stable at zero equilibrium. The output in the neighborhood of the equilibrium can be represented as follows[115].

$$x(t) = \sum_{\bar{n}=1}^N \int_{-\infty}^{\infty} \dots \int_{-\infty}^{\infty} h_{\bar{n}}(\tau_1, \dots, \tau_{\bar{n}}) \prod_{i=1}^{\bar{n}} u(t - \tau_i) d\tau_i \quad (2.27)$$

where  $N$  is the maximum order of the system nonlinearity;  $h_{\bar{n}}(\tau_1, \dots, \tau_{\bar{n}})$  is the  $\bar{n}$ th order Volterra kernel.



The Volterra series is always considered as a powerful tool for analyzing nonlinear systems and has been extensively researched in the last several decades. Basic principles about the Volterra series are systematically introduced in Refs. [116, 117]. Its development is reviewed by Billings [118], Korenberg and Hunter [119, 120]. Kotsios [121] studied the possible problems when an infinite Volterra system was transformed to a finite input/output form and proposed an effective operator to solve them. The application of the Volterra series involves studies in different fields including civil and mechanical engineering, electrical engineering, biological engineering and control system.

The multi-dimensional Fourier transforms of the Volterra kernels are defined as higher-order frequency response functions (HFRFs) or generalized frequency response functions (GFRFs)[122].

$$H_{\bar{n}}(j\omega_1, \dots, j\omega_{\bar{n}}) = \int_{-\infty}^{\infty} \dots \int_{-\infty}^{\infty} h_{\bar{n}}(\tau_1, \dots, \tau_{\bar{n}}) e^{-(\omega_1\tau_1 + \dots + \omega_{\bar{n}}\tau_{\bar{n}})} d\tau_1 \dots d\tau_{\bar{n}} \quad (2.28)$$

So the response of a nonlinear system in the frequency domain to a general input can be described by [123]

$$\left\{ \begin{array}{l} X(j\omega) = \sum_{\bar{n}=1}^N X_{\bar{n}}(j\omega) \quad \text{for } \forall \omega \\ X_{\bar{n}}(j\omega) = \frac{1/\sqrt{\bar{n}}}{(2\pi)^{\bar{n}-1}} \int_{\omega_1 + \dots + \omega_{\bar{n}} = \omega} H_{\bar{n}}(j\omega_1, \dots, j\omega_{\bar{n}}) \prod_{i=1}^{\bar{n}} U(j\omega_i) d\sigma_{\bar{n}\omega} \end{array} \right. \quad (2.29)$$

Here  $X_{\bar{n}}(j\omega)$  denotes the  $\bar{n}$ th order frequency response of the system's response.

The term

$$\int_{\omega_1 + \dots + \omega_{\bar{n}} = \omega} H_{\bar{n}}(j\omega_1, \dots, j\omega_{\bar{n}}) \prod_{i=1}^{\bar{n}} U(j\omega_i) d\sigma_{\bar{n}\omega}$$

represents the integration of  $H_{\bar{n}}(j\omega_1, \dots, j\omega_{\bar{n}}) \prod_{i=1}^{\bar{n}} U(j\omega_i)$  over the  $\bar{n}$ -dimensional hyper-plane  $\omega_1 + \dots + \omega_{\bar{n}} = \omega$ .

The  $n^{\text{th}}$  order GFRF is the extension of the frequency response function of a linear system to the  $\bar{n}$ th order nonlinear case. The GFRFs can be used to describe the nonlinear system characteristics. The algorithm for determining GFRFs was studied in Refs. [31, 124-129]. The GFRFs of discrete-time system are introduced in Refs. [124, 125, 129] and have been applied to analyze the Duffing's equation and a Van der Pol model successfully. For continuous-time systems, harmonic probing method is a useful tool to determine the GFRFs [126-128]. Rijlaarsdam [130, 131] analyzed the relationship between the GFRFs and the higher order sinusoidal input describing function, and verified his conclusions by numerical examples. The nonlinear information in GFRFs can be used in damage detection [132-134] and system control [135].

### 2.5.3 NOFRFs

The GFRFs are difficult to measure and interpret in practical engineering because they are multi-dimensional. So Lang proposed the novel concept of nonlinear output frequency response functions (NOFRFs) which are determined by both the input and the GFRFs of a nonlinear system and defined as follows [31].

$$G_{\bar{n}}(j\omega) = \frac{\int_{\omega_1+\dots+\omega_{\bar{n}}=\omega} H_{\bar{n}}(j\omega_1, \dots, j\omega_{\bar{n}}) \prod_{i=1}^{\bar{n}} U(j\omega_i) d\sigma_{\bar{n}\omega}}{\int_{\omega_1+\dots+\omega_{\bar{n}}=\omega} \prod_{i=1}^{\bar{n}} U(j\omega_i) d\sigma_{\bar{n}\omega}} \quad (2.30)$$

under the condition that

$$\int_{\omega_1+\dots+\omega_{\bar{n}}=\omega} \prod_{i=1}^{\bar{n}} U(j\omega_i) d\sigma_{\bar{n}\omega} \neq 0 \quad (2.31)$$

By introducing the NOFRFs, the output frequency response of a nonlinear system can be written as

$$\begin{cases} X(j\omega) = \sum_{\bar{n}=1}^N X_{\bar{n}}(j\omega) & i = 1, \dots, n \\ X_{\bar{n}}(j\omega) = G_{\bar{n}}(j\omega)U_{\bar{n}}(j\omega) \end{cases} \quad (2.32)$$

Here,  $U_{\bar{n}}(j\omega)$  is the Fourier transform of the  $\bar{n}$  order power of the input,  $u^{\bar{n}}(t)$ , it can be written as follows.

$$U_{\bar{n}}(j\omega) = \frac{1/\sqrt{\bar{n}}}{(2\pi)^{\bar{n}-1}} \int_{\omega_1+\dots+\omega_{\bar{n}}=\omega} \prod_{i=1}^{\bar{n}} U(j\omega_i) d\sigma_{\bar{n}\omega} \quad (2.33)$$

The NOFRFs  $G_{\bar{n}}(j\omega)$  defined by Eq. (2.30) can be regarded as an alternative extension of the frequency response function of a linear system to the  $\bar{n}^{\text{th}}$  order nonlinear case. The most distinctive characteristic of the NOFRFs is their one-dimensional nature, which can significantly facilitate the analysis of nonlinear systems in the frequency domain. Lang explained the energy transfer phenomenon in a nonlinear system using the concept of NOFRFs[31]. The NOFRFs could also be used to explain resonances and determine resonant frequencies in nonlinear systems [136] and nonlinear effects in cracked beams[137, 138]. Lang and Peng also studied the properties of the NOFRFs for a kind of periodic structures in Refs.[139-141] and applied the results to the detection and localization of nonlinear components in the systems [28, 142-145].

#### 2.5.4 Transmissibility based damage detection and localization

Traditionally, the transmissibility is defined as the ratio of the spectra of two different system outputs, has been comprehensively studied, and is widely used for damage detection and localization. For example, Cao [146] investigated the rate of change of both the system transmissibility and the system frequency response functions when a damage occurred, and found that the transmissibility was much more sensitive to the damage than the FRF. Maia [147] conducted a comprehensive research on the transmissibility based damage detection technique, and proposed a DRQ (Detection and Relative Damage Quantification) Indicator, which was the correlation

between the measured system response and the response estimated from the undamaged transmissibility function. He also proposed the concept of TDI (Transmissibility Damage Indicator) in [25], which was defined as the correlation between the transmissibility of a undamaged system and the transmissibility of a damaged system. The performance of these transmissibility based indicators in damage detection has been verified by experimental studies. In addition to damage detection, the transmissibility has also been used for damage localization. Zhang [148] studied the influence of damage on the transmissibility, and found that the transmissibility near the damaged area could cause a more significant change. Consequently, he proposed several damage indicators based on translational transmissibility and curvature transmissibility and verified that these damage indicators could help to find the location of damage correctly by both simulation studies and experimental tests. Jonson [26, 29, 149] analyzed the characteristics of the transmissibility response function and concluded that transmissibility response function was entirely independent of the poles but solely dependent on the zeros of the system transfer function so that the damage could be trapped and identified. Sampaio and Maia [27] pointed out that the summation of the difference between the damaged and the undamaged transmissibility would mask the true damage location if the frequency range was inappropriate. This is because the transmissibility difference near the resonances and anti-resonances was much larger than that in the other frequency range. So he counted the occurrences of maximum transmissibility difference at different frequencies and considered the result as a damage indicator. But if the location of operational forces changes, the transmissibility between responses at two fixed points will also change making such techniques become invalid. Devriendt [150] found that the transmissibility around the natural resonance frequencies changed slightly when the location of operational forces changed. So he considered the occurrence times of maximum transmissibility around the resonance frequencies as a damage location indicator and demonstrated its effectiveness by

simulation and experimental studies. Chesne' [151] reviewed available transmissibility based damage detection and localization techniques and pointed out the possible factors which affect the results of transmissibility analysis and should be taken into consideration such as frequency bands, force location and environment.

## **2.6 SHM under changing environmental and operational conditions**

### **2.6.1 The effect of Environmental and operational conditions**

It is known that structural damage usually causes variations in the dynamic characteristics of the structure and changes features of the measured signals from the structure. Here, the signal features can be extracted from signal processing methods, and those which change because of the existence and different severities of damage are known as damage sensitive features. SHM and damage localization are always implemented by evaluating how much the damage sensitive features extracted from the measurements on a monitored structure deviate from the same features extracted from a healthy structure. A significant departure will cause damage alarm, while a similarity in the features is considered as an indication of being normal, namely, no damage occurs at the moment. The potential problem with these SHM and damage localization techniques is that the variability of the signal features can be the results of the changing environmental factors and operating parameters, but most available techniques do not take these effects into account. Environmental factors are the environmental conditions where the signals are measured such as temperature, wind, and humidity, while the operating parameters include different loading conditions. Sohn reviewed the possible environmental and operational conditions which will affect structural dynamic behaviours [24].

### **2.6.1.1 Temperature**

Variation of environmental temperature can cause more significant fluctuation in structural dynamic features than damage in some circumstances. The environmental temperature always changes hour by hour, and day by day. When the process of the measuring signals lasts quite a long time and the temperature varies a lot, the variation of the damage sensitive features can be the results of both damage and the environmental temperature. Temperature changes the damage sensitive features in two ways. One is by altering the material characteristics of the structure, particularly, material stiffness which the natural frequency depends on. So the natural frequency will change with the variation of the temperature. The other is by varying the structural boundary conditions [24].

Several investigations have been conducted to study the temperature effect on the dynamic features of a structural system [18]. The measurements on a footbridge which were conducted by Askegaard and Mossing and lasted 3 years show that the natural frequency changes about 10% and seasonal temperature variation contributes partially to this [19]. Brenner found that the temperature could also cause the change of bridge deflection and strains [152]. As for gearbox, Loutas [153] researched how the features of the vibration and acoustic emission (AE) signals in the frequency domain changed when the gearbox kept working until the 4 teeth were cut and considerable damage on the shaft happened. It was concluded that the oil temperature had an effect on the recordings.

Ambient temperature can also alter the dynamic responses of a structure by changing its boundary condition. Alampalli compared the first three natural frequencies of a damaged bridge with their counterpart on a the healthy bridge when the bridge deck was in different ambient temperature and found that the first three natural frequencies of the damaged bridge at above-freezing temperatures were all slightly lower than those of the healthy bridge, while the first three natural frequencies of the

damaged bridge at below-freezing temperatures increased significantly and were about 1.5 times those of the healthy bridge [154].

### **2.6.1.2 Unpredicted loadings**

Unpredicted loadings such as wind-induced and traffic-induced loadings on bridges would be a factor that is difficult to measure, but may change the dynamic responses of a structure significantly. It is intuitive that moving vehicles and passengers on a bridge will increase its mass and change its modal frequencies. But the number of vehicles and passengers and their masses usually keep changing from time to time and cannot be measured accurately. Wind is able to induce certain distributed pressure on a structure and make it vibrate even though there is no external loading at all. Therefore, these unpredicted loadings play an important role on the structure dynamics.

Many researchers pay attention to the effects of traffic loadings on the structural dynamics. Zhang [20] analysed the ambient vibration measured on a cable-stayed bridge during a 24 hours period and concluded that the modal frequencies of the bridge changed as much as 1% during a day period and the damping ratios depended on the traffic mass, especially when the vibration of the deck exceeded a critical level. However, the modal amplitudes and modal deflection were insensitive to the traffic conditions. Kim [155] compared traffic-induced vibration of three bridges with different lengths and reported that the traffic changed the natural frequencies of the shortest bridge most obviously. The second natural frequency of the shortest bridge was decreased by as much as 5.4% as a result of the heavy traffic. Sohn [24] concluded that the mass loading effect on the bridge depended on the traffic mass relative to the bridge magnitude. He also [156] investigated feature changes of a theme park ride and found that the feature variation caused by mass loading (customers simulated by rock dummies) in a train was much larger than that caused by the delamination damage.

Wind-induced loading should also be considered when analysing the structure dynamic behaviours. Metwally [21] investigated the dependency of bridge modal parameters and responses on wind speed based on the vibration data of a bridge measured over 100 continuous hours. It is observed that the vertical vibration amplitude of the bridge was almost a quadratic function of the wind speed; both damping ratio and higher order mode shapes depended on the vibration amplitude when the wind speed was up to 13m/s. Other researchers studied the vibration of bridges caused by wind and rain and found that this kind of vibration could be considered as an instability phenomenon [157, 158].

### **2.6.1.3 Operational speed**

The temperature and unpredicted loadings usually affect structural dynamics by changing the modal parameters of the structures as reviewed above, while operational speed such as rotating speed of a rotor system will cause unexpected dynamic responses. Han [22] studied the stability of a rotor system suffering rub-impact damage under different rotating speeds and found that the rotor behaved in the state of a stable periodic motion firstly when the rotating speed of the system was low, while if the speed increased up to a certain range, the system exhibited period-doubling bifurcations and then reached stable periodic motion again when the rotating speed kept increasing. Ma [23] also observed the bifurcation phenomena in another rotor system which was also subject to the rub-impact damage when the rotating speeds became faster, and verified it by experimental studies.

Different environmental factors such as temperature and humidity and operational conditions may affect the structural dynamic responses at the same time and their effects cannot be separated from each other easily [12, 24, 159]. Pirner [159] found it was difficult to directly distinguish wind-induced loadings and temperature-induced ones in a TV tower by using time histories.



In summary, the change of measured features can be contributed not only by damage but also by environmental and operational conditions. It is obvious that neglect of these factors, which often impact on structural dynamics and sensor measurements, will make some features of sensor measurements not show what happens with inspected components. Therefore, the effect of changing environmental and operational conditions should be filtered out when conducting SHM so that any change in the signal features which are literally produced by abnormality of components and/or system can be correctly identified.

### **2.6.2 SHM under changing environmental and operational conditions**

Some researchers have paid attention to the influence of changing environmental and operational conditions on the system behaviours, and tried to eliminate the effect of the non-damage factors so as to enhance the reliability of damage detection. The corresponding techniques can be divided into three different categories. Firstly, when variable environmental factors and operational parameters, such as temperature and operational speed, can be measured directly, extensive modelling methods can help to build the relationship among the damage-sensitive features, damage situation and non-damage factors including environmental factors and operational parameters. Secondly, if it is difficult and impractical to measure environmental and operational conditions, such as unpredicted loadings, these changing conditions can be considered as intrinsic characteristics of the system itself, so that the damage-sensitive features, which are 'orthogonal' to the variation induced by changing environmental and operational conditions, can be extracted. Thirdly, some researchers try to extract signal features explicitly which are insensitive to changing environmental and operational conditions but are still sensitive to damage situation. It should be pointed out that in this case it is possible to distinguish feature variation caused by damage from those induced by changing environmental and operational parameters even though no measurements on environmental and operational parameters are available.

The models which describe the damage-sensitive features, damage situation and environmental and operational factors can indicate quantitatively the contribution of variable environmental and operational factors to the change of damage-sensitive features so that the effects of these non-damage factors can be eliminated when conducting SHM. De Roeck and Peeters [160] monitored the Z24 Bridge in Switzerland for one year and then considered the environmental factors including air temperature, humidity, rain, wind speed and wind direction when conducting damage detection on this bridge. The results demonstrated that once the effects of these environmental influences were filtered out, stiffness degradations could be detected if the corresponding frequency shifts were more than just 1%. They [161] also built an ARX (autoregressive model with an exogenous input) model for modal frequencies and temperature, and determined the possible health threshold of the simulation errors between measured modal frequencies and these predicted from the ARX model by statistical analysis. It is expected that the predicted errors based on modal frequencies of the healthy bridge should be within the threshold. Yang [162] pointed out that most research about gearbox damage detection always assumed that the load was a constant and the vibration signals caused by a fluctuating load were not interpreted correctly. Therefore, the model developed under the constant load assumption cannot recognize whether the vibration signature changes are caused by the load variation or by a failure occurrence. To settle this problem, he proposed a proper approach which considered load as additional information in a time series ARX model. Sohn [163] conducted damage detection by using AR-ARX (auto-regression and auto-regression with exogenous) models from time series of the vibration signals. Firstly, the reference data set which is assumed to be collected under the same environmental and operational conditions as the new data set was selected when the sum of the squared differences between reference AR model coefficients and that of the new data set was minimum. Then the damage-sensitive feature was defined as the residual error between the new data set and the predicted value of the ARX model which was

modelled based on the selected reference data set. This AR-ARX models based method was verified by experimental tests from an 8DOF mass-spring system. He further employed outlier analysis with the Mahalanobis distance measure for AR model coefficients in the above AR-ARX models based method to identify the abnormal variation of a patrol boat. The effectiveness of this outlier analysis technique and AR-ARX models based method was validated by the strain data sets measured from the patrol boat under different conditions [164]. Worden [165] considered the coefficients of the AR model from a data set as damage sensitive features and revised conventional outlier analysis method by replacing traditional mean vector of the damage sensitive features with features at the same temperature predicted from a polynomial regression model in terms of the temperature and the mean vector of damage sensitive features at this temperature. He further demonstrated by simulation studies that the higher AR model order was able to help to identify the damage state more clearly. Finally Worden pointed out that interpolation could be applied to predict the mean vector of damage sensitive features when more environmental and/or operational factors were considered.

When the values of environmental and operational factors are difficult to measure but the signal features under different environmental and operational conditions are available, certain techniques such as neural network and singular value decomposition (SVD) can help to take environmental and operational variation into consideration while conducting SHM. Zhou [166] applied back-propagation neural network (BPNN) technique to build the correlation model between the temperature and modal feature of a bridge in Hong Kong so as to eliminate the temperature effect, and then auto-associative neural network (AANN) was employed to detect damage in the bridge. Experimental studies showed that this technique could detect the natural frequency change caused by damage as small as 1%. Sohn [167] proposed that if the reference signal wasn't selected based on the AR model, an auto-associative neural network could be employed to distinguish the change of the damage-sensitive feature caused

by damage and that caused by variation of ambient conditions; this proposal was also verified by the experimental tests from an 8DOF mass-spring system. Besides, in order to monitor the health state of a bridge in the USA effectively, Sohn built a linear adaptive filter model for the modal parameters including fundamental frequency and temperature inputs to reduce the temperature effect on the measured modal parameters [168]. Moreover, Sohn summarized the possible environmental and operational factors which may affect the structural health monitoring and reviewed available techniques to eliminate these effects including regression analysis, subspace-based identification method, novelty detection, singular value decomposition, auto-associative neural network, factor analysis and lamb-wave propagation method [24]. Ruotolo and Surace [169] think that when damage-sensitive feature vectors under possible environmental and operational conditions are put together into a matrix, the rank of this matrix will increase by 1 if another damage-sensitive feature vector extracted from damaged structure is added into this matrix while the rank of this matrix will keep the same if the new feature vector is collected from a healthy structure. So a singular value decomposition technique was developed and its capability in SHM was illustrated by both simulation investigation and experimental studies on a cantilever beam. The results indicated that the proposed technique was able to successfully detect not only damage occurrence but also damage severity. Another SVD based method was applied to a composite beam in Ref. [170]. Surace and Worden [171, 172] proposed a negative selection approach to distinguish the feature fluctuation induced by the environmental and operational conditions and that caused by damage occurrence. This negative selection is to simulate the human immune system which can differentiate the antigens from human body. Kullaa [173] removed the effects of operational and environmental fluctuations by using linear factor analysis (FA) or the nonlinear combination of linear factor analyzers, then the application of this factor analysis based method was verified by both simulated data sets from a wooden bridge and a vehicle crane.

Finally, several methods have been proposed to construct signal features which are only sensitive to damage but insensitive to changing environments and operational conditions. Cross and Worden [174] combined linearly several damage sensitive features to produce a new feature which was independent to environmental and operational variation but was sensitive to damage. They [175] also tried to extract signal features which are insensitive to environmental variation but still damage-sensitive by three different methods including the co-integration technique as discussed above, outlier analysis and the minor principal components techniques. A univariate novelty index was used to select this kind of feature for outlier analysis. The minor components were assumed to be independent from environmental changes. Devriendt [150] reduced the frequency range to a small frequency band around the resonance frequencies of a structure, so that the transmissibility based SHM was more robust because it became independent of the changing loading condition to a certain extent. Figueiredo [176] reviewed machine learning algorithms including factor analysis, Mahalanobis squared distance (MSD), singular value decomposition and auto-associative neural network and compared the damage detection results for a three floor building under changing stiffness and mass conditions and concluded that the algorithms based on the first two methods were more suitable to minimize the false-positive damage indications, while the algorithm based on the last two methods is more applicable to minimize false-negative damage indications.

All above techniques treat features under all possible environmental and operational conditions equally, the judgment criteria on the occurrence of damage are determined when the whole variable range of environmental and operational parameters are taken into consideration. The problem is the features of measurements are always only sensitive to damage under certain values of environmental and operating parameters, and the features in such range can represent the healthy condition more effectively. Motivated by this phenomenon, a new SHM method considering changing environmental and operational conditions is proposed in this thesis. The overall

environmental and operational conditions are divided into several ranges (bins) which contain different values of operating parameters, then an SHM strategy is conducted within these different ranges separately.

## **2.7 Damage localization under changing environmental and operational conditions**

As stated above, transmissibility analysis methods is one class of the most popular techniques to detect damage location. However, because the transmissibility is basically a linear system concept, all the techniques above assume the systems behave linearly. This has several limitations [151]. Firstly, the transmissibility between responses at two fixed points depends on the location of the excitation. Namely, if the loading is applied on the system at different locations, the transmissibility even between responses at two fixed points will also change. Secondly, the potential of the available transmissibility based techniques in damage localization requires the use signals of an appropriate frequency band. An unsuitable frequency band used in transmissibility analysis may cause a false alarm in fault location. Finally, because traditional transmissibility is basically a linear system concept, it cannot be used to propose a systematic approach to detecting and locating damage of nonlinear features. Therefore, alternative damage sensitive features need to be explored to overcome these limitations. The new method can be based on the nonlinear features in the responses of the damaged system.

In MDOF (Multi-Degree-Of-Freedom) structural systems, certain types of damage often manifest themselves as the introduction of non-linearity into an otherwise linear system. One obvious example is crack. The breathing crack [177], which may open and close as loading increases and decreases [178], will change the stiffness of the operating structure and further induce nonlinear behaviors in the whole system [137, 179, 180]. At the same time, the super-harmonic components and sub-harmonic

resonances can be observed when the cracked object is excited by a harmonic loading [137, 138, 180-182]. Another common example is clearances between subassemblies. This gap can be caused by the long-time wear or extreme deflection or displacement due to excessive loading so that different structural parts interfere with each other and induce piecewise linear response [183, 184]. Ref. [185] also indicated that high order harmonic components such as 2X, 3X appeared and changed with the variation of looseness clearance when a bolt on the pedestal became loosened. In rotary machineries, rub-impact damage in rotor systems makes the rotor rubbing the stator regularly so that the stiffness of the system becomes bilinear. This will induce super- and/or sub-harmonic components of the driving frequency [186-188]. Similarly, some damage, including misalignment [189-191] and oil whirl [192], can potentially cause nonlinear frequency components. Overall, nonlinear behaviors often manifest in many damaged MDOF structural systems and nonlinear components can be used to represent damage with nonlinear features in such systems.

Some damage in the electrical system could also induce a system's nonlinear behavior. For example, in power transmission line, the insulation of power cables may be degraded because of electric stress after a long-time work. When the water tree deterioration occurs, the relationship between the voltage and the current will become nonlinear, so that the whole system behaves nonlinearly [193, 194]. Besides, if the power cables electrically contact with poor conductive surface, such as a tree branch and a road surface, the current will be restricted to a lower level. In this case, nonlinear high-impedance ground damage happens [195, 196].

### **2.7.1 Alternative transmissibility analysis based on nonlinear features**

In order to extend the transmissibility based damage detection and localization approaches to MDOF structural systems which can behave nonlinearly due to the occurrence of damage with nonlinear features, several methods have recently been

developed [28, 137-139, 142-145, 193]. These methods are based on the concept of nonlinear output frequency response functions [31, 197] and use the system response signals to deterministic inputs including sinusoids to detect and locate such damage in the systems. Moreover, Lang et al. [28] proposed the concept of transmissibility of the NOFRFs which systematically extends the transmissibility concept to the nonlinear case, and has been used to develop a technique that can detect and locate damage with linear and/or nonlinear features in MDOF structural systems. The effectiveness of the technique has been verified by both numerical simulation studies and experimental tests [28]. However there are many limitations with these recently developed techniques. All but the one in [142] of these methods assume that when damage occurs in a MDOF system and makes the system behave nonlinearly, there is only one nonlinear component in the system. Although the method proposed in [142] has overcome this problem and can deal with more than one nonlinear components, the method requires that the loading on structural systems is measurable, which is difficult in many practical applications.

One of the important studies in this thesis is concerned with the development of a new and more general transmissibility analysis method for the detection and location of damage via nonlinear features in MDOF structural systems. By evaluating and analyzing the transmissibility at super-harmonics/ frequencies generated by nonlinearity a concept that will be introduced in the thesis for MDOF nonlinear structural systems, the method can deal with more than one nonlinearly damaged components in the system and does not require that loadings on inspected structural systems are measurable.



## Chapter 3

### **A novel health probability based structural health monitoring method**

Structural health monitoring is traditionally concerned with fitting sensors inside or outside systems and analyzing the features of signals from sensor measurements using appropriate signal processing techniques to reveal the system's condition and health status. However, the conventional signal only based analysis often cannot distinguish the normal changes due to the differences in system environmental or operating parameters from the changes which are induced by damage. This is because the changes revealed by sensor signal analysis can not only show what happens with the condition and health status of inspected systems but also reflect normal changes in the system such as changes in system environmental or operating conditions.

Motivated by the need to correctly identify the changes in signal features which are produced by abnormality in inspected systems, a novel health probability based structural health monitoring method is proposed in this chapter. In this method, the relationship between a signal feature and the normal changes in the system environmental and operating parameters, known as baseline model, is first established. Then, a tolerance range of the signal feature's deviation from what is determined by the baseline model is evaluated via a data based training process. Furthermore, the health probability, which is defined as the proportion of the cases where the system's working status as represented by the signal feature is within the tolerance range, is used to decide whether the system is in a normal working condition or not so as to implement SHM. Both simulation studies and experimental data analyses have been conducted to demonstrate the performance of the proposed new technique.

## 3.1 Methodology

### 3.1.1 B-spline baseline model

The purpose of building a baseline model is to map the system environmental and operating parameters to a signal feature extracted from the sensor measurements so that the effects of these environmental and operating conditions can be taken into consideration when conducting structural health monitoring. Many methods can be employed to build the baseline model, such as polynomial regression, least squares method and maximum likelihood estimation. In this chapter, a B-spline approximation model which has been extensively applied in modelling due to its excellent capability in smoothly data fitting is used to determine the baseline model.

Given  $n+1$  control coefficients  $\alpha_0, \alpha_1, \dots, \alpha_n$ , a knot vector  $\mathbf{x} = \{x_0, x_1, \dots, x_m\}$  and degree  $p$ , univariate B-spline approximation model between variables  $x$  and  $\tilde{z}$  can be determined as [198]

$$\tilde{z} = f(x) = \sum_{i=0}^n \alpha_i N_{i,p}(x) \quad (3.1)$$

where  $N_{i,p}(x)$  is  $i^{\text{th}}$  B-spline basis functions with degree  $p$  and is usually defined by Cox-de Boor recursion formula as

$$N_{i,0}(x) = \begin{cases} 1 & \text{if } x_i \leq x \leq x_{i+1} \\ 0 & \text{otherwise} \end{cases} \quad (3.2)$$

$$N_{i,p}(x) = \frac{x - x_i}{x_{i+p} - x_i} N_{i,p-1}(x) + \frac{x_{i+p+1} - x}{x_{i+p+1} - x_{i+1}} N_{i+1,p-1}(x)$$

Here,  $N_{0,p}(x) = 1$ ,  $n, m$  and  $p$  must satisfy the relationship  $m = n + p$ . Namely, if a B-spline approximation model with degree  $p$  and  $n+1$  control coefficients is expected,  $m = n + p$  knots are needed.

If there are  $N$  variables, say,  $x^{(1)}, x^{(2)}, \dots, x^{(N)}$ , multivariate B-spline approximation model is defined as [198]

$$\tilde{z} = f(x^{(1)}, \dots, x^{(N)}) = \sum_{i_1=0}^{n_1} \dots \sum_{i_N=0}^{n_N} \alpha_{i_1, i_2, \dots, i_N} N_{i_1, p}(x^{(1)}) N_{i_2, p}(x^{(2)}) \dots N_{i_N, p}(x^{(N)}) \quad (3.3)$$

Similarly,  $N_{i_1, p}(x^{(1)}), N_{i_2, p}(x^{(2)}), \dots, N_{i_N, p}(x^{(N)})$  are the B-spline basis functions of degree  $p$  with respect to variables  $x^{(1)}, x^{(2)}, \dots, x^{(N)}$ , respectively, and can be determined according to Eq.(3.2) with  $N_{0, p}(x^{(i)})=1$ ;  $\alpha_{i_1, i_2, \dots, i_N}$  are the corresponding control coefficients.

The major problem in using the B-spline approximation model as shown in Eq. (3.1) or Eq. (3.3) is the significant increase in the number of B-spline basis functions and the terms associated with the multiplication of these functions when there are a large number of knots and variables. These lead to complicated and tedious computations when fitting a B-spline approximation model. In addition, the contribution of some B-spline basis functions and their multiplications is often insignificant and can be ignored. Therefore, recursive forward-regression orthogonal estimator proposed by Billings [199] will be employed to select the important terms and to avoid under-fitting or over-fitting a B-spline approximation model. The detail of this estimator is introduced in Appendix A.

In order to ensure the obtained baseline model is a good representation of the underlying process, Mean Square Error (MSE), that is the average of the squares of the errors between the features extracted from sensor measurements  $z$  and predicted features by baseline model  $\tilde{z}$ , is defined as Eq. (3.4) to assess model performance:

$$MSE = \frac{1}{\bar{N}} \sum_{i=1}^{\bar{N}} (z - \tilde{z})^2 \quad (3.4)$$

where  $\bar{N}$  is the number of  $z$ . If the MSE level for the training dataset is similar to that

for remaining datasets, the obtained baseline model is capable of representing the underlying process and can be used for structural health monitoring purpose.

### **3.1.2 Modeling error tolerance range and bins for environmental and operating parameters**

Denote the error between the feature extracted from a sensor measurement and the feature predicted by a baseline model as

$$\varepsilon = z - \tilde{z} \quad (3.5)$$

where  $z$  is the feature extracted from a sensor measurement and  $\tilde{z}$  is the feature predicted by a baseline model in Eqs. (3.1) or (3.3),  $\varepsilon$  is the error between  $z$  and  $\tilde{z}$ . This error is generally determined by many factors, including modelling error, noise, and the effects of less significant environmental and operating parameter changes which can't be covered by the baseline model. In principle, all of these factors can be neglected in the system normal working conditions if the baseline model is good enough in representing the changes in sensor signal features in these conditions. However, a possible damage in the system can make a significant increase in the error, and this phenomenon can be exploited for the system health monitoring purpose.

Under the assumption that error  $\varepsilon$  follows a normal distribution when the system is working normally, that is,  $\varepsilon \sim N(\mu, \sigma^2)$ , where  $\mu$  is the mean and  $\sigma$  is the standard deviation,  $[\mu - 3\sigma, \mu + 3\sigma]$  can cover 99.73% of the error values in the system normal working conditions. Therefore, the tolerance range of the error between the feature of a sensor measurement and the feature predicted by a baseline model can be set as  $[\mu - 3\sigma, \mu + 3\sigma]$ .

However, the error between the feature of a sensor measurement from health structures and the feature predicted by a baseline model is likely to vary with the environmental and operating conditions, which means that the error is large in some

conditions but small in other conditions. In addition, in practice, sensor signal features of damaged systems change slightly in some environmental and operating conditions but change significantly in other environmental and operating conditions. Motivated by these phenomena, the whole operating conditions are divided into several cases/bins according to the value of operating parameters, so that the errors which have the similar level can be calculated and their tolerance range can be determined in each bin. The bins can be defined as:

$$B_{n_1, n_2, \dots, n_N} = \{x^{(1)}, x^{(2)}, \dots, x^{(N)}\}, n_i = 1, 2, \dots, M_i, i = 1, 2, \dots, N \quad (3.6)$$

$$x^{(i)} \in [x_{\min}^{(i)} + S_1^{(i)} + S_2^{(i)} + \dots + S_{n_i-1}^{(i)}, x_{\min}^{(i)} + S_1^{(i)} + S_2^{(i)} + \dots + S_{n_i}^{(i)}]$$

where  $M_i$  is the number of the segments for  $i^{\text{th}}$  variable  $x^{(i)}$ ;  $x_{\min}^{(i)}$  is the minimum value of variable  $x^{(i)}$ ,  $S_{n_i}^{(i)}$  is the length of  $n_i^{\text{th}}$  segment for variable  $x^{(i)}$ .

When the length is fixed for the same operating parameter, the bins can be written as:

$$B_{n_1, n_2, \dots, n_N} = \{x^{(1)}, x^{(2)}, \dots, x^{(N)}\}, n_i = 1, 2, \dots, M_i, i = 1, 2, \dots, N \quad (3.7)$$

$$x^{(i)} \in \left[ x_{\min}^{(i)} + \frac{(n_i - 1)(x_{\max}^{(i)} - x_{\min}^{(i)})}{M_i}, x_{\min}^{(i)} + \frac{n_i(x_{\max}^{(i)} - x_{\min}^{(i)})}{M_i} \right]$$

In order to describe bins more precisely, the bins are numbered by single subscript. Fig. 3.1 demonstrates one simple way to number the bins in one dimension case and two dimensions case respectively.



(a) One dimension case (b) Two dimensions case

Fig. 3.1 Definition of bins

### 3.1.3 Health probability

According to the definition of tolerance range above, if a monitored structural system is operating in a healthy status, most of errors  $\varepsilon$  should fall into the tolerance range associated with a corresponding bin. If there is a change or damage, only a small number of values of  $\varepsilon$  should be within the corresponding tolerance range. This phenomenon can be represented quantitatively by the concept of health probability defined as follows:

$$P = N_{in}/N_{all} \quad (3.8)$$

where  $N_{in}$  is the number of the values of  $\varepsilon$  which are within the tolerance range, and  $N_{all}$  is the total number of  $\varepsilon$  evaluated in a particular bin.

In order to illustrate how health probability  $P$  is evaluated and how bin is related to this concept, a simple example is provided in the following.

**Example 3.1:** Calculate health probability  $P$  in different bins based on data shown in Fig. 3.2

In Fig.3.2, horizontal axis represents the environmental parameter  $x$ , vertical axis reveals signal features either extracted from measurements or predicted from baseline model; the line represents baseline model, blue points represent signal features of healthy structure and red points represent signal features of monitored structure. The whole value of  $x$  are divided into three bins which cover the range of  $x \in [0,3)$ ,  $x \in [3,6)$ ,  $x \in [6,9]$ , and denoted by bin 1, bin 2 and bin 3 respectively. There are 100 signal features of healthy structure in range of  $x \in [0,3)$ , namely, bin 1, and mean  $\mu_1$  and standard deviation  $\sigma_1$  of the errors between these 100 signal features and corresponding features predicted by baseline model are used to calculate error tolerance range for bin 1, that is  $[\mu_1 - 3\sigma_1, \mu_1 + 3\sigma_1]$ . There are 20 signal features of monitored structure in range of  $x \in [0,3)$ , and errors between these 20 signal

features and corresponding features predicted by baseline model are also calculated and 14 errors are within the error tolerance range  $[\mu_1 - 3\sigma_1, \mu_1 + 3\sigma_1]$ . Therefore, the health probability  $P$  for bin 1 is  $14/20 = 0.70$ . Similarly, health probability  $P$  for bin 2 and bin 3 can be calculated. The results are shown in Table 3.1.

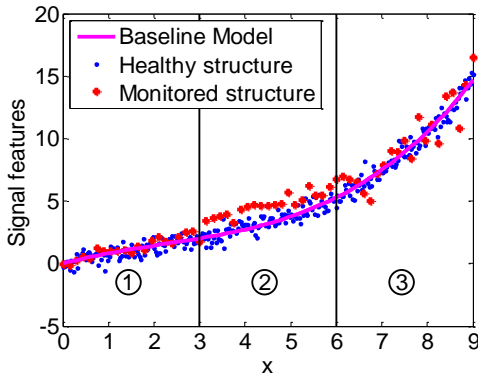


Table 3.1 Calculation of health probability

Bin index	$N_{in}$	$N_{all}$	$p$
Bin 1	14	20	0.70
Bin 2	7	20	0.35
Bin 3	19	20	0.95

Fig. 3.2 Signal features

## 3.2 Simulation case study

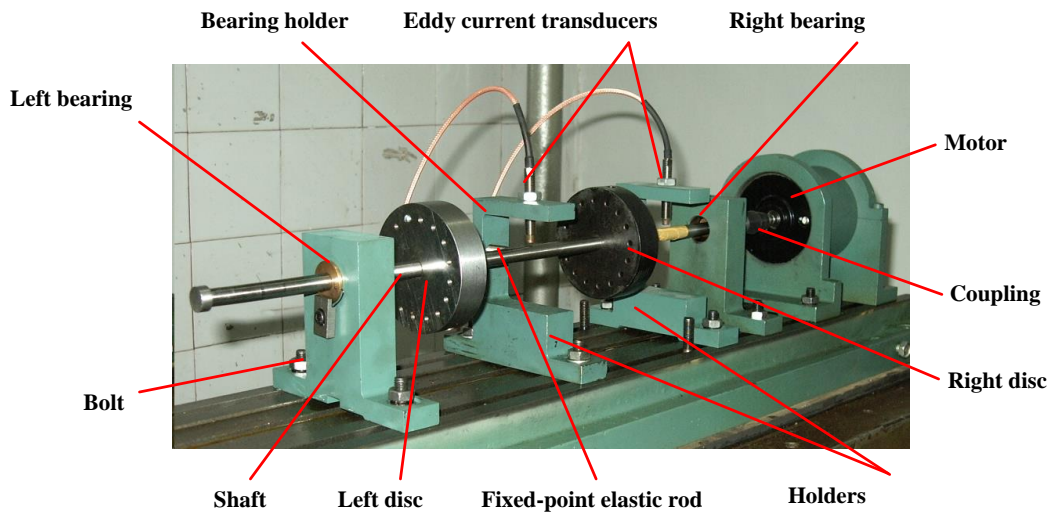
### 3.2.1 Simulation model

In this section, the health probability based structural health monitoring technique is applied on a dual-disc rotor system suffering rub-impact damage by numerical simulation study. The test rig of a dual-disc rotor system is shown in Fig. 3.3 (a); the simplified finite element (FE) model of the test rig is shown in Fig. 3.3 (b). If the vibration caused by unbalance mass is very serious so that elastic rod in the test rig contact the shaft, the additional nonlinear force will be produced. This can simulate the rub-impact damage between rotor and stator in the rotor system and is represented by nonlinear spring and damper in FE model.

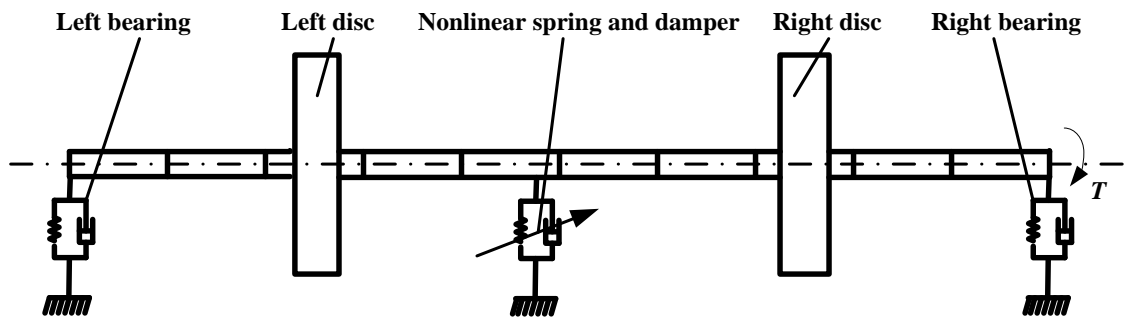
The dynamic equation of the rotor system suffering rub-impact damage is as follows.

$$M\ddot{u} + (C + \omega G)\dot{u} + Ku = F + F_{rub} \quad (3.9)$$

where  $\mathbf{u}$  is the displacement vector;  $\mathbf{M}, \mathbf{C}, \mathbf{G}, \mathbf{K}$  are mass matrix, damping matrix, gyroscopic moment matrix and stiffness matrix of the rotor system respectively;  $\mathbf{F}$  and  $\mathbf{F}_{rub}$  represent the input force vector and the effects of rub-impact damage, respectively. Detailed information about the model and rub-impact mechanism can be found in Ref. [187]. Equation (3.9) can be solved by the Newmark method to find the vibration responses of the rotor system.



(a) Test rig



(b) Simplified FE model

Fig. 3.3 A dual-disc rotor system and FE model

### 3.2.2 Simulation data analysis

The vibration of right disc in horizontal direction is measured when the rotating speed changes from 60 Hz to 100Hz. Many signal signatures of sensor measurements can be



considered, including kurtosis, crest factor, standard deviation, median, total energy, root mean square (RMS) in the time domain and the frequency, amplitude, and phase etc in the frequency domain. RMS is a signal signature that has been widely employed in many structural health monitoring methods [36, 200, 201] and therefore, is used as damage sensitive feature in this chapter. When there is no damage in the rotor system, namely, it is operating under healthy status, the vibration level of right disc represented by RMS feature is shown in Fig. 3.4 by ‘•’. When there is a rub-impact damage in the rotor system, the vibration level of right disc represented by RMS feature is displayed in Fig.3.4 by ‘\*’.

The measured vibration data are divided into 8 groups; the data in the first group are used to fit the baseline model, the remaining ones are used to validate the model by assessing MSE error. In this simulation case study, there is only one variable, namely, rotating speed, so baseline model is fitted by univariate B-spline approximation model in Eq. (3.1). In this model, the order of B-spline basis functions is set as  $p = 3$ , and it is assumed that there are 14 knots which are 60, 65.6, 68.4, 71.2, 74, 76.8, 79.6, 82.4, 85.2, 88, 90.8, 93.6, 96.4, 100, respectively. In order to enable the model be capable of representing the data at two ends, the first and last knots are extended three times, thus, the knot series become 60, 60, 60, 60, 65.6, 68.4, 71.2, 74, 76.8, 79.6, 82.4, 85.2, 88, 90.8, 93.6, 96.4, 100, 100, 100 and 100, respectively. Then, B-spline basis functions  $N_{i,p}(x)$  can be determined according to Eq. (3.2), and some of them are displayed in Fig. 3.5. By using recursive forward-regression orthogonal estimator which is introduced in Ref. [199] and Appendix A, when ERR (Error Reduction Ratio) is set as 1, the selected terms and corresponding coefficients are listed in Table 3.2. Consequently, baseline model is determined by B-spline approximation model represented by Eq.(3.1) with selected terms and corresponding coefficients in Table 3.2.

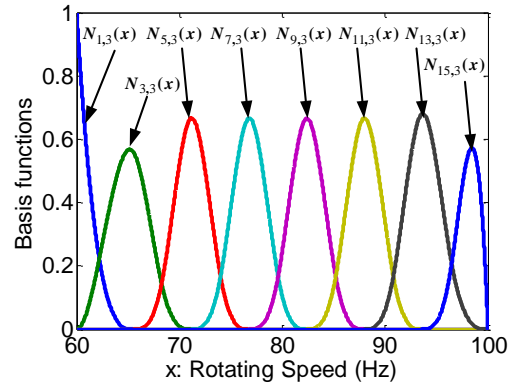
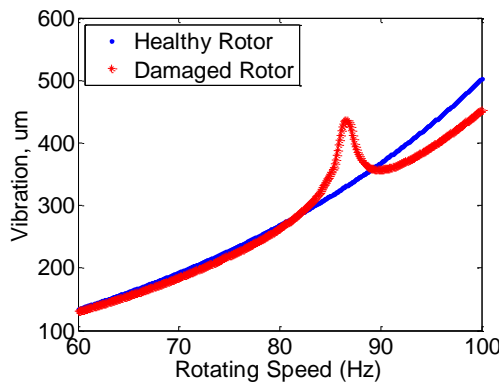


Fig. 3.4 Vibration levels of the rotor system      Fig. 3.5 Basis functions for B-spline approximation model

Table 3.2 Selected terms and corresponding coefficients for B-spline approximation model

Terms	Coefficient	Terms	Coefficient	Terms	Coefficient	Terms	Coefficient
$N_{14,3}(x)$	452.3393	$N_{16,3}(x)$	502.4466	$N_{15,3}(x)$	483.7022	$N_{7,3}(x)$	241.7277
$N_{12,3}(x)$	377.2505	$N_{6,3}(x)$	220.3154	$N_{13,3}(x)$	411.5025	$N_{5,3}(x)$	200.4327
$N_{10,3}(x)$	316.6062	$N_{4,3}(x)$	181.9595	$N_{11,3}(x)$	345.7081	$N_{1,3}(x)$	134.1698
$N_{8,3}(x)$	264.8062	$N_{2,3}(x)$	143.71	$N_{9,3}(x)$	289.7054	$N_{3,3}(x)$	159.0669

The suitability of the B-spline approximation model represented by Eq.(3.1) with selected terms and corresponding coefficients in Table 3.2 is validated by assessing MSE error with remaining 7 data groups which are not involved in modeling, the results are shown by bar charts in Fig. 3.6. It can be obviously observed that the values of MSE errors for the data groups that have not been used for the modeling are only slightly different from the MSE for the modeling data. So the model is considered to be valid to be used for condition monitoring.

Bins are constructed by using Eq.(3.7) and the method in Fig. 3.1 (a) according to the

minimum and maximum of measured rotating speed when  $M_1 = 4$  and  $N = 1$ , and are numbered as bin 1, bin 2, bin 3 and bin 4, respectively. In each bin, not only the errors of the healthy rotor systems and their tolerance range are calculated, but the errors of the damaged rotor systems are also calculated, the result is displayed in Fig. 3.7 which reveals that the tolerance ranges capture very few error data points of damaged rotor system. In order to describe this quantitatively, health probability for each bin is calculated according to Eq. (3.8) and listed in Table 3.3 which indicates that the health probabilities for all bins are 0. Therefore, it can be concluded that there is damage in this rotor system, which is consistent with the real situation of the simulated system.

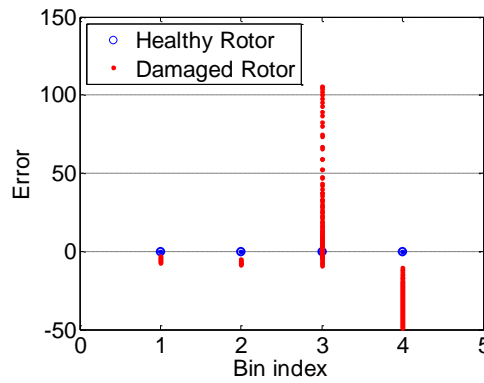
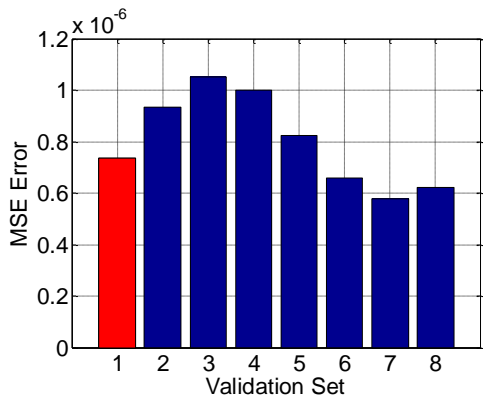


Fig. 3.6 Validation of baseline model

Fig. 3.7 Errors and tolerance ranges

Table 3.3 Health probability for rotor system suffering rub-impact damage

Bin index	Bin 1	Bin 2	Bin 3	Bin 4
$P$	0	0	0	0

### 3.3 Experimental case study

In order to demonstrate the potential of the proposed structural health monitoring method in practical applications, it was applied to analyse the experimental data from an operating wind turbine in this section.

### 3.3.1 Experimental measurements

The gearbox, the function of which is to transform input power from hub to shaft between the gearbox and the generator, and the generator, which will transmit mechanical power initially from wind to electrical power, are two of the most critical components for wind turbines but likely to suffering from damage particularly after serving long time. For example, in the gearbox, the surface of gear teeth can be wearred because of inadequate lubration film, debris, abrasive, or initial cracks, then the kissing surfaces will not be able to contact smoothly which eventually induces abnormal vibration. The vibration levels change with the rotating speed of gear and seriousness of wear or damage in gearbox componnets. Therefore, the vibration levels need to be monitored when conducting health monitoring on gearbox.

However, vibration signals only cover the low frequency range (under 20k Hz) and can be detected if the defects/damage is serious enough. Accoustic emission (AE) signals which covers the frequency range from 100kHz to 1MHz in most cases, can be a supplementary. AE is defined as transient accoustic (elastic) wave which is produced from a rapid release of local strain energy due to a damage or deformation within or on the surface of a structure. Since AE is at microscopic level, AE is sensitive to early stage defects/damage and can be used to detect the damage at an early stage and monitor its develop. Therefore, in this experiments, two accelerometers and two accoustic emission(AE) sensors are installed on the top of gearbox (labelled as AE sensor 1 and vibration accelerometer 1) and at the back of generator near the high speed shaft (labelled as AE sensor 2 and vibration accelerometer 2) respectively, so that the possible useful information in both low and high frequency range can be exploited from these sensor measurements. During data collection, data acquisition from each sensor in one second duration are recorded, at the same time, the average values of the wind speeds and power outputs are also recorded over a ten minutes period, and are considered as the representation of the operating conditions, as

shown in Fig.3.8. The types and locations of the sensors are listed in Table 3.4.

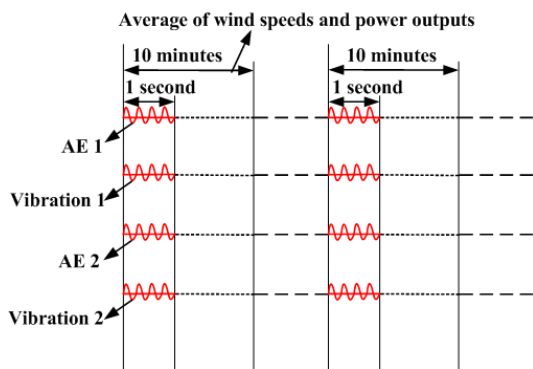


Fig. 3.8 Data acquisition schedule

Table 3.4 Location of each sensor

Type of sensor	Location
Acoustic Emission 1	On the top of gearbox
Accelerometer 1	On the top of gearbox
Acoustic Emission 2	Back of generator
Accelerometer 2	Back of generator

Because it is impossible to inject damage into healthy wind turbine systems without great expense, the measurements were conducted on an operating wind turbine without artificial damage. Data were recorded over three periods: November 2010, December 2010 and February 2011. For data analysis in this section, one part of the data in November 2010 is used to build the baseline model which can represent the relationship between the signal feature of sensor measurements and the turbine operating parameters including wind speed and power output, the remaining data in November 2010 are used to validate this model, and the tolerance range of modeling error  $\varepsilon$  between the signal feature extracted directly from sensor measurements and feature predicted from the baseline model is determined according to the datasets in November 2010. Datasets in December 2010 and February 2011 are used to demonstrate the capability of the proposed method in health monitoring of wind turbine.

### 3.3.2 Experimental data analyses

In experimental data analyses, the measurement data from each sensor in November 2010 are divided into 8 groups, the data in the first group are used to build the baseline model, and the remaining ones are used to validate the baseline model by

assessing MSE error.

When wind speed is represented by  $x$ , power output is represented by  $y$ , and the order of basis functions is set as 3, the bivariate B-spline approximation model for the relationship between the predicted signal feature  $\tilde{z}$  and  $x, y$  can be derived from Eq. (3.3) and expressed by

$$\tilde{z} = f(x, y) = \sum_{i_1=0}^{n_1} \dots \sum_{i_2=0}^{n_2} \alpha_{i_1, i_2} N_{i_1, 3}(x) N_{i_2, 3}(y) \quad (3.10)$$

In this experimental case study, it is assumed that there are 21 knots for variable  $x$  and 20 knots for variable  $y$ , then B-spline basis functions  $N_{i_1, 3}(x)$  and  $N_{i_2, 3}(y)$  can be determined according to Eq.(3.2), and some of them are shown in Fig. 3.9. By using the forward-regression orthogonal estimator, which is introduced in Ref. [199] and Appendix A, when ERR is set as 0.95, 0.935, 0.985 and 0.955 for AE 1, AE 2, vibration 1 and vibration 2, respectively, the selected terms and corresponding coefficients for each sensor measurement are listed in Table 3.5. Consequently, the baseline model is determined by bivariate B-spline approximation model represented by Eq. (3.10) with selected terms and corresponding coefficients in Table 3.5.

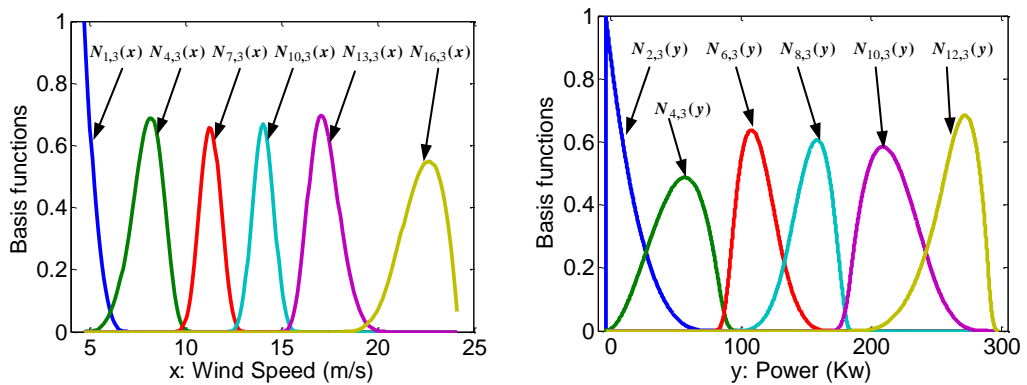
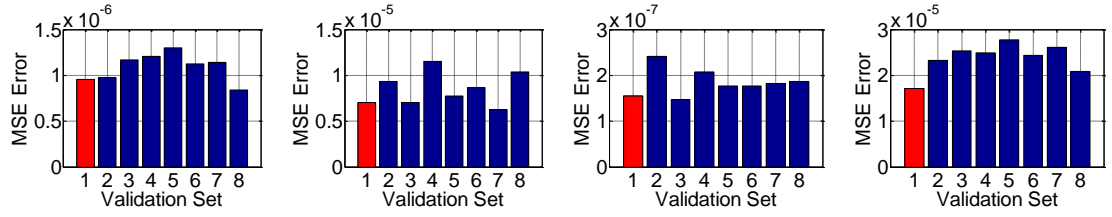


Fig. 3.9 Basis functions for B-spline approximation model

Table 3.5 Selected terms and corresponding coefficients for B-spline approximation model

AE 1		Vibration 1		AE 2		Vibration 2	
Terms	$\alpha_{i_1,i_2}$	Terms	$\alpha_{i_1,i_2}$	terms	$\alpha_{i_1,i_2}$	terms	$\alpha_{i_1,i_2}$
$\alpha_{0,0}$	0.007682	$\alpha_{0,0}$	0.033153	$\alpha_{0,0}$	0.002775	$\alpha_{0,0}$	0.027974
$N_{2,3}(y)$	-0.00488	$N_{2,3}(y)$	-0.0265	$N_{2,3}(y)$	-0.00219	$N_{2,3}(y)$	-0.02678
$N_{13,3}(y)$	0.005279	$N_{1,3}(y)$	-0.03273	$N_{14,3}(y)$	0.001704	$N_{12,3}(y)$	0.017192
$N_{11,3}(y)$	0.005514	$N_{14,3}(x)$	0.01063	$N_{12,3}(x)$	0.001172	$N_{14,3}(x)$	0.023969
$N_{1,3}(y)$	-0.00688	$N_{2,3}(x)$	-0.0149	$N_{1,3}(y)$	-0.00238	$N_{10,3}(y)$	0.022916
$N_{14,3}(x)$	0.007622	$N_{3,3}(x)$	-0.03447	$N_{4,3}(y)$	-0.00131	$N_{1,3}(y)$	-0.02771
$N_{14,3}(x)N_{13,3}(y)$	-0.0101	$N_{3,3}(x)N_{2,3}(y)$	0.041281			$N_{3,3}(x)$	-0.04292
$N_{4,3}(y)$	-0.00414					$N_{3,3}(x)N_{2,3}(y)$	0.049619
$N_{3,3}(x)$	-0.00489						

The suitability of the B-spline approximation models represented by Eq.(3.10) with selected terms and corresponding coefficients given in Table 3.5 is validated by assessing MSE with remaining 7 data groups which are not involved in the modeling process, the results are shown by bar charts in Fig. 3.10. It can be observed that the values of MSE errors for the data groups not used in the modeling process are all only slightly different from those for modeling data. So the modeling results are validated and can therefore be used for condition monitoring.



(a) Acoustic emission 1    (b) Vibration 1    (c) Acoustic emission 2    (d) Vibration 2

Fig. 3.10 Validation of each model

When there are two variables, and the length of each bin is fixed for the same operating parameter, the bins are determined according to Eq. (3.11) as follows:

$$B_{n_1, n_2} = \{x, y\}$$

$$x \in \left[ x_{\min} + \frac{(n_1 - 1)(x_{\max} - x_{\min})}{M_1}, x_{\min} + \frac{n_1(x_{\max} - x_{\min})}{M_1} \right] \quad (3.11)$$

$$y \in \left[ y_{\min} + \frac{(n_2 - 1)(y_{\max} - y_{\min})}{M_2}, y_{\min} + \frac{n_2(y_{\max} - y_{\min})}{M_2} \right]$$

where  $x_{\min}$ ,  $x_{\max}$ ,  $y_{\min}$  and  $y_{\max}$  are the minimum and maximum of measured wind speed and power outputs. When it is assumed that  $M_1 = M_2 = 3$ , bins are constructed according to Eq. (3.11), and the results are shown in Fig. 3.11. After neglecting bins where very few or no measured wind speeds and power outputs fall inside, five bins are retained and numbered as shown in Fig. 3.11.

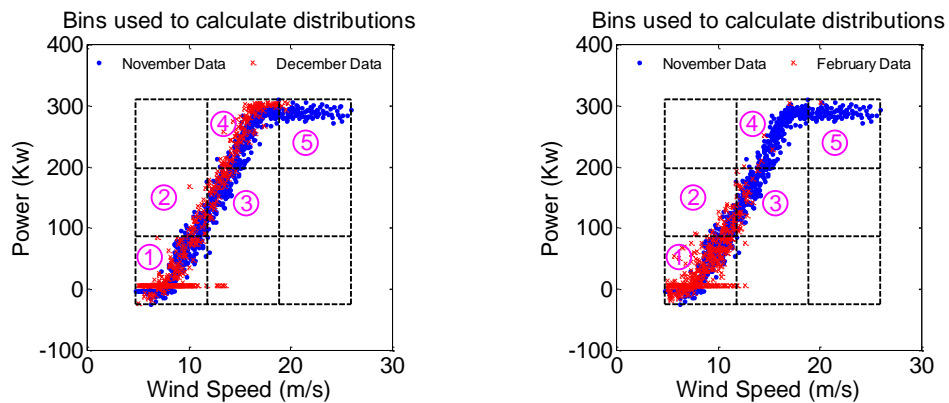


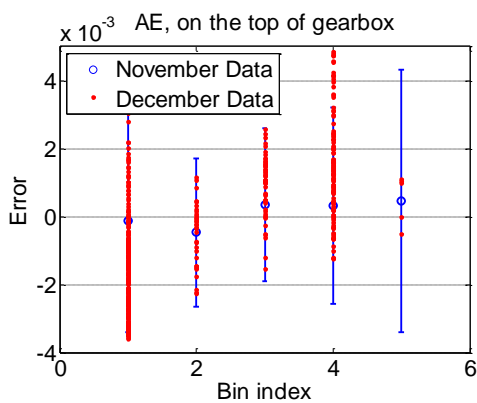
Fig. 3.11 Bins used to calculate error distribution

In each bin, the errors between signal RMS features extracted directly from sensor

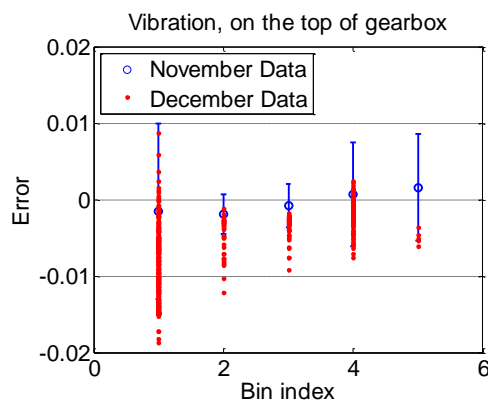


measurements in November 2010 and the RMS features predicted using the baseline model and its tolerance range are calculated. The results are shown in Figs. 3.12 and 3.13. In addition, the errors between the predicted RMS and the RMS of signals measured in December 2010 and February 2011, respectively, are also evaluated and shown in Figs. 3.12 and 3.13. It can be observed from Fig. 3.12 that most data points for AE sensor 1 and accelerometer 2 are inside the corresponding tolerance range, while a significant number of data points for accelerometer 1 and AE sensor 2 are outside the corresponding tolerance range, and a similar phenomenon can be observed from Fig 3.13.

In order to represent this phenomenon quantitatively, health probability for each bin is calculated according to Eq. (3.8) and shown in Tables 3.6 and 3.7. In the tables, all the probabilities highlighted are smaller than 0.8, which indicates that a possible change has taken place. This indication is consistent with the practical situation of the wind turbine as some parts in the wind turbine were replaced after November 2010. In addition to this correct inference that has been made from the baseline model based analysis, the analysis results also show that AE signals are more sensitive to the condition variation in generator while vibration is more sensitive to the condition change in gearbox. This conclusion is clearly very helpful for the use of appropriate sensors for the condition monitoring of different wind turbine components.



(a) Acoustic emission 1



(b) Vibration 1

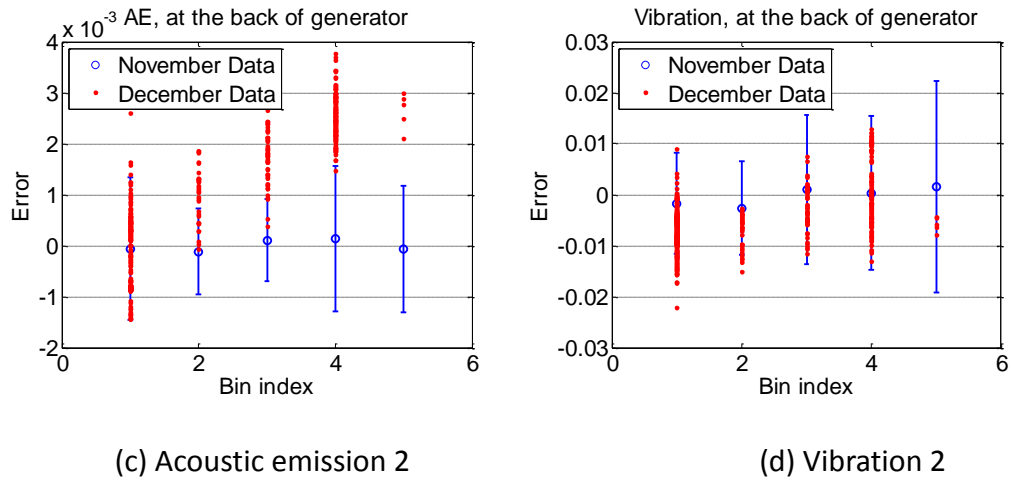


Fig. 3.12 The tolerance range of errors in each bin and errors between signal features of measurements in December 2010 and predicted features

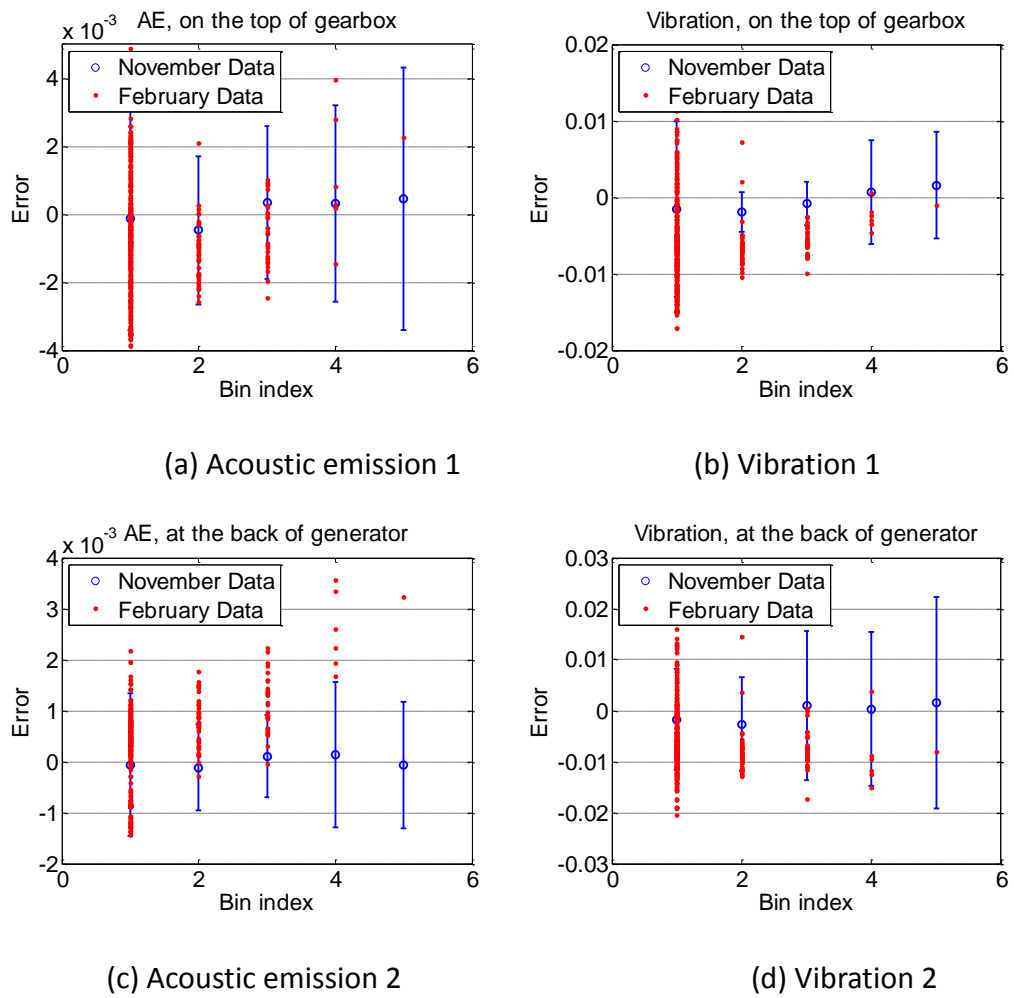


Fig. 3.13 The tolerance range of errors in each bin and errors between signal features of measurements on February 2011 and predicted features

Table 3.6 Health probability for measurements in December 2010

Bin index	On the top of gearbox		At the back of generator	
	AE 1	Vibration 1	AE 2	Vibration 2
Bin 1	0.89557	0.734177	0.987342	0.892405
Bin 2	1	0.515152	0.333333	0.848485
Bin 3	1	0.72549	0.039216	1
Bin 4	0.808	0.976	0.008	1
Bin 5	1	0.6	0	1

Table 3.7 Health probability for measurements in February 2011

Bin index	On the top of gearbox		At the back of generator	
	AE 1	Vibration 1	AE 2	Vibration 2
Bin 1	0.897143	0.828571	0.957143	0.86
Bin 2	0.977273	0.022727	0.454545	0.886364
Bin 3	0.935484	0.129032	0.451613	0.967742
Bin 4	0.833333	1	0	0.833333
Bin 5	1	1	0	1

### 3.4 Conclusions

A novel health probability based structural health monitoring method has been proposed in this chapter and its effectiveness has been investigated by both simulation studies and field data analysis.

The effects of operating and environmental parameters on structural health monitoring can be systematically taken into account by a baseline model which represents the relationship between the RMS feature of sensor data and the changes in the system environmental and operating parameters. From the baseline model and corresponding data, the tolerance range of baseline modelling error can be

determined; the health probability defined as the proportion of the cases where the system's working status as represented by the signal RMS feature is within the tolerance range can be used to determine whether an inspected system is in an expected working condition or not, so as to implement the system condition and health monitoring.

The simulation study on the rotor system indicates that the technique can correctly find out the system's damage condition. The correct analysis of the field data from an operating wind turbine has demonstrated the potential engineering significance of the new baseline model based condition and health monitoring approach.

## Chapter 4

# **Transmissibility analysis method for detection and localization of damage via nonlinear features in MDOF structural systems**

In Chapter 3, the effect of environmental and operational conditions has been taken into consideration when conducting SHM by building a model between the features of the measured signals and the environmental and operational conditions. In this chapter, an alternative damage sensitive feature which is insensitive to the change of environmental and operational conditions is exploited. This damage sensitive feature is analyzed based on the transmissibility analysis and can be used to find the location of the damage with nonlinear features in Multi-Degree-Of-Freedom (MDOF) structural systems.

Traditional transmissibility of two system responses depends on the location of the system input. When a system is excited by the same input but at different locations, the traditional transmissibility analysis results will be different. Therefore, if the traditional transmissibility is employed in damage detection or localization, the input location should be taken into consideration carefully; otherwise the variation of input locations may mask the damage information. In this chapter, a new transmissibility analysis method is proposed for the detection and location of damage via nonlinear features in MDOF structural systems. The method is derived based on the transmissibility of Nonlinear Output Frequency Response Functions (NOFRFs), a concept recently proposed to extend the traditional transmissibility concept to nonlinear cases. The implementation of the method is only based on measured system output responses and by evaluating and analyzing the transmissibility of these system

responses at super-harmonics. The new method can overcome the problems with traditional transmissibility analysis based methods, which are normally loading input location dependent and can only be applied in locating damage with linear features. In addition, the method can also overcome the problems with available NOFRF transmissibility based techniques which either assume that there is only one damaged component with nonlinear features in the system and/or require the loading on inspected structural systems is measurable. Both numerical simulation studies and experimental data analysis have been conducted to verify the effectiveness and demonstrate the potential practical applications of the new method.

#### 4.1 MDOF nonlinear structural systems and associated engineering backgrounds

In engineering practice the behaviors of many mechanical and civil structural systems, such as, rotary machineries[202-204], multi-storey buildings [28, 205, 206] and multi-span bridges [207, 208], should be described by more than one set of coordinates and can, therefore, be modeled by MDOF systems. A simplified representation of these mechanical and civil structural systems is shown in Fig. 4.1 where the motion of all masses is one-dimensional and the input force  $f$  is applied on one of the masses.

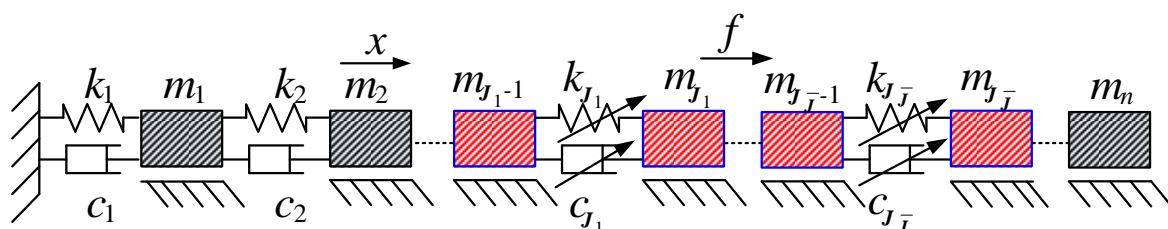


Fig. 4.1 An MDOF nonlinear structural system

If all the springs and dampers in the system in Fig. 4.1 are linear, then the system is a linear MDOF system with governing equation

$$\mathbf{M}\ddot{\mathbf{x}}(t) + \mathbf{C}\dot{\mathbf{x}}(t) + \mathbf{K}\mathbf{x}(t) = \mathbf{F}(t) \quad (4.1)$$

where

$$\mathbf{M} = \begin{bmatrix} m_1 & 0 & \cdots & 0 \\ 0 & m_2 & \cdots & 0 \\ \vdots & \vdots & \ddots & 0 \\ 0 & 0 & 0 & m_n \end{bmatrix}, \quad \mathbf{C} = \begin{bmatrix} c_1 + c_2 & -c_2 & 0 & \cdots & 0 \\ -c_2 & c_2 + c_3 & -c_3 & \ddots & \vdots \\ 0 & \ddots & \ddots & \ddots & \vdots \\ \vdots & \ddots & -c_{n-1} & c_{n-1} + c_n & -c_n \\ 0 & 0 & 0 & -c_n & c_n \end{bmatrix},$$

$$\mathbf{K} = \begin{bmatrix} k_1 + k_2 & -k_2 & 0 & \cdots & 0 \\ -k_2 & k_2 + k_3 & -k_3 & \ddots & \vdots \\ 0 & \ddots & \ddots & \ddots & \vdots \\ \vdots & \ddots & -k_{n-1} & k_{n-1} + k_n & -k_n \\ 0 & 0 & 0 & -k_n & k_n \end{bmatrix}, \quad \mathbf{x}(t) = [x_1(t), \dots, x_n(t)]^T$$

are the system mass matrix, damping matrix, stiffness matrix and displacement vector, respectively.  $\mathbf{F}(t)$  is the force vector. When, as shown in Fig 4.1, only one input force is applied on the system, the MDOF system is a Single-Input Multi-Output (SIMO) system. While if many input forces are applied on the system at the same time, the system is a Multi-Input Multi-Output (MIMO) system. In this chapter, the case of one input force applied on the  $S^{\text{th}}$  mass will be considered so that

$$\mathbf{F}(t) = \left[ \overbrace{0 \ \dots \ 0}^{S-1} \ f(t) \ \overbrace{0 \ \dots \ 0}^{n-S} \right]^T.$$

The MDOF structural systems described by Eq. (4.1) are also known as periodic structures which consist fundamentally of several identical structural components that are joined together side by side and/or to end to end form the whole structure [209]. A wide class of engineering structures including multi-blade turbines and rotary compressors, multi-storey buildings, multi-span bridges and elevated guideways for high speed transportation vehicles, etc. can be or have been treated as periodic structures. For example, the model can be used to describe the transversal vibration on each floor of multi-storey buildings as shown in Fig. 4.2 where floor  $i$  is modeled

by inertial  $m_i$ , stiffness  $k_i$  and power dissipation  $c_i$ . The bending and shear of a beam can be approximated by transverse and rotational springs respectively. So a beam can also be represented by some discrete blocks which are connected side by side by transverse springs and rotational springs as shown in Fig. 4.3. Similarly, a rotor-bearing system can be modelled by lumped masses connected by horizontal and vertical springs as shown in Fig. 4.4. When the motions of a structural system in different directions are considered as in the examples shown in Figs 4.3 and 4.4,  $m_i, k_i$  and  $c_i$  in Eq. (4.1) should be replaced by matrixes. However, if the motion in one direction is significantly more considerable than in other directions, the motion in only one particular direction needs to be studied. In such cases, the system can be well represented by Eq. (4.1).

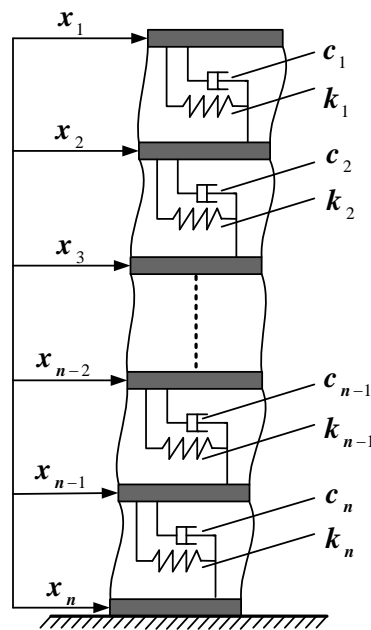


Fig. 4.2 Modelling of a multi-storey building

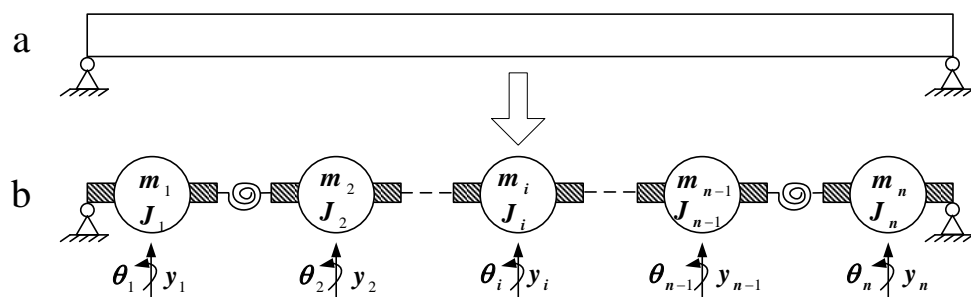


Fig.4.3 Modelling of a simple supported beam



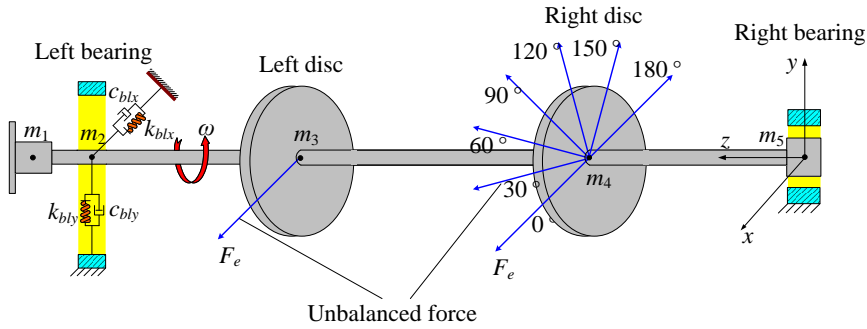


Fig. 4.4 Modelling of a rotor-bearing system

In engineering practice, all structural systems are prone to suffering certain damage due to long service time, improper use or hostile working environments. And certain types of damage often manifest themselves as the introduction of nonlinearity into an otherwise linear system, such as breathing cracks, pedestal looseness and rub-impacts as reviewed in Section 2.7. In the MDOF system shown in Fig. 4.1, damaged components can often be represented by nonlinear springs/dampers denoted by the spring and damper symbols with an arrow.

When there are  $\bar{J} (\bar{J} \geq 1)$  nonlinear springs/dampers in the system which are located between the  $J_i - 1$  and  $J_i$ th masses, namely  $J_i$ th springs/dampers, ( $i = 1, 2, \dots, \bar{J}$ ) (it is assumed that  $J_1 < J_2 < \dots < J_{\bar{J}}$ ), and the first spring and damper, which are connected to the fixed ground, are not nonlinear, that is,  $J_1 > 1$ , the restoring forces of these nonlinear springs/dampers are the nonlinear functions of the deformation/the deformation derivative. Under the assumption that these functions are continuous, they can be approximated by a polynomial with its nonlinear part represented by

$$\begin{cases} f_{si}(t) = \sum_{\bar{n}=2}^{\bar{N}} r_{(J_i, \bar{n})} (x_{J_i}(t) - x_{J_i-1}(t))^{\bar{n}} \\ f_{di}(t) = \sum_{\bar{n}=2}^{\bar{N}} w_{(J_i, \bar{n})} (\dot{x}_{J_i}(t) - \dot{x}_{J_i-1}(t))^{\bar{n}} \end{cases} \quad i = 1, \dots, \bar{J} \quad (4.2)$$

where  $r_{(J_i, \bar{n})}$  and  $w_{(J_i, \bar{n})}$  are the polynomial coefficients. Denote

$$nf_i(t) = \left[ \underbrace{0 \dots 0}_{J_i-2} \quad -(f_{si}(t) + f_{di}(t)) \quad f_{si}(t) + f_{di}(t) \quad \underbrace{0 \dots 0}_{n-J_i} \right]^T \quad i = 1, \dots, \bar{J} \quad (4.3)$$

and

$$\mathbf{NF}(t) = \sum_{i=1}^{\bar{J}} nf_i(t) \quad (4.4)$$

Then, the motion of MDOF system in Fig. 4.1 can be described by

$$\mathbf{M}\ddot{\mathbf{x}}(t) + \mathbf{C}\dot{\mathbf{x}}(t) + \mathbf{K}\mathbf{x}(t) = \mathbf{F}(t) + \mathbf{NF}(t) \quad (4.5)$$

Eq. (4.5) represents a class of SIMO nonlinear systems with the input and outputs being  $f(t)$  and  $x_i(t)$ ,  $i = 1, \dots, n$ , respectively, and  $\mathbf{NF}(t)$  represents the effects of nonlinear springs/dampers in the system.

The detection and localization of nonlinear components in such structural systems are equivalent to detecting and locating a wide class of damage in the systems and, therefore, have significant implications in engineering practices. The present study is motivated by this practical need and aims to address the basic issues of how to detect whether there exist nonlinear components in the system (4.5) and to find their location from the system output responses measured on the masses. The solution to these issues with system (4.5) can be directly applied to address damage detection and location problems of simple rotor and building etc. structures [210, 211] and, more importantly, has potential to be extended to address more complicated damage detection and location problems with similar natures. Therefore, this chapter and the following chapters 5 and 6 will address the nonlinear component detection and localization problems with system (4.5) when the system is subject to single sinusoidal loading, multiple sinusoidal loadings, and multiple general loadings, respectively in order to systematically develop a series of method to address relevant engineering problems.

## 4.2 The NOFRFs of Single-Input Multi-Output nonlinear systems

In engineering structures especially mechatronic systems such as rotors [185-187, 203, 212] and civil structures such as buildings [28, 210], the appearance of super-harmonics, i.e., the system responses contain integer multiples of the driving frequency, often indicates the occurrence of structural damage, and such phenomena are often referred to 2×, 3×, etc harmonics in engineering practice [185]. Theoretically, these engineering structural systems can often be represented by a SIMO nonlinear system of a Volterra series model as follows [115, 213].

$$x_i(t) = \sum_{\bar{n}=1}^N \int_{-\infty}^{\infty} \dots \int_{-\infty}^{\infty} h_{(i,\bar{n})}(\tau_1, \dots, \tau_{\bar{n}}) \prod_{i=1}^{\bar{n}} f(t - \tau_i) d\tau_i \quad i = 1, 2, \dots, n \quad (4.6)$$

where  $x_i(t)$  and  $f(t)$  are the  $i^{\text{th}}$  output and the input of the system, respectively;  $n$  is the number of the system outputs;  $N$  is the maximum order of the system nonlinearity;  $h_{(i,\bar{n})}(\tau_1, \dots, \tau_{\bar{n}})$  is the  $\bar{n}^{\text{th}}$  order Volterra kernel associated with the  $i^{\text{th}}$  system output. Super-harmonic is a typical phenomenon with nonlinear systems described by equation Eq. (4.6). For example, Eq. (4.6) can represent a slightly damaged rotor system. In this case,  $f(t)$  is an unbalanced force acting on rotor shaft, which is periodic and of the same frequency as that of rotor rotation.  $x_i(t) \quad i = 1, 2, \dots, n$  are vibration measurements at different positions of the shaft,  $N$  is the highest order of super-harmonics observed from the vibration measurements, and  $h_{(i,\bar{n})}(\tau_1, \dots, \tau_{\bar{n}}) \quad i = 1, 2, \dots, n, \bar{n}=1, \dots, N$  are the functions determined by the rotor dynamics.

The output frequency responses of system (4.6) to a general input can be described by [123, 213]

$$\begin{cases} X_i(j\omega) = \sum_{\bar{n}=1}^N X_{(i,\bar{n})}(j\omega) \quad \forall \omega \\ X_{(i,\bar{n})}(j\omega) = \frac{1/\sqrt{\bar{n}}}{(2\pi)^{\bar{n}-1}} \int_{\omega_1+\dots+\omega_{\bar{n}}=\omega} H_{(i,\bar{n})}(j\omega_1, \dots, j\omega_{\bar{n}}) \prod_{i=1}^{\bar{n}} F(j\omega_i) d\sigma_{\bar{n}\omega} \end{cases} \quad (4.7)$$

Here  $X_i(j\omega)$  and  $F(j\omega)$  are the spectra of the  $i^{\text{th}}$  system output  $x_i$  and the system input  $f(t)$ , respectively;  $X_{(i,\bar{n})}(j\omega)$  denotes the  $\bar{n}^{\text{th}}$  order frequency response of the system's  $i^{\text{th}}$  output, and

$$H_{(i,\bar{n})}(j\omega_1, \dots, j\omega_{\bar{n}}) = \int_{-\infty}^{\infty} \dots \int_{-\infty}^{\infty} h_{(i,\bar{n})}(\tau_1, \dots, \tau_{\bar{n}}) e^{-(\omega_1\tau_1+\dots+\omega_{\bar{n}}\tau_{\bar{n}})} d\tau_1 \dots d\tau_{\bar{n}} \quad (4.8)$$

is known as the  $\bar{n}^{\text{th}}$  order Generalized Frequency Response Function(GFRF) associated with the  $i^{\text{th}}$  system output, which is the extension of the frequency response functions (FRF) of a SIMO linear system to the  $\bar{n}^{\text{th}}$  order nonlinear case [31]. In Eq. (4.7),

$$\int_{\omega_1+\dots+\omega_{\bar{n}}=\omega} H_{(i,\bar{n})}(j\omega_1, \dots, j\omega_{\bar{n}}) \prod_{i=1}^{\bar{n}} F(j\omega_i) d\sigma_{\bar{n}\omega}$$

represents the integration of  $H_{(i,\bar{n})}(j\omega_1, \dots, j\omega_{\bar{n}}) \prod_{i=1}^{\bar{n}} F(j\omega_i)$  over the  $\bar{n}$ -dimensional hyper-plane  $\omega_1 + \dots + \omega_{\bar{n}} = \omega$ . Eq. (4.7) is the representation of system (4.6) in the frequency domain and a theoretical basis for studying super-harmonics and many well-known nonlinear phenomena.

As shown in Eq. (4.8), the GFRFs are multi-dimensional functions of frequency variables. This makes the frequency domain analysis of nonlinear systems considerably difficult. In order to solve this problem, the concept of NOFRFs was proposed by Lang and Billings [31]. For the SIMO nonlinear system (4.6), the NOFRFs are defined as

$$G_{(i,\bar{n})}(j\omega) = \frac{\int_{\omega_1+\dots+\omega_{\bar{n}}=\omega} H_{(i,\bar{n})}(j\omega_1, \dots, j\omega_{\bar{n}}) \prod_{i=1}^{\bar{n}} F(j\omega_i) d\sigma_{\bar{n}\omega}}{\int_{\omega_1+\dots+\omega_{\bar{n}}=\omega} \prod_{i=1}^{\bar{n}} F(j\omega_i) d\sigma_{\bar{n}\omega}}, \quad \bar{n} = 1, \dots, N, i = 1, \dots, n \quad (4.9)$$

under the condition that

$$\int_{\omega_1 + \dots + \omega_{\bar{n}} = \omega} \prod_{i=1}^{\bar{n}} F(j\omega_i) d\sigma_{\bar{n}\omega} \neq 0 \quad (4.10)$$

From Eqs. (4.7) and (4.9), it can be shown that the output frequency responses of SIMO nonlinear systems can be represented using the NOFRFs as

$$\begin{cases} X_i(j\omega) = \sum_{\bar{n}=1}^N X_{(i,\bar{n})}(j\omega) & i = 1, \dots, n \\ X_{(i,\bar{n})}(j\omega) = G_{(i,\bar{n})}(j\omega) F_{\bar{n}}(j\omega) \end{cases} \quad (4.11)$$

where

$$F_{\bar{n}}(j\omega) = \frac{1/\sqrt{\bar{n}}}{(2\pi)^{\bar{n}-1}} \int_{\omega_1 + \dots + \omega_{\bar{n}} = \omega} \prod_{i=1}^{\bar{n}} F(j\omega_i) d\sigma_{\bar{n}\omega} \quad (4.12)$$

which is the Fourier Transform of  $f^{\bar{n}}(t)$ . Eq. (4.11) shows that, using the NOFRFs, the output spectra of nonlinear systems can be represented in a way similar to the FRF based representation of the output spectra of linear systems. This has significantly facilitated the analysis of nonlinear systems in the frequency domain [137, 211].

### 4.3 The NOFRF transmissibility of MDOF nonlinear structural systems

For SIMO linear systems, the transmissibility is defined as the ratio between the spectra of two different outputs and is equal to the ratio between the systems FRFs corresponding to the two outputs [25, 29]. To extend this well-known concept to the SIMO nonlinear system case, the transmissibility of the NOFRFs between the  $i^{\text{th}}$  and  $k^{\text{th}}$  outputs of the system (4.5) was introduced in [28] as

$$T_{i,k}^{NL}(j\omega) = \frac{G_{(i,N)}(j\omega)}{G_{(k,N)}(j\omega)} \quad (4.13)$$

where  $i, k \in \{1, \dots, n\}$ . It can be observed that when  $N = 1$ , the transmissibility of the NOFRFs as defined in (4.13) reduces to the traditional concept of transmissibility for

linear systems. Besides, as the NOFRFs do not depend on the change of the system input strength [31, 139, 143], the NOFRF transmissibility also is dependent from the system input strength. This property is the same as the input amplitude independent property with the traditional transmissibility concept.

Because system (4.5) is a SIMO nonlinear system, traditional transmissibility analysis methods can't be applied directly to the system. In [28], the NOFRF transmissibility given by Eq. (4.13) was introduced, which for the first time extended the transmissibility concept to the nonlinear case. In order to apply transmissibility analysis to the system (4.5), a series of relationships regarding the NOFRF transmissibility of the system are derived and the results are summarized in Proposition 4.1 as follows.

**Proposition 4.1 The properties of the NOFRF transmissibility of the SIMO nonlinear system**

If the outputs of system (4.5) can also be represented by the Volterra series model (4.6), there exit following results regarding the NOFRF transmissibility of the system:

(i) When  $\bar{J} > 1$ , that is, there are multiple nonlinear components in the system,

$$\begin{cases} T_{i,k}^{NL}(j\omega) = \frac{G_{(i,\bar{n})}(j\omega)}{G_{(k,\bar{n})}(j\omega)} = \bar{Q}_{i,k}(j\omega), \bar{n} \in \{2, \dots, N-1\}; \\ \quad \text{if } 1 \leq i < k \leq J_1 - 1 \text{ or } J_J \leq i < k \leq n \\ T_{i,k}^{NL}(j\omega) \neq \frac{G_{(i,\bar{n})}(j\omega)}{G_{(k,\bar{n})}(j\omega)}, \bar{n} \in \{2, \dots, N-1\}. \quad \text{Otherwise} \end{cases} \quad (4.14)$$

where  $\bar{Q}_{i,k}(j\omega)$  is only dependent on the  $M$ ,  $C$ , and  $K$ , that is, the linear characteristic parameters of the system (4.5).

(ii) When  $\bar{J} = 1$ , that is, there is only one nonlinear component in system (4.5),

$$T_{i,k}^{NL}(j\omega) = \frac{G_{(i,\bar{n})}(j\omega)}{G_{(k,\bar{n})}(j\omega)} = \bar{Q}_{i,k}(j\omega), \bar{n} \in \{2, \dots, N-1\}; \text{if } i, k \in \{1, \dots, n\}, i < k \quad (4.15)$$

where  $\bar{Q}_{i,k}(j\omega)$  are of the same nature as  $\bar{Q}_{i,k}(j\omega)$ , that is, only dependent on  $M$ ,  $C$ , and  $K$ .

In addition, if  $S \geq J_1$ ,

$$\left\{ \begin{array}{l} T_{i,k}^L(j\omega) = \frac{G_{(i,1)}(j\omega)}{G_{(k,1)}(j\omega)} = Q_{i,k}(j\omega) = \frac{G_{(i,\bar{n})}(j\omega)}{G_{(k,\bar{n})}(j\omega)} = T_{i,k}^{NL}(j\omega), \bar{n} \in \{2, \dots, N-1\}; \\ \quad \text{if } 1 \leq i < k \leq J_1 - 1 \text{ or } S \leq i < k \leq n \\ \\ T_{i,k}^L(j\omega) = \frac{G_{(i,1)}(j\omega)}{G_{(k,1)}(j\omega)} = Q_{i,k}(j\omega) \neq \frac{G_{(i,\bar{n})}(j\omega)}{G_{(k,\bar{n})}(j\omega)} = T_{i,k}^{NL}(j\omega), \bar{n} \in \{2, \dots, N-1\}; \\ \quad \text{otherwise} \end{array} \right. \quad (4.16)$$

and if  $S < J_1$ ,

$$\left\{ \begin{array}{l} T_{i,k}^L(j\omega) = \frac{G_{(i,1)}(j\omega)}{G_{(k,1)}(j\omega)} = Q_{i,k}(j\omega) = \frac{G_{(i,\bar{n})}(j\omega)}{G_{(k,\bar{n})}(j\omega)} = T_{i,k}^{NL}(j\omega), \bar{n} \in \{2, \dots, N-1\}; \\ \quad \text{if } 1 \leq i < k \leq S \text{ or } J_1 \leq i < k \leq n \\ \\ T_{i,k}^L(j\omega) = \frac{G_{(i,1)}(j\omega)}{G_{(k,1)}(j\omega)} = Q_{i,k}(j\omega) \neq \frac{G_{(i,\bar{n})}(j\omega)}{G_{(k,\bar{n})}(j\omega)} = T_{i,k}^{NL}(j\omega), \bar{n} \in \{2, \dots, N-1\}; \\ \quad \text{otherwise} \end{array} \right. \quad (4.17)$$

In Eqs. (4.16) and (4.17),  $T_{i,k}^L(j\omega)$  represents the traditional transmissibility and  $Q_{i,k}(j\omega)$  is again only dependent on  $M$ ,  $C$ , and  $K$ .

**Proof:** The conclusions of the Proposition 4.1 can be reached by using the analysis results in [139] for the system (4.5) and the definition of transmissibility of the NOFRFs given by Eq. (4.13).

Point (i) of Proposition 4.1 indicates that the NOFRF transmissibility and the ratio between other higher order NOFRFs are the same and only dependent on the system linear characteristic parameter  $M$ ,  $C$ , and  $K$  when associated system output points are on either side of the nonlinear components, but this relationship does not hold when the output points are within the span of nonlinear components.

Point (ii) of Proposition 4.1 shows that, if there is only one nonlinear component in system (4.5), the NOFRF transmissibility and the ratio between other higher order

NOFRFs are the same as the traditional linear transmissibility when associated system output points are both on the same side of the only nonlinear component and the input force. Otherwise, the relationships do not hold.

These results are the theoretical basis for reaching the conclusions of Proposition 4.3 in the Section 4.4 below, from which effective algorithms will be derived in Section 4.5 for the detection and localization of nonlinear components in system (4.5).

## 4.4 Transmissibility at super-harmonics

In order to more clearly demonstrate the main ideas, the study in this chapter assumes that the input force  $f(t)$  to the system (4.5) is sinusoidal and the location  $S$  where the input is applied is known a priori. These assumptions are, in fact, valid in many practical cases. For example, in rotors, the input is sinusoidal with frequency the same as rotating frequency and located in the position where the unbalanced force is applied [185-187]; in buildings, the ground motions due to earthquakes can also be considered to be sinusoidal in many cases [214, 215]. Under these assumptions, the output frequency response of the system (4.5) can be represented using the system NOFRFs as described in Proposition 4.2 below.

### Proposition 4.2 Frequency properties of the SIMO system to a harmonic input

Under the condition that the outputs of the system (4.5) can be represented by the Volterra series (4.6) and the input to the system is a harmonic

$$f(t) = A\cos(\omega_F t + \beta) \quad (4.18)$$

the range of the system output frequencies are  $\Omega = \{0, \pm 1\omega_F, \pm 2\omega_F, \dots, \pm N\omega_F\}$  and the system output responses at these frequencies can be determined by



$$\left\{ \begin{array}{l} X_i(j\omega_F) = G_{(i,1)}(j\omega_F)F_1(j\omega_F) + G_{(i,3)}(j\omega_F)F_3(j\omega_F) + \\ \quad \dots + G_{(i,N)}(j\omega_F)F_N(j\omega_F) \\ X_i(j2\omega_F) = G_{(i,2)}(j2\omega_F)F_2(j2\omega_F) + G_{(i,4)}(j2\omega_F)F_4(j2\omega_F) + \\ \quad \dots + G_{(i,N-1)}(j2\omega_F)F_{N-1}(j2\omega_F) \\ \quad \quad \quad \dots \quad \dots \quad \dots \\ X_i(jN\omega_F) = G_{(i,N)}(jN\omega_F)F_N(jN\omega_F) \end{array} \right. \quad (4.19)$$

for  $i = 1, \dots, n$  when  $N$  is odd or

$$\left\{ \begin{array}{l} X_i(j\omega_F) = G_{(i,1)}(j\omega_F)F_1(j\omega_F) + G_{(i,3)}(j\omega_F)F_3(j\omega_F) + \\ \quad \dots + G_{(i,N-1)}(j\omega_F)F_{N-1}(j\omega_F) \\ X_i(j2\omega_F) = G_{(i,2)}(j2\omega_F)F_2(j2\omega_F) + G_{(i,4)}(j2\omega_F)F_4(j2\omega_F) + \\ \quad \dots + G_{(i,N)}(j2\omega_F)F_N(j2\omega_F) \\ \quad \quad \quad \dots \quad \dots \quad \dots \\ X_i(jN\omega_F) = G_{(i,N)}(jN\omega_F)F_N(jN\omega_F) \end{array} \right. \quad (4.20)$$

when  $N$  is even.

**Proof:** See Appendix B.

Proposition 4.2 indicates that when subject to a sinusoidal input with frequency  $\omega_F$ , the output frequencies of the system (4.5) are  $\omega_F$  and  $2\omega_F, 3\omega_F, \dots$  etc. super-harmonics, which are the output frequencies generated by system nonlinearity [137, 138, 185-187], and the system output responses at these super-harmonic frequencies are determined by the system higher order NOFRFs and the Fourier Transform of system input raised to corresponding orders .

The concept of transmissibility at super-harmonics is introduced and defined as the ratio of the super-harmonic responses on two consecutive masses, that is

$$ST^{i,i+1}(j\bar{k}\omega_F) = \frac{X_i(j\bar{k}\omega_F)}{X_{i+1}(j\bar{k}\omega_F)} \quad \bar{k} = 2, \dots, N \text{ and } i = 1, \dots, n-1 \quad (4.21)$$

Moreover, from Propositions 4.1 and 4.2, the relationship between the transmissibility at super-harmonics as defined in (4.21) and the NOFRF transmissibility can be derived. The result is summarized in Proposition 4.3 as follows.

**Proposition 4.3 Properties of transmissibility at super-harmonics for the SIMO**

**nonlinear system**

Under the same condition of Proposition 4.2,

(i) When there are multiple nonlinear components in the system (4.5), that is  $\bar{J} > 1$ , if two consecutive masses of the system are all on the left or right side of the nonlinear components, namely,  $1 \leq i \leq J_1 - 2$  or  $J_{\bar{J}} \leq i \leq n - 1$ , then

$$ST^{i,i+1}(j\bar{k}\omega_F) = T_{i,i+1}^{NL}(j\bar{k}\omega_F) = \bar{Q}_{i,i+1}(j\bar{k}\omega_F), \bar{k} = 2, \dots, N \quad (4.22)$$

If at least one mass is within the range of nonlinear components, namely,  $J_1 - 1 \leq i \leq J_{\bar{J}} - 1$ , then

$$ST^{i,i+1}(j\bar{k}\omega_F) \neq T_{i,i+1}^{NL}(j\bar{k}\omega_F) \quad \bar{k} = 2, \dots, N \quad (4.23)$$

(ii) When there is only one nonlinear component in the system, that is,  $\bar{J} = 1$ , then

$$ST^{i,i+1}(j\bar{k}\omega_F) = T_{i,i+1}^{NL}(j\bar{k}\omega_F) = \bar{Q}_{i,i+1}(j\bar{k}\omega_F), i = 1, \dots, n - 1, \bar{k} = 2, \dots, N \quad (4.24)$$

and

$$\begin{cases} ST^{i,i+1}(j\omega_F) = T_{i,i+1}^L(j\omega_F) = Q_{i,i+1}(j\omega_F), \\ \quad \text{if } 1 \leq i \leq J_1 - 2 \text{ or } S \leq i \leq n - 1 \text{ when } S \geq J_1; \\ \quad \text{or if } 1 \leq i \leq S - 1 \text{ or } J_1 \leq i \leq n - 1 \text{ when } S < J_1 \\ ST^{i,i+1}(j\omega_F) \neq T_{i,i+1}^L(j\omega_F) = Q_{i,i+1}(j\omega_F) \\ \quad \text{otherwise} \end{cases} \quad (4.25)$$

(iii) Results (i) and (ii) above hold for  $\bar{k} = 2, 4, \dots, N$  if  $\bar{k}$  and  $N$  are all even; for  $\bar{k} = 3, 5, \dots, N$ , if  $\bar{k}$  and  $N$  are all odd; for  $\bar{k} = 2, 4, \dots, N - 1$  if  $\bar{k}$  is even but  $N$  is odd; and for  $\bar{k} = 3, 5, \dots, N - 1$  if  $\bar{k}$  is odd but  $N$  is even.

**Proof:** See Appendix C.

Result (i) of Proposition 4.3 indicates that if there are multiple nonlinear components in the system and the two consecutive masses involved in the transmissibility evaluation are located both on the same side of the nonlinear components, then the transmissibility at super-harmonics only depends on the system linear characteristic

parameters and is, therefore, independent from the system input. Otherwise, that is, when the two masses involved in the transmissibility evaluation are located inside the area of system nonlinear components, the transmissibility at super-harmonics may be dependent on the system input. This observation implies that the transmissibility at super-harmonics can be exploited to find the locations of nonlinear components when there are multiple nonlinear components in the system.

Result (ii) of Proposition 4.3 indicates that if there is only one nonlinear component in the system, the transmissibility at super-harmonics is completely dependent on the system linear characteristic parameters and independent from the system input. This implies that whether there is only one nonlinear component in the system or not can also be determined from the analysis of transmissibility at super-harmonics.

In addition, result (ii) of Proposition 4.3 indicates that if there is only one nonlinear component in the system, and the two consecutive masses involved in the transmissibility evaluation are not located between this nonlinear component and the mass where an input excitation is applied, the transmissibility at driving frequency also only depends on the system linear characteristic parameters and is independent from the system input. This implies that the transmissibility at driving frequency can be exploited to find the location of the only nonlinear component in this case.

According to [137, 185, 187], the damage with nonlinear features in MDOF systems can make the whole system behave nonlinearly and, particularly, produce super-harmonics. Therefore, as far as the systems' damage detection and location are concerned, the phenomena of higher order harmonics can be used to determine whether there exists such damage in the system, and the observations from Proposition 4.3 can be exploited to find out whether there is only one or multiple damaged components with nonlinear features in the system and the locations of the damage. These are the basis of a new method that will be proposed in the following for detection and localization of damage in MDOF systems via nonlinear features.

## 4.5 Detection and location of damage via nonlinear features using a new transmissibility analysis method

### 4.5.1 Basic ideas

According to [137, 185, 187], the damage with nonlinear features in MDOF systems can make the whole system behave nonlinearly and, particularly, produce super-harmonics. So the higher order harmonics can be used to determine whether there exists such damage in the system.

When damage with nonlinear features has been detected in system (4.5), the results of Proposition 4.3 can be used to find out whether there is only one or more than one damage with nonlinear features in the system and the locations of the damage. This is based on the following observations.

First, Eq. (4.24) in Proposition 4.3 (ii) indicates that when there is only one nonlinear component in MDOF system (4.5), the transmissibility at super-harmonics depends only on the system parameters  $M, C, K$  and does not change with the system input. This is a very distinctive feature and can be used, if damage with nonlinear features has been detected in system (4.5), to determine whether there is only one nonlinear component in the system or not.

Secondly, if there is only one nonlinear component in the system, Eq. (4.25) in Proposition 4.3 (ii) indicates that whether the transmissibility at base frequency  $\omega_F$  varies with a change in the system input depends on the location of the two masses involved in the transmissibility evaluation. This property can be exploited to find the location of the only nonlinear component in the system.

Finally, if there are multiple nonlinear components in the system (4.5), Eqs. (4.22) and (4.23) in Proposition 4.3 (i) indicate that whether the transmissibility at super-harmonics varies with a change in the system input depends on the location of

the two masses involved in the transmissibility evaluation. This can be used to find the locations of nonlinear components in the system.

#### 4.5.2 The method

From the super-harmonic analysis based damage detection idea, and the above observations from Proposition 4.3, a new transmissibility analysis method for the detection and localization of damage with nonlinear features in system (4.5) can be proposed under the following two assumptions.

a) The output responses of system (4.5) to two different sinusoidal inputs

$$f(t) = f^{(1)}(t) = A_1 \sin(\omega_F t + \beta_1) \quad \text{and} \quad f(t) = f^{(2)}(t) = A_2 \sin(\omega_F t + \beta_2) \quad (4.26)$$

can be obtained, respectively, so that two sets of transmissibility analysis results

$$\begin{cases} ST1^{i,i+1}(j\bar{k}\omega_F) = \frac{X_i^1(j\bar{k}\omega_F)}{X_{i+1}^1(j\bar{k}\omega_F)} = \frac{X_i(j\bar{k}\omega_F)}{X_{i+1}(j\bar{k}\omega_F)} \Big|_{f(t)=f^{(1)}(t)=A_1 \sin(\omega_F t + \beta_1)} \\ ST2^{i,i+1}(j\bar{k}\omega_F) = \frac{X_i^2(j\bar{k}\omega_F)}{X_{i+1}^2(j\bar{k}\omega_F)} = \frac{X_i(j\bar{k}\omega_F)}{X_{i+1}(j\bar{k}\omega_F)} \Big|_{f(t)=f^{(2)}(t)=A_2 \sin(\omega_F t + \beta_2)} \end{cases} \quad (4.27)$$

and their differences

$$S\delta^{i,i+1}(j\bar{k}\omega_F) = |ST1^{i,i+1}(j\bar{k}\omega_F) - ST2^{i,i+1}(j\bar{k}\omega_F)| \quad (4.28)$$

can be determined. Here,  $i = 1, \dots, n - 1$ ;  $\bar{k} = 1, 2, \dots, N$ . In (4.27),  $X_i^1(j\bar{k}\omega_F)$  and  $X_i^2(j\bar{k}\omega_F)$  are the spectra of the  $\bar{k}^{\text{th}}$  harmonic responses of the system to inputs  $f^{(1)}(t)$  and  $f^{(2)}(t)$ , respectively, and  $A_1 \neq A_2$ .

b) The location where the input force  $f(t)$  is applied to the system, that is, mass number  $S$  is known a priori.

The detailed procedures of the new method can be described as follows.

Step 1) Evaluate the spectra of the output responses of the system (4.5) to inputs  $f_1(t)$  and  $f_2(t)$ , respectively, and determine the amplitudes of these spectra at all the harmonics, that is,  $X_i^1(j\bar{k}\omega_F)$  and  $X_i^2(j\bar{k}\omega_F)$ , for  $i = 1, \dots, n$  and

$\bar{k} = 2, \dots, N$ . Here,  $N$  can be determined as the highest order at which the harmonics are observed in the system outputs. Determine the value of index  $IND_1$  as defined below to represent the strength of higher order harmonics in the system output responses

$$IND_1 = \max \left\{ \left| \frac{X_i^1(j\bar{k}\omega_F)}{X_i^1(j\omega_F)} \right|, \left| \frac{X_i^2(j\bar{k}\omega_F)}{X_i^2(j\omega_F)} \right|, i = 1, \dots, n, \text{ and } \bar{k} = 2, \dots, N \right\} \quad (4.29)$$

If

$$IND_1 \geq \varepsilon_1 \quad (4.30)$$

then it can be concluded that there exists damage with nonlinear features in the system. Otherwise, there is no such damage in the system. In (4.30),  $\varepsilon_1$  is a threshold to be determined a priori.

Step 2) If Step 1) indicates there is damage with nonlinear features in the system, select a  $\tilde{k} \in \{2, \dots, N\}$  such that both  $X_i^1(j\tilde{k}\omega_F)$   $i = 1, \dots, n$  and  $X_i^2(j\tilde{k}\omega_F)$   $i = 1, \dots, n$  have significant amplitudes. Calculate  $ST1^{i,i+1}(j\tilde{k}\omega_F)$ ,  $ST2^{i,i+1}(j\tilde{k}\omega_F)$ , and  $S\delta^{i,i+1}(j\tilde{k}\omega_F)$  for  $i = 1, \dots, n - 1$  using (4.27) and (4.28). Then, evaluate

$$S\delta_{\max}(\tilde{k}) = \max\{S\delta^{i,i+1}(j\tilde{k}\omega_F), i \in \{1, 2, \dots, n - 1\}\} \quad (4.31)$$

to see whether

$$S\delta_{\max}(\tilde{k}) \leq \varepsilon_2 \quad (4.32)$$

where  $\varepsilon_2$  is another a priori determined threshold. If (4.32) holds, it can be concluded that there exists only one damaged component with nonlinear features in the system. Otherwise, there are more than one damaged components with nonlinear features.

Step 3) If Step 2) indicates there exists only one damaged component with nonlinear features, calculate  $ST1^{i,i+1}(j\omega_F)$ ,  $ST2^{i,i+1}(j\omega_F)$ , and  $S\delta^{i,i+1}(j\omega_F)$  for  $i = 1, \dots, n - 1$  using (4.27) and (4.28). Then evaluate

$$S\delta_{\max}(1) = \max\{S\delta^{i,i+1}(j\omega_F), i \in \{1, 2, \dots, n-1\}\} \quad (4.33)$$

and

$$\overline{S\delta}^{i,i+1}(j\omega_F) = \frac{S\delta^{i,i+1}(j\omega_F)}{S\delta_{\max}(1)} \text{ for } i = 1, \dots, n-1 \quad (4.34)$$

to find those  $i$ 's such that

$$\overline{S\delta}^{i,i+1}(j\omega_F) \geq \varepsilon_3 \quad (4.35)$$

where  $\varepsilon_3$  is again a priori determined threshold.

Denote those  $i$ 's such that (4.35) holds as

$$i', i' + 1, \dots, i' + m' - 1$$

where  $m' \geq 1$ .

Then, there are only two possibilities which are  $S = i'$  or  $S = i' + m'$ . If  $S = i'$ , it can be concluded that the only nonlinear component is located between mass  $(i' + m' - 1)$  and mass  $(i' + m')$ . Otherwise,  $S = i' + m'$ , and it can be concluded that the only nonlinear component is located between mass  $i'$  and mass  $(i' + 1)$ .

Step 4) If Step 2) indicates there exist more than one damaged components with nonlinear features in the system, evaluate

$$\overline{S\delta}^{i,i+1}(j\tilde{k}\omega_F) = \frac{S\delta^{i,i+1}(j\tilde{k}\omega_F)}{S\delta_{\max}(\tilde{k})} \text{ for } i = 1, \dots, n-1 \quad (4.36)$$

to find those  $i$ 's such that

$$\overline{S\delta}^{i,i+1}(j\tilde{k}\omega_F) \geq \varepsilon_4 \quad (4.37)$$

where  $\varepsilon_4$  is also a priori determined threshold. Denote those  $i$ 's such that (4.37)

hold as

$$i'', i'' + 1, \dots, i'' + m'' - 1$$

where  $m'' > 1$ . Then, it can be concluded that these nonlinear components are located between mass  $i''$  and mass  $i'' + m''$ .

The method above can be represented by the flow chart in Fig. 4.5 which illustrates each step and the order of the whole procedure clearly.

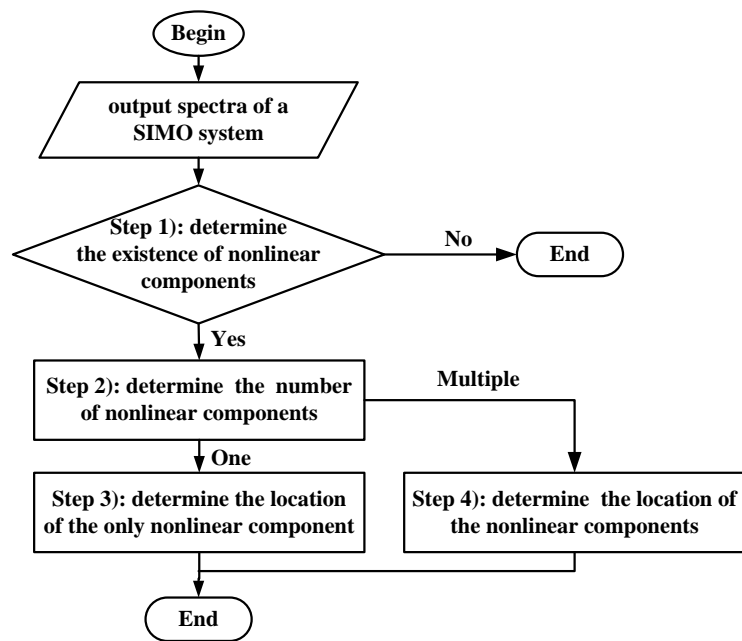


Fig. 4.5 Flow chart of damage detection and localization method for SIMO systems

### 4.5.3 Remarks

For the new method described above, following remarks can be made regarding the theoretical basis of relevant steps and the choice of the threshold parameters that are required to be determined a priori.

- a) Step 1) of the method is based on the well-known fact that nonlinearity will generate harmonics in the system output response. Step 2) exploits the property of system (4.5) described in the first point of Proposition 4.3 (ii), which indicates if



there is only one nonlinear component in the system, the transmissibility at super-harmonics is completely determined by the system linear characteristic parameters and, therefore, independent of the system input. The theoretical basis of Step 3) is the second point of Proposition 4.3 (ii), which reveals an important relationship between the transmissibility at base frequency and the location of the only nonlinear component in the system. Step 4) makes use of the property of the transmissibility at super-harmonics of system (4.5) described by Proposition 4.3 (i) , which shows where the transmissibility at super-harmonics is only dependent on the system linear characteristic parameters and, therefore, independent of the system input and where this is not the case.

- b)  $\varepsilon_1, \varepsilon_2, \varepsilon_3, \varepsilon_4$  are four threshold parameters in the method. In practice, these thresholds are determined a priori from experimental data using statistical analyses. For example,  $\varepsilon_1$  can be a small number associated with a noise threshold in the cases where the system basically behaves linearly and can be determined as the mean plus three times the standard deviation of the values of  $IND_1$  in the situations when there is no damage with nonlinear features in the system.  $\varepsilon_2, \varepsilon_3, \varepsilon_4$  can be determined in the same way but based on the mean and standard deviation of  $S\delta_{\max}(\tilde{k})$ ,  $\overline{S\delta}^{i,i+1}(j\omega_F)$ , and  $\overline{S\delta}^{i,i+1}(j\tilde{k}\omega_F)$ , respectively, in corresponding situations. The details of this threshold determination procedure will be demonstrated in Section 4.7. The threshold parameters thus determined allow the effects of un-modeled dynamics, noise, and inherent but less significant system nonlinearity to be neglected when the new method is used in practice.
- c) The determination of  $N$  and  $\tilde{k}$  can be achieved by observing the spectra of the system outputs, which will also be demonstrated in Section 4.7.
- d) It is worth pointing out that as the method only uses structural output response measurements, it can readily be implemented in real time by directly processing signals from a network of sensors such as accelerometers fitted in structural systems for condition monitoring purposes.

In the next two sections, simulation and experimental studies will be conducted to demonstrate the performance of the proposed method and its potential in practical applications.

## 4.6 Simulation studies

In order to verify the effectiveness of the proposed method, simulation studies are conducted in this section. For this purpose, a 10DOF system as described by Eq. (4.5) is considered where:  $m_1 = m_2 = \dots = m_{10} = 1$ ,

$$k_1 = k_2 = \dots = k_5 = k_{10} = 3.6 \times 10^4,$$

$$k_6 = k_7 = k_8 = 0.8k_1, \quad k_9 = 0.9k_1, \quad \mu = 0.01, \quad C = \mu K,$$

and the parameters of nonlinear springs and dampers are

$$\bar{N} = 3, \quad r_{(J_i,2)} = 0.8k_1^2, \quad r_{(J_i,3)} = 0.4k_1^3, \quad w_{(J_i,2)} = w_{(J_i,3)} = 0, \quad i = 1, \dots, \bar{J}.$$

where  $\bar{J}$ , the number of nonlinear components in the system, is  $\bar{J} = 3$  and  $\bar{J} = 1$ , respectively in the two cases of simulation studies below. In addition, the position of loading on the system is  $S = 7$  and  $S = 3$  in the following two simulation studies, respectively.

### 4.6.1 Simulation study: case 1

In this case, there are three ( $\bar{J} = 3$ ) nonlinear components in the system, which are the 3<sup>rd</sup>, 5<sup>th</sup> and 6<sup>th</sup> springs. Two loading conditions are considered where the input forces are

$$f(t) = f^{(1)}(t) = 10\sin(40\pi t)$$

$$\text{and } f(t) = f^{(2)}(t) = 20\sin(40\pi t)$$

respectively, and are applied on the 7<sup>th</sup> mass, that is,  $S = 7$ . The new method was applied to the spectra of the output responses of the system under the two loading

conditions, that is,

$$X_i^1(j\bar{k}\omega_F) \text{ and } X_i^2(j\bar{k}\omega_F), \quad i = 1, \dots, 10, \quad \bar{k} = 1, \dots, N.$$

where  $N$  was determined as 4. The four threshold parameters  $\varepsilon_1, \varepsilon_2, \varepsilon_3, \varepsilon_4$  were determined using the procedure introduced in Remark b) in Section 4.5.3. The results are given in Table 4.1.

Table 4.1 Threshold parameters used in the simulation studies

Threshold parameter	$\varepsilon_1$	$\varepsilon_2$	$\varepsilon_3$	$\varepsilon_4$
Value	$8.42 \times 10^{-6}$	0.0099	$9.82 \times 10^{-6}$	0.0015

The results of the simulation study obtained in each step of the proposed method are given as follows.

**Step 1)**

In this case, the index  $IND_1$  was evaluated using Eq. (4.29) as

$$IND_1 = \max \left\{ \left| \frac{X_i^1(j\bar{k}\omega_F)}{X_i^1(j\omega_F)} \right|, \left| \frac{X_i^2(j\bar{k}\omega_F)}{X_i^2(j\omega_F)} \right|, i = 1, \dots, 10, \text{ and } \bar{k} = 2, \dots, 4 \right\} = 0.0287 \geq \varepsilon_1 = 8.42 \times 10^{-6}$$

Therefore, it is concluded that damage with nonlinear features exists in the system.

**Step 2)**

At this step,  $\tilde{k}$  was determined as  $\tilde{k} = 2$ . So

$$ST1^{i,i+1}(j2\omega_F), \quad ST2^{i,i+1}(j2\omega_F), \text{ and } S\delta^{i,i+1}(j2\omega_F) \quad i = 1, \dots, 9$$

were evaluated using Eqs. (4.27) and (4.28). Then,  $S\delta_{\max}(2)$  was determined using Eq. (4.31); the result is

$$S\delta_{\max}(2) = 1.5349 > \varepsilon_2 = 0.0099$$

So it is known that there are multiple nonlinear components in the system.

**Step 4)**

As Step 2) has shown that there are multiple nonlinear components in the system, Step 4) rather than Step 3) of the proposed method is needed in this case. At this step,  $\overline{S\delta}^{i,i+1}(j\tilde{k}\omega_F) = \overline{S\delta}^{i,i+1}(j2\omega_F)$ ,  $i = 1, \dots, 9$  were evaluated using Eq. (4.36). The results are shown in Table 4.2, in which it can be observed that

$$\overline{S\delta}^{i,i+1}(j2\omega_F) \geq \varepsilon_4 = 0.0015, \quad i = 2,3,4,5$$

Therefore  $i'' = 2$  and  $m'' = 4$ , and it can be concluded that nonlinear components are located between mass  $i'' = 2$  and mass  $i'' + m'' = 6$  in the system.

Table 4.2 The value of  $\overline{S\delta}^{i,i+1}(j2\omega_F)$  when the 3rd, 5th and 6th springs are nonlinear

$i$	$\overline{S\delta}^{i,i+1}(j2\omega_F)$	$i$	$\overline{S\delta}^{i,i+1}(j2\omega_F)$	$i$	$\overline{S\delta}^{i,i+1}(j2\omega_F)$
1	$5.16 \times 10^{-5}$	4	1	7	0.000133
2	0.109899	5	0.340627	8	$8.63 \times 10^{-5}$
3	0.071504	6	$9.63 \times 10^{-5}$	9	$9.59 \times 10^{-6}$

Obviously, the conclusions reached at each step are all consistent with the real situation of the simulated system. So the effectiveness of the proposed method is verified by this simulation study.

#### 4.6.2 Simulation study: case 2

In this case, there is only one ( $\bar{J} = 1$ ) nonlinear component in the system, which is the 8<sup>th</sup> spring. The same two loading conditions as in the above simulation study case 1 were considered and the input force was applied on the 3<sup>rd</sup> mass, that is,  $S = 3$ . The new method was again applied to the spectra of the output responses of the system under the two loading conditions. Again,  $N$  was determined as 4 and the same threshold parameters  $\varepsilon_1, \varepsilon_2, \varepsilon_3, \varepsilon_4$  as given in Table 4.1 were used. The results obtained in each step of the method are given as follows.

**Step 1)**

In this case, the index  $IND_1$  was evaluated by (4.29) as

$$IND_1 = \max \left\{ \left| \frac{X_i^1(j\bar{k}\omega_F)}{X_i^1(j\omega_F)} \right|, \left| \frac{X_i^2(j\bar{k}\omega_F)}{X_i^2(j\omega_F)} \right|, i = 1, \dots, 10, \text{ and } \bar{k} = 2, \dots, 4 \right\}$$

$$= 0.0387 \geq \varepsilon_1 = 8.42 \times 10^{-6}$$

So, damage with nonlinear features exists in the system.

**Step 2)**

At this step,  $\tilde{k}$  is again determined as  $\tilde{k} = 2$ . Therefore, in the same way as in Step 2), simulation case study 1,  $S\delta_{\max}(2)$  was determined; the result is

$$S\delta_{\max}(2) = 6.7163 \times 10^{-4} < \varepsilon_2 = 0.0099$$

So it is known that there is only one nonlinear component in the system.

**Step 3)**

Because Step 2) indicates there is only one nonlinear component in the system, Step 3) of the proposed method was followed to evaluate  $ST1^{i,i+1}(j\omega_F)$ ,  $ST2^{i,i+1}(j\omega_F)$ , and  $S\delta^{i,i+1}(j\omega_F)$  for  $i = 1, \dots, 9$  using Eqs. (4.27) and (4.28). Then,  $\overline{S\delta}^{i,i+1}(j\omega_F)$  for  $i = 1, \dots, 9$  were evaluated using Eqs. (4.33) and (4.34). The results are shown in Table 4.3 indicating

$$\overline{S\delta}^{i,i+1}(j\omega_F) \geq \varepsilon_3 = 9.82 \times 10^{-6}, i = 3, \dots, 7$$

So  $i' = 3$  and  $m' = 5$ . As  $S = 3 = i'$ , it is known that the only nonlinear component is located between mass  $(i' + m' - 1) = 7$  and mass  $(i' + m') = 8$ .

Again, the conclusions reached at each step above are all consistent with the real situation of the simulated system. So the effectiveness of the proposed method is further verified by the second simulation study.

Table 4.3 The value of  $\overline{S\delta}^{i,i+1}(j\omega_F)$  when the 8th spring is nonlinear

$i$	$\overline{S\delta}^{i,i+1}(j\omega_F)$	$i$	$\overline{S\delta}^{i,i+1}(j\omega_F)$	$i$	$\overline{S\delta}^{i,i+1}(j\omega_F)$
1	$2.2 \times 10^{-6}$	4	0.112423	7	1
2	$3.56 \times 10^{-6}$	5	0.305335	8	$5.79 \times 10^{-6}$
3	0.076072	6	0.986996	9	$3.44 \times 10^{-6}$

## 4.7 Experimental studies

### 4.7.1 Experimental setup

In order to demonstrate the potential of the new transmissibility analysis based damage detection and location method in practical applications, the method was applied to analyse the experimental data from a three-storey building structure shown in Fig.4.6. The structure consists of aluminum plates and columns, which are assembled together by bolted joints. The bottom and top aluminum plates are connected by four columns between them, which form a 4DOF structural system. An electromagnetic shaker is used to excite the ground floor directly. The whole building structure can move on rails in only one direction. There are four accelerometers to measure the response of floors, which are installed to each floor at the opposite side from the electromagnetic shaker. In addition, the top of each floor suspends a center column, which can contact a bumper fitted on bottom of the floor so as to produce nonlinear behaviors. The strength of the nonlinearity can be changed by adjusting the location of the bumper. This kind of nonlinearity can simulate the fatigue cracks which are open and close under different loading conditions.

The three-storey building structure can be described by a spring-damper model shown in Fig. 4.7, which is clearly a specific case of the nonlinear MDOF model in Fig. 4.1.

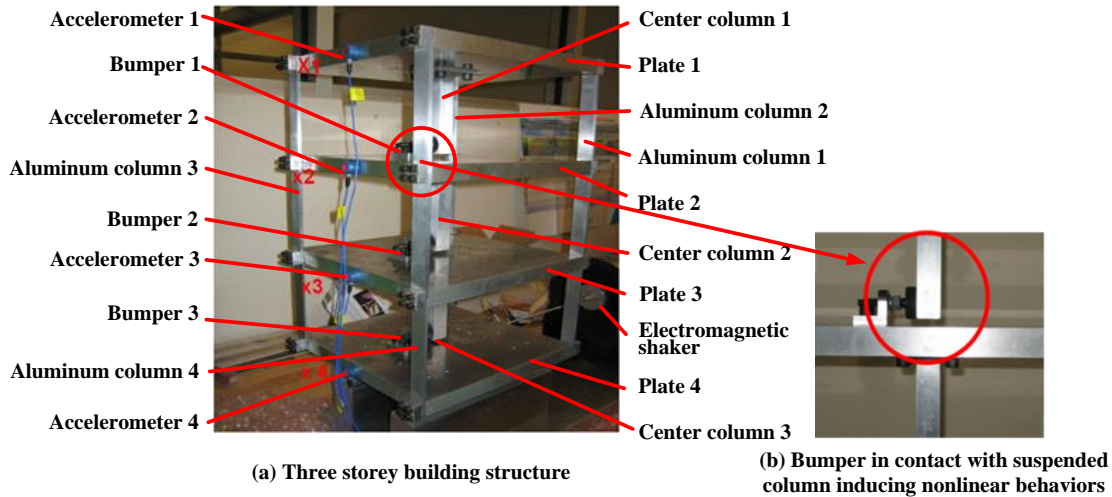


Fig. 4.6 Three-storey building structure used for the experimental studies

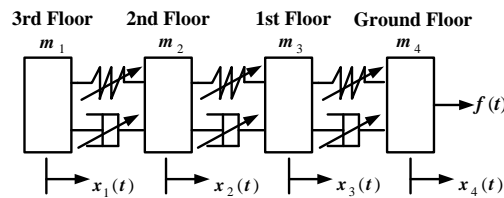


Fig. 4.7 4DOF system model of the three-storey building structure

#### 4.7.2 Experiments and experimental data analyses

Data were collected from six different experiments on the three-storey building structure. The details of the experiments are summarized in Table 4.4. Three different state conditions of the structure were investigated. These are the structural state conditions under Experiments #1 and #2, under Experiments #3 and #4, and under Experiments #5 and #6, respectively. The data collected from Experiments #1 and #2 were used to determine the situation of state condition 1, the data collected from Experiments #3 and #4 were used to determine the situation of state condition 2, and the data collected from Experiments #5 and #6 were used to determine the situation of state condition 3. The objectives of the experimental data analysis were to apply the method proposed in this chapter for each state condition to detect whether there exist nonlinear components in the experimental system and, if this is the case, determine the location of the nonlinear components in the system.

Table 4.4 Details of the experiments

Experiments	Input excitation applied by shaker control computer	Structure state condition under which experiment was conducted
Experiment #1	25 Hz sinusoidal with amplitude 2	State Condition 1: A 0.13mm gap was introduced between the column and bumper on the first floor to generate a nonlinear effect.
Experiment #2	25 Hz sinusoidal with amplitude 2.5	
Experiment #3	25 Hz sinusoidal with amplitude 2	State Condition 2: A 0.20mm gap was introduced between the column and bumper on the second (top) floor to generate a nonlinear effect.
Experiment #4	25 Hz sinusoidal with amplitude 2.5	
Experiment #5	25 Hz sinusoidal with amplitude 1	State Condition 3: A 0.30mm gap was introduced between the column and bumper on both the ground (bottom) floor and on the first floor to produce two nonlinear components in the structure.
Experiment #6	25 Hz sinusoidal with amplitude 1.5	

Before the proposed method was applied to analyze the experimental data,  $N$  and  $\tilde{k}$  were determined as  $N = 3$  and  $\tilde{k} = 3$  from observing the spectra of the system outputs in the six experiments shown in Fig. 4.7.

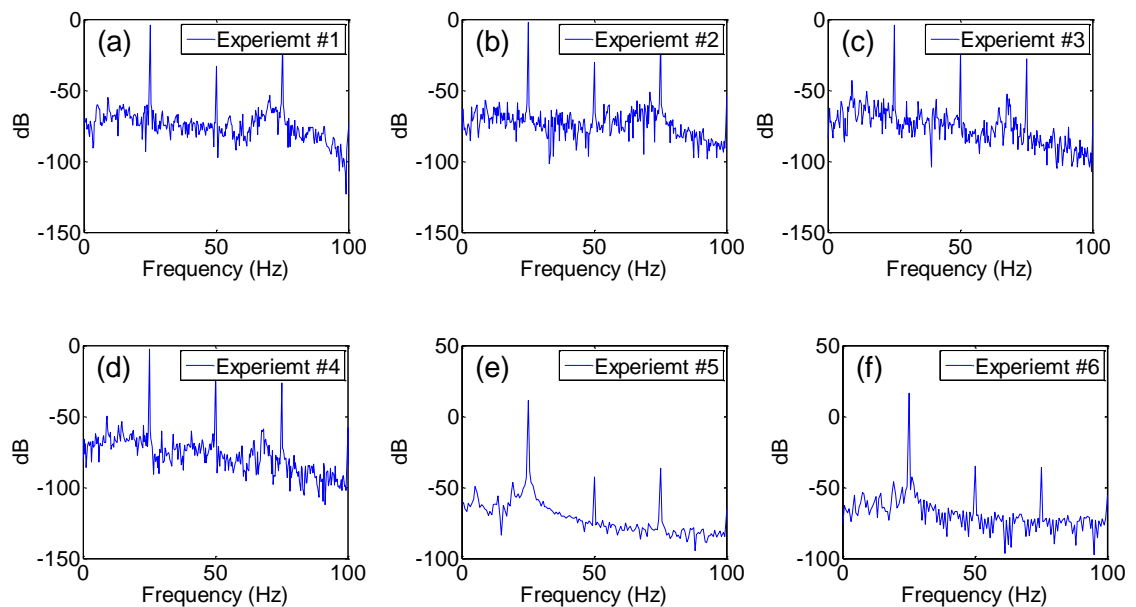


Fig.4.7 Output spectra on the first floor in Experiments #1 - #6



By using the procedure introduced in Remark b) in Section 4.5.3 again, threshold parameters  $\varepsilon_1, \varepsilon_2, \varepsilon_3, \varepsilon_4$  in this case were determined as shown in Table 4.5.

Table 4.5 The threshold parameters used in the experimental data analysis

Threshold parameters	$\varepsilon_1$	$\varepsilon_2$	$\varepsilon_3$	$\varepsilon_4$
Value	0.019897	0.0179	0.0483	0.0881

In order to demonstrate how these thresholds were obtained using this procedure for the experimental data analysis, take the process of determining  $\varepsilon_1$ , as an example, Table 4.6 shows the values of  $IND_1$  evaluated from Eq. (4.29) using data collected from 16 different tests where there are no nonlinear components introduced in the experimental structural system. By using the results in Table 4.6, it was obtained that

$$\overline{IND}_1 = \frac{\sum_{i=1}^{16} IND_1(i)}{16} = 0.011722$$

$$\sigma = \sqrt{\frac{\sum_{i=1}^{16} (IND_1(i) - \overline{IND}_1(i))^2}{16}} = 0.002725$$

Consequently,  $\varepsilon_1 = \overline{IND}_1 + 3\sigma = 0.019897$ .

Table 4.6 The values of  $IND_1$  evaluated using data for different tests where no nonlinear components were introduced

Tests	Values of $IND_1$			
Tests 1-4	0.012792	0.015297	0.010087	0.00882
Tests 5-8	0.013415	0.015845	0.010125	0.008762
Tests 9-12	0.014219	0.01538	0.009981	0.009003
Tests 13-16	0.015069	0.009937	0.009317	0.009499

Table 4.7 shows all the results of experimental data analyses. Because  $IND_1=0.3453 > \varepsilon_1 = 0.019897$  in state condition 1,  $IND_1=0.1714 > \varepsilon_1 = 0.019897$  in

state condition 2, and  $IND_1=0.1604 > \varepsilon_1 = 0.019897$  in state condition 3, it was concluded that there exists nonlinear damage in the structural system in all the three state conditions.

Moreover, because

$$S\delta_{\max}(\tilde{k}) = S\delta_{\max}(3) = 0.016 < \varepsilon_2 = 0.0179$$

in state condition 1,

$$S\delta_{\max}(\tilde{k}) = S\delta_{\max}(3) = 0.013 < \varepsilon_2 = 0.0179$$

in state condition 2, and

$$S\delta_{\max}(\tilde{k}) = S\delta_{\max}(3) = 0.8988 > \varepsilon_2 = 0.0179$$

in state condition 3, it was concluded that there is only one nonlinear component in state conditions 1 and 2 but there are more than one nonlinear components in state condition 3. Therefore, Step 3) of the proposed method should be used to find the location of the nonlinear component under state conditions 1 and 2, but Step 4) of the proposed method should be used to find the location of the nonlinear components under state condition 3.

The last row of Table 4.7 shows the data analysis results for localization of nonlinear components in the three state conditions. The analysis results for state condition 1 using Step 3) of the proposed method indicate

$$\overline{S\delta}^{i,i+1}(j\omega_F) \geq \varepsilon_3 = 0.0483, \quad i = 2,3$$

So  $i' = 2$  and  $i' + m' - 1 = 3 \rightarrow m' = 2$ . Because  $L = 4 = i' + m'$  in this case, it is known that the nonlinear component is located between mass  $i' = 2$  and mass  $i' + 1 = 3$  in state condition 1, that is, on the first floor.

The analysis results for state condition 2 again using Step 3) of the proposed method indicate

$$\overline{S\delta}^{i,i+1}(j\omega_F) \geq \varepsilon_3 = 0.0483, \quad i = 1,2,3$$

So  $i' = 1$  and  $i' + m' - 1 = 3 \rightarrow m' = 3$ . Because again  $L = 4 = i' + m'$  in this case, it is known that the nonlinear component is located between mass  $i' = 1$  and mass  $i' + 1 = 2$  in state condition 2, that is, on the second floor.

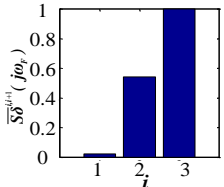
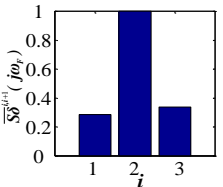
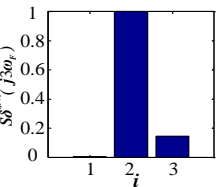
The analysis results for state condition 3 using Step 4) of the proposed method indicate

$$\overline{S\delta}^{i,i+1}(j\tilde{k}\omega_F) = \overline{S\delta}^{i,i+1}(j3\omega_F) \geq \varepsilon_4 = 0.0881, \quad i = 2,3$$

Therefore  $i'' = 2$  and  $m'' + i'' - 1 = 3 \rightarrow m'' = 2$ , and it can be concluded that nonlinear components are located between mass  $i'' = 2$  and mass  $i'' + m'' = 4$  in the system in state condition 3, that is, on the ground and first floors.

Obviously, the conclusions reached by the analysis of the experimental data from the three state conditions of the experimental system using the proposed method are completely consistent with the real situations of the system. Therefore, the potential of the proposed method in engineering applications have been verified.

Table 4.7 Details of the experimental data analysis results

	The experimental data analysis results for the three-storey building structure under state condition 1	The experimental data analysis results for the three-storey building structure under state condition 2	The experimental data analysis results for the three-storey building structure under state condition 3
$N$	3	3	3
$IND_1$	$0.3453 > \varepsilon_1$ $= 0.019897$	$0.1747 > \varepsilon_1$ $= 0.019897$	$0.1604 > \varepsilon_1$ $= 0.019897$
$\tilde{k}$	3	3	3
$S\delta_{\max}(\tilde{k})$	$0.016 < \varepsilon_2 = 0.0179$	$0.013 < \varepsilon_2 = 0.0179$	$0.8988 > \varepsilon_2 = 0.0179$
$\overline{S\delta}^{i,i+1}(j\omega_F)$ or $\overline{S\delta}^{i,i+1}(j3\omega_F)$ for $i = 1, \dots, 3$			

## 4.8 Conclusions

Transmissibility analysis is a well-established method and has been widely applied in structural analysis including damage detection and localization. However, traditional transmissibility is a linear system concept which cannot be directly applied to the analysis of nonlinear structural systems. Recently, the concept of transmissibility of the NOFRFs has been introduced to extend the transmissibility concept to nonlinear cases, and the NOFRF transmissibility based/related techniques have been developed to detect and locate damage in MDOF structural systems. However, these techniques assume that there is only one nonlinear component in a damaged system and /or require that the loading on inspected structural systems is measurable. To address these issues so as to enable NOFRF transmissibility based damage detection and location to be applicable in engineering practice, a new transmissibility analysis method has been developed in this chapter for the detection and location of damage via nonlinear features in MDOF structural systems. The new method is derived using the NOFRF transmissibility concept and can be implemented by evaluation and analysis of the transmissibility of system responses at super-harmonics. Both numerical simulation studies and experimental data analysis have been conducted to verify the effectiveness and demonstrate the potential practical applications of the proposed new technique. Although, for convenience of introducing main ideas, a relatively simple MDOF system model and sinusoidal loadings are considered in this study, the method can be extended to more complicated systems and more general multi-frequency and band limited loading cases and, therefore, has potential to be applied in practice to tackle nonlinear damage detection and location problems. The research in the next two chapters will be focused on these more general loading conditions to enable the ideas to be applicable in a much wider range of practical structural systems.

## Chapter 5

### **Nonlinearity detection and location for MIMO nonlinear systems using transmissibility analysis**

Chapter 4 deals with the problem of nonlinearity detection and localization when the structural system is subject to only one input. In this chapter, the case where several loadings are applied on a structural system simultaneously is studied. The concept of the NOFRFs is extended to multi-input case so that the outputs of multi-input multi-output (MIMO) nonlinear systems can be analysed and transmissibility analysis based method can be used to detect and localize nonlinear components in MIMO systems. The distinctive differences of output responses between the SIMO and MIMO systems are that the NOFRFs of MIMO systems are much more complicated and the frequency components of output responses are more abundant. For example, in the case of two sinusoidal inputs with frequencies  $\omega_{f1}$  and  $\omega_{f2}$ , respectively, not only the harmonics of the driving frequencies such as  $2\omega_{f1}$ ,  $3\omega_{f1}$  as mentioned in Chapter 4 can be observed in the frequency spectra of output responses, but also the combination of driving frequencies such as  $\omega_{f1} + \omega_{f2}$  and  $2\omega_{f1} + \omega_{f2}$  will appear. Both super-harmonic frequencies and the combination of driving frequencies are induced by the system nonlinearity, are unique phenomena with nonlinear systems, and are, later on, referred to as nonlinearity generated frequencies.

In this chapter, after the description of the model and mathematical representation of a class of MIMO systems, the concept of the NOFRFs of MIMO nonlinear systems is introduced and the properties of the transmissibility of the NOFRFs of MIMO nonlinear systems are derived. Then, the transmissibility at nonlinearity generated frequency is proposed and its properties are investigated. Finally, a transmissibility analysis based method is developed to detect and localize nonlinear components in MIMO nonlinear

systems and the effectiveness of this method is verified by simulation case studies.

## 5.1 A class of MIMO dynamic systems

The MIMO systems studied in this chapter are similar to the MDOF systems considered in Chapter 4, but there are  $m$  rather than one inputs applied at different locations as shown in Fig. 5.1. In this system description, the nonlinear components are also represented by nonlinear springs and dampings, which is denoted by the spring and damper symbols with arrows, these components can represent structural damage with nonlinear features in many practical systems as mentioned in Chapter 4.

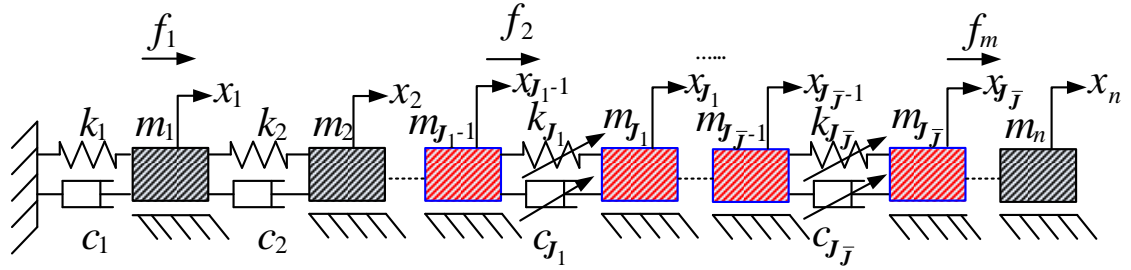


Fig. 5.1 MIMO nonlinear structural system subject to  $m$  inputs

The motion of the MIMO system in Fig. 5.1 can be described by

$$\mathbf{M}\ddot{\mathbf{x}}(t) + \mathbf{C}\dot{\mathbf{x}}(t) + \mathbf{K}\mathbf{x}(t) = \mathbf{F}_m(t) + \mathbf{NF}(t) \quad (5.1)$$

where the mass matrix  $\mathbf{M}$ , damping matrix  $\mathbf{C}$ , stiffness matrix  $\mathbf{K}$ , and displacement vector  $\mathbf{x}(t)$  are exactly the same as that in Eq. (4.5); the effects of nonlinear components represented by  $\mathbf{NF}(t)$  are also the same as that described by Eqs. (4.2), (4.3) and (4.4). But, because  $m$  inputs are applied on the  $S_1, S_2, \dots, S_m^{\text{th}}$  masses respectively, assuming  $S_1 < S_2 < \dots < S_m$ , the force vector can be described as

$$\mathbf{F}_m(t) = [0 \quad \dots \quad f_1(t) \quad \dots \quad f_2(t) \quad \dots \quad f_m(t) \quad \dots \quad 0]^T \quad (5.2)$$

## 5.2 Description of MIMO nonlinear systems in the time and frequency domains

Volterra series are capable of representing not only SIMO nonlinear systems but also MIMO systems. However, the Volterra kernels of MIMO nonlinear systems are more complicated. When MIMO nonlinear systems are stable at zero equilibrium, the system outputs around equilibrium can be represented by the multi-input Volterra series as follows.

$$x_i(t) = \sum_{\bar{n}=1}^N x_i^{(\bar{n})}(t) \quad (5.3)$$

where

$$\begin{aligned} x_i^{(\bar{n})}(t) = & \sum_{n_1+n_2+\dots+n_m=\bar{n}} \int_{-\infty}^{+\infty} \dots \int_{-\infty}^{+\infty} h_{(i,p_1=n_1,p_2=n_2,\dots,p_m=n_m)}^{(\bar{n})}(\tau_1, \tau_2, \dots, \tau_{\bar{n}}) f_1(t \\ & - \tau_1) \dots f_1(t - \tau_{n_1}) f_2(t - \tau_{n_1+1}) \dots f_2(t - \tau_{n_1+n_2}) \dots f_m(t \\ & - \tau_{n_1+n_2+\dots+n_{m-1}+1}) \dots f_m(t - \tau_{n_1+n_2+\dots+n_m}) d\tau_1 \dots d\tau_{\bar{n}} \end{aligned} \quad (5.4)$$

where,  $x_i(t)$ , and  $f_1(t)$ ,  $f_2(t)$ , ...,  $f_m(t)$  are the system  $i^{\text{th}}$  output and inputs, respectively;  $\bar{n}$  denotes the order of system nonlinearity;  $N$  is the maximum order of the system nonlinearity,  $h_{(i,p_1=n_1,p_2=n_2,\dots,p_m=n_m)}^{(\bar{n})}(\tau_1, \tau_2, \dots, \tau_{\bar{n}})$  is the  $\bar{n}^{\text{th}}$  order Volterra kernel of  $i^{\text{th}}$  output associated with the first input  $f_1(t)$  with order  $n_1$ , the second input  $f_2(t)$  with order  $n_2$ , ..., the  $m^{\text{th}}$  inputs  $f_m(t)$  with order  $n_m$ , and  $n_1 + n_2 + \dots + n_m = \bar{n}$ . Given the order, the Volterra kernel of SIMO nonlinear system is unique, while there are many more Volterra kernels in MIMO nonlinear systems where the contribution of each input is different [126]. For example, if the system is excited by two inputs at different locations, there are two first order Volterra kernels for the  $i^{\text{th}}$  output, namely,  $h_{(i,p_1=1,p_2=0)}^{(1)}(\tau_1)$  and  $h_{(i,p_1=0,p_2=1)}^{(1)}(\tau_2)$ ; three second

order Volterra kernels, namely,  $h_{(i,p_1=2,p_2=0)}^{(2)}(\tau_1, \tau_2)$  ,  $h_{(i,p_1=1,p_2=1)}^{(2)}(\tau_1, \tau_2)$  and  $h_{(i,p_1=0,p_2=2)}^{(2)}(\tau_1, \tau_2)$ .

The output frequency responses of system (5.3) to input (5.2) can be described as follows [197].

$$X_i(j\omega) = \sum_{\bar{n}=1}^N X_i^{(\bar{n})}(j\omega) \quad (5.5)$$

$$\begin{aligned} X_i^{(\bar{n})}(j\omega) &= \frac{1}{\sqrt{\bar{n}}} \left( \frac{1}{2\pi} \right)^{\bar{n}-1} \sum_{n_1+n_2+\dots+n_m=\bar{n}} \int_{\omega_1+\omega_2+\dots+\omega_{\bar{n}}=\omega} H_{(i,p_1=n_1,p_2=n_2,\dots,p_m=n_m)}^{(\bar{n})}(j\omega_1, j\omega_2, \dots, j\omega_{\bar{n}}) \\ &\prod_{q=1}^m \prod_{p=n_0+n_1+\dots+n_{q-1}+1}^{n_1+\dots+n_q} F_q(j\omega_p) d\sigma_{\bar{n}\omega} \end{aligned} \quad (5.6)$$

where,  $n_0 = 0$ ;  $X_i^{(\bar{n})}(j\omega)$  is the  $\bar{n}^{\text{th}}$  order nonlinear output spectrum of the  $i^{\text{th}}$  output;  $F_q(j\omega_p)$  is the frequency spectrum of the  $q^{\text{th}}$  input;  $\int_{\omega_1+\omega_2+\dots+\omega_{\bar{n}}(\blacksquare)} d\sigma_{\bar{n}\omega}$  represents the integration of  $(\blacksquare)$  over the  $\bar{n}$ -dimensional hyper-plane  $\omega_1 + \omega_2 + \dots + \omega_{\bar{n}} = \omega$ ;  $H_{(i,p_1=n_1,p_2=n_2,\dots,p_m=n_m)}^{(\bar{n})}(j\omega_1, j\omega_2, \dots, j\omega_{\bar{n}})$  is the Fourier Transform of the  $\bar{n}^{\text{th}}$  order Volterra kernel  $h_{(i,p_1=n_1,p_2=n_2,\dots,p_m=n_m)}^{(\bar{n})}(\tau_1, \tau_2, \dots, \tau_{\bar{n}})$ , and is named as  $\bar{n}^{\text{th}}$  Generalized Frequency Response Function(GFRF) associated with  $i^{\text{th}}$  output and  $n_1$  first input  $f_1(t)$ ,  $n_2$  second input  $f_2(t)$ , ..., and  $n_m$   $m^{\text{th}}$  input  $f_m(t)$ . It should be noticed that for every GFRF, the sum of every input order is equal to the order of the GFRF, namely,  $n_1 + n_2 + \dots + n_m = \bar{n}$ . The GFRFs here are the extension of the frequency response function (FRF) of MIMO linear systems to nonlinear cases. Obviously, one MIMO nonlinear system can have several GFRFs at each order.



### 5.3 The NOFRFs and NOFRF transmissibility of MIMO nonlinear systems

Similar to the GFRFs of SIMO nonlinear system, the GFRFs of MIMO nonlinear systems are also multi-dimensional which makes it difficult for them to be used in analysing the nonlinear systems directly. Therefore, Lang and Peng proposed the concept of the NOFRFs of MIMO nonlinear systems to address this problem [31, 197].

For the MIMO system (5.5), the NOFRFs are defined as

$$G_{(i,p_1=n_1,\dots,p_m=n_m)}^{(\bar{n})}(j\omega) = \frac{\int_{\omega_1+\omega_2+\dots+\omega_{\bar{n}}=\omega} H_{(i,p_1=n_1,\dots,p_m=n_m)}^{(\bar{n})}(j\omega_1, \dots, j\omega_{\bar{n}}) \prod_{q=1}^m \prod_{p=n_0+n_1+\dots+n_{q-1}+1}^{n_1+\dots+n_q} F_q(j\omega_p) d\sigma_{\bar{n}\omega}}{\int_{\omega_1+\omega_2+\dots+\omega_{\bar{n}}=\omega} \prod_{q=1}^m \prod_{p=n_0+n_1+\dots+n_{q-1}+1}^{n_1+\dots+n_q} F_q(j\omega_p) d\sigma_{\bar{n}\omega}} \quad (5.7)$$

under the condition that

$$\int_{\omega_1+\omega_2+\dots+\omega_{\bar{n}}=\omega} \prod_{q=1}^m \prod_{p=n_0+n_1+\dots+n_{q-1}+1}^{n_1+\dots+n_q} F_q(j\omega_p) d\sigma_{\bar{n}\omega} \neq 0 \quad (5.8)$$

Define

$$X_{(i,p_1=n_1,\dots,p_m=n_m)}^{(\bar{n})}(j\omega) = \frac{1}{\sqrt{\bar{n}}} \left(\frac{1}{2\pi}\right)^{\bar{n}-1} \int_{\omega_1+\dots+\omega_{\bar{n}}=\omega} H_{(i,p_1=n_1,\dots,p_m=n_m)}^{(\bar{n})}(j\omega_1, \dots, j\omega_{\bar{n}}) \prod_{q=1}^m \prod_{p=n_0+n_1+\dots+n_{q-1}+1}^{n_1+\dots+n_q} F_q(j\omega_p) d\sigma_{\bar{n}\omega} \quad (5.9)$$

Eq.(5.6) can be rewritten as following.

$$X_i^{(\bar{n})}(j\omega) = \sum_{n_1+n_2+\dots+n_m=\bar{n}} X_{(i,p_1=n_1,\dots,p_m=n_m)}^{(\bar{n})}(j\omega) \quad (5.10)$$

Based on the definition of the NOFRFs in Eq. (5.7), Eq.(5.9) can be rewritten as following.

$$X_{(i,p_1=n_1,\dots,p_m=n_m)}^{(\bar{n})}(j\omega) = G_{(i,p_1=n_1,\dots,p_m=n_m)}^{(\bar{n})}(j\omega)F_{(i,p_1=n_1,\dots,p_m=n_m)}^{(\bar{n})}(j\omega) \quad (5.11)$$

where

$$F_{(i,p_1=n_1,\dots,p_m=n_m)}^{(\bar{n})}(j\omega) = \frac{1}{\sqrt{\bar{n}}} \left( \frac{1}{2\pi} \right)^{\bar{n}-1} \int_{\omega_1+\dots+\omega_{\bar{n}}=\omega} \prod_{q=1}^m \prod_{p=n_0+n_1+\dots+n_{q-1}+1}^{n_1+\dots+n_q} F_q(j\omega_p) d\sigma_{\bar{n}\omega} \quad (5.12)$$

and Eq.(5.10) can further be rewritten as following.

$$X_i^{(\bar{n})}(j\omega) = \sum_{n_1+n_2+\dots+n_m=\bar{n}} G_{(i,p_1=n_1,\dots,p_m=n_m)}^{(\bar{n})}(j\omega)F_{(i,p_1=n_1,\dots,p_m=n_m)}^{(\bar{n})}(j\omega) \quad (5.13)$$

Consequently, the frequency domain representation of system outputs in Eqs. (5.3) and (5.4) can be written as follows.

$$\left\{ \begin{array}{l} X_i(j\omega) = \sum_{\bar{n}=1}^N X_i^{(\bar{n})}(j\omega) \\ X_i^{(\bar{n})}(j\omega) = \sum_{n_1+n_2+\dots+n_m=\bar{n}} G_{(i,p_1=n_1,\dots,p_m=n_m)}^{(\bar{n})}(j\omega)F_{(i,p_1=n_1,\dots,p_m=n_m)}^{(\bar{n})}(j\omega) \end{array} \right. \quad (5.14)$$

According to [31, 197], the NOFRF  $G_{(i,p_1=n_1,\dots,p_m=n_m)}^{(\bar{n})}(j\omega)$  has the following properties:

- (i) The  $G_{(i,p_1=n_1,\dots,p_m=n_m)}^{(\bar{n})}(j\omega)$  is valid only over the frequency range where  $F_{(i,p_1=n_1,\dots,p_m=n_m)}^{(\bar{n})}(j\omega) \neq 0$ .
- (ii) As indicated by Eq. (5.11),  $G_{(i,p_1=n_1,\dots,p_m=n_m)}^{(\bar{n})}(j\omega)$  makes it possible for  $X_{(i,p_1=n_1,\dots,p_m=n_m)}^{(\bar{n})}(j\omega)$  to be represented in a manner which is similar to the description for the output frequency system response of linear systems.
- (iii)  $G_{(i,p_1=n_1,\dots,p_m=n_m)}^{(\bar{n})}(j\omega)$  is independent from the amplitude change of the input spectra by constant gains, namely,

$$G_{(i,p_1=n_1,\dots,p_m=n_m)}^{(\bar{n})}(j\omega)\Big|_{F_1=\alpha_1\bar{F}_1,\dots,F_m=\alpha_m\bar{F}_m} = G_{(i,p_1=n_1,\dots,p_m=n_m)}^{(\bar{n})}(j\omega)\Big|_{F_1=\bar{F}_1,\dots,F_m=\bar{F}_m} \quad (5.15)$$

Here,  $\alpha_1, \alpha_2, \dots, \alpha_m$  are constant gains. This means that the NOFRFs keep the same when the strength of inputs changes only by constant gains.

Similar to the NOFRF transmissibility of SIMO nonlinear system, the transmissibility of the NOFRFs between two outputs of the MIMO nonlinear system, say  $i^{\text{th}}$  and  $k^{\text{th}}$ , is defined as follows.

$$\gamma_{(i,k,p_1=n_1,\dots,p_m=n_m)}^{(N)}(j\omega) = \frac{G_{(i,p_1=n_1,\dots,p_m=n_m)}^{(N)}(j\omega)}{G_{(k,p_1=n_1,\dots,p_m=n_m)}^{(N)}(j\omega)} \quad (5.16)$$

where  $i, k \in \{1, \dots, n\}$  and  $n_1 + n_2 + \dots + n_m = N$ . In this definition, the NOFRFs are associated with the first input  $f_1(t)$  with order  $n_1$ , the second input  $f_2(t)$  with order  $n_2$ , ..., the  $m^{\text{th}}$  inputs  $f_m(t)$  with order  $n_m$ . Obviously, when  $N = 1$ , the transmissibility of the NOFRFs as defined in Eq. (5.16) reduces to the traditional concept of transmissibility for MIMO linear systems; when  $m = 1$ , the NOFRF transmissibility in Eq. (5.16) is the same as that in Eq. (4.13). Besides, as stated above, the NOFRFs are independent of the change of the system input amplitude, the NOFRF transmissibility defined in Eq.(5.16) does not change with the system input amplitude either. This is the same as the input amplitude independent property with the traditional transmissibility concept. Some important properties of the NOFRF transmissibility of MIMO nonlinear systems are summarized in Proposition 5.1 below.

**Proposition 5.1 Properties of the NOFRF transmissibility of MIMO nonlinear systems**

If the system (5.1) can be represented by the Volterra series model (5.3), and it is assumed that  $\bar{n} \in \{2,3,4, \dots, N - 1\}$ ,  $n_{i,\bar{n}}, i = 1,2, \dots, m$  are integer, and  $\sum_{i=1}^m n_{i,\bar{n}} = \bar{n}$ , the following significant properties regarding the NOFRF transmissibility of MIMO nonlinear systems can be derived.

- (i) When  $\bar{J} > 1$ , namely, there are more than one nonlinear components in system (5.1),

$$\left\{ \begin{array}{l} \gamma_{(i,k,p_1=n_1,\dots,p_m=n_m)}^{(N)}(j\omega) = \frac{G_{(i,p_1=n_1,\bar{n},\dots,p_m=n_m,\bar{n})}^{(\bar{n})}(j\omega)}{G_{(k,p_1=n_1,\bar{n},\dots,p_m=n_m,\bar{n})}^{(\bar{n})}(j\omega)} = \bar{Q}_{i,k}(j\omega) \\ \quad \text{if } 1 \leq i < k \leq J_1 - 1 \text{ or } J_J \leq i < k \leq n \\ \gamma_{(i,k,p_1=n_1,\dots,p_m=n_m)}^{(N)}(j\omega) \neq \frac{G_{(i,p_1=n_1,\bar{n},\dots,p_m=n_m,\bar{n})}^{(\bar{n})}(j\omega)}{G_{(k,p_1=n_1,\bar{n},\dots,p_m=n_m,\bar{n})}^{(\bar{n})}(j\omega)} \text{ otherwise} \end{array} \right. \quad (5.17)$$

where  $\bar{Q}_{i,k}(j\omega)$  is the same as that in Eq. (4.14), and is only dependent on the linear characteristic parameters of system (5.1), namely,  $\mathbf{M}, \mathbf{C}, \mathbf{K}$ .

- (ii) When  $\bar{J} = 1$ , that is, there is only one nonlinear component in system (5.1),

$$\gamma_{(i,k,p_1=n_1,\dots,p_m=n_m)}^{(N)}(j\omega) = \frac{G_{(i,p_1=n_1,\bar{n},\dots,p_m=n_m,\bar{n})}^{(\bar{n})}(j\omega)}{G_{(k,p_1=n_1,\bar{n},\dots,p_m=n_m,\bar{n})}^{(\bar{n})}(j\omega)} = \bar{\bar{Q}}_{i,k}(j\omega) \quad 1 \leq i < k \leq n \quad (5.18)$$

where  $\bar{\bar{Q}}_{i,k}(j\omega)$  is the same as that in Eq. (4.15), and holds the same nature as  $\bar{Q}_{i,k}(j\omega)$ , that is, dependent only on the linear parameters of the system (5.1).

In addition, if the multiple inputs are all sinusoidal, the driving frequency of  $\tilde{m}^{\text{th}}$  input is considered, that is  $\omega = \omega_{f\tilde{m}}$ , and the  $\tilde{m}^{\text{th}}$  input is on the right side of the nonlinear component, that is  $S_{\tilde{m}} \geq J_1$ , then,

$$\left\{ \begin{array}{l} \gamma_{(i,k,p_1=0,\dots,p_{\tilde{m}}=1,\dots,p_m=0)}^{(1)}(j\omega_{f\tilde{m}}) = \frac{G_{(i,p_1=n_1,\bar{n},\dots,p_m=n_m,\bar{n})}^{(\bar{n})}(j\omega_{f\tilde{m}})}{G_{(k,p_1=n_1,\bar{n},\dots,p_m=n_m,\bar{n})}^{(\bar{n})}(j\omega_{f\tilde{m}})} = Q_{i,k}(j\omega_{f\tilde{m}}) = \gamma_{(i,k,p_1=n_1,\dots,p_m=n_m)}^{(N)}(j\omega_{f\tilde{m}}) \\ \quad \text{if } 1 \leq i < k \leq J_1 - 1 \text{ or } S_{\tilde{m}} \leq i < k \leq n \\ \gamma_{(i,k,p_1=0,\dots,p_{\tilde{m}}=1,\dots,p_m=0)}^{(1)}(j\omega_{f\tilde{m}}) \neq \frac{G_{(i,p_1=n_1,\bar{n},\dots,p_m=n_m,\bar{n})}^{(\bar{n})}(j\omega_{f\tilde{m}})}{G_{(k,p_1=n_1,\bar{n},\dots,p_m=n_m,\bar{n})}^{(\bar{n})}(j\omega_{f\tilde{m}})} = Q_{i,k}(j\omega_{f\tilde{m}}) = \gamma_{(i,k,p_1=n_1,\dots,p_m=n_m)}^{(N)}(j\omega_{f\tilde{m}}) \\ \quad \text{otherwise} \end{array} \right. \quad (5.19)$$

if the  $\tilde{m}^{\text{th}}$  input is on the left side of the nonlinear component, that is  $S_{\tilde{m}} < J_1$ ,

$$\left\{ \begin{array}{l} \gamma_{(i,k,p_1=0,\dots,p_{\tilde{m}}=1,\dots,p_m=0)}^{(1)}(j\omega_{f\tilde{m}}) = \frac{G_{(i,p_1=n_1,\bar{n},\dots,p_m=n_m,\bar{n})}^{(\bar{n})}(j\omega_{f\tilde{m}})}{G_{(k,p_1=n_1,\bar{n},\dots,p_m=n_m,\bar{n})}^{(\bar{n})}(j\omega_{f\tilde{m}})} = Q_{i,k}(j\omega_{f\tilde{m}}) = \gamma_{(i,k,p_1=n_1,\dots,p_m=n_m)}^{(N)}(j\omega_{f\tilde{m}}) \\ \quad \text{if } 1 \leq i < k \leq S_{\tilde{m}} \text{ or } J_1 \leq i < k \leq n \\ \gamma_{(i,k,p_1=0,\dots,p_{\tilde{m}}=1,\dots,p_m=0)}^{(1)}(j\omega_{f\tilde{m}}) \neq \frac{G_{(i,p_1=n_1,\bar{n},\dots,p_m=n_m,\bar{n})}^{(\bar{n})}(j\omega_{f\tilde{m}})}{G_{(k,p_1=n_1,\bar{n},\dots,p_m=n_m,\bar{n})}^{(\bar{n})}(j\omega_{f\tilde{m}})} = Q_{i,k}(j\omega_{f\tilde{m}}) = \gamma_{(i,k,p_1=n_1,\dots,p_m=n_m)}^{(N)}(j\omega_{f\tilde{m}}) \\ \quad \text{otherwise} \end{array} \right. \quad (5.20)$$

**Proof:** See Appendix D.

Point (i) of Proposition 5.1 indicates that if there are multiple nonlinear components in system (5.1), no matter where the system's multiple inputs are located and what effects these inputs have on the system, the NOFRF transmissibility is the same as the ratio between other higher order NOFRFs; they are all independent of the system inputs and only dependent on system linear characteristic parameters  $M$ ,  $C$ , and  $K$  when the locations of associated system output responses are on either side of the nonlinear components. However, these relationships do not hold when at least one output location is within the span of the nonlinear components. This property is similar to that in point (i) of Proposition 4.1.

Point (ii) of Proposition 5.1 shows that, if there is only one nonlinear component in system (5.1), the NOFRF transmissibility and the ratio between other higher order NOFRFs are always the same and only dependent on system linear characteristic parameters  $M$ ,  $C$ , and  $K$ , no matter where the associated system output responses and system inputs are. However, they are only the same as the traditional linear transmissibility when associated system output responses are both on the same side of the only nonlinear component and the input forces. Otherwise, the relationships do not hold when at least one output locates within the span of the nonlinear component and the input forces. This property is similar to that in point (ii) of Proposition 4.1.

The results of Proposition 5.1 are the theoretical basis for deriving the properties of the transmissibility at nonlinearity generated frequencies for the MIMO nonlinear system in Proposition 5.3 in the following section, from which effective nonlinearity detection and localization method for MIMO nonlinear system (5.1) will be derived in Section 5.5.

## 5.4 Transmissibility at nonlinearity generated frequencies

In order to demonstrate the main ideas more clearly, the loadings to the MIMO nonlinear system are all assumed to be harmonic in this chapter. Under this assumption, the output frequency responses of MIMO system (5.1) can be easily represented using the NOFRFs as described in Proposition 5.2 below.

### Proposition 5.2 Frequency responses of MIMO systems subject to multiple harmonic inputs

When the loadings on the MIMO system (5.1) are all harmonics as follows,

$$\begin{cases} f_1(t) = \alpha_1 \sin(\omega_{f_1}t + \beta_1) \\ f_2(t) = \alpha_2 \sin(\omega_{f_2}t + \beta_2) \\ \vdots \\ f_m(t) = \alpha_m \sin(\omega_{f_m}t + \beta_m) \end{cases} \quad (5.21)$$

according to Eq. (5.14), the system output responses can be represented by

$$X_i(j\omega) = \sum_{\bar{n}=1}^N \sum_{n_1+\dots+n_m=\bar{n}} G_{(i,p_1=n_1,\dots,p_m=n_m)}^{(\bar{n})}(j\omega) F_{(i,p_1=n_1,\dots,p_m=n_m)}^{(\bar{n})}(j\omega) \quad (5.22)$$

and the terms on the right hand side of Eq. (5.22) which can make real contribution to the frequency component of the system output at frequency  $\omega$  are associated with those  $n_1, n_2, \dots, n_m$  such that

$$\begin{cases} n_1^+ + n_1^- = n_1 \\ n_2^+ + n_2^- = n_2 \\ \vdots \\ n_m^+ + n_m^- = n_m \\ n_1 + n_2 + \dots + n_m = \bar{n} \\ \bar{n} = 1, 2, \dots, N \end{cases} \quad (5.23)$$

where  $N$  is the highest order of system nonlinearity, and  $n_1^+, n_2^+, \dots, n_m^+, n_1^-, n_2^-, \dots, n_m^-$  are all nonnegative integers and satisfy the following relationship.

$$\omega = (n_1^+ - n_1^-)\omega_{f_1} + (n_2^+ - n_2^-)\omega_{f_2} + \dots + (n_m^+ - n_m^-)\omega_{f_m} \quad (5.24)$$

**Proof:** Proposition 5.2 can be derived directly by using the frequency output representation of nonlinear system in Eq.(5.14) and requirements of frequency  $\omega$  in Eq.(5.6), that is,  $\omega_1 + \omega_2 + \dots + \omega_{\bar{n}} = \omega$ .

In order to demonstrate how to determine the system output responses using Proposition 5.2, one example is provided in the following.

**Example 5.1:** Determine the system output responses where  $m = 2$ ,  $\omega_{f_1} = 30$ ,  $\omega_{f_2} = 40$  and  $N = 4$ .

Firstly, the frequency components are calculated by solving equations in Eqs. (5.23) and (5.24), the possible value of  $n_1^+, n_1^-, n_2^+, n_2^-, \bar{n}$  and  $\omega$  are listed in the Table 5.1.

Table 5.1 Frequency components when  $m = 2$ ,  $\omega_{f_1} = 30$ ,  $\omega_{f_2} = 40$  and  $N = 4$

$n_1^+$	$n_1^-$	$n_2^+$	$n_2^-$	$\bar{n}$	$\omega$		$n_1^+$	$n_1^-$	$n_2^+$	$n_2^-$	$\bar{n}$	$\omega$	
0	0	1	1	2	$(1-1)\omega_{f_2} = 0$		2	0	0	0	2	$2\omega_{f_1} = 60$	60
0	0	2	2	4	$(2-2)\omega_{f_2} = 0$		2	0	1	1	4	$2\omega_{f_1} - (1-1)\omega_{f_2} = 60$	
1	1	0	0	2	$(1-1)\omega_{f_1} = 0$	0	3	1	0	0	4	$(3-1)\omega_{f_1} = 60$	
1	1	1	1	4	$(1-1)\omega_{f_1} + (1-1)\omega_{f_2} = 0$		1	0	1	0	2	$\omega_{f_1} + \omega_{f_2} = 70$	70
2	2	0	0	4	$(2-2)\omega_{f_1} = 0$		1	0	2	1	4	$\omega_{f_1} + (2-1)\omega_{f_2} = 70$	
0	1	1	0	2	$-\omega_{f_1} + \omega_{f_2} = 10$		2	1	1	0	4	$(2-1)\omega_{f_1} + \omega_{f_2} = 70$	
0	1	2	1	4	$-\omega_{f_1} + (2-1)\omega_{f_2} = 10$	10	0	0	2	0	2	$2\omega_{f_2} = 80$	80
1	2	1	0	4	$(1-2)\omega_{f_1} + \omega_{f_2} = 10$		0	0	3	1	4	$(3-1)\omega_{f_2} = 80$	
0	2	2	0	4	$-2\omega_{f_1} + 2\omega_{f_2} = 20$		1	1	2	0	4	$(1-1)\omega_{f_1} + 2\omega_{f_2} = 80$	
2	0	0	1	3	$2\omega_{f_1} - \omega_{f_2} = 20$	20	0	1	3	0	4	$-1\omega_{f_1} + 3\omega_{f_2} = 90$	90
1	0	0	0	1	$\omega_{f_1} = 30$		3	0	0	0	3	$3\omega_{f_1} = 90$	
1	0	1	1	3	$\omega_{f_1} - (1-1)\omega_{f_2} = 30$	30	2	0	1	0	3	$2\omega_{f_1} + \omega_{f_2} = 100$	
2	1	0	0	3	$(2-1)\omega_{f_1} = 30$		1	0	2	0	3	$\omega_{f_1} + 2\omega_{f_2} = 110$	110
0	0	1	0	1	$\omega_{f_2} = 40$		0	0	3	0	3	$3\omega_{f_2} = 120$	120
0	0	2	1	3	$(2-1)\omega_{f_2} = 40$	40	4	0	0	0	4	$4\omega_{f_1} = 120$	
1	1	1	0	3	$(1-1)\omega_{f_1} + \omega_{f_2} = 40$		3	0	1	0	4	$3\omega_{f_1} + \omega_{f_2} = 130$	
0	1	2	0	3	$\omega_{f_1} + 2\omega_{f_2} = 50$	50	2	0	2	0	4	$2\omega_{f_1} + 2\omega_{f_2} = 140$	140
3	0	0	1	4	$3\omega_{f_1} - \omega_{f_2} = 50$		1	0	3	0	4	$\omega_{f_1} + 3\omega_{f_2} = 150$	150
							0	0	4	0	4	$4\omega_{f_2} = 160$	160





frequencies is overlapped with that of driving frequencies, for example,  $\omega_{f_1} - (1 - 1)\omega_{f_2} = \omega_{f_1} = 30$ , the overlapped frequencies are treated as driving frequencies. Furthermore, the first order NOFRFs does not contribute to the frequency components at nonlinearity generated frequencies. This can be concluded easily by observing the system responses at nonlinearity generated frequencies represented in Eq.(5.26).

Because the NOFRFs cannot be measured directly, but it is possible to measure the system output responses by installing sensors at corresponding locations in practice, the transmissibility of system output responses instead of the NOFRF transmissibility will be used for the system analysis and nonlinearity localization. Besides, Proposition 5.1 indicates that, for nonlinear MIMO system (5.1), the NOFRF transmissibility is independent of the system inputs but only dependent on the system linear characteristic parameters  $\mathbf{M}$ ,  $\mathbf{C}$ , and  $\mathbf{K}$  when the locations of associated system output responses are on the same side of the nonlinear components. Considering this and the fact revealed in Proposition 5.2 that when subject to sinusoidal inputs with frequencies  $\omega_{f_1}, \omega_{f_2} \dots \omega_{f_m}$ , nonlinearity will induce nonlinearity generated frequencies in the output responses of system (5.1), including  $2\omega_{f_1}, 2\omega_{f_2}, \dots$  etc super-harmonics and  $\omega_{f_1} + \omega_{f_2}$ , etc combined frequencies, the concept of the transmissibility at nonlinearity generated frequencies is introduced and defined as the ratio of the system responses on two consecutive masses at nonlinearity generated frequencies, that is

$$ST_{i,i+1}^{NL}(j\omega_{NL}) = \frac{X_i(j\omega_{NL})}{X_{i+1}(j\omega_{NL})} \quad (5.27)$$

where,  $X_i(j\omega_{NL})$  and  $X_{i+1}(j\omega_{NL})$  are the spectrum of the  $i^{\text{th}}$  and  $(i + 1)^{\text{th}}$  system outputs respectively;  $\omega_{NL}$  is a nonlinearity generated frequency. Apparently, the concept of transmissibility at super-harmonics proposed in Chapter 4 is a special case of transmissibility at nonlinearity generated frequencies.

The relationship between the transmissibility at nonlinearity generated frequencies

and the NOFRF transmissibility is summarized in Proposition 5.3 as follows.

**Proposition 5.3 The properties of transmissibility at nonlinearity generated frequencies**

(i) When there are more than one nonlinear components in system (5.1), that is  $\bar{J} > 1$ , if two consecutive masses of the system are both on the left or right side of the nonlinear components, namely,  $1 \leq i \leq J_1 - 2$  or  $J_{\bar{J}} \leq i \leq n - 1$ , then

$$ST_{i,i+1}^{NL}(j\omega_{NL}) = \gamma_{(i,i+1,p_1=n_1,\dots,p_m=n_m)}^{(N)}(j\omega_{NL}) = \bar{Q}_{i,i+1}(j\omega_{NL}) \quad (5.28)$$

If at least one mass is within the range of nonlinear components, namely,  $J_1 - 1 \leq i \leq J_{\bar{J}} - 1$ , then

$$ST_{i,i+1}^{NL}(j\omega_{NL}) \neq \gamma_{(i,i+1,p_1=n_1,\dots,p_m=n_m)}^{(N)}(j\omega_{NL}) \neq \bar{Q}_{i,i+1}(j\omega_{NL}), \quad (5.29)$$

(ii) When there is only one nonlinear component in the system, that is  $\bar{J} = 1$ , then

$$ST^{i,i+1}(j\omega_{NL}) = \gamma_{(i,i+1,p_1=n_1,\dots,p_m=n_m)}^{(N)}(j\omega_{NL}) = \bar{Q}_{i,i+1}(j\omega_{NL}), i = 1, \dots, n - 1 \quad (5.30)$$

and if the driving frequency of  $\tilde{m}^{\text{th}}$  input is considered, that is  $\omega = \omega_{f\tilde{m}}$ , and the  $\tilde{m}^{\text{th}}$  input is applied on the  $S_{\tilde{m}}^{\text{th}}$  mass, then,

$$\left\{ \begin{array}{l} ST^{i,i+1}(j\omega_{f\tilde{m}}) = \gamma_{(i,i+1,p_1=0,\dots,p_{\tilde{m}}=1,\dots,p_m=0)}^{(1)}(j\omega_{f\tilde{m}}) = Q_{i,i+1}(j\omega_{f\tilde{m}}), \tilde{m} = 1, 2, \dots, m \\ \quad \text{if } 1 \leq i \leq S_{\tilde{m}} - 1 \text{ or } J_1 \leq i < n \text{ when } S_{\tilde{m}} < J_1 \\ \quad \text{or if } 1 \leq i \leq J_1 - 2 \text{ or } S_{\tilde{m}} \leq i < n \text{ when } S_{\tilde{m}} \geq J_1 \\ ST^{i,i+1}(j\omega_{f\tilde{m}}) \neq \gamma_{(i,i+1,p_1=0,\dots,p_{\tilde{m}}=1,\dots,p_m=0)}^{(1)}(j\omega_{f\tilde{m}}) = Q_{i,i+1}(j\omega_{f\tilde{m}}) \tilde{m} = 1, 2, \dots, m \\ \quad \text{otherwise} \end{array} \right. \quad (5.31)$$

**Proof:** See Appendix E.

Proposition 5.3 describes the relationship between the transmissibility of the NOFRFs and transmissibility of system responses at nonlinearity generated frequencies for the MIMO nonlinear system (5.1), which is an extension of the results for SIMO system described in Proposition 4.3.

Result (i) of Proposition 5.3 indicates in the case that there are multiple nonlinear components in the MIMO nonlinear system, if the locations of outputs involved in the transmissibility evaluation are on the same side of nonlinear components, the transmissibility of the system responses at nonlinearity generated frequencies is equal to the corresponding NOFRF transmissibility; and they only depend on the system linear characteristic parameters and are independent from the system inputs. Otherwise, the conclusions do not hold. Therefore, the locations of nonlinear components can be identified from the analysis of transmissibility of the system responses at nonlinearity generated frequencies when there are multiple nonlinear components in the MIMO nonlinear system.

First part of result (ii) of Proposition 5.3 indicates that in the case that there is only one nonlinearity in the MIMO nonlinear system, the transmissibility of the system responses at nonlinearity generated frequencies is always the same as the NOFRF transmissibility and they also only depend on the system linear characteristic parameters and are independent of the system inputs, no matter where the locations of output responses are. Therefore, the number of nonlinear components (one or multiple) can be determined by exploiting the sensitivity of the transmissibility of the system responses at nonlinearity generated frequencies.

Second part of result (ii) of Proposition 5.3 indicates that in the case that there is only one nonlinearity in the MIMO nonlinear system, if the locations of outputs involved in the transmissibility evaluation are on the same side of the nonlinear component and any one of system inputs, the transmissibility of the system responses at corresponding driving frequency is equal to the NOFRF transmissibility and they all depend on the system linear characteristic parameters and are independent from the system inputs. Therefore, the location of the only nonlinear component can be identified by analysing the transmissibility of the system responses at a driving frequency.

For MIMO nonlinear system (5.1), many features discussed above are unique with the transmissibility at nonlinearity generated frequencies while the transmissibility at driving frequencies, that is, the transmissibility traditionally used for system analysis is generally dependent on the locations of inputs.

## 5.5 Detection and location of damage via nonlinear features using a transmissibility analysis method for MIMO nonlinear systems

### 5.5.1 The method

The observations from Proposition 5.3 above show that, when outputs involved in the transmissibility evaluation are located on the same side of nonlinear components, the transmissibility of system responses at nonlinearity generated frequencies only depends on the system linear characteristic parameters and is, to a great extent, insensitive to loading conditions. These are properties that can be exploited to conduct structural health monitoring and damage localization under changing environments. Consequently, a new transmissibility analysis method for the detection and location of damage with nonlinear features for MIMO structural system (5.1) can be proposed under the following assumptions.

The output responses of system (5.1) to two loading conditions

$$\begin{cases} f_1(t) = f_1^{(1)}(t) = \alpha_1^{(1)} \sin(\omega_{f_1} t + \beta_1^{(1)}) \\ f_2(t) = f_2^{(1)}(t) = \alpha_2^{(1)} \sin(\omega_{f_2} t + \beta_2^{(1)}) \\ \dots \\ f_m(t) = f_m^{(1)}(t) = \alpha_m^{(1)} \sin(\omega_{f_m} t + \beta_m^{(1)}) \end{cases} \quad (5.32)$$

and

$$\begin{cases} f_1(t) = f_1^{(2)}(t) = \alpha_1^{(2)} \sin(\omega_{f_1} t + \beta_1^{(2)}) \\ f_2(t) = f_2^{(2)}(t) = \alpha_2^{(2)} \sin(\omega_{f_2} t + \beta_2^{(2)}) \\ \dots \\ f_m(t) = f_m^{(2)}(t) = \alpha_m^{(2)} \sin(\omega_{f_m} t + \beta_m^{(2)}) \end{cases} \quad (5.33)$$

can be obtained, respectively, so that two sets of transmissibility analysis results

$$\begin{cases} ST1^{i,i+1}(j\omega) = \frac{X_i^1(j\omega)}{X_{i+1}^1(j\omega)} = \frac{X_i(j\omega)}{X_{i+1}(j\omega)} \Big|_{f_1(t)=f_1^{(1)}(t), \dots, f_m(t)=f_m^{(1)}(t)} \\ ST2^{i,i+1}(j\omega) = \frac{X_i^2(j\omega)}{X_{i+1}^2(j\omega)} = \frac{X_i(j\omega)}{X_{i+1}(j\omega)} \Big|_{f_1(t)=f_1^{(2)}(t), \dots, f_m(t)=f_m^{(2)}(t)} \end{cases} \quad (5.34)$$

and their differences

$$S\delta^{i,i+1}(j\omega) = |ST1^{i,i+1}(j\omega) - ST2^{i,i+1}(j\omega)| \quad (5.35)$$

can be obtained, where,  $[\alpha_1^{(1)}, \alpha_2^{(1)}, \dots, \alpha_m^{(1)}]^T \neq [\alpha_1^{(2)}, \alpha_2^{(2)}, \dots, \alpha_m^{(2)}]^T$  so that second loading condition is different from first one;  $i = 1, \dots, n - 1$ ;  $X_i^1(j\omega)$  and  $X_i^2(j\omega)$  are the spectra of the responses of the system subject to the first and second loading conditions, respectively, and  $\omega$  are frequencies observed in the spectra of outputs which can be determined by solving Eqs. (5.23) and (5.24).

The new method involves procedures similar to that in Section 4.5.2 and can be described as follows.

Step 1) Evaluate the spectra of the output responses of system (5.1) to two different loading conditions as shown in Eqs. (5.32) and (5.33), respectively and determine the amplitudes of these observed spectra, that is,  $X_i^1(j\omega)$  and  $X_i^2(j\omega)$ , for  $i = 1, \dots, n$ ; determine  $N$  as the highest order of the nonlinearity which takes a significant part in the system responses from observing the spectra of the system outputs and calculate all nonlinearity generated frequencies  $\omega_{NL}$  according to the highest order of the nonlinearity  $N$  and the frequencies of system inputs by using Proposition 5.2; evaluate the ratio between the system response at every nonlinearity generated frequency and maximum amplitude of system inputs and calculate the value of index  $IND_1$  as defined below to represent the strength of nonlinearity generated frequencies in the system output responses

$$IND_1 = \max \left\{ \left| \frac{X_i^1(j\omega_{NL})}{\max\{X_i^1(j\omega_{f1}), \dots, X_i^1(j\omega_{fm})\}} \right|, \left| \frac{X_i^2(j\omega_{NL})}{\max\{X_i^2(j\omega_{f1}), \dots, X_i^2(j\omega_{fm})\}} \right|, i = 1, \dots, n \right\} \quad (5.36)$$

If

$$IND_1 \geq \varepsilon_1 \quad (5.37)$$

then it can be concluded that there exists nonlinear components in the system. Otherwise, there are no such components in the system. In Eq. (5.37),  $\varepsilon_1$  is a threshold to be determined a priori.

Step 2) If Step 1) indicates there is nonlinear component in the system, select a nonlinearity generated frequency  $\omega_{NL1}$  such that both  $X_i^1(j\omega_{NL1})$   $i = 1, \dots, n$  and  $X_i^2(j\omega_{NL1})$   $i = 1, \dots, n$  have significant amplitudes. Calculate  $ST1^{i,i+1}(j\omega_{NL1})$ ,  $ST2^{i,i+1}(j\omega_{NL1})$ , and  $S\delta^{i,i+1}(j\omega_{NL1})$  for  $i = 1, \dots, n - 1$  using Eqs. (5.34) and (5.35). Then, evaluate

$$S\delta_{\max}(j\omega_{NL1}) = \max\{S\delta^{i,i+1}(j\omega_{NL1}), i \in \{1, 2, \dots, n - 1\}\} \quad (5.38)$$

to check whether

$$S\delta_{\max}(j\omega_{NL1}) \leq \varepsilon_2 \quad (5.39)$$

where  $\varepsilon_2$  is another priori determined threshold. If Eq. (5.39) holds, it can be concluded that there exists only one nonlinear component in the system. Otherwise, there are more than one nonlinear components.

Step 3) If Step 2) indicates there exists only one nonlinear component in the system, select the driving frequency of the  $\widetilde{m}1^{\text{th}}$  input, namely,  $\omega_{f\widetilde{m}1}$ , such that both  $X_i^1(\omega_{f\widetilde{m}1})$   $i = 1, \dots, n$  and  $X_i^2(\omega_{f\widetilde{m}1})$   $i = 1, \dots, n$  have significant amplitudes, calculate  $ST1^{i,i+1}(j\omega_{f\widetilde{m}1})$ ,  $ST2^{i,i+1}(j\omega_{f\widetilde{m}1})$  and  $S\delta^{i,i+1}(j\omega_{f\widetilde{m}1})$  for  $i = 1, \dots, n - 1$  using Eqs (5.34) and (5.35). Then evaluate

$$S\delta_{\max}(j\omega_{f\widetilde{m}_1}) = \max\{S\delta^{i,i+1}(j\omega_{f\widetilde{m}_1}), i \in \{1, 2, \dots, n-1\}\} \quad (5.40a)$$

and

$$\overline{S\delta}^{i,i+1}(j\omega_{f\widetilde{m}_1}) = \frac{S\delta^{i,i+1}(j\omega_{f\widetilde{m}_1})}{S\delta_{\max}(j\omega_{f\widetilde{m}_1})} \text{ for } i = 1, \dots, n-1 \quad (5.41a)$$

to find those  $i$ 's such that

$$\overline{S\delta}^{i,i+1}(j\omega_{f\widetilde{m}_1}) \geq \varepsilon_3 \quad (5.42a)$$

where  $\varepsilon_3$  is again a priori determined threshold.

Denote those  $i$ 's such that Eq. (5.42a) holds respectively as

$$i', i' + 1, \dots, i' + m' - 1$$

where  $m' \geq 1$ .

Then, for  $i$ 's, there are only two possibilities which are  $S_{\widetilde{m}_1} = i'$  or  $S_{\widetilde{m}_1} = i' + m'$ . If  $S_{\widetilde{m}_1} = i'$ , it can be concluded that the only nonlinear component is located between mass  $(i' + m' - 1)$  and mass  $(i' + m')$ . Otherwise,  $S_{\widetilde{m}_1} = i' + m'$ , it can be concluded that the only nonlinear component is located between mass  $i'$  and mass  $(i' + 1)$ .

Until now, two possible locations of nonlinear component have been identified. But if the location of the  $\widetilde{m}_1^{\text{th}}$  input is unknown, the exact location of the only nonlinear component still cannot be determined. Therefore, more information is needed.

For this purpose, the calculation above is repeated by considering the driving frequency of another input, say the  $\widetilde{m}_2^{\text{th}}$  input, with driving frequency  $\omega_{f\widetilde{m}_2} \neq \omega_{f\widetilde{m}_1}$ , calculating  $ST1^{i,i+1}(j\omega_{f\widetilde{m}_2})$ ,  $ST2^{i,i+1}(j\omega_{f\widetilde{m}_2})$  and  $S\delta^{i,i+1}(j\omega_{f\widetilde{m}_2})$  for  $i = 1, \dots, n-1$  using Eqs (5.34) and (5.35), and evaluating

$$S\delta_{\max}(j\omega_{f\bar{m}2}) = \max\{S\delta^{i,i+1}(j\omega_{f\bar{m}2}), i \in \{1, 2, \dots, n-1\}\} \quad (5.40b)$$

and

$$\overline{S\delta}^{i,i+1}(j\omega_{f\bar{m}2}) = \frac{S\delta^{i,i+1}(j\omega_{f\bar{m}2})}{S\delta_{\max}(j\omega_{f\bar{m}2})} \text{ for } i = 1, \dots, n-1 \quad (5.41b)$$

to find those  $i$ 's such that

$$\overline{S\delta}^{i,i+1}(j\omega_{f\bar{m}2}) \geq \varepsilon_3 \quad (5.42b)$$

Denote those  $i$ 's such that Eq. (5.42b) holds respectively as

$$\bar{i}, \bar{i} + 1, \dots, \bar{i} + \bar{m} - 1$$

where  $\bar{m} \geq 1$ .

Similarly, there are also only two possibilities which are  $S_{\bar{m}2} = \bar{i}$  or  $S_{\bar{m}2} = \bar{i} + \bar{m}$ . If  $S_{\bar{m}2} = \bar{i}$ , it can be concluded that the only nonlinear component is located between mass  $(\bar{i} + \bar{m} - 1)$  and mass  $(\bar{i} + \bar{m})$ . Otherwise,  $S_{\bar{m}2} = \bar{i} + \bar{m}$ , it can be concluded that the only nonlinear component is located between mass  $\bar{i}$  and mass  $(\bar{i} + 1)$ .

Because it has been concluded that there is only one nonlinear component in the system in Step 2), two of the four numbers  $i', i' + m' - 1, \bar{i}$  and  $\bar{i} + \bar{m} - 1$  must be the same. By finding this number and denoting it as  $J'$ , it can then be concluded that the only nonlinear component is located between mass  $J'$  and mass  $(J' + 1)$ .

Step 4) If Step 2) indicates there exist more than one nonlinear components in the system, evaluate

$$\overline{S\delta}^{i,i+1}(j\omega_{NL1}) = \frac{S\delta^{i,i+1}(j\omega_{NL1})}{S\delta_{\max}(j\omega_{NL1})} \text{ for } i = 1, \dots, n-1 \quad (5.43)$$

to find those  $i$ 's such that



$$\overline{S\delta}^{i,i+1}(j\omega_{NL1}) \geq \varepsilon_4 \tag{5.44}$$

where  $\varepsilon_4$  is also a priori determined threshold. Denote those  $i$ 's such that (5.44) hold as

$$i'', i'' + 1, \dots, i'' + m'' - 1$$

where  $m'' > 1$ . Then, it can be concluded that these nonlinear components are located between mass  $i''$  and mass  $i'' + m''$ .

Similar to the method for detection and localization of damage with nonlinear features in Chapter 4, each step and the order of the whole procedure in the method above can be also represented by the flow chart shown in Fig. 5.2.

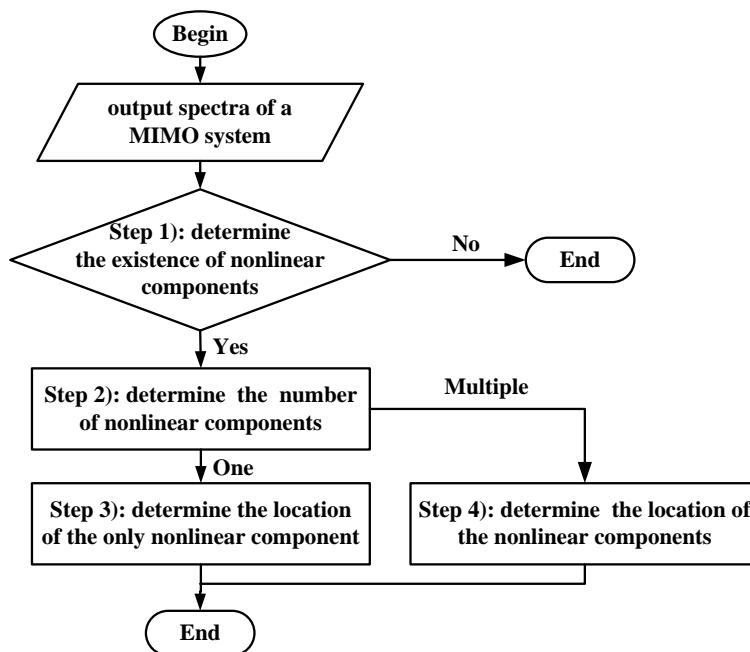


Fig. 5.2 Flow chart of damage detection and localization method for MIMO systems

The theoretical basis of each step, determination of the threshold parameters and advantage of the new nonlinearity detection and location method described above will be discussed in the following remarks.

### 5.5.2 Remarks

- a) Step 1) of the method is based on the well-known fact that nonlinearity will produce new frequency components in the system output responses. Step 2) exploits the property of system (5.1) described in the first point of Proposition 5.3 (ii), which indicates if there is only one nonlinear component in the system, the transmissibility at nonlinearity generated frequency is completely determined by the system linear characteristic parameters and, therefore, independent of the system inputs. The theoretical basis of Step 3) is the second point of Proposition 5.3 (ii), which reveals an important relationship between the transmissibility at driving frequencies and the location of the only nonlinear component in the system. Step 4) makes use of the property of the transmissibility at nonlinearity generated frequencies of system (5.3) described by Proposition 5.3 (i), which shows where the transmissibility at nonlinearity generated frequencies is only dependent on the system linear characteristic parameters and, therefore, independent of the system inputs and where this is not the case.
- b) Similar to that in Chapter 4,  $\varepsilon_1, \varepsilon_2, \varepsilon_3, \varepsilon_4$  are four threshold parameters in the method which need to be determined a priori from experimental data using statistical analyses as described by Remark b) in section 4.5.3.
- c) The method in Chapter 4 assumes that the location of input is known a priori, however, it can be seen from Step 3) and Step 4) above that when the system is subject to multiple inputs with different driving frequencies, the locations of nonlinear components can always be identified without any knowledge about the locations of these inputs. Thus, the application of the proposed method is independent from the locations of inputs. This is a distinctive advantage of the new nonlinearity detection and location method proposed in this chapter.

- d) According to results of Proposition 5.3, the transmissibility of the system responses at nonlinearity generated frequencies is independent from the system inputs if the locations of outputs involved in the transmissibility evaluation are on the same side of the nonlinear components; but the transmissibility at driving frequency always depends on the locations of system inputs. Therefore, in the cases where there are more than one nonlinear components in the system, the method allows the multiple inputs in the considered different loading conditions to be at different locations. However, in the cases where there is only one nonlinear component in the system, the method requires the locations of the multiple inputs in the considered different loading conditions to be the same.

## 5.6 Simulation studies

In order to verify the effectiveness of the above proposed approach, three simulation studies are conducted in this section; the 10DOF system used in Chapter 4 but subject to multiple inputs is considered again for the simulation studies.

### 5.6.1 Simulation study: case 1

In this case, there are three ( $\bar{J} = 3$ ) nonlinear components in the system, which are the 3<sup>rd</sup>, 5<sup>th</sup> and 6<sup>th</sup> springs. So  $J_1 = 3, J_2 = 5, J_3 = 6$ . Two loading conditions are considered as

$$\begin{cases} f_1(t) = f_1^{(1)}(t) = 3 \sin(30\pi t) \\ f_2(t) = f_2^{(1)}(t) = 6 \sin(40\pi t) \end{cases} \quad (5.45)$$

and

$$\begin{cases} f_1(t) = f_1^{(2)}(t) = 6 \sin(30\pi t) \\ f_2(t) = f_2^{(2)}(t) = 12 \sin(40\pi t) \end{cases} \quad (5.46)$$

respectively. In this case, two loading conditions are applied on the same locations, say,  $S_1 = 3$  and  $S_2 = 8$ .

The new method was applied to the spectra of the system output responses under the two loading conditions, that is,

$$X_i^1(j\omega) \text{ and } X_i^2(j\omega), i = 1, \dots, 10.$$

The highest order of system nonlinearity is determined to be  $N = 3$  from the observation on spectra of the system output responses, for example, the output response of the 5<sup>th</sup> mass when the system is subject to the first loading condition as shown Fig. 5.3. So the possible frequencies can be calculated by Eqs. (5.23) and (5.24) and nonlinearity related frequencies are

$$\omega_{NL} = \{0, 10\pi, 20\pi, 50\pi, 60\pi, 70\pi, 80\pi, 90\pi, 100\pi, 110\pi, 120\pi\} \quad (5.47)$$

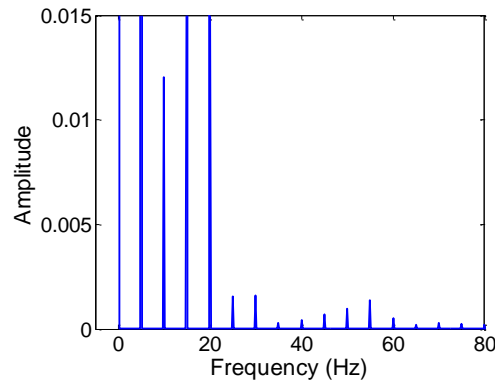


Fig. 5.3 Output responses of the 5<sup>th</sup> mass when the system is subject to the 1<sup>st</sup> loading condition

In this simulation study, the value of linear and nonlinear parameters of the system are the same as that in simulation studies in Section 4.6. Therefore, the value of thresholds  $\varepsilon_1$ ,  $\varepsilon_2$ ,  $\varepsilon_3$  and  $\varepsilon_4$  are assumed the same as that listed in Table 4.1.

The results of the simulation study obtained in each step of the proposed method are given as follows.

**Step 1)**

In this case, the ratio between the system response at every nonlinearity generated frequency in Eq. (5.47) and maximum amplitude of system inputs was calculated and the index  $IND_1$  was evaluated using (5.36) as

$$IND_1 = \max \left\{ \left| \frac{X_i^1(j\omega_{NL})}{\max\{X_i^1(j\omega_{f1}), X_i^1(j\omega_{f2})\}} \right|, \left| \frac{X_i^2(j\omega_{NL})}{\max\{X_i^2(j\omega_{f1}), X_i^2(j\omega_{f2})\}} \right|, i = 1, \dots, 10 \right\}$$

$$= 0.3591 \geq \varepsilon_1 = 8.42 \times 10^{-6}$$

where  $\omega_{NL}$  is shown in Eq. (5.47). Therefore, it is concluded that nonlinear components exist in the system.

**Step 2)**

At this step, the nonlinearity generated frequency  $\omega_{NL1} = \omega_{f2} - \omega_{f1} = 10\pi$  was used. So

$$ST1^{i,i+1}(j10\pi), ST2^{i,i+1}(j10\pi), \text{ and } S\delta^{i,i+1}(j10\pi) \quad i = 1, \dots, 9$$

were evaluated using Eqs. (5.34) and (5.35). Then,  $S\delta_{\max}(j10\pi)$  was determined using (5.38), the result is

$$S\delta_{\max}(j10\pi) = 0.1398 > \varepsilon_2 = 0.0099$$

So it is known that there are more than one nonlinear components in the system.

**Step 4)**

As Step 2) has shown that there are more than one nonlinear components in the system, the two loading conditions can be applied on any locations, in this case, they are applied on the same locations; and Step 4) rather than Step 3) of the proposed method is needed in this case. At this step,  $\overline{S\delta}^{i,i+1}(j\omega_{NL1}) = \overline{S\delta}^{i,i+1}(j10\pi)$ ,  $i = 1, \dots, 9$  were evaluated using (5.43). The results are shown in Table 5.2, in which it can be observed that

$$\overline{S\delta}^{i,i+1}(j10\pi) \geq \varepsilon_4 = 0.0015, \quad i = 2,3,4,5$$

Therefore,  $i'' = 2$  and  $m'' = 4$ , and it can be concluded that nonlinear components are located between mass  $i'' = 2$  and mass  $i'' + m'' = 6$  in the system.

Table 5.2 The value of  $\overline{S\delta}^{i,i+1}(j\omega_{NL1})$  when the 3<sup>rd</sup>, 5<sup>th</sup> and 6<sup>th</sup> springs are nonlinear

$i$	$\overline{S\delta}^{i,i+1}(j\omega_{NL1})$	$i$	$\overline{S\delta}^{i,i+1}(j\omega_{NL1})$	$i$	$\overline{S\delta}^{i,i+1}(j\omega_{NL1})$
1	$3.96 \times 10^{-6}$	4	0.866718	7	$3.73 \times 10^{-6}$
2	1	5	0.501518	8	$6.79 \times 10^{-6}$
3	0.246067	6	$3.84 \times 10^{-6}$	9	$4.29 \times 10^{-6}$

Obviously, the conclusions reached at each step are all consistent with the real situation of the simulated system. So the effectiveness of the proposed method is verified by this simulation study.

### 5.6.2 Simulation study: case 2

This study was conducted in order to demonstrate the effectiveness of the proposed method when the loading inputs are applied on different locations in the considered different loading conditions. In this case study, the loading in the first loading condition is shown in Eq. (5.45) and applied on the 3<sup>rd</sup> and 8<sup>th</sup> masses respectively, namely,  $S_1^{(1)} = 3$ ,  $S_2^{(1)} = 8$ , and the loading in the second loading condition is shown in Eq. (5.46) and is applied on the 4<sup>th</sup> and 7<sup>th</sup> masses respectively, namely,  $S_1^{(2)} = 4$ ,  $S_2^{(2)} = 7$ . The other conditions are exactly the same as that in case study 1. The results of the simulation study obtained in each step of the proposed method are given as

follows.

**Step 1)**

In this case, the ratio between the system response at every nonlinearity generated frequency in Eq. (5.47) and maximum amplitude of system inputs is calculated and the index  $IND_1$  was evaluated using (5.36) as

$$IND_1 = \max \left\{ \left| \frac{X_i^1(j\omega_{NL})}{\max\{X_i^1(j\omega_{f1}), X_i^1(j\omega_{f2})\}} \right|, \left| \frac{X_i^2(j\omega_{NL})}{\max\{X_i^2(j\omega_{f1}), X_i^2(j\omega_{f2})\}} \right|, i = 1, \dots, 10 \right\}$$

$$= 0.3591 \geq \varepsilon_1 = 8.42 \times 10^{-6}$$

where  $\omega_{NL}$  is shown in Eq. (5.47). Therefore, it is concluded that nonlinear component exists in the system.

**Step 2)**

At this step, the nonlinearity generated frequency  $\omega_{NL1} = \omega_{f2} - \omega_{f1} = 10\pi$  was used again. So

$$ST1^{i,i+1}(j10\pi), ST2^{i,i+1}(j10\pi), \text{ and } S\delta^{i,i+1}(j10\pi) \quad i = 1, \dots, 9$$

were evaluated using Eqs. (5.34) and (5.35). Then,  $S\delta_{\max}(j10\pi)$  was determined using Eq. (5.38); the result is

$$S\delta_{\max}(j10\pi) = 0.4255 > \varepsilon_2 = 0.0099$$

So it is known that there are more than one nonlinear components in the system.

**Step 4)**

As Step 2) has shown that there are more than one nonlinear components in the system, Step 4) rather than Step 3) of the proposed method is used in this case. At this step,  $\overline{S\delta}^{i,i+1}(j\omega_{NL1}) = \overline{S\delta}^{i,i+1}(j10\pi)$ ,  $i = 1, \dots, 9$  were evaluated using Eq. (5.43).

The results are shown in Table 5.3, in which it can be observed that

$$\overline{S\delta}^{i,i+1}(j10\pi) \geq \varepsilon_4 = 0.0015, \quad i = 2,3,4,5$$

Therefore  $i'' = 2$  and  $m'' = 4$ , and it can be concluded that nonlinear components are located between mass  $i'' = 2$  and mass  $i'' + m'' = 6$  in the system.

Table 5.3 The value of  $\overline{S\delta}^{i,i+1}(j\omega_{NL1})$  when the 3<sup>rd</sup>, 5<sup>th</sup> and 6<sup>th</sup> springs are nonlinear

$i$	$\overline{S\delta}^{i,i+1}(j\omega_{NL1})$	$i$	$\overline{S\delta}^{i,i+1}(j\omega_{NL1})$	$i$	$\overline{S\delta}^{i,i+1}(j\omega_{NL1})$
1	$9.74 \times 10^{-6}$	4	0.952396	7	$3.35 \times 10^{-6}$
2	1	5	0.540621	8	$3.18 \times 10^{-6}$
3	0.28236	6	$2.87 \times 10^{-6}$	9	$1.5 \times 10^{-6}$

Obviously, the conclusions reached at each step are all consistent with the real situation of the simulated system. So the effectiveness of the proposed method is again verified by this simulation study.

### 5.6.3 Simulation study: case 3

In this case, there is only one ( $\bar{J} = 1$ ) nonlinear component in the system, which is the 6<sup>th</sup> spring. The same two loading conditions as in simulation study case 1 (shown in Eqs.(5.45) and (5.46) and  $S_1 = 3$  and  $S_2 = 8$ ) were considered. The new method was applied to the spectra of the output responses of the system under the two loading conditions. Again,  $N$  was determined as 3 from the observation on spectra of the system output responses, for example, the output response of the 8th mass when the system is subject to the second loading condition as shown Fig. 5.4, and  $\omega_{NL}$  is the same as that in Eq.(5.47), and the same threshold parameters  $\varepsilon_1, \varepsilon_2, \varepsilon_3, \varepsilon_4$  as given in Table 4.1 were used. The results obtained in each step of the method are given as follows.



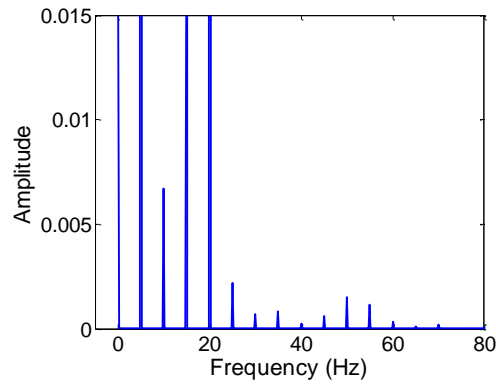


Fig. 5.4 Output response of the 8<sup>th</sup> mass when the system is subject to the 2<sup>nd</sup> loading condition

**Step 1)**

In this case, the ratio between the system response at every nonlinearity generated frequency in Eq.(5.47) and maximum amplitude of system inputs is calculated and the index  $IND_1$  was evaluated by (5.36) as

$$IND_1 = \max \left\{ \left| \frac{X_i^1(j\omega_{NL})}{\max\{X_i^1(j\omega_{f1}), X_i^1(j\omega_{f2})\}} \right|, \left| \frac{X_i^2(j\omega_{NL})}{\max\{X_i^2(j\omega_{f1}), X_i^2(j\omega_{f2})\}} \right|, i = 1, \dots, 10 \right\}$$

$$= 0.1348 \geq \varepsilon_1 = 8.42 \times 10^{-6}$$

So, damage with nonlinear features exists in the system.

**Step 2)**

At this step,  $\omega_{NL1} = \omega_{f2} - \omega_{f1} = 10\pi$ . Therefore, in the same way as in Step 2), simulation case study 1,  $S\delta_{\max}(j\omega_{NL1})$  was determined; the result is

$$S\delta_{\max}(j\omega_{NL2}) = 2.2383 \times 10^{-6} < \varepsilon_2 = 0.0099$$

So it is known that there is only one nonlinear component in the system.

**Step 3)**

Because Step 2) indicates there is only one nonlinear component in the system, Step 3) of the proposed method was followed to evaluate  $ST1^{i,i+1}(j\omega_{f\tilde{m}1})$ ,  $ST1^{i,i+1}(j\omega_{f\tilde{m}2})$ ,  $ST2^{i,i+1}(j\omega_{f\tilde{m}1})$ ,  $ST2^{i,i+1}(j\omega_{f\tilde{m}2})$ ,  $S\delta^{i,i+1}(j\omega_{f\tilde{m}1})$  and

$S\delta^{i,i+1}(j\omega_{f\bar{m}2})$  for  $i = 1, \dots, 9$  using Eqs. (5.34) and (5.35). In this case,  $\omega_{f\bar{m}1} = \omega_{f1} = 30\pi$ , and  $\omega_{f\bar{m}2} = \omega_{f2} = 40\pi$ . Then,  $\overline{S\delta}^{i,i+1}(j30\pi)$  and  $\overline{S\delta}^{i,i+1}(j40\pi)$  for  $i = 1, \dots, 9$  were evaluated using Eqs. (5.40a), (5.41a), (5.40b) and (5.41b). The results are shown in Tables 5.4 and 5.5 indicating

$$\begin{cases} \overline{S\delta}^{i,i+1}(j30\pi) \geq \varepsilon_3 = 9.82 \times 10^{-6} & i = 3,4,5 \\ \overline{S\delta}^{i,i+1}(j40\pi) \geq \varepsilon_3 = 9.82 \times 10^{-6} & i = 5,6,7 \end{cases}$$

So  $i' = 3, i' + m' - 1 = 5, \bar{i} = 5$  and  $\bar{i} + \bar{m} - 1 = 7$ , then

$$J' = i' + m' - 1 = \bar{i} = 5$$

Therefore, the only nonlinear component is located between mass  $J' = 5$  and mass  $(J' + 1) = 6$ .

Table 5.4 The value of  $\overline{S\delta}^{i,i+1}(j\omega_{f1})$  when the 6<sup>th</sup> spring is nonlinear

$i$	$\overline{S\delta}^{i,i+1}(j\omega_{f1})$	$i$	$\overline{S\delta}^{i,i+1}(j\omega_{f1})$	$i$	$\overline{S\delta}^{i,i+1}(j\omega_{f1})$
1	$3.86 \times 10^{-7}$	4	0.346388	7	$9.74 \times 10^{-7}$
2	$7.06 \times 10^{-7}$	5	1	8	$6.65 \times 10^{-7}$
3	0.219297	6	$1.22 \times 10^{-6}$	9	$2.31 \times 10^{-7}$

Table 5.5 The value of  $\overline{S\delta}^{i,i+1}(j\omega_{f2})$  when the 6<sup>th</sup> spring is nonlinear

$i$	$\overline{S\delta}^{i,i+1}(j\omega_{f2})$	$i$	$\overline{S\delta}^{i,i+1}(j\omega_{f2})$	$i$	$\overline{S\delta}^{i,i+1}(j\omega_{f2})$
1	$2.27 \times 10^{-6}$	4	$3.15 \times 10^{-6}$	7	0.176738
2	$4.97 \times 10^{-6}$	5	1	8	$3.23 \times 10^{-6}$
3	$2.27 \times 10^{-6}$	6	0.356747	9	$1.18 \times 10^{-6}$

Again, the conclusions reached at each step above are all consistent with the real situation of the simulated system. So the effectiveness of the proposed method is further verified by the third simulation study.

## 5.7 General case

The properties of systems (5.1) and (4.5) and the proposed nonlinearity detection and location methods in this and the last chapters can be extended to the more general case as follows.

$$\mathbf{A}_{\bar{N}}\mathbf{x}^{\{\bar{N}\}} + \mathbf{A}_{\bar{N}-1}\mathbf{x}^{\{\bar{N}-1\}} + \dots + \mathbf{A}_3\ddot{\mathbf{x}} + \mathbf{A}_2\dot{\mathbf{x}} + \mathbf{A}_1\dot{\mathbf{x}} + \mathbf{A}_0\mathbf{x} = \mathbf{F}(t) + \mathbf{NF}(t) \quad (5.48)$$

where,  $\mathbf{F}(t)$  and  $\mathbf{x}(t)$  are system input and output vectors respectively;  $\mathbf{NF}(t)$  is extra term produced by nonlinear components in the system.  $\mathbf{x}^{\{\bar{n}\}}$ ,  $\bar{n} = 1, 2, \dots, \bar{N}$  is the  $\bar{n}^{\text{th}}$  derivative of  $\mathbf{x}(t)$ ; there are  $m$  inputs which correspond to the  $S_1, S_2, \dots, S_m^{\text{th}}$  outputs respectively; the number of the system outputs is  $n$ ;  $\mathbf{A}_{\bar{N}}, \mathbf{A}_{\bar{N}-1}, \dots, \mathbf{A}_1$  are the coefficient matrices associated with  $\bar{N}^{\text{th}}, (\bar{N} - 1)^{\text{th}}, \dots, 1^{\text{st}}$  order derivative of the system outputs, respectively;  $\mathbf{A}_0$  is the coefficient matrix of system output.

The capability of the proposed method for detecting and locating nonlinearity in more general system (5.48) will be demonstrated by another case study in the following where water tree degradation detection issue with power cables will be studied. The power cables have a significant application in power distribution and transmission lines. The water tree degradation is one of the most common damages in the power cable system after long time service and will incur nonlinear behaviours of the whole system [217, 218]. The proposed technique will be applied to a power cable with water tree degradation to find the location of the degradation in this case study.

### 5.7.1 Power cable systems

Research studies have demonstrated that water tree degradations will cause the

power cable system to behave nonlinearly. The V-I relationship of water tree degradation can be approximated by the following nonlinear function [217]:

$$i_{wt}(t) = \frac{1}{R_{wt}} (u_{wt}(t) + ru_{wt}^3(t)) \quad (5.49)$$

where  $i_{wt}(t)$ ,  $u_{wt}(t)$  are the current and voltage and  $R_{wt}$  and  $r$  are the parameters in the water tree degradation V-I relationship. Fig. 5.5 shows the equivalent circuit of a typical 35kV, single-core, XLPE insulated power cable in transmission line where the  $J_j^{\text{th}}$  ( $j = 1, 2, \dots, \bar{J}$ ) component have a water tree damage and consequently become nonlinear [193, 195], and  $R_j$ ,  $L_j$ ,  $G_i$ ,  $C_i$ ,  $j = 1, \dots, n + 1$ ,  $i = 1, \dots, n$ , are the section resistance, section inductance, shunt conductance and shunt capacitance of the power cable system respectively;  $u_i(t)$  and  $i_i(t)$  are the voltage and the current of the  $i$ th cable section with  $i_i(t)$   $i = 1, 2, \dots, n$  being considered as system output in the analysis.

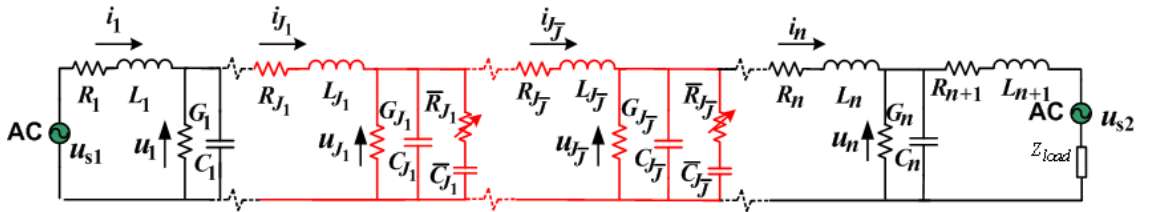


Fig. 5.5 Equivalent circuit of power cable system

Applying Kirchhoff's voltage and current laws to the power cable shown in Fig. 5.5, the mathematical model of the circuit system can be deduced (See Appendix F for details) showing that the model is of the form of Eq.(5.48) where  $\bar{N} = 3$  and

$$F(t) = [f_1(t) \ 0 \ \dots \ f_2(t)]^T$$

$$A_3 = \begin{bmatrix} 0 & 0 & 0 & \dots & 0 \\ 0 & L_2 C_2 C_1 & 0 & \ddots & 0 \\ \vdots & \ddots & \ddots & \ddots & \vdots \\ 0 & \ddots & \ddots & L_{n-1} C_{n-1} C_{n-2} & 0 \\ 0 & 0 & 0 & \dots & 0 \end{bmatrix}$$

$$\mathbf{A}_2 = \begin{bmatrix} A_2(1,1) & 0 & 0 & \cdots & 0 \\ 0 & A_2(2,2) & 0 & \ddots & 0 \\ \vdots & \ddots & \ddots & \ddots & \vdots \\ 0 & \ddots & 0 & A_2(n-1, n-1) & 0 \\ 0 & 0 & 0 & -L_{n+1}C_n & A_2(n, n) \end{bmatrix}$$

$$\mathbf{A}_1 = \begin{bmatrix} A_1(1,1) & 0 & 0 & \cdots & 0 \\ -G_2 & A_1(2,2) & -G_1 & \ddots & \vdots \\ \vdots & \ddots & \ddots & \ddots & 0 \\ 0 & \ddots & -G_{n-1} & A_1(n-1, n-1) & -G_{n-2} \\ 0 & 0 & 0 & A_1(n, n-1) & A_1(n, n) \end{bmatrix}$$

$$\mathbf{A}_0 = \begin{bmatrix} A_0(1,1) & -1 & 0 & \cdots & 0 \\ -C_2 & A_0(2,2) & -C_1 & \ddots & 0 \\ \vdots & \ddots & \ddots & \ddots & \vdots \\ 0 & \ddots & -C_{n-1} & A_0(n-1, n-1) & -C_{n-2} \\ 0 & 0 & 0 & A_0(n, n-1) & A_0(n, n) \end{bmatrix}$$

$$f_1(t) = \dot{u}_{s1}(s)C_1 + u_{s1}(s)G_1$$

$$f_2(t) = C_{n-1}\dot{u}_{s2}(t) + G_{n-1}u_{s2}(t)$$

$$A_2(1,1) = L_1C_1$$

$$A_2(p, p) = R_pC_{p-1}C_p + L_pG_{p-1}C_p + L_pC_{p-1}G_p, \quad p = 2, 3, \dots, n-1$$

$$A_2(n, n) = L_{n+1}C_{n-1} + C_nL_{n+1}$$

$$A_1(1,1) = R_1C_1 + L_1G_1$$

$$A_1(p, p) = R_pC_pG_{p-1} + R_pC_{p-1}G_p + L_pG_{p-1}G_p + C_{p-1} + C_p \quad p = 2, 3, \dots, n-1$$

$$A_1(n, n) = R_{n+1}C_{n-1} + z_{load}C_{n-1} + L_{n+1}G_{n-1} + G_nL_{n+1} + C_nR_{n+1} + C_nz_{load}$$

$$A_1(n, n-1) = C_nR_{n+1} + C_nz_{load} + G_nL_{n+1}$$

$$A_0(1,1) = R_1G_1 + 1$$

$$A_0(p, p) = R_pG_{p-1}G_p + G_{p-1} + G_p$$

$$A_0(n, n) = R_{n+1}G_{n-1} + z_{load}G_{n-1} + 1 + G_nR_{n+1} + G_nz_{load}$$

$$A_0(n, n-1)G_nR_{n+1} + G_nz_{load} - 1$$

In power transmission line, the mains frequency is fixed (either 50Hz or 60Hz). However, communications can be realised via power transmission line by using a modulated carrier signal to carry and transmit useful information such as current, voltage, switch status, temperature and oil level, etc between the base and substations[219]. In this study, carrier signal with low amplitude but very high carrier frequency is employed as the system input signal for water tree damage detection and location purposes. Such carrier signal has advantage in terms of low effect on the normal power transmission and good performance of anti-chirp [219].

### 5.7.2 Application of proposed method on power cable system

In order to verify the effectiveness of the proposed approach when applied in the more general system (5.48), a power cable system as described by Eq. (5.48) is considered where:.

$$n = 5; R_1 = R_2 = \dots = R_6 = 3.61 \times 10^{-4}\Omega; L_1 = L_2 = \dots = L_6 = 5.50 \times 10^{-7}\text{H};$$

$$G_1 = G_2 = \dots = G_5 = 3.58 \times 10^{-10}\text{S}; C_1 = C_2 = \dots = C_5 = 2.85 \times 10^{-10}\text{F};$$

$$Z_{load} = 1.5 \times 10^4\Omega.;$$

and the parameters of the nonlinear components representing water tree damage are

$$r_{J(i)} = 1.7 \times 10^{-5}, R_{J(i)} = 2 \times 10^5\Omega, C_{rJ(i)} = 0, i = 1, \dots, \bar{J} .$$

In this case, there are two ( $\bar{J} = 2$ ) nonlinear components in the system, which are in the 3<sup>rd</sup> and 4<sup>th</sup> sections. Two input conditions implemented by carrier signals are considered as

$$\begin{cases} f_1(t) = f_1^{(1)}(t) = 2.5 \sin(4 \times 10^5 \pi t) \\ f_2(t) = f_2^{(1)}(t) = 7.5 \sin(2 \times 10^5 \pi t) \end{cases} \quad (5.50)$$

and

$$\begin{cases} f_1(t) = f_1^{(1)}(t) = 5 \sin(4 \times 10^5 \pi t) \\ f_2(t) = f_2^{(1)}(t) = 15 \sin(2 \times 10^5 \pi t) \end{cases} \quad (5.51)$$

respectively, and the inputs are applied on two ends of the system as shown in Fig. 5.5. It should be noted that the mains frequency (either 50Hz or 60Hz) are still in the power system but it cannot be detected because of very high sampling frequency and short sampling time which are  $5 \times 10^7$  Hz and 0.001 second respectively. The new method was applied to the spectra of the output responses of the system under the two input conditions, that is,

$$X_i^1(j\omega) \text{ and } X_i^2(j\omega), \quad i = 1,2,3,4,5.$$

The highest order of nonlinearity is determined as  $N = 4$  from the observation on spectra of the system output responses, for example, spectra of the third current when the system is subject to the second loading condition as shown Fig. 5.6, so the possible frequencies produced by system nonlinearity are

$$\omega_{NL} = \{0,6 \times 10^5\pi, 8 \times 10^5\pi, 10 \times 10^5\pi, 12 \times 10^5\pi, 14 \times 10^5\pi, 16 \times 10^5\pi\} \quad (5.52)$$

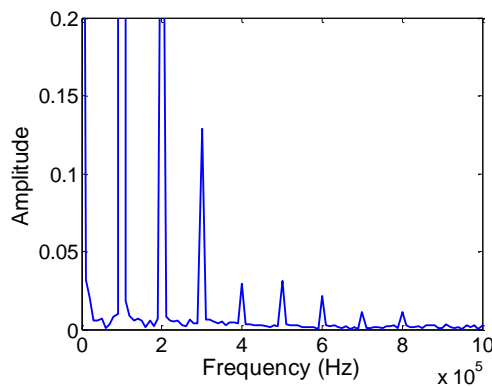


Fig. 5.6 Spectra of the 3<sup>rd</sup> current when the system is subject to the 2<sup>nd</sup> loading condition

The four threshold parameters  $\varepsilon_1, \varepsilon_2, \varepsilon_3, \varepsilon_4$  were determined using the procedure introduced in Remark b) in Section 4.5.2. The results are given in Table 5.6.

Table 5.6 Threshold parameters used in the simulation study on power cable system

Threshold parameters	$\varepsilon_1$	$\varepsilon_2$	$\varepsilon_3$	$\varepsilon_4$
Value	$3.81 \times 10^{-5}$	0.000561	0.008441	$9.8 \times 10^{-5}$

The results of this case study obtained in each step of the proposed method are given as follows.

**Step 1)**

In this case, the ratio between the system response at every nonlinearity generated frequency in Eq. (5.52) and maximum amplitude of system inputs is calculated and the index  $IND_1$  was evaluated using Eq. (5.36) as

$$IND_1 = \max \left\{ \left| \frac{X_i^1(j\omega_{NL})}{\max\{X_i^1(j\omega_{f1}), X_i^1(j\omega_{f2})\}} \right|, \left| \frac{X_i^2(j\omega_{NL})}{\max\{X_i^2(j\omega_{f1}), X_i^2(j\omega_{f2})\}} \right|, i = 1, \dots, 5 \right\}$$

$$= 0.2707 \geq \varepsilon_1 = 3.81 \times 10^{-5}$$

The value of  $\omega_{NL}$  is shown in Eq. (5.52). Therefore, it is concluded that damage with nonlinear features exists in the system.

**Step 2)**

At this step,  $\omega_{NL1}$  was determined as  $\omega_{NL1} = \omega_{f1} + \omega_{f2} = 6 \times 10^5 \pi$ . So

$$ST1^{i,i+1}(j6 \times 10^5 \pi), ST2^{i,i+1}(j6 \times 10^5 \pi), \text{ and } S\delta^{i,i+1}(j6 \times 10^5 \pi) \quad i = 1, \dots, 5$$

were evaluated using Eqs. (5.34) and (5.35). Then,  $S\delta_{\max}(j6 \times 10^5 \pi)$  was determined using Eq. (5.38); the result is

$$S\delta_{\max}(j6 \times 10^5 \pi) = 5.4424 > \varepsilon_2 = 0.000561$$

So it is known that there are more than one nonlinear components in the system.

**Step 4)**

As Step 2) has shown that there are more than one nonlinear components in the system, Step 4) rather than Step 3) of the proposed method is used in this case. At this step,  $\overline{S\delta}^{i,i+1}(j\omega_{NL1}) = \overline{S\delta}^{i,i+1}(j6 \times 10^5 \pi)$ ,  $i = 1, \dots, 5$  were evaluated using Eq. (5.43). The results are shown in Table 5.7, in which it can be observed that

$$\overline{S\delta}^{i,i+1}(j6 \times 10^5 \pi) \geq \varepsilon_4 = 9.8 \times 10^{-5}, \quad i = 3, 4$$



Therefore  $i'' = 3$  and  $m'' = 2$ , and it can be concluded that nonlinear components are located between output  $i'' = 3$  and output  $i'' + m'' = 5$  in the system.

Obviously, the conclusions reached at each step are all consistent with the real situation of the simulated power cable system. So the effectiveness of the proposed method when applied to the detection and location of damage in the more general power cable system has been verified.

Table 5.7 The value of  $\overline{S\delta}^{i,i+1}(j\omega_{NL1})$  in the simulation study on power cable system

$i$	1	2	3	4
$\overline{S\delta}^{i,i+1}(j\omega_{NL1})$	$5 \times 10^{-6}$	$4.82 \times 10^{-5}$	1	0.039863

## 5.8 Conclusions

By analysing the NOFRFs and the NOFRF transmissibility of MIMO nonlinear systems, this chapter investigates the transmissibility at nonlinearity generated frequency and proposes a transmissibility based nonlinearity detection and location method for a class of MIMO structural systems. From the NOFRF transmissibility based analysis, it is found that the transmissibility at nonlinearity generated frequency is insensitive to the locations and strength of loading inputs. According to this observation, a novel technique is proposed to detect the existence and find the locations of nonlinear components in the MIMO structural systems. Moreover, the effectiveness of the new technique is verified by simulation case studies.

Furthermore, the proposed nonlinearity detection and location method is applied to a more general case of higher order dynamics and used to detect and locate water tree damage in power cable system. Simulation studies have again verified the more general application.

## Chapter 6

### **Transmissibility analysis based nonlinearity localization and modal identification for nonlinear MDOF systems**

Chapters 4 and 5 deal with the problem of nonlinearity detection and localization when SIMO/MIMO structural systems are subject to only one or multiple harmonic inputs. However, in engineering practice, structural systems are often subject to loadings with band limited frequencies such as, for example, loadings on the blades of wind turbines and traffic loadings on bridges, etc. In order to address these more general problems, in this chapter, the new nonlinearity detection and localization methods proposed in chapters 4 and 5 are extended to the cases where structural systems are subject to loadings with band limited frequencies. The results also provide useful guidelines for the application of transmissibility analysis based modal identification methods [220] to nonlinear structural systems.

In this chapter, the output frequencies of MIMO nonlinear systems subject to loadings with band limited frequencies are first analyzed to determine the nonlinearity generated frequencies in this more general case. Then the new methods proposed in chapters 4 and 5 are extended for the detection and localization of nonlinear components in a class of nonlinear systems subject to loadings with band limited frequencies, and the effectiveness of new developments is verified by numerical simulation studies. Finally, based on the results of nonlinearity detection and localization, some guidelines are provided for how to apply the transmissibility analysis based modal identification methods to nonlinear structural systems.

## 6.1 Output frequencies of multi-input nonlinear systems

It is well known that for linear systems, the frequency range of outputs is exactly the same as that of system inputs. However, for nonlinear systems, new frequencies will be produced and the frequency components are much more complicated. Eqs. (4.11) and (5.14) show the output responses of nonlinear systems subject to one and multiple inputs, respectively and Eqs. (5.23) and (5.24) shows the output frequencies of nonlinear systems when subjected to multiple harmonic inputs. Lang [216] developed an algorithm to calculate the frequency ranges of output responses of single input nonlinear systems when the systems are subject to an input with frequency components within a limited range  $[a, b]$ . For  $m$ -input nonlinear systems, when the frequency ranges of the  $m$  inputs are  $[a_1, b_1]$ ,  $[a_2, b_2]$ , ..., and  $[a_m, b_m]$ , respectively, the output frequency ranges can be determined by Proposition 6.1 as follows.

### Proposition 6.1 Output frequencies of multi-input nonlinear systems

If a multi-input nonlinear system is subject to  $m$  inputs, the frequency ranges of which are  $[a_1, b_1]$ ,  $[a_2, b_2]$ , ..., and  $[a_m, b_m]$ , respectively, the system output frequencies can be determined as

$$\omega = \Omega(n_1^+, n_1^-, a_1, b_1) + \Omega(n_2^+, n_2^-, a_2, b_2) + \cdots + \Omega(n_m^+, n_m^-, a_m, b_m) \quad (6.1)$$

where,

$$\Omega(n_i^+, n_i^-, a_i, b_i) = \begin{cases} [n_i^+ a_i - n_i^- b_i, n_i^+ b_i - n_i^- a_i] & \text{if } n_i^+ a_i - n_i^- b_i > 0 \\ [0, n_i^+ b_i - n_i^- a_i] & \text{if } n_i^+ a_i - n_i^- b_i \leq 0 \end{cases} \quad (6.2)$$

and  $i = 1, 2, \dots, m$ ,  $n_1^+$ ,  $n_2^+$ , ...,  $n_m^+$ ,  $n_1^-$ ,  $n_2^-$ , ...,  $n_m^-$  are nonnegative integer satisfying the following relationships:

$$\begin{cases} n_1^+ + n_1^- = n_1 \\ n_2^+ + n_2^- = n_2 \\ \vdots \\ n_m^+ + n_m^- = n_m \\ n_1 + n_2 + \dots + n_m = \bar{n} \\ \bar{n} = 1, 2, \dots, N \end{cases} \quad (6.3)$$

where  $N$  is the highest order of system nonlinearity.

**Proof:** Proposition 6.1 can be derived directly by using the frequency output representation of nonlinear system and the requirements of frequency  $\omega$  in Eq.(5.6), that is,  $\omega_1 + \omega_2 + \dots + \omega_{\bar{n}} = \omega$ .

Two examples are provided in the following to show how to determine the frequencies of system output responses using the algorithm in Eqs. (6.1)-(6.3).

**Example 6.1:** Determine the system output frequencies where  $m = 1$ ,  $[a_1, b_1] = [90, 100]$  and  $N = 4$ .

Firstly, the frequency components are calculated by solving Eqs. (6.1)-(6.3) in Proposition 6.1, the possible values of  $n_1^+, n_1^-, \bar{n}$  and  $\omega$  are listed in Table 6.1.

Table 6.1 Frequency components when  $m = 1$ ,  $[a_1, b_1] = [90, 100]$  and  $N = 4$

$n_1^+$	$n_1^-$	$\bar{n}$	$n_1^+ a_1 - n_1^- b_1$	$n_1^+ b_1 - n_1^- a_1$	$\omega$
1	1	2	-10	10	[0,20]
2	2	4	-20	20	
1	0	1	90	100	[80,110]
2	1	3	80	110	
2	0	2	180	200	[170,210]
3	1	4	170	210	
3	0	3	270	300	[270,300]
4	0	4	360	400	[360,400]

Then the system output frequencies are determined as:

$$\omega = [0,20] \cup [80,110] \cup [170,210] \cup [270,300] \cup [360,400] \quad (6.4)$$

In addition, it can be observed from Table 6.1 that the frequency range determined by nonlinearity order  $\bar{n}$  contains that determined by nonlinearity order  $\bar{n} - 2i$ , if  $\bar{n} - 2i > 0$ , where  $i$  is positive integer and  $i < \frac{\bar{n}}{2}$ . This is consistent with the conclusions made by Lang in Ref. [216].

**Example 6.2:** Determine the system output frequencies where  $m = 2$ ,  $[a_1, b_1] = [90,100]$ ,  $[a_2, b_2] = [30,35]$  and  $N = 2$ .

Firstly, the frequency components can be calculated by solving Eqs. (6.1)-(6.3) in Proposition 6.1, the possible values of  $n_1^+, n_1^-, n_2^+, n_2^-, \bar{n}$  and  $\omega$  are listed in Table 6.2.

Table 6.2 Frequency components when  $m = 2$ ,  $[a_1, b_1] = [90,100]$ ,  $[a_2, b_2] = [30,35]$  and  $N = 2$

$n_1^+$	$n_1^-$	$n_2^+$	$n_2^-$	$\bar{n}$	$n_1^+ a_1 - n_1^- b_1$	$n_1^+ b_1 - n_1^- a_1$	$\omega$
0	0	1	1	2	-5	5	[0,10]
1	1	0	0	2	-10	10	
0	0	1	0	1	30	35	[30,50]
0	0	2	0	2	60	70	[55,70]
1	0	0	1	2	55	70	
1	0	0	0	1	90	100	[90,100]
1	0	1	0	2	120	135	[120,135]
2	0	0	0	2	180	200	[180,200]

Then the system output frequencies are determined as:

$$\omega = [0,10] \cup [30,50] \cup [55,70] \cup [90,100] \cup [120,130] \cup [180,200] \quad (6.5)$$

Just as in Chapter 5, the frequencies which are produced by system nonlinearity and do not overlap with the frequency range of system inputs are again referred to as nonlinearity generated frequencies in the following.

## 6.2 Transmissibility based nonlinearity detection and localization for MDOF nonlinear systems subject to band limited loading inputs

In order to apply the nonlinearity detection and localization techniques proposed in Chapters 4 and 5 to the case where structural systems are subject to inputs with band limited frequencies as,

$$\mathbf{F}(t) = [0 \quad \dots \quad f_1(t) \quad \dots \quad f_2(t) \quad \dots \quad f_m(t) \quad \dots \quad 0]^T \quad (6.6)$$

where  $f_1(t)$ ,  $f_2(t)$ , ...,  $f_m(t)$  are  $m$  inputs with band limited frequencies and are applied on the  $S_1$ ,  $S_2$ , ...,  $S_m^{\text{th}}$  masses respectively, an alternative transmissibility index is proposed as follows.

$$STI^{i,i+1} = \frac{1}{\omega_2 - \omega_1} \int_{\omega_1}^{\omega_2} ST^{i,i+1}(j\omega) d\omega = \frac{1}{\omega_2 - \omega_1} \int_{\omega_1}^{\omega_2} \frac{X_i(j\omega)}{X_{i+1}(j\omega)} d\omega \quad (6.7)$$

where  $ST^{i,i+1}(j\omega)$  is the transmissibility at frequency  $\omega$ . In addition, the following two assumptions are made:

- a) Two different loading conditions can be considered, and the frequency ranges of the loading inputs are known a priori but their locations applied on the system can be unknown when there are multiple inputs applied on the system. However, the location of the input is required to be known when there is only one input applied.
- b) The output spectra of structural systems to the two loading conditions are available, say,  $X_i^1(j\omega)$  and  $X_i^2(j\omega)$ , and the following transmissibility indices

$$\begin{cases} STI1^{i,i+1} = \frac{1}{\omega_2 - \omega_1} \int_{\omega_1}^{\omega_2} \frac{X_i^1(j\omega)}{X_{i+1}^1(j\omega)} d\omega = \frac{1}{\omega_2 - \omega_1} \int_{\omega_1}^{\omega_2} \frac{X_i(j\omega)}{X_{i+1}(j\omega)} d\omega \Big|_{f_1(t)=f_1^{(1)}(t), \dots, f_m(t)=f_m^{(1)}(t)} \\ STI2^{i,i+1} = \frac{1}{\omega_2 - \omega_1} \int_{\omega_1}^{\omega_2} \frac{X_i^2(j\omega)}{X_{i+1}^2(j\omega)} d\omega = \frac{1}{\omega_2 - \omega_1} \int_{\omega_1}^{\omega_2} \frac{X_i(j\omega)}{X_{i+1}(j\omega)} d\omega \Big|_{f_1(t)=f_1^{(2)}(t), \dots, f_m(t)=f_m^{(2)}(t)} \end{cases} \quad (6.8)$$

and their difference

$$SI\delta^{i,i+1} = |STI1^{i,i+1} - STI2^{i,i+1}| \quad i = 1, \dots, n - 1 \quad (6.9)$$

can be determined, where,  $\omega$  can be within the range of any driving frequencies or the nonlinearity generated frequencies.

Based on the new transmissibility index defined above and under the two assumptions, the nonlinearity detection and localization techniques in Chapters 4 and 5 can be applied to the case where a structural system is subject to the inputs with band limited frequencies. The details will be demonstrated in the following two case studies where the system considered is the same as that in Chapters 4 and 5.

### 6.2.1 Simulation study: case 1

In this simulation study, system (4.5) is considered with the value of linear and nonlinear parameters the same as that in simulation studies in Section 4.6. Therefore, thresholds  $\varepsilon_1$ ,  $\varepsilon_2$ ,  $\varepsilon_3$  and  $\varepsilon_4$  listed in Table 4.1 are used.

It is assumed that there are three nonlinear components which are 5<sup>th</sup>, 6<sup>th</sup> and 7<sup>th</sup> springs, namely,  $\bar{J} = 3$ ,  $J_1 = 5$ ,  $J_2 = 6$  and  $J_3 = 7$  and only one input which is applied on the 4<sup>th</sup> mass, namely,  $m = 1$ ,  $S_1 = 4$ . The following two loading conditions are considered

$$f(t) = f^{(1)}(t) = \frac{A_1(\sin(\omega_{f_2}t + \beta_2) - \sin(\omega_{f_1}t + \beta_1))}{2\pi(t - t_1)} \quad (6.10)$$

and

$$f(t) = f^{(2)}(t) = \frac{A_2(\sin(\omega_{f_2}t + \beta_2) - \sin(\omega_{f_1}t + \beta_1))}{2\pi(t - t_1)} \quad (6.11)$$

where the frequency components are all within the range of  $\omega_F = [\omega_{f1}, \omega_{f2}]$ ,  $A_1 = 10$ ,  $A_2 = 15$ ,  $\omega_{f1} = 90\pi$ ,  $\omega_{f2} = 100\pi$ ,  $\beta_1 = \beta_2 = 0$  and  $t_1 = 5$  seconds.

According to Proposition 6.1, when the system is subject to the input as shown in Eqs. (6.10) and (6.11); and the highest order of system nonlinearity is taken as  $N = 3$  from the observation on spectra of the system output responses, for example, the output response of the 5th mass when the system is subject to the second loading condition as shown Fig. 6.1, the frequency range of system output can be calculated by solving Eqs. (6.1)-(6.3) in Proposition 6.1 and then the nonlinearity generated frequencies can be determined as

$$\omega_{NL} = [0, 10\pi] \cup [80\pi, 90\pi] \cup (100\pi, 110\pi] \cup [180\pi, 200\pi] \cup [270\pi, 300\pi] \quad (6.12)$$

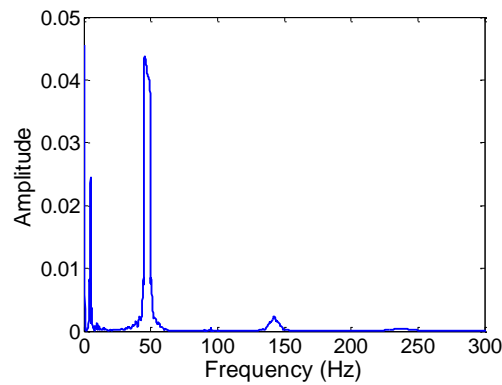


Fig. 6.1 Output response of the 5<sup>th</sup> mass when the system is subject to the 2<sup>nd</sup> loading condition

Because there is only one input applied to the system, the technique in Chapter 4 is employed in this case, and the results obtained in each step are given as follows.

### Step 1)

In this case, the ratio between the system response at every nonlinearity generated frequency in Eq. (6.12) and maximum amplitude of system inputs is calculated and the index  $IND_1$  was evaluated by



$$IND_1 = \max \left\{ \left| \frac{\max\{X_i^1(j\omega'_{NL})\}}{\max\{X_i^1(j\omega'_F)\}} \right|, \left| \frac{\max\{X_i^2(j\omega'_{NL})\}}{\max\{X_i^2(j\omega'_F)\}} \right|, i = 1, \dots, 10, \omega'_F \in \omega_F \text{ and } \omega'_{NL} \in \omega_{NL} \right\} \quad (6.13)$$

where  $\omega_{NL}$  is shown in Eq. (6.12) and it indicates that

$$IND_1 = 3.0104 \geq \varepsilon_1 = 8.42 \times 10^{-6}$$

Therefore, it is concluded that at least one nonlinear component exists in the system.

### Step 2)

At this step, the nonlinearity generated frequency range  $\omega_{NL1} = [\omega_1, \omega_2] = [3\omega_{f1}, 3\omega_{f2}] = [270\pi, 300\pi]$  is used, and

$$STI1^{i,i+1}, STI2^{i,i+1} \text{ and } SI\delta^{i,i+1}, i = 1, \dots, 9$$

were evaluated using Eqs. (6.8) and (6.9). Then,  $SI\delta_{\max}$  was determined using

$$SI\delta_{\max} = \max\{SI\delta^{i,i+1}, i \in \{1, 2, \dots, 9\}\} \quad (6.14)$$

the result is

$$SI\delta_{\max} = 0.3111 > \varepsilon_2 = 0.0099$$

So it is known that there are more than one nonlinear components in the system.

### Step 4)

As Step 2) has shown that there are more than one nonlinear components in the system, Step 4) rather than Step 3) of the proposed method is used in this case. At this step,  $\overline{SI\delta}^{i,i+1}$ ,  $i = 1, \dots, 9$  were evaluated by

$$\overline{SI\delta}^{i,i+1} = \frac{SI\delta^{i,i+1}}{SI\delta_{\max}} \text{ for } i = 1, \dots, 9 \quad (6.15)$$

The results are shown in Table 6.3, in which it can be observed that

$$\overline{SI\delta}^{i,i+1} \geq \varepsilon_4 = 0.0015, i = 4, 5, 6$$

Therefore,  $i'' = 4$ , and  $m'' = 3$ , and it can be concluded that the nonlinear

components are located between mass  $i'' = 4$  and mass  $i'' + m'' = 7$  in the system.

Table 6.3 The value of  $\overline{SI\delta}^{i,i+1}$  when the 5<sup>th</sup>, 6<sup>th</sup> and 7<sup>th</sup> springs are nonlinear

$i$	$\overline{SI\delta}^{i,i+1}$	$i$	$\overline{SI\delta}^{i,i+1}$	$i$	$\overline{SI\delta}^{i,i+1}$
1	0.000177	4	0.473247	7	0.000459
2	0.000323	5	0.833626	8	0.000985
3	0.000192	6	1	9	0.001132

Obviously, the conclusions reached at each step are all consistent with the real situation of the simulated system.

## 6.2.2 Simulation study: case 2

In this simulation study, system (5.1) is considered with the value of linear and nonlinear parameters the same as that in simulation studies in Section 5.6. Therefore,  $\varepsilon_1$ ,  $\varepsilon_2$ ,  $\varepsilon_3$  and  $\varepsilon_4$  listed in Table 4.1 are used again.

It is assumed that there is only one nonlinear component which is the 6<sup>th</sup> spring, namely,  $\bar{J} = 1$ ,  $J_1 = 6$  and two inputs which are applied on the 3<sup>rd</sup> and 4<sup>th</sup> masses at the same time, namely,  $m = 2$ ,  $S_1 = 3$  and  $S_2 = 4$ . Two following different loading conditions are considered

$$\begin{cases} f_1(t) = f_1^{(1)}(t) = \frac{A_1(\sin(\omega_{f_2}t + \beta_2) - \sin(\omega_{f_1}t + \beta_1))}{2\pi(t - t_1)} \\ f_2(t) = f_2^{(1)}(t) = \frac{B_1(\sin(\omega_{f_4}t + \beta_4) - \sin(\omega_{f_3}t + \beta_3))}{2\pi(t - t_1)} \end{cases} \quad (6.16)$$

and

$$\begin{cases} f_1(t) = f_1^{(2)}(t) = \frac{A_2(\sin(\omega_{f_2}t + \beta_2) - \sin(\omega_{f_1}t + \beta_1))}{2\pi(t - t_1)} \\ f_2(t) = f_2^{(2)}(t) = \frac{B_2(\sin(\omega_{f_4}t + \beta_4) - \sin(\omega_{f_3}t + \beta_3))}{2\pi(t - t_1)} \end{cases} \quad (6.17)$$

where,  $A_1 = B_1 = 10$ ,  $A_2 = B_2 = 20$ ,  $\omega_{f_1} = 40\pi$ ,  $\omega_{f_2} = 50\pi$ ,  $\omega_{f_3} = 60\pi$ ,  $\omega_{f_4} = 70\pi$ ,  $\beta_1 = \beta_2 = \beta_3 = \beta_4 = 0$  and  $t_1 = 5$ . Eqs. (6.16) and (6.17) imply that under each loading condition, the loading input frequency ranges are  $\omega_{F1} = [\omega_{f_1}, \omega_{f_2}]$  and  $\omega_{F2} = [\omega_{f_3}, \omega_{f_4}]$  for the two inputs, respectively. Therefore, the range of driving frequencies are

$$\omega_F = \omega_{F1} \cup \omega_{F2} = [\omega_{f_1}, \omega_{f_2}] \cup [\omega_{f_3}, \omega_{f_4}] = [40\pi, 50\pi] \cup [60\pi, 70\pi]$$

According to Proposition 6.1, when the nonlinear system is subject to loading condition shown in Eqs. (6.16) and (6.17) and the highest order of system nonlinearity is considered as  $N = 3$  from the observation on spectra of the system output responses, for example, the output response of the 3<sup>rd</sup> mass when the system is subject to the second loading condition as shown Fig. 6.2, the frequency range of system output can be calculated by solving Eqs. (6.1)-(6.3) in Proposition 6.1 and the nonlinearity generated frequencies can be determined as

$$\omega_{NL} = [0, 40\pi) \cup (50\pi, 60\pi) \cup (70\pi, 210\pi] \quad (6.18)$$

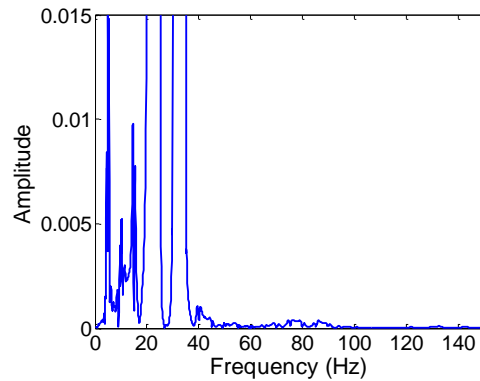


Fig. 6.2 Output response of the 3<sup>rd</sup> mass when the system is subject to the 2<sup>nd</sup> loading condition

Because there are two system inputs, the technique in Chapter 5 is applied in this case, and the results obtained in each step are given as follows.

### Step 1)

In this case, the ratio between the system response at every nonlinearity generated frequency in Eq. (6.18) and maximum amplitude of system inputs is calculated and the index  $IND_1$  was evaluated using Eq. (6.11) as

$$IND_1 = \max \left\{ \left| \frac{\max\{X_i^1(j\omega'_{NL})\}}{\max\{X_i^1(j\omega'_F)\}} \right|, \left| \frac{\max\{X_i^2(j\omega'_{NL})\}}{\max\{X_i^2(j\omega'_F)\}} \right|, i = 1, \dots, 10, \omega'_F \in \omega_F \text{ and } \omega'_{NL} \in \omega_{NL} \right\}$$

$$= 0.4952 \geq \varepsilon_1 = 8.42 \times 10^{-6}$$

where  $\omega_{NL}$  is shown in Eq. (6.18). Therefore, it is concluded that at least one nonlinear component exists in the system.

### Step 2)

At this step, the nonlinearity generated frequency range  $\omega_{NL1}$  was determined as

$$\omega_{NL1} = [\omega_1, \omega_2] = [\omega_{f3} - \omega_{f2}, \omega_{f4} - \omega_{f1}] = [10\pi, 30\pi].$$

So

$$STI1^{i,i+1}, STI2^{i,i+1} \text{ and } SI\delta^{i,i+1}, i = 1, \dots, 9$$

were evaluated using Eqs. (6.8) and (6.9). Then,  $S\delta_{\max}$  was determined using Eq. (6.14); the result is

$$SI\delta_{\max} = 1.4866 \times 10^{-4} < \varepsilon_2 = 0.0099$$

So it is known that there is only one nonlinear component in the system.

### Step 3)

Because Step 2) indicates there is only one nonlinear component in the system, Step 3) of the proposed method was followed. At this step, the range of driving frequency  $\omega_F^1 = [\omega_1, \omega_2] = [\omega_{f1}, \omega_{f2}]$  was used first to evaluate

$$STI1_1^{i,i+1}, STI2_1^{i,i+1} \text{ and } SI\delta_1^{i,i+1}, i = 1, \dots, 9$$

using Eqs. (6.8) and (6.9) and  $\overline{SI\delta}_1^{i,i+1}$ ,  $i = 1, \dots, 9$  were evaluated using Eqs. (6.14) and (6.15). Then the range of driving frequency  $\omega_F^2 = [\omega_1, \omega_2] = [\omega_{f3}, \omega_{f4}]$  was used to evaluate

$$STI1_2^{i,i+1}, STI2_2^{i,i+1} \text{ and } SI\delta_2^{i,i+1}, i = 1, \dots, 9$$

using Eqs. (6.8) and (6.9) and  $\overline{SI\delta}_2^{i,i+1}$ ,  $i = 1, \dots, 9$  were evaluated by Eqs. (6.14) and (6.15). The results are shown in Tables 6.4 and 6.5 indicating

$$\begin{cases} \overline{SI\delta}_1^{i,i+1} \geq \varepsilon_3 = 9.82 \times 10^{-6} & i = 3, 4, 5 \\ \overline{SI\delta}_2^{i,i+1} \geq \varepsilon_3 = 9.82 \times 10^{-6} & i = 4, 5 \end{cases}$$

So  $i' = 3, i' + m' - 1 = 5, \bar{i} = 4$  and  $\bar{i} + \bar{m} - 1 = 5$ , then

$$J' = i' + m' - 1 = \bar{i} + \bar{m} - 1 = 5$$

Therefore, the only nonlinear component is located between mass  $J' = 5$  and mass  $(J' + 1) = 6$ .

Table 6.4 The value of  $\overline{SI\delta}_1^{i,i+1}$  when the 6<sup>th</sup> spring is nonlinear

$i$	$\overline{SI\delta}_1^{i,i+1}$	$i$	$\overline{SI\delta}_1^{i,i+1}$	$i$	$\overline{SI\delta}_1^{i,i+1}$
1	$9.73 \times 10^{-7}$	4	0.564982	7	$2.81 \times 10^{-6}$
2	$2.71 \times 10^{-6}$	5	1	8	$1.13 \times 10^{-6}$
3	0.331382	6	$3.89 \times 10^{-6}$	9	$2.58 \times 10^{-7}$

Table 6.5 The value of  $\overline{SI\delta}_2^{i,i+1}$  when the 6<sup>th</sup> spring is nonlinear

$i$	$\overline{S\delta}_2^{i,i+1}$	$i$	$\overline{S\delta}_2^{i,i+1}$	$i$	$\overline{S\delta}_2^{i,i+1}$
1	$1.98 \times 10^{-6}$	4	0.83277	7	$8.26 \times 10^{-6}$
2	$4.27 \times 10^{-6}$	5	1	8	$3.74 \times 10^{-6}$
3	$4.48 \times 10^{-6}$	6	$2.28 \times 10^{-6}$	9	$1.41 \times 10^{-6}$

Again, the conclusions reached at each step above are all consistent with the real situation of the simulated system.

From the results in Chapter 4, 5 and 6, it can be concluded that using the transmissibilities at nonlinearity generated frequencies, the location of nonlinear components can always be identified correctly, no matter what number and form of loading inputs are applied on the system.

### 6.3 Modal identification

Modal identification is one of the most important parts when conducting dynamic analysis on structural systems. Transmissibility analysis based method is an effective modal identification method by using output response measurements only [220]. But the method assumes that the system is linear; the effectiveness of the method in the case where the system is nonlinear has never been studied. Therefore, transmissibility analysis based modal identification method of nonlinear structural systems is investigated in this section.

### 6.3.1 Modal identification of linear MDOF systems using transmissibility analysis

If all springs and dampers are linear, the governing equation of the systems shown in Fig. 4.1 and Fig. 5.1 are described by Eq. (4.1) or Eq.(5.1) without nonlinear term  $\mathbf{NF}(t)$ , respectively. The modal parameters of the linear systems including natural frequency and damping ratio can be identified by transmissibility analysis as summarized in Proposition 6.2 below [220-222].

#### Proposition 6.2 Transmissibility analysis based modal identification of linear systems

For linear systems described by Eq. (4.1) or Eq.(5.1) without nonlinear term  $\mathbf{NF}(t)$  and subject to different loading conditions, define,

$$\Delta^{-1}T_{i,k}^{S',S''}(\omega) = \frac{1}{T_{i,k}^{S'}(\omega) - T_{i,k}^{S''}(\omega)} \quad (6.19)$$

where  $S'$  and  $S''$  indicate two different loading conditions, namely, the loadings are applied on different masses under the two conditions (detailed definition and relevant discussions about different loading conditions can be found in Ref. [222]);  $T_{i,k}^{S'}(\omega)$  and  $T_{i,k}^{S''}(\omega)$  are transmissibilities between  $i^{\text{th}}$  and  $k^{\text{th}}$  outputs under the loading condition  $S'$  and  $S''$ , respectively. Then, under the small damping assumption, the pole of the system's  $\bar{m}$ th mode  $\lambda_{\bar{m}}$

$$\lambda_{\bar{m}} = \sigma_{\bar{m}} + j\omega_{\bar{m}}, \quad \bar{m} = 1, 2, \dots, n \quad (6.20)$$

can be obtained by identifying the peaks of  $\Delta^{-1}T_{i,k}^{S',S''}(\omega)$ . Consequently, the  $\bar{m}^{\text{th}}$  order natural frequency  $\omega_{\bar{m}}$  and corresponding damping ratio  $\zeta_{\bar{m}} = -\sigma_{\bar{m}} / \sqrt{\sigma_{\bar{m}}^2 + \omega_{\bar{m}}^2}$  can be obtained

**Proof of Proposition 6.2** [220-222]

For linear system described by Eq. (4.1) or Eq.(5.1) without nonlinear term  $\mathbf{NF}(t)$ , under the small damping assumption, the transfer function matrix can be described by

$$H(\omega) = \sum_{\bar{m}=1}^n \left( \frac{\{\phi_{\bar{m}}\}\{v_{\bar{m}}\}^T}{j\omega - \lambda_{\bar{m}}} + \frac{\{\phi_{\bar{m}}\}^*\{v_{\bar{m}}\}^H}{j\omega - \lambda_{\bar{m}}^*} \right) \quad (6.21)$$

where  $\{\mathbf{■}\}^T$ ,  $\{\mathbf{■}\}^*$  and  $\{\mathbf{■}\}^H$  are all mathematical operators, indicating transpose, complex conjugate and Hermitian conjugate respectively;  $n$  is the number of modes and is also the number of DOFs of linear system;  $\phi_{\bar{m}}$  and  $v_{\bar{m}}$  are the modal shape and modal participation factor of mode  $\bar{m}$ , respectively. The objective of modal identification is to find the value of natural frequency  $\omega_{\bar{m}}$  and damping ratio  $\zeta_{\bar{m}}$  from the system's pole  $\lambda_{\bar{m}}$ .

When the system is subject to the loading condition  $S'$ , and there are  $m$  inputs which are applied on the  $S_1, S_2, \dots, S_m^{\text{th}}$  masses respectively, the transmissibility between the  $i^{\text{th}}$  and  $k^{\text{th}}$  outputs is

$$\begin{aligned} T_{i,k}^{S'}(\omega) &= \frac{X_i(\omega)}{X_k(\omega)} = \frac{\sum_{p=1}^m H_{iS_p}(\omega)F_{S_p}(\omega)}{\sum_{p=1}^m H_{kS_p}(\omega)F_{S_p}(\omega)} \\ &= \frac{\sum_{p=1}^m \sum_{\bar{m}=1}^n \left( \frac{\{\phi_{i\bar{m}}\}v_{S_p\bar{m}}}{j\omega - \lambda_{\bar{m}}} + \frac{\{\phi_{i\bar{m}}\}^*v_{S_p\bar{m}}^*}{j\omega - \lambda_{\bar{m}}^*} \right) F_{S_p}(\omega)}{\sum_{p=1}^m \sum_{\bar{m}=1}^n \left( \frac{\{\phi_{k\bar{m}}\}v_{S_p\bar{m}}}{j\omega - \lambda_{\bar{m}}} + \frac{\{\phi_{k\bar{m}}\}^*v_{S_p\bar{m}}^*}{j\omega - \lambda_{\bar{m}}^*} \right) F_{S_p}(\omega)} \end{aligned} \quad (6.22)$$

where  $F_{S_p}(\omega)$  is the spectrum of the  $p^{\text{th}}$  input.

When  $\omega$  approaches to one of the system's poles, say,  $\lambda_{\bar{i}}$ , then the value of  $T_{i,k}^{S'}(\omega)$  can be calculated using Eq.(6.22) according to limiting algorithm.

$$\lim_{\omega \rightarrow \lambda_{\bar{i}}} T_{i,k}^{S'}(\omega) = \frac{\phi_{i\bar{i}} \sum_{p=1}^{\bar{S}} v_{S_p\bar{i}} F_{S_p}(\omega)}{\phi_{k\bar{i}} \sum_{p=1}^{\bar{S}} v_{S_p\bar{i}} F_{S_p}(\omega)} = \frac{\phi_{i\bar{i}}}{\phi_{k\bar{i}}} \quad (6.23)$$

Eq. (6.23) indicates that when the frequency is equal to one of the system's poles, the



transmissibility between two fixed DOFs becomes independent of the locations of inputs. This accords with the fact that transmissibility changes with the positions of the inputs, but it is independent of them and becomes convergent at the system's poles.

Define the subtraction of two transmissibility functions as

$$\Delta T_{i,k}^{S',S''}(\omega) = T_{i,k}^{S'}(\omega) - T_{i,k}^{S''}(\omega) \quad (6.24)$$

Consequently, the following relationship can be satisfied.

$$\lim_{\omega \rightarrow \lambda_{\bar{i}}} \Delta T_{i,k}^{S',S''}(\omega) = \lim_{\omega \rightarrow \lambda_{\bar{i}}} \{T_{i,k}^{S'}(\omega) - T_{i,k}^{S''}(\omega)\} = \frac{\phi_{i\bar{i}}}{\phi_{k\bar{i}}} - \frac{\phi_{i\bar{i}}}{\phi_{k\bar{i}}} = 0 \quad (6.25)$$

This indicates that the system's poles are zeroes of function  $\Delta T_{i,k}^{S',S''}(\omega)$ , and consequently, poles of its inverse, namely,  $\Delta^{-1}T_{i,k}^{S',S''}$ . Therefore, it is possible to identify the system poles  $\lambda_{\bar{m}}$  by analyzing the transmissibility functions  $T_{i,k}^{S'}(\omega), T_{i,k}^{S''}(\omega)$  and associated  $\Delta^{-1}T_{i,k}^{S',S''}(\omega)$ . Thus, the Proposition 6.2 is proved.

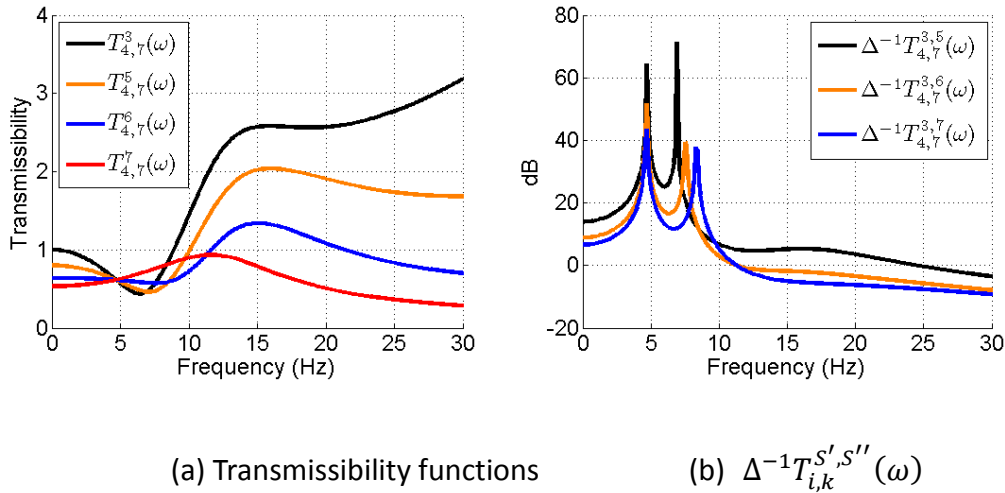


Fig. 6.3 Some transmissibility functions and associated  $\Delta^{-1}T_{i,k}^{S',S''}(\omega)$  of linear system

$$(4.1)$$

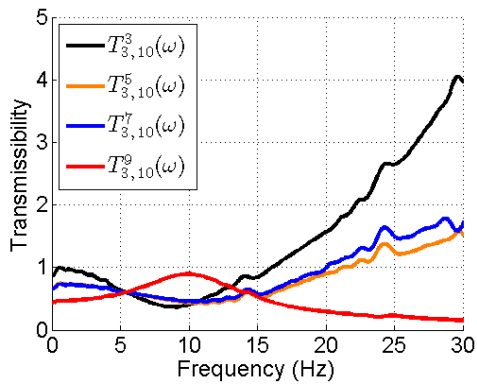
For system (4.1) with the same linear parameters as that in simulation studies in Section 6.2, some transmissibility functions  $T_{i,k}^{S'}(\omega)$ ,  $T_{i,k}^{S''}(\omega)$  and associated

$\Delta^{-1}T_{i,k}^{S',S''}(\omega)$  are shown in Fig. 6.3 where  $i = 4$  and  $k = 7$ . It can be observed that all transmissibility functions intersect at the same points when  $\omega \approx 4.7\text{Hz}$  in Fig. 6.3(a) and all  $\Delta^{-1}T_{i,k}^{S',S''}(\omega)$  functions have a peak when  $\omega \approx 4.7\text{Hz}$  in Fig. 6.3(b). These are in agreement with the above analysis.

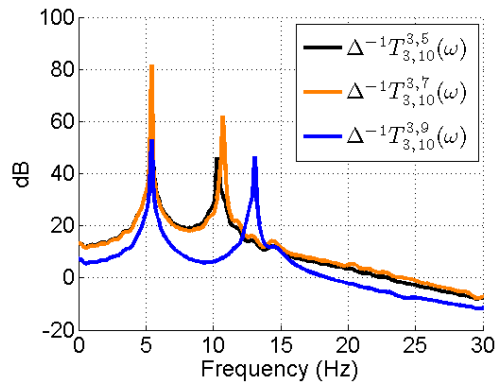
### 6.3.2 Modal identification of nonlinear MODF systems using transmissibility analysis

Proposition 6.2 describes the theoretical principle of modal identification of linear MODF systems by analysing transmissibility functions and associated  $\Delta^{-1}T_{i,k}^{S',S''}(\omega)$ . However, when there are multiple nonlinear components in the system, the effectiveness of this method depends on the output DOFs used for transmissibility evaluations.

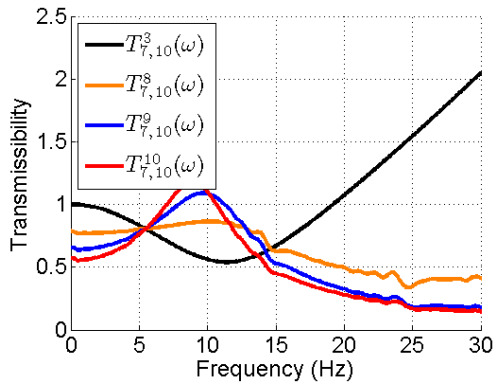
For example, Fig. 6.4 shows some transmissibility functions  $T_{i,k}^{S'}(\omega)$ ,  $T_{i,k}^{S''}(\omega)$  and associated  $\Delta^{-1}T_{i,k}^{S',S''}(\omega)$  with system (4.5) where the 5<sup>th</sup>, 6<sup>th</sup> and 7<sup>th</sup> springs become nonlinear and output DOFs are chosen as  $i = 3$  and  $k = 10$ ,  $i = 7$  and  $k = 10$ ,  $i = 2$  and  $k = 4$  respectively. It can be found that all transmissibility functions intersect at one point in Figs. 6.4(a), (c) and (e) and all  $\Delta^{-1}T_{i,k}^{S',S''}(\omega)$  reach a peak at  $\omega \approx 5.4\text{Hz}$  in Figs. 6.4(b), (d) and (f). Therefore, the modal analysis method for the linear MDOF system is able to be used to identify the pole of the nonlinear system in these cases. In addition, a comparison between Fig. 6.3 and Fig. 6.4 reveals that even common peaks in these two figures can indicate the system's pole, but the specific values of the pole that can be observed from the two figures are slightly different. This can be due to the fact that an introduction of nonlinearity can cause the change in a system's equivalent stiffness and, consequently, slightly change the system's natural frequency.



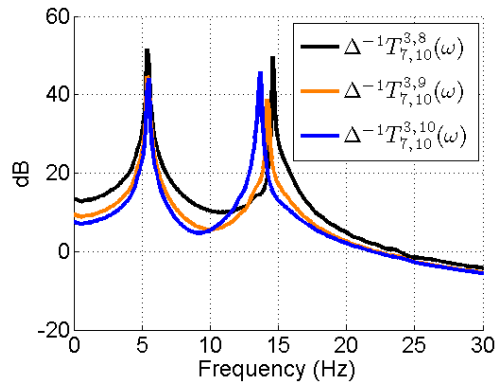
(a) Transmissibility functions



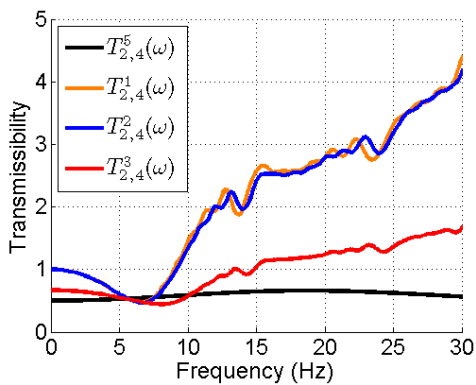
(b)  $\Delta^{-1}T_{i,k}^{S',S''}(\omega)$



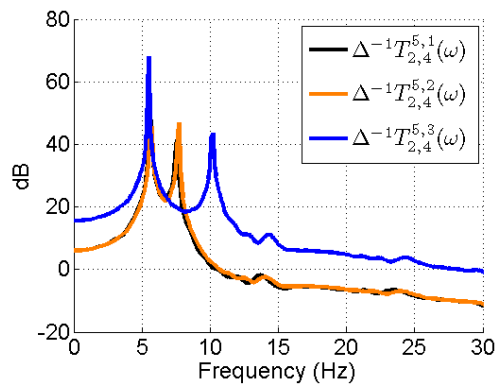
(c) Transmissibility functions



(d)  $\Delta^{-1}T_{i,k}^{S',S''}(\omega)$



(e) Transmissibility functions



(f)  $\Delta^{-1}T_{i,k}^{S',S''}(\omega)$

Fig. 6.4 Some transmissibility functions and associated  $\Delta^{-1}T_{i,k}^{S',S''}(\omega)$  of the nonlinear system (4.5)

Fig. 6.5 shows some transmissibility functions  $T_{i,k}^{S'}(\omega)$ ,  $T_{i,k}^{S''}(\omega)$  and associated  $\Delta^{-1}T_{i,k}^{S',S''}(\omega)$  when the output DOFs are selected as  $i = 4$ ,  $k = 7$ . It can be seen that there are many intersection points among different transmissibility functions in Fig. 6.5(a) and many common peaks at different frequencies in Fig. 6.5(b). Therefore, the system's pole cannot be identified in this case.

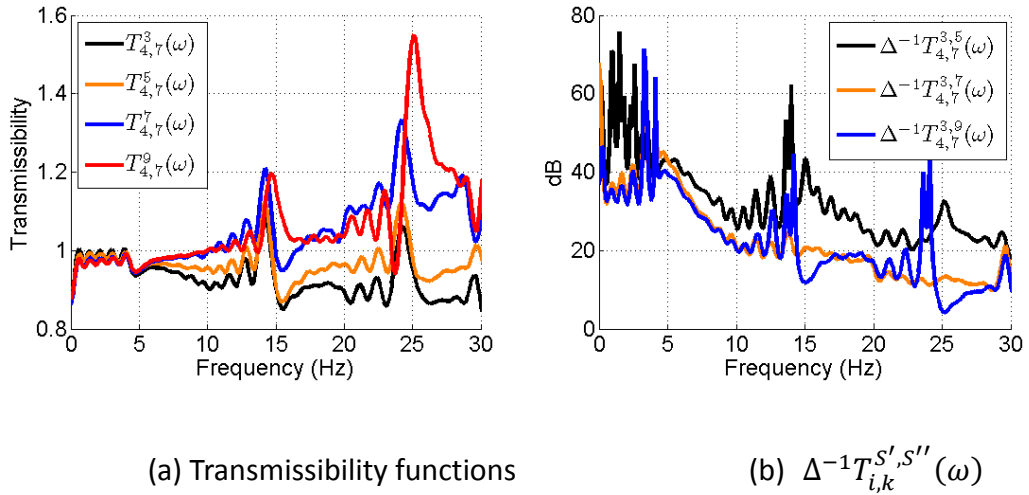


Fig. 6.5 Some transmissibility functions and associated  $\Delta^{-1}T_{i,k}^{S',S''}(\omega)$  of the nonlinear system (4.5)

It can be concluded from above analysis on Figs. 6.4 and 6.5 that for the nonlinear systems described by (4.5) or (5.1), the linear method becomes invalid if the output DOFs are not appropriately selected; but if two output DOFs involved in transmissibility evaluation are both located outside the range of nonlinear components including on the same side and on the different sides of nonlinear components, transmissibility analysis based technique can still be used to identify the modal parameters. This can be because for a nonlinear system with several nonlinear components, if both output DOFs involved in transmissibility evaluations are outside of the locations of these nonlinear components, the nonlinear components can together be considered as one integrated part of the system that can approximately be represented by an equivalent linear subsystem.

In addition, there are always many peaks in the figure of every  $\Delta^{-1}T_{i,k}^{S',S''}(\omega)$ , but only the common peaks of different  $\Delta^{-1}T_{i,k}^{S',S''}(\omega)$  are capable of representing the system poles. Therefore, the transmissibility functions of two system responses under at least three different loading conditions are required to identify the system modal parameters by transmissibility analysis method.

Based on the above observations and similar assumptions as that in Section 6.2, that is, the output responses of the structural system to three different loading conditions, which are within the same frequency range but applied on different locations, are available, the following procedure can be proposed to identify the modal parameters of nonlinear systems by transmissibility analysis.

Step 1) Evaluate  $X_i^1(j\omega)$ ,  $X_i^2(j\omega)$  and  $X_i^3(j\omega)$ ,  $i = 1, \dots, n$ , the spectra of the output responses of structural system under three different loading conditions, and determine the amplitudes of these spectra at all nonlinearity generated frequencies in the system outputs, that is,  $X_i^1(j\omega_{NL})$ ,  $X_i^2(j\omega_{NL})$  and  $X_i^3(j\omega_{NL})$ , for  $i = 1, \dots, n$ ; determine the highest order  $N$  of the system nonlinearity from observing the system output frequency responses; and calculate the value of index  $IND_1$  as defined by Eq. (6.13) to represent the strength of the effect of system nonlinearity on the system output responses. If

$$IND_1 \geq \varepsilon_1 \quad (6.26)$$

then it can be concluded that there exists nonlinear component in the system. Otherwise, there is no nonlinear component in the system. In Eq. (6.26),  $\varepsilon_1$  is a threshold to be determined a priori.

Step 2) If Step 1) indicates there is nonlinear component in the system, select a nonlinearity generated frequency range  $\omega_{NL1} = [\omega_1, \omega_2]$  such that  $X_i^1(j\omega_{NL1})$ ,  $X_i^2(j\omega_{NL1})$  and  $X_i^3(j\omega_{NL1})$   $i = 1, \dots, n$  have significant amplitudes. Select any two sets of system frequency responses, say,  $X_i^1(j\omega_{NL1})$  and  $X_i^2(j\omega_{NL1})$  to

calculate  $ST1^{i,i+1}$ ,  $ST2^{i,i+1}$ , and  $S\delta^{i,i+1}$  for  $i = 1, \dots, n - 1$  using Eqs. (6.8) and (6.9). Then, evaluate  $SI\delta_{\max}$  using Eq.(6.14) to check whether

$$SI\delta_{\max} \leq \varepsilon_2 \quad (6.27)$$

where  $\varepsilon_2$  is another a priori determined threshold. If Eq. (6.27) holds, it can be concluded that there exists only one nonlinear component in the system. Otherwise, there are more than one nonlinear components.

Step 3) If Step 2) indicates there exists only one nonlinear component, then, the modal parameters can be identified by using the same method as that in the linear case.

Step 4) If Step 2) indicates there exist more than one nonlinear components in the system, evaluate  $\overline{SI\delta}^{i,i+1}$ ,  $i = 1, \dots, n - 1$  by using Eq.(6.15) to find those  $i$ 's such that

$$\overline{SI\delta}^{i,i+1} \geq \varepsilon_4 \quad (6.28)$$

where  $\varepsilon_4$  is a priori determined threshold. Denote those  $i$ 's such that (6.28) holds as

$$i'', i'' + 1, \dots, i'' + m'' - 1$$

where  $m'' > 1$ . Then, it can be concluded that these nonlinear components are located between mass  $i''$  and mass  $i'' + m''$ .

Step 5) When the locations of nonlinear components are determined, two output DOFs involved in transmissibility evaluation can be chosen so that

$$i, k \notin \{i'', i'' + 1, \dots, i'' + m'' - 1\}$$

This includes two possibilities:

- a) Both output DOFs involved are on the same side of nonlinear components, that is

$$1 \leq i, k \leq i'' \text{ or } i'' + m'' \leq i, k \leq n \quad i \neq k \quad (6.29)$$

- b) Two output DOFs involved are on the different sides of nonlinear components, that is

$$\left\{ \begin{array}{l} 1 \leq i \leq i'' \\ i'' + m'' \leq k \leq n \end{array} \right. \text{ or } \left\{ \begin{array}{l} i'' + m'' \leq i \leq n \\ 1 \leq k \leq i'' \end{array} \right. \quad (6.30)$$

Then evaluate  $\Delta^{-1}T_{i,k}^{S',S''}(\omega)$  by using Eq. (6.19) in the situations where two different loading conditions are considered including, for example, situation 1): first and second loading conditions are considered, situation 2): first and third loading conditions are considered, etc. Consequently, the system's poles can be identified from the common peaks of these  $\Delta^{-1}T_{i,k}^{S',S''}(\omega)$ .

The theoretical basis of each step and some requirements for loading conditions are discussed in the following remarks.

### 6.3.3 Remarks

- a) Steps 1), 2) and 4) can be used to detect the nonlinear components in the system and find their locations, the theoretical basis of these three steps are the same as corresponding steps of nonlinearity localization procedure in Chapters 4 and 5. Steps 3) and 5) are used to identify poles of the nonlinear system, they exploit the conclusion in Proposition 6.2 and the observations from Figs. 6.4 and 6.5.  $\varepsilon_1, \varepsilon_2, \varepsilon_4$  are three threshold parameters in the method which are determined in the same way as determining the corresponding thresholds in the nonlinearity localization procedure in Chapters 4 and 5.
- b) According to Proposition 6.2, the system can be subject to one input or multiple inputs. However, in different loading conditions, the loading inputs should be applied on different locations, and have the same frequency range which covers some natural frequencies of the system.

- c) The proposed procedure for modal identification of nonlinear systems can be used for all cases where the nonlinear phenomenon is local including the cases when the system is subject to damage with nonlinear features and the cases when the nonlinearity is caused by other factors, such as extremely large loadings.

### 6.3.4 Simulation study

In order to demonstrate how to use above proposed procedure to identify poles of nonlinear systems, one simulation study is conducted in this section. The 10DOF system used in Chapter 4 with the value of linear and nonlinear parameters the same as that in simulation studies in Section 4.6 is considered again for the simulation study. Therefore, thresholds  $\varepsilon_1$ ,  $\varepsilon_2$ , and  $\varepsilon_4$  listed in Table 4.1 are used again.

It is assumed that there are three nonlinear components which are 5<sup>th</sup>, 6<sup>th</sup> and 7<sup>th</sup> springs, namely,  $\bar{J} = 3$ ,  $J_1 = 5$ ,  $J_2 = 6$  and  $J_3 = 7$ , and the inputs under three different conditions are exactly the same, but applied on different locations, in this case, 2<sup>nd</sup>, 6<sup>th</sup> and 9<sup>th</sup> masses respectively. The input is shown as

$$f(t) = \frac{A \sin(\omega_f t + \beta)}{2\pi(t - t_1)} \quad (6.31)$$

where,  $A = 3$ ,  $\omega_f = 80\pi$ ,  $\beta = 0$  and  $t_1 = 5$  seconds. Therefore, the frequency range of the loadings is  $\omega_F = [0, \omega_f] = [0, 80\pi]$ ; the highest order of system nonlinearity is determined as  $N = 6$  from the observation on spectra of the system output responses, for example, the output response of the 7<sup>th</sup> mass when the input is applied on the 2<sup>nd</sup> mass as shown Fig. 6.6; the nonlinearity generated frequencies are calculated by solving Eqs. (6.1)-(6.3) in Proposition 6.1 and the results are

$$\omega_{NL} = (80, 480\pi] \quad (6.32)$$



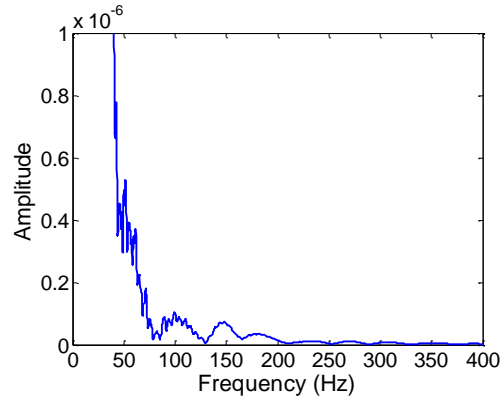


Fig. 6.6 Output response of the 7<sup>th</sup> mass when the input is applied on the 2<sup>nd</sup> mass

The results of the simulation study obtained in each step of the proposed method are given as follows.

**Step 1)**

In this case, the ratio between the system response at every nonlinearity generated frequency in Eq. (6.32) and maximum amplitude of system inputs is calculated and the index  $IND_1$  was evaluated using (6.11) as

$$IND_1 = \max \left\{ \left| \frac{\max\{X_i^1(j\omega'_{NL})\}}{\max\{X_i^1(j\omega'_F)\}} \right|, \left| \frac{\max\{X_i^2(j\omega'_{NL})\}}{\max\{X_i^2(j\omega'_F)\}} \right|, i = 1, \dots, 10, \omega'_F \in \omega_F \text{ and } \omega'_{NL} \in \omega_{NL} \right\} \quad (6.33)$$

$$= 0.0035 \geq \varepsilon_1 = 8.42 \times 10^{-6}$$

where  $\omega_{NL}$  is shown in Eq.(6.32). Therefore, it can be concluded that there exists nonlinear component in the system.

**Step 2)**

At this step, the nonlinearity generated frequency range was determined as  $\omega_{NL1} = [\omega_1, \omega_2] = (80,160]$  , and  $X_i^1(j\omega_{NL1})$  and  $X_i^2(j\omega_{NL1})$  are used for nonlinearity localization. So

$$STI1^{i,i+1}, STI2^{i,i+1} \text{ and } SI\delta^{i,i+1}, i = 1, \dots, 9$$

were evaluated using Eqs. (6.8) and (6.9). Then,  $SI\delta_{\max}$  was determined using Eq.

(6.14), the result is

$$SI\delta_{\max} = 2.6245 > \varepsilon_2 = 0.0099$$

So it is known that there are more than one nonlinear components in the system.

**Step 4)**

As Step 2) has shown that there are more than one nonlinear components in the system, Step 4) rather than Step 3) of the proposed method is used in this case. At this step,  $\overline{SI\delta}^{i,i+1}$ ,  $i = 1, \dots, 9$  were evaluated by Eq. (6.15), the results are shown in Table 6.6, in which it can be observed that

$$\overline{SI\delta}^{i,i+1} \geq \varepsilon_4 = 0.0015, \quad i = 4,5,6$$

Therefore,  $i'' = 4$ , and  $m'' = 3$ , and it can be concluded that the nonlinear components are located between mass  $i'' = 4$  and mass  $i'' + m'' = 7$  in the system.

Table 6.6 The value of  $\overline{SI\delta}^{i,i+1}$  when the 5<sup>th</sup>, 6<sup>th</sup> and 7<sup>th</sup> springs are nonlinear

$i$	$\overline{SI\delta}^{i,i+1}$	$i$	$\overline{SI\delta}^{i,i+1}$	$i$	$\overline{SI\delta}^{i,i+1}$
1	0.000424	4	1	7	0.000617
2	0.000379	5	0.249364	8	0.000554
3	0.000215	6	0.135129	9	0.000263

**Step 5)**

As Step 4) has determined the nonlinear components are located between 4<sup>th</sup> mass and 7<sup>th</sup> mass, therefore, two output DOFs involved in transmissibility evaluation can be chosen as 3<sup>rd</sup> and 8<sup>th</sup>. Then  $\Delta^{-1}T_{i,k}^{S',S''}(\omega)$  are determined to obtain  $\Delta^{-1}T_{3,8}^{2,6}(\omega)$  and  $\Delta^{-1}T_{3,8}^{2,9}(\omega)$  using Eq. (6.19), the results are shown in Fig. 6.7.

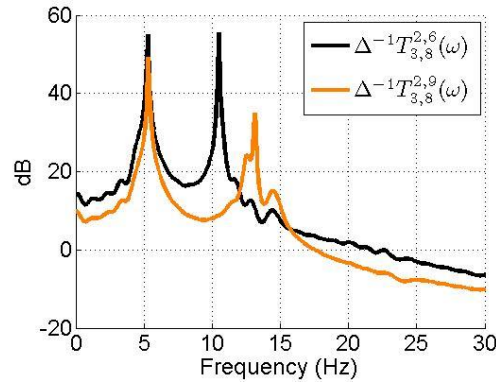


Fig. 6.7  $\Delta^{-1}T_{3,8}^{2,6}(\omega)$  and  $\Delta^{-1}T_{3,8}^{2,9}(\omega)$  of the nonlinear system (4.5)

It can be seen that the two  $\Delta^{-1}T_{i,k}^{S',S''}(\omega)$  both reach a peak at  $\omega \approx 5.4\text{Hz}$  in Fig. 6.7.

Therefore, the modal analysis method for the nonlinear MDOF system can be used to identify the pole of the nonlinear system in this case. Obviously, the conclusions reached at each step are all consistent with the real situation of the simulated system.

## 6.4 Conclusions

This chapter studied the determination of the output frequency components of nonlinear systems subject to the loading inputs with band limited frequencies, and demonstrated, by examples, that the MIMO nonlinear system output frequency ranges can be correctly determined using the analysis results.

Then the detection and localization of nonlinear components in the systems subject to inputs with band limited frequencies were studied by extending the results introduced in Chapters 4 and 5 to the more general and practical systems.

Finally, the theoretical principle of transmissibility analysis based modal identification method for linear systems is introduced and demonstrated by simulation examples. Furthermore, studies were conducted to combine this method with the newly proposed nonlinearity detection and localization technique to identify the poles of nonlinear systems to implement a transmissibility analysis based modal identification for nonlinear structural systems.

## Chapter 7

### Conclusions

Structural health monitoring, which is concerned with damage detection and identification, is always applied for engineering systems in order to guarantee systems' safety and reliability. Although extensive research works have been conducted in the area of SHM, there is still no approach that can systematically take the effect of system operational and environmental conditions on SHM results into account.

Transmissibility analysis is a well-known technique for SHM. But traditional transmissibility is basically a linear system concept and relevant techniques assume the systems behave linearly. Consequently, the analysis results generally depend on the locations of system input and can therefore also be affected by system operational and environmental conditions.

In order to address these fundamental problems with SHM, in the present study, a general structural health monitoring method is first proposed which can be used to address a wide class of SHM problems via systematically taking the effects of operating conditions and environmental changes into account. Moreover, considering the well-known facts that damage can often make a structural system behave nonlinearly, new transmissibility analysis methods have been developed for the detection and localization of damage with nonlinear features in MDOF structural systems. These methods do not require that much structural loading input information as needed by traditional transmissibility analysis, so as to be able to solve input location dependent problem with traditional transmissibility analysis when dealing with detection and localization of damage with nonlinear features for a wide range of engineering systems. In addition, new guidelines have also been proposed based on the new transmissibility analysis for the modal analysis for nonlinear structural systems.

## 7.1 Main contributions of this thesis

The main contributions of this thesis can be summarized as follows.

(1) A novel health probability based structural health monitoring method for changing environmental and operational conditions

A baseline model, which represents the relationship between the RMS feature of sensor data and the changes in the system environmental and operating parameters, is built by a B-spline function based modeling approach. The tolerance range of baseline modelling error is determined by using a statistical analysis. Then the health probability, which is defined as the proportion of the cases where the modeling errors are within the tolerance range, is used to determine whether an inspected system is working in a normal or damaged working condition.

(2) Transmissibility analysis methods for detection and location of damage via nonlinear features in MDOF structural systems

New methods have been developed to determine the output frequencies of nonlinear systems under different types of inputs. The characteristics of NOFRFs transmissibility and transmissibility of system responses at frequencies generated by system nonlinearity are investigated to reveal the damage sensitive features which are independent from the locations of system inputs. A series of new transmissibility analysis based methods are then proposed to detect and localize damage with nonlinear features in MDOF structural systems. Furthermore, the proposed nonlinearity detection and location methods are extended to more general case of higher order dynamics and applied to study the detection and localization of water tree damage in power cable system.

(3) Transmissibility analysis based modal identification for nonlinear MDOF systems

Effects of damage with nonlinear features on the transmissibility analysis based modal

identification method are also investigated. Based on the results of nonlinearity detection and localization, new guidelines are developed for applying the transmissibility analysis based modal identification to nonlinear structural systems.

These results provide a series of new SHM methods, which can systematically take many effects of system operating conditions and environmental changes on SHM results into account and provide more effective solutions to a wide range of engineering structural health monitoring problems. Both numerical simulation studies and experimental data analysis have been conducted to verify the effectiveness and demonstrate the potential practical applications of these new methods.

## **7.2 Suggestions for further work**

Although, the present research has developed many new methods for structural health monitoring and damage localization, there are many further issues yet to be addressed. These issues mainly involve the extension of the new transmissibility methods to structural systems where there exist both damage which induces changes in system linear characteristics and damage with nonlinear features. Traditional transmissibility is a linear system concept, and can only be applied to detect and locate damage which mainly induce system linear characteristic changes. The new transmissibility analysis based methods developed in this thesis are mainly concerned with detection and location of damage with nonlinear features. However, in engineering practice, damage which induce system linear characteristic changes and damage with nonlinear features can exist simultaneously in a system. Thus, the development of methods which can deal with the detection and location of damage with these different natures at the same time are important for engineering applications of the new transmissibility analysis methods proposed in this study.

## Publication list

- [1]. **X. Y. Zhao**, Z. Q. Lang, G. Park, C. R. Farrar, M. D. Todd, Z. Mao, "Transmissibility analysis method for detection and location of damage via nonlinear features in MDOF structural systems," IEEE/ASME Transactions on Mechatronics, 2014. (Accepted).
- [2]. **X. Y. Zhao** and Z. Lang, "Structural health monitoring under changing environmental conditions," 2014 PhD Presentation Showcase, pp. 1-9. The Royal Society, London, UK, Oct. 2014.
- [3]. **X. Y. Zhao** and Z. Lang, " A novel health probability-based engineering system condition and health monitoring method," the 11th International Conference on Condition Monitoring and Machinery Failure Prevention Technologies, pp. 107(1-13), Manchester, UK, June, 2014.
- [4]. **X. Y. Zhao** and Z. Lang, "Transmissibility analysis for damage detection and location using nonlinear features of structural system response," the 3rd International Conference on Recent Advances in Nonlinear Mechanics, Harbin, China, Jan., 2014.
- [5]. **X. Y. Zhao** and Z. Lang, "Detecting location of damaged components in MDOF structural systems using transmissibility at super-harmonic," 2012 PhD Presentation Showcase, pp. 1-11. IET, Savoy Place, London, UK, Oct. 2012.
- [6]. **X. Y. Zhao** and Z. Lang, "A novel health probability for structural health monitoring," 18th International Conference on Automation and Computing (ICAC), pp. 1-6. Loughborough University, Leicestershire, UK, Sep. 2012.

## Appendix A

### Recursive forward-regression orthogonal estimator

Identification of MIMO nonlinear systems using a forward-regression orthogonal estimator can be introduced as follows according to Ref. [199 ].

Consider the following linear regression function:

$$\mathbf{Y} = \mathbf{X}\boldsymbol{\beta} + \boldsymbol{\xi} \quad (\text{A.1})$$

where  $\mathbf{X}$ ,  $\mathbf{Y}$  are variable vectors,  $\boldsymbol{\beta}$  is coefficient vector,  $\boldsymbol{\xi}$  is error vector,  $\mathbf{Y} = \{y(1), y(2), \dots, y(N)\}^T$ ,  $\mathbf{X} = \{X(1), X(2), \dots, X(N)\}^T$ ,  $\boldsymbol{\beta} = \{\beta_1, \beta_2, \dots, \beta_M\}^T$  and  $X(t) = \{x_1(t), x_2(t), \dots, x_M(t)\}^T$ . The purpose of this estimator is to select the terms in  $X(t) = \{x_1(t), x_2(t), \dots, x_M(t)\}$  which contribute significantly to the model between  $\mathbf{X}$  and  $\mathbf{Y}$ , and identify their coefficients.

There are the assumptions for Eq.(A.1) are made as follows:

- 1).  $\boldsymbol{\xi}$  is a zero mean white sequence and is uncorrelated with  $\mathbf{X}$ ;
- 2). All stochastic process involved are ergodic;
- 3).  $\mathbf{X}^T \mathbf{X}$  is positive definite so that it can be decomposed into:

$$\mathbf{X}^T \mathbf{X} = \mathbf{A}^T \mathbf{D} \mathbf{A} \quad (\text{A.2})$$

where  $\mathbf{A}$  is an upper triangular matrix with unity diagonal elements, and  $\mathbf{D}$  is a diagonal matrix with positive diagonal elements.

Then, Eq.(A.1) can be rewritten as:

$$\mathbf{Y} = \mathbf{X}(\mathbf{A}^{-1}\mathbf{A})\boldsymbol{\beta} + \boldsymbol{\xi} = \mathbf{W}\mathbf{g} \quad (\text{A.3})$$

where



$$\begin{cases} \mathbf{W} = \mathbf{X}\mathbf{A}^{-1} \\ \mathbf{g} = \mathbf{A}\boldsymbol{\beta} \end{cases} \quad (\text{A.4})$$

Because

$$\mathbf{W}^T\mathbf{W} = (\mathbf{X}\mathbf{A}^{-1})^T(\mathbf{X}\mathbf{A}^{-1}) = \mathbf{D} \quad (\text{A.5})$$

the matrix  $\mathbf{W}$  is an orthogonal matrix.

Auxiliary regressors  $w_i$  can be obtained recursively from:

$$\mathbf{W} = \mathbf{X} - \mathbf{W}(\mathbf{A} - \mathbf{I}) \quad (\text{A.6})$$

The upper triangular matrix  $\mathbf{A}$  satisfies

$$\mathbf{A} = \mathbf{D}^{-1}\mathbf{W}^T\mathbf{P} \quad (\text{A.7})$$

The auxiliary parameter vector  $\mathbf{A}$  satisfies:

$$\mathbf{g} = \mathbf{D}^{-1}\mathbf{W}^T\mathbf{Y} - \mathbf{D}^{-1}\mathbf{W}^T\boldsymbol{\xi} \quad (\text{A.8})$$

So that the estimated  $\mathbf{g}$  is given by

$$\hat{\mathbf{g}} = \mathbf{D}^{-1}\mathbf{W}^T\mathbf{Y} \quad (\text{A.9})$$

The estimates of the original parameters can be computed from

$$\hat{\boldsymbol{\beta}} = \hat{\mathbf{g}} - (\mathbf{A} - \mathbf{I})\hat{\boldsymbol{\beta}} \quad (\text{A.10})$$

The error reduction ratio (ERR) due to  $i$ th term is defined as:

$$[err]_i = \frac{\hat{g}_i \sum_{t=1}^N w_i^2(t)}{\sum_{t=1}^N y^2(t)} \quad (\text{A.11})$$

The terms that contribute greatly to the model can be selected as follows:

Firstly, all the  $x_i(t), i = 1, 2, \dots, M$  are considered as possible candidates for  $w_1(t)$ .

For  $i = 1, 2, \dots, M$ , calculate

$$w_1^{(l)}(t) = x_i(t), \hat{g}_1^{(l)} = \frac{\sum_{t=1}^N w_1^{(l)}(t)y(t)}{\sum_{t=1}^N (w_1^{(l)}(t))^2}, [err]_1^{(l)} = \frac{(\hat{g}_1^{(l)})^2 \sum_{t=1}^N (w_1^{(l)}(t))^2}{\sum_{t=1}^N z^2(t)} \quad (\text{A.12})$$

Find the maximum of  $[err]_1^{(l)}$ , for example,  $[err]_1^{(f)} = \max\{[err]_1^{(l)}, 1 \leq l \leq M\}$ .

Then the first term  $w_1(t) = w_1^{(f)}(t), x_f(t)$  is selected with  $\hat{g}_1 = \hat{g}_1^{(f)}$  and  $[err]_1 = [err]_1^{(f)}$ .

Secondly, all the  $x_i(t), i = 1, 2, \dots, M, i \neq f$  are considered as possible candidates for  $w_2(t)$ . For  $i = 1, 2, \dots, M, i \neq f$ , calculate

$$\begin{aligned} w_2^{(l)}(t) = x_i(t) - \alpha_{12}^{(l)} w_1(t), \hat{g}_2^{(l)} &= \frac{\sum_{t=1}^N w_2^{(l)}(t)y(t)}{\sum_{t=1}^N (w_2^{(l)}(t))^2}, [err]_2^{(l)} \\ &= \frac{(\hat{g}_2^{(l)})^2 \sum_{t=1}^N (w_2^{(l)}(t))^2}{\sum_{t=1}^N z^2(t)} \end{aligned} \quad (\text{A.13})$$

where

$$\alpha_{12}^{(l)} = \frac{\sum_{t=1}^N w_1(t)x_i(t)}{\sum_{t=1}^N w_1^2(t)} \quad (\text{A.14})$$

Find the maximum of  $[err]_2^{(l)}$ , for example,  $[err]_2^{(k)} = \max\{[err]_2^{(l)}, 1 \leq l \leq M, i \neq f\}$ . Then the second term  $w_2(t) = w_2^{(k)}(t) = x_1(t) - \alpha_{12} w_1(t), x_k(t)$  is selected with  $\alpha_{12} = \alpha_{12}^{(k)}, \hat{g}_2 = \hat{g}_2^{(k)}$  and  $[err]_2 = [err]_2^{(k)}$ .

The procedure is terminated at the  $M_s$ th step either when

$$1 - \sum_{i=1}^{M_s} [err]_i < a \text{ desired tolerance}, M_s < M \quad (\text{A.15})$$

or when  $M_s = M$ .

After the terms which contribute significantly to the model are selected by above procedure, their coefficients can be identified by using least square method.

## Appendix B

### Proof of Proposition 4.2

According to Ref. [123], the  $\bar{n}$ th order frequency response of the system's  $i$ th output can be expressed as

$$X_{(i,\bar{n})}(j\omega) = \frac{1}{2^{\bar{n}}} \sum_{\omega_1 + \dots + \omega_{\bar{n}} = \omega} A(j\omega_1) \dots A(j\omega_{\bar{n}}) H_{(i,\bar{n})}(j\omega_1, \dots, j\omega_{\bar{n}}) \quad (\text{B.1})$$

where

$$A(j\omega_k) = \begin{cases} Ae^{j\beta} & \text{if } \omega_k = \omega_F \\ Ae^{-j\beta} & \text{if } \omega_k = -\omega_F \\ 0 & \text{otherwise} \end{cases} \quad (\text{B.2})$$

Obviously, if  $b$  ( $b \in \{0, 1, 2, \dots, \bar{n}\}$ )  $\omega_k$ 's in  $\omega_1, \dots, \omega_{\bar{n}}$  take the value of  $\omega_F$ , then the remaining  $(\bar{n} - b)$   $\omega_k$ 's in  $\omega_1, \dots, \omega_{\bar{n}}$  take the value of  $-\omega_F$ . Consequently, the possible frequency components in  $X_{(i,\bar{n})}(j\omega)$  can be obtained as

$$\Omega_{\bar{n}} = \{(-\bar{n} + 2b)\omega_F, b = 0, 1, \dots, \bar{n}\} = \{-\bar{n}\omega_F, -(\bar{n} - 2)\omega_F, \dots, (\bar{n} - 2)\omega_F, \bar{n}\omega_F\} \quad (\text{B.3})$$

and the possible frequency components of system output are given by [46]

$$\begin{aligned} \Omega &= \bigcup_{\bar{n}=N-1}^N \Omega_{\bar{n}} = \{-N\omega_F, -(N-2)\omega_F, \dots, (N-2)\omega_F, N\omega_F\} \\ &\cup \{-(N-1)\omega_F, -(N-3)\omega_F, \dots, (N-3)\omega_F, (N-1)\omega_F\} \\ &= \{0, \pm 1\omega_F, \pm 2\omega_F, \dots, \pm N\omega_F\} \end{aligned} \quad (\text{B.4})$$

From Eq. (B.1), it is known that

$$X_{(i,\bar{n})}(j\omega) = G_{(i,\bar{n})}(j\omega) F_{\bar{n}}(j\omega) \quad (\text{B.5})$$

where

$$G_{(i,\bar{n})}(j\omega) = \frac{\sum_{\omega_1+\dots+\omega_{\bar{n}}=\omega} A(j\omega_1) \dots A(j\omega_{\bar{n}}) H_{(i,\bar{n})}(j\omega_1, \dots, j\omega_{\bar{n}})}{\sum_{\omega_1+\dots+\omega_{\bar{n}}=\omega} A(j\omega_1) \dots A(j\omega_{\bar{n}})}$$

and

$$F_{\bar{n}}(j\omega) = \frac{1}{2^{\bar{n}}} \sum_{\omega_1+\dots+\omega_{\bar{n}}=\omega} A(j\omega_1) \dots A(j\omega_{\bar{n}})$$

in this case. As Eq. (B.3) indicates even order harmonics are produced by even order nonlinearity and odd order harmonics are produced by odd order nonlinearity, Eqs. (4.19) and (4.20) can be obtained from (B.5) from the case of  $N$  is odd and from the case of  $N$  is even, respectively. Thus, the proof of Proposition 4.2 is completed.

## Appendix C

### Proof of Proposition 4.3

Consider  $\bar{k}$  and  $N$  are all even first. In this case, it is known from (4.20) that

$$X_i(j\bar{k}\omega_F) = G_{(i,\bar{k})}(j\bar{k}\omega_F)F_{\bar{k}}(j\bar{k}\omega_F) + G_{(i,\bar{k}+2)}(j\bar{k}\omega_F)F_{\bar{k}+2}(j\bar{k}\omega_F) + \cdots + G_{(i,N)}(j\bar{k}\omega_F)F_N(j\bar{k}\omega_F) \quad (C.1)$$

and

$$X_{i+1}(j\bar{k}\omega_F) = G_{(i+1,\bar{k})}(j\bar{k}\omega_F)F_{\bar{k}}(j\bar{k}\omega_F) + G_{(i+1,\bar{k}+2)}(j\bar{k}\omega_F)F_{\bar{k}+2}(j\bar{k}\omega_F) + \cdots + G_{(i+1,N)}(j\bar{k}\omega_F)F_N(j\bar{k}\omega_F) \quad (C.2)$$

where  $\bar{k} = 2, 4, \dots, N-2, N$ . It is known from Property (i) of the NOFRF transmissibility given by Eq. (4.14) that if  $\bar{J} > 1$ , for  $1 \leq i \leq J_1 - 2$  or  $J_{\bar{J}} \leq i \leq n - 1$ ,

$$\begin{aligned} \frac{G_{(i,\bar{k})}(j\bar{k}\omega_F)F_{\bar{k}}(j\bar{k}\omega_F)}{G_{(i+1,\bar{k})}(j\bar{k}\omega_F)F_{\bar{k}}(j\bar{k}\omega_F)} &= \frac{G_{(i,\bar{k}+2)}(j\bar{k}\omega_F)F_{\bar{k}+2}(j\bar{k}\omega_F)}{G_{(i+1,\bar{k}+2)}(j\bar{k}\omega_F)F_{\bar{k}+2}(j\bar{k}\omega_F)} = \cdots \\ &= \frac{G_{(i,N)}(j\bar{k}\omega_F)F_N(j\bar{k}\omega_F)}{G_{(i+1,N)}(j\bar{k}\omega_F)F_N(j\bar{k}\omega_F)} = T_{i,i+1}^{NL}(j\bar{k}\omega_F) \\ &= \bar{Q}_{i,i+1}(j\bar{k}\omega_F) \end{aligned} \quad (C.3)$$

Eqs. (C.1)-(C.3) imply that

$$\begin{aligned} ST^{i,i+1}(j\bar{k}\omega_F) &= \frac{X_i(j\bar{k}\omega_F)}{X_{i+1}(j\bar{k}\omega_F)} = \\ &= \frac{G_{(i,\bar{k})}(j\bar{k}\omega_F)F_{\bar{k}}(j\bar{k}\omega_F) + G_{(i,\bar{k}+2)}(j\bar{k}\omega_F)F_{\bar{k}+2}(j\bar{k}\omega_F) + \cdots + G_{(i,N)}(j\bar{k}\omega_F)F_N(j\bar{k}\omega_F)}{G_{(i+1,\bar{k})}(j\bar{k}\omega_F)F_{\bar{k}}(j\bar{k}\omega_F) + G_{(i+1,\bar{k}+2)}(j\bar{k}\omega_F)F_{\bar{k}+2}(j\bar{k}\omega_F) + \cdots + G_{(i+1,N)}(j\bar{k}\omega_F)F_N(j\bar{k}\omega_F)} \\ &= T_{i,i+1}^{NL}(j\bar{k}\omega_F) = \bar{Q}_{i,i+1}(j\bar{k}\omega_F) \end{aligned} \quad (C.4)$$

Therefore, Eq. (4.22) holds.

Also according to Property (i) of the NOFRF transmissibility, it is known that if

$\bar{J} > 1$ , for  $J_1 - 1 \leq i \leq J_J - 1$ ,

$$\begin{aligned} \frac{G_{(i,\bar{k})}(j\bar{k}\omega_F)F_{\bar{k}}(j\bar{k}\omega_F)}{G_{(i+1,\bar{k})}(j\bar{k}\omega_F)F_{\bar{k}}(j\bar{k}\omega_F)} &\neq T_{i,i+1}^{NL}(j\bar{k}\omega_F), \\ \frac{G_{(i,\bar{k}+2)}(j\bar{k}\omega_F)F_{\bar{k}+2}(j\bar{k}\omega_F)}{G_{(i+1,\bar{k}+2)}(j\bar{k}\omega_F)F_{\bar{k}+2}(j\bar{k}\omega_F)} &\neq T_{i,i+1}^{NL}(j\bar{k}\omega_F), \dots, \\ \text{and } \frac{G_{(i,N-2)}(j\bar{k}\omega_F)F_N(j\bar{k}\omega_F)}{G_{(i+1,N-2)}(j\bar{k}\omega_F)F_N(j\bar{k}\omega_F)} &\neq T_{i,i+1}^{NL}(j\bar{k}\omega_F), \end{aligned}$$

so that

$$\begin{aligned} ST^{i,i+1}(j\bar{k}\omega_F) &= \frac{X_i(j\bar{k}\omega_F)}{X_{i+1}(j\bar{k}\omega_F)} \\ &= \frac{G_{(i,\bar{k})}(j\bar{k}\omega_F)F_{\bar{k}}(j\bar{k}\omega_F) + G_{(i,\bar{k}+2)}(j\bar{k}\omega_F)F_{\bar{k}+2}(j\bar{k}\omega_F) + \dots + G_{(i,N)}(j\bar{k}\omega_F)F_N(j\bar{k}\omega_F)}{G_{(i+1,\bar{k})}(j\bar{k}\omega_F)F_{\bar{k}}(j\bar{k}\omega_F) + G_{(i+1,\bar{k}+2)}(j\bar{k}\omega_F)F_{\bar{k}+2}(j\bar{k}\omega_F) + \dots + G_{(i+1,N)}(j\bar{k}\omega_F)F_N(j\bar{k}\omega_F)} \\ &\neq T_{i,i+1}^{NL}(j\bar{k}\omega_F) \end{aligned} \tag{C.5}$$

Therefore, Eq. (4.23) holds.

According to Property (ii) of the NOFRF transmissibility given by (4.15), if  $\bar{J} = 1$ , for  $i = 1, \dots, n - 1$

$$\begin{aligned} \frac{G_{(i,\bar{k})}(j\bar{k}\omega_F)F_{\bar{k}}(j\bar{k}\omega_F)}{G_{(i+1,\bar{k})}(j\bar{k}\omega_F)F_{\bar{k}}(j\bar{k}\omega_F)} &= \frac{G_{(i,\bar{k}+2)}(j\bar{k}\omega_F)F_{\bar{k}+2}(j\bar{k}\omega_F)}{G_{(i+1,\bar{k}+2)}(j\bar{k}\omega_F)F_{\bar{k}+2}(j\bar{k}\omega_F)} = \dots \\ &= \frac{G_{(i,N)}(j\bar{k}\omega_F)F_N(j\bar{k}\omega_F)}{G_{(i+1,N)}(j\bar{k}\omega_F)F_N(j\bar{k}\omega_F)} = T_{i,i+1}^{NL}(j\bar{k}\omega_F) = \bar{Q}_{i,i+1}(j\bar{k}\omega_F) \end{aligned} \tag{C.6}$$

Eqs. (C.1), (C.2) and (C.6) imply that

$$\begin{aligned} ST^{i,i+1}(j\bar{k}\omega_F) &= \frac{X_i(j\bar{k}\omega_F)}{X_{i+1}(j\bar{k}\omega_F)} \\ &= \frac{G_{(i,\bar{k})}(j\bar{k}\omega_F)F_{\bar{k}}(j\bar{k}\omega_F) + G_{(i,\bar{k}+2)}(j\bar{k}\omega_F)F_{\bar{k}+2}(j\bar{k}\omega_F) + \dots + G_{(i,N)}(j\bar{k}\omega_F)F_N(j\bar{k}\omega_F)}{G_{(i+1,\bar{k})}(j\bar{k}\omega_F)F_{\bar{k}}(j\bar{k}\omega_F) + G_{(i+1,\bar{k}+2)}(j\bar{k}\omega_F)F_{\bar{k}+2}(j\bar{k}\omega_F) + \dots + G_{(i+1,N)}(j\bar{k}\omega_F)F_N(j\bar{k}\omega_F)} \end{aligned}$$

$$= T_{i,i+1}^{NL}(j\bar{k}\omega_F) = \bar{Q}_{i,i+1}(j\bar{k}\omega_F) \quad (C.7)$$

Therefore, Eq. (4.24) holds.

As  $N$  is assumed to be even, for  $\bar{J} = 1$ , it is known from the first equation in Eqs. (4.16) and (4.17) and the first Eq. of (4.20) that

when  $S \geq J_1$ , if  $1 \leq i \leq J_1 - 2$  or  $S \leq i \leq n - 1$ , or when  $S < J_1$  if  $1 \leq i \leq S - 1$  or  $J_1 \leq i \leq n - 1$ ,

$$\begin{aligned} ST^{i,i+1}(j\omega_F) &= \frac{X_i(j\omega_F)}{X_{i+1}(j\omega_F)} \\ &= \frac{G_{(i,1)}(j\omega_F)F_1(j\omega_F) + G_{(i,3)}(j\omega_F)F_3(j\omega_F) + \cdots + G_{(i,N-1)}(j\omega_F)F_{N-1}(j\omega_F)}{G_{(i+1,1)}(j\omega_F)F_1(j\omega_F) + G_{(i+1,3)}(j\omega_F)F_3(j\omega_F) + \cdots + G_{(i+1,N-1)}(j\omega_F)F_{N-1}(j\omega_F)} \\ &= T_{i,i+1}^L(j\omega_F) = Q_{i,i+1}(j\omega_F) \end{aligned} \quad (C.8)$$

that is, the first equation of Eq. (4.25) holds. Otherwise, it is known from the second equation of Eqs. (4.16) and (4.17) and the first Eq. of (4.20) that

$$\begin{aligned} ST^{i,i+1}(j\omega_F) &= \frac{X_i(j\omega_F)}{X_{i+1}(j\omega_F)} \\ &= \frac{G_{(i,1)}(j\omega_F)F_1(j\omega_F) + G_{(i,3)}(j\omega_F)F_3(j\omega_F) + \cdots + G_{(i,N-1)}(j\omega_F)F_{N-1}(j\omega_F)}{G_{(i+1,1)}(j\omega_F)F_1(j\omega_F) + G_{(i+1,3)}(j\omega_F)F_3(j\omega_F) + \cdots + G_{(i+1,N-1)}(j\omega_F)F_{N-1}(j\omega_F)} \\ &\neq T_{i,i+1}^L(j\omega_F) = Q_{i,i+1}(j\omega_F) \end{aligned} \quad (C.9)$$

So the second equation of Eq. (4.26) holds.

For all the other cases of  $N$  and  $\bar{k}$ , i.e.,  $N$  and  $\bar{k}$  are all odd, or  $N$  is odd but  $\bar{k}$  is even, or  $N$  is even but  $\bar{k}$  is odd, Eqs. (4.22)-(4.25) can be proved by following the same approach as above. Thus, the proof of Proposition 4.3 is completed.

## Appendix D

### Proof of Proposition 5.1

When the inputs applied on the MIMO nonlinear system (5.1) are

$$\left\{ \begin{array}{l} f_1(t) = \sum_{q=1}^{n_1} e^{j\omega_q t} \\ \vdots \\ f_l(t) = \sum_{q=n_1+\dots+n_{l-1}+1}^{n_1+\dots+n_l} e^{j\omega_q t} \\ \vdots \\ f_m(t) = \sum_{q=n_1+\dots+n_{m-1}+1}^{n_1+\dots+n_m} e^{j\omega_q t} \end{array} \right. \quad (\text{D.1})$$

where  $n_1 + n_2 + \dots + n_m = \bar{n}$  and  $\bar{n} \geq 2$ , the corresponding  $i$ th output according to the Volterra series is

$$\begin{aligned} x_i = & \sum_{q=1}^{n_1} H_{(i,p_1=1,p_2=0,\dots,p_m=0)}^{(1)}(j\omega_q) e^{j\omega_q t} + \dots \\ & + \sum_{q=n_1+\dots+n_{l-1}+1}^{n_1+\dots+n_l} H_{(i,p_1=0,\dots,p_l=1,\dots,p_m=0)}^{(1)}(j\omega_q) e^{j\omega_q t} + \dots \\ & + \sum_{q=n_1+\dots+n_{m-1}+1}^{n_1+\dots+n_m} H_{(i,p_1=0,\dots,p_m=1)}^{(1)}(j\omega_q) e^{j\omega_q t} + \dots \\ & + \chi H_{(i,p_1=n_1,p_2=n_2,\dots,p_m=n_m)}^{(\bar{n})}(j\omega_1, j\omega_2, \dots, j\omega_{\bar{n}}) e^{j(\omega_1+\omega_2+\dots+\omega_{\bar{n}})t} + \dots \end{aligned} \quad (\text{D.2})$$

where,  $\chi$  is the coefficient of

$$H_{(i,p_1=n_1,p_2=n_2,\dots,p_m=n_m)}^{(\bar{n})}(j\omega_1, j\omega_2, \dots, j\omega_{\bar{n}}) e^{j(\omega_1+\omega_2+\dots+\omega_{\bar{n}})t}.$$

Substitute Eqs.(D.1) and (D.2) into Eq.(5.1), and extract the coefficients of  $e^{j(\omega_1+\omega_2+\dots+\omega_m)t}$  in each row, and assume that  $\omega_1 + \omega_2 + \dots + \omega_{\bar{n}} = \omega$ , the following



relationships can be achieved.

For the first row,

$$\begin{aligned} & (-m_1\omega^2 + j(c_1 + c_2)\omega + k_1 + k_2)H_{(1,p_1=n_1,p_2=n_2,\dots,p_m=n_m)}^{(\bar{n})}(j\omega_1, j\omega_2, \dots, j\omega_{\bar{n}}) \\ & - (jc_2\omega + k_2)H_{(2,p_1=n_1,p_2=n_2,\dots,p_m=n_m)}^{(\bar{n})}(j\omega_1, j\omega_2, \dots, j\omega_{\bar{n}}) = 0 \end{aligned} \quad (D.3)$$

Then,

$$\frac{H_{(1,p_1=n_1,p_2=n_2,\dots,p_m=n_m)}^{(\bar{n})}(j\omega_1, j\omega_2, \dots, j\omega_{\bar{n}})}{H_{(2,p_1=n_1,p_2=n_2,\dots,p_m=n_m)}^{(\bar{n})}(j\omega_1, j\omega_2, \dots, j\omega_{\bar{n}})} = \frac{jc_2\omega + k_2}{-m_1\omega^2 + j(c_1 + c_2)\omega + k_1 + k_2} \quad (D.4)$$

According to the definition of NOFRF of MIMO nonlinear system in Eq. (5.7), it can be obtained that

$$\begin{aligned} & G_{(1,p_1=n_1,\dots,p_m=n_m)}^{(\bar{n})}(j\omega) \\ & = \frac{\int_{\omega_1+\omega_2+\dots+\omega_{\bar{n}}=\omega} Q_1(j\omega)H_{(2,p_1=n_1,\dots,p_m=n_m)}^{(\bar{n})}(j\omega_1, \dots, j\omega_{\bar{n}}) \prod_{q=1}^m \prod_{p=n_0+n_1+\dots+n_{q-1}+1}^{n_1+\dots+n_q} F_q(j\omega_p) d\sigma_{\bar{n}\omega}}{\int_{\omega_1+\omega_2+\dots+\omega_{\bar{n}}=\omega} \prod_{q=1}^m \prod_{p=n_0+n_1+\dots+n_{q-1}+1}^{n_1+\dots+n_q} F_q(j\omega_p) d\sigma_{\bar{n}\omega}} \\ & = Q_1(j\omega)G_{(2,p_1=n_1,\dots,p_m=n_m)}^{(\bar{n})}(j\omega) \end{aligned} \quad (D.5)$$

where  $Q_1(j\omega) = \frac{jc_2\omega + k_2}{-m_1\omega^2 + j(c_1 + c_2)\omega + k_1 + k_2}$ . Therefore,

$$\frac{G_{(1,p_1=n_1,\dots,p_m=n_m)}^{(\bar{n})}(j\omega)}{G_{(2,p_1=n_1,\dots,p_m=n_m)}^{(\bar{n})}(j\omega)} = Q_1(j\omega) \quad (D.6)$$

It can be similarly deduced that, for the last mass, the GFRFs satisfy the following relationships:

$$\begin{aligned} & (-m_n\omega^2 + jc_n\omega + k_n)H_{(n,p_1=n_1,p_2=n_2,\dots,p_m=n_m)}^{(\bar{n})}(j\omega_1, j\omega_2, \dots, j\omega_{\bar{n}}) \\ & - (jc_n\omega + k_n)H_{(n-1,p_1=n_1,p_2=n_2,\dots,p_m=n_m)}^{(\bar{n})}(j\omega_1, j\omega_2, \dots, j\omega_{\bar{n}}) = 0 \end{aligned} \quad (D.7)$$

Then,

$$\frac{H_{(n,p_1=n_1,p_2=n_2,\dots,p_m=n_m)}^{(\bar{n})}(j\omega_1, j\omega_2, \dots, j\omega_{\bar{n}})}{H_{(n-1,p_1=n_1,p_2=n_2,\dots,p_m=n_m)}^{(\bar{n})}(j\omega_1, j\omega_2, \dots, j\omega_{\bar{n}})} = \frac{jc_n\omega + k_n}{-m_n\omega^2 + jc_n\omega + k_n} \quad (\text{D.8})$$

According to the definition of NOFRF of MIMO nonlinear system in Eq. (5.7), it can be obtained that

$$\begin{aligned} & G_{(n,p_1=n_1,\dots,p_m=n_m)}^{(\bar{n})}(j\omega) \\ &= \frac{\int_{\omega_1+\omega_2+\dots+\omega_{\bar{n}}=\omega} Q'_n(j\omega) H_{(n-1,p_1=n_1,\dots,p_m=n_m)}^{(\bar{n})}(j\omega_1, \dots, j\omega_{\bar{n}}) \prod_{q=1}^m \prod_{p=n_0+n_1+\dots+n_{q-1}+1}^{n_1+\dots+n_q} F_q(j\omega_p) d\sigma_{\bar{n}\omega}}{\int_{\omega_1+\omega_2+\dots+\omega_{\bar{n}}=\omega} \prod_{q=1}^m \prod_{p=n_0+n_1+\dots+n_{q-1}+1}^{n_1+\dots+n_q} F_q(j\omega_p) d\sigma_{\bar{n}\omega}} \\ &= Q'_n(j\omega) G_{(n-1,p_1=n_1,\dots,p_m=n_m)}^{(\bar{n})}(j\omega) \end{aligned} \quad (\text{D.9})$$

where  $Q'_n(j\omega) = \frac{jc_n\omega + k_n}{-m_n\omega^2 + jc_n\omega + k_n}$ . Therefore,

$$\frac{G_{(n,p_1=n_1,\dots,p_m=n_m)}^{(\bar{n})}(j\omega)}{G_{(n-1,p_1=n_1,\dots,p_m=n_m)}^{(\bar{n})}(j\omega)} = Q'_n(j\omega) \quad (\text{D.10})$$

For the masses that not connected to the  $J_i$ th ( $i = 1, \dots, J_J$ ) spring, the GFRFs satisfy the following relationships:

$$\begin{aligned} & (-m_i\omega^2 + j(c_i + c_{i+1})\omega + k_i + k_{i+1}) H_{(i,p_1=n_1,p_2=n_2,\dots,p_m=n_m)}^{(\bar{n})}(j\omega_1, j\omega_2, \dots, j\omega_{\bar{n}}) \\ & - (jc_i\omega + k_i) H_{(i-1,p_1=n_1,p_2=n_2,\dots,p_m=n_m)}^{(\bar{n})}(j\omega_1, j\omega_2, \dots, j\omega_{\bar{n}}) \\ & - (jc_{i+1}\omega + k_{i+1}) H_{(i+1,p_1=n_1,p_2=n_2,\dots,p_m=n_m)}^{(\bar{n})}(j\omega_1, j\omega_2, \dots, j\omega_{\bar{n}}) = 0 \end{aligned} \quad (\text{D.11})$$

Then,

$$\begin{aligned} & \frac{H_{(i,p_1=n_1,p_2=n_2,\dots,p_m=n_m)}^{(\bar{n})}(j\omega_1, j\omega_2, \dots, j\omega_{\bar{n}})}{H_{(i+1,p_1=n_1,p_2=n_2,\dots,p_m=n_m)}^{(\bar{n})}(j\omega_1, j\omega_2, \dots, j\omega_{\bar{n}})} \\ &= \frac{jc_{i+1}\omega + k_{i+1}}{\left( -m_i\omega^2 + j(c_i + c_{i+1})\omega + k_i + k_{i+1} - (jc_i\omega + k_i) \frac{H_{(i-1,p_1=n_1,p_2=n_2,\dots,p_m=n_m)}^{(\bar{n})}(j\omega_1, j\omega_2, \dots, j\omega_{\bar{n}})}{H_{(i,p_1=n_1,p_2=n_2,\dots,p_m=n_m)}^{(\bar{n})}(j\omega_1, j\omega_2, \dots, j\omega_{\bar{n}})} \right)} \end{aligned} \quad (\text{D.12})$$

If mass  $i$  and mass  $i + 1$  are both on the left side of all nonlinear components, namely,  $1 < i \leq J_1 - 2$ , then

$$\begin{aligned}
 & G_{(i,p_1=n_1,\dots,p_m=n_m)}^{(\bar{n})}(j\omega) \\
 &= \frac{\int_{\omega_1+\omega_2+\dots+\omega_{\bar{n}}=\omega} Q_i(j\omega) H_{(i+1,p_1=n_1,\dots,p_m=n_m)}^{(\bar{n})}(j\omega_1, \dots, j\omega_{\bar{n}}) \prod_{q=1}^m \prod_{p=n_0+n_1+\dots+n_{q-1}+1}^{n_1+\dots+n_q} F_q(j\omega_p) d\sigma_{\bar{n}\omega}}{\int_{\omega_1+\omega_2+\dots+\omega_{\bar{n}}=\omega} \prod_{q=1}^m \prod_{p=n_0+n_1+\dots+n_{q-1}+1}^{n_1+\dots+n_q} F_q(j\omega_p) d\sigma_{\bar{n}\omega}} \\
 &= Q_i(j\omega) G_{(i+1,p_1=n_1,\dots,p_m=n_m)}^{(\bar{n})}(j\omega)
 \end{aligned} \tag{D.13}$$

where  $Q_i(j\omega) = \frac{jc_{i+1}\omega + k_{i+1}}{(-m_i\omega^2 + j(c_i + c_{i+1})\omega + k_i + k_{i+1} + (jc_i\omega + k_i)Q_{i-1}(j\omega))}$ . Therefore,

$$\frac{G_{(i,p_1=n_1,\dots,p_m=n_m)}^{(\bar{n})}(j\omega)}{G_{(i+1,p_1=n_1,\dots,p_m=n_m)}^{(\bar{n})}(j\omega)} = Q_i(j\omega) \tag{D.14}$$

Consequently, if mass  $i$  and mass  $k$  are both on the left side of the nonlinear components, that is,  $1 \leq i < k \leq J_1 - 1$ , then

$$\frac{G_{(i,p_1=n_{1,\bar{n}},\dots,p_m=n_{m,\bar{n}})}^{(\bar{n})}(j\omega)}{G_{(k,p_1=n_{1,\bar{n}},\dots,p_m=n_{m,\bar{n}})}^{(\bar{n})}(j\omega)} = Q_i(j\omega) Q_{i+1}(j\omega) \dots Q_{k-1}(j\omega) \tag{D.15}$$

It can also be obtained from Eq. (D.11) that

$$\begin{aligned}
 & \frac{H_{(i,p_1=n_1,p_2=n_2,\dots,p_m=n_m)}^{(\bar{n})}(j\omega_1, j\omega_2, \dots, j\omega_{\bar{n}})}{H_{(i-1,p_1=n_1,p_2=n_2,\dots,p_m=n_m)}^{(\bar{n})}(j\omega_1, j\omega_2, \dots, j\omega_{\bar{n}})} \\
 &= \frac{j c_i \omega + k_i}{\left( -m_i \omega^2 + j(c_i + c_{i+1})\omega + k_i + k_{i+1} - (j c_{i+1} \omega + k_{i+1}) \frac{H_{(i+1,p_1=n_1,p_2=n_2,\dots,p_m=n_m)}^{(\bar{n})}(j\omega_1, j\omega_2, \dots, j\omega_{\bar{n}})}{H_{(i,p_1=n_1,p_2=n_2,\dots,p_m=n_m)}^{(\bar{n})}(j\omega_1, j\omega_2, \dots, j\omega_{\bar{n}})} \right)}
 \end{aligned} \tag{D.16}$$

If mass  $i$  and mass  $i + 1$  are both on the right side of all nonlinear components, namely,  $J_j + 1 \leq i < n$ , then

$$\begin{aligned}
 & G_{(i,p_1=n_1,\dots,p_m=n_m)}^{(\bar{n})}(j\omega) \\
 &= \frac{\int_{\omega_1+\omega_2+\dots+\omega_{\bar{n}}=\omega} Q'_i(j\omega) H_{(i-1,p_1=n_1,\dots,p_m=n_m)}^{(\bar{n})}(j\omega_1, \dots, j\omega_{\bar{n}}) \prod_{q=1}^m \prod_{p=n_0+n_1+\dots+n_{q-1}+1}^{n_1+\dots+n_q} F_q(j\omega_p) d\sigma_{\bar{n}\omega}}{\int_{\omega_1+\omega_2+\dots+\omega_{\bar{n}}=\omega} \prod_{q=1}^m \prod_{p=n_0+n_1+\dots+n_{q-1}+1}^{n_1+\dots+n_q} F_q(j\omega_p) d\sigma_{\bar{n}\omega}} \\
 &= Q'_i(j\omega) G_{(i-1,p_1=n_1,\dots,p_m=n_m)}^{(\bar{n})}(j\omega)
 \end{aligned} \tag{D.17}$$

where  $Q'_i(j\omega) = \frac{j c_i \omega + k_i}{-m_i \omega^2 + j(c_i + c_{i+1})\omega + k_i + k_{i+1} - (j c_{i+1} \omega + k_{i+1}) Q'_{i+1}(j\omega)}$ . Therefore,

$$\frac{G_{(i,p_1=n_1,\dots,p_m=n_m)}^{(\bar{n})}(j\omega)}{G_{(i-1,p_1=n_1,\dots,p_m=n_m)}^{(\bar{n})}(j\omega)} = Q'_i(j\omega) \quad (\text{D.18})$$

Consequently, if mass  $i$  and mass  $i + 1$  are both on the right side of the nonlinear components, that is,,  $J_{\bar{J}} \leq i < k \leq n$ , then

$$\frac{G_{(i,p_1=n_1,\bar{n},\dots,p_m=n_m,\bar{n})}^{(\bar{n})}(j\omega)}{G_{(k,p_1=n_1,\bar{n},\dots,p_m=n_m,\bar{n})}^{(\bar{n})}(j\omega)} = \frac{1}{Q'_{i+1}(j\omega)Q'_i(j\omega) \dots Q'_k(j\omega)} \quad (\text{D.19})$$

it can be concluded according to eqs.(D.15) and (D.19) that, if  $1 \leq i < k \leq J_1 - 1$  or  $J_{\bar{J}} \leq i < k \leq n$

$$\gamma_{(i,k,p_1=n_1,\dots,p_m=n_m)}^{(N)}(j\omega) = \frac{G_{(i,p_1=n_1,\bar{n},\dots,p_m=n_m,\bar{n})}^{(\bar{n})}(j\omega)}{G_{(k,p_1=n_1,\bar{n},\dots,p_m=n_m,\bar{n})}^{(\bar{n})}(j\omega)} = \bar{Q}_{i,k}(j\omega) \quad (\text{D.20})$$

where,

$$\bar{Q}_{i,k}(j\omega) \in \left\{ \frac{1}{Q'_{i+1}(j\omega)Q'_i(j\omega) \dots Q'_k(j\omega)}, Q_i(j\omega)Q_{i+1}(j\omega) \dots Q_{k-1}(j\omega) \right\} \quad (\text{D.21})$$

Therefore, first equation in Eq.(5.17) holds.

For the masses that are connected to nonlinear springs, the GFRFs satisfy the following relationships:

$$\begin{aligned} & (-m_i\omega^2 + j(c_i + c_{i+1})\omega + k_i + k_{i+1})H_{(i,p_1=n_1,p_2=n_2,\dots,p_m=n_m)}^{(\bar{n})}(j\omega_1, j\omega_2, \dots, j\omega_{\bar{n}}) \\ & - (jc_i\omega + k_i)H_{(i-1,p_1=n_1,p_2=n_2,\dots,p_m=n_m)}^{(\bar{n})}(j\omega_1, j\omega_2, \dots, j\omega_{\bar{n}}) \\ & - (jc_{i+1}\omega + k_{i+1})H_{(i+1,p_1=n_1,p_2=n_2,\dots,p_m=n_m)}^{(\bar{n})}(j\omega_1, j\omega_2, \dots, j\omega_{\bar{n}}) \\ & - NF_{(i,p_1=n_1,p_2=n_2,\dots,p_m=n_m)}^{(\bar{n})}(j\omega_1, j\omega_2, \dots, j\omega_{\bar{n}}) = 0 \end{aligned} \quad (\text{D.22})$$

Then,

Appendix D Proof of Proposition 5.1

$$\begin{aligned} & \frac{H_{(i,p_1=n_1,p_2=n_2,\dots,p_m=n_m)}^{(\bar{n})}(j\omega_1, j\omega_2, \dots, j\omega_{\bar{n}})}{H_{(i+1,p_1=n_1,p_2=n_2,\dots,p_m=n_m)}^{(\bar{n})}(j\omega_1, j\omega_2, \dots, j\omega_{\bar{n}})} \\ &= Q_i(j\omega) \left( 1 + \frac{NF_{(i,p_1=n_1,p_2=n_2,\dots,p_m=n_m)}^{(\bar{n})}(j\omega_1, j\omega_2, \dots, j\omega_{\bar{n}})}{(jc_{i+1}\omega + k_{i+1})H_{(i+1,p_1=n_1,p_2=n_2,\dots,p_m=n_m)}^{(\bar{n})}(j\omega_1, j\omega_2, \dots, j\omega_{\bar{n}})} \right) \end{aligned} \quad (D.23)$$

where  $NF_{(i,p_1=n_1,p_2=n_2,\dots,p_m=n_m)}^{(\bar{n})}(j\omega_1, j\omega_2, \dots, j\omega_{\bar{n}})$  denotes the extra terms produced by nonlinear components. When  $\bar{n} = 2$  and  $p_1 = 1, p_2 = 1, p_3 = 0, \dots, p_m = 0$  and if the  $i$ th mass is connected with only one nonlinear component and is on the left hand side, it can be expressed as follows.

$$\begin{aligned} NF_{(i,p_1=n_1,p_2=n_2,\dots,p_m=n_m)}^{(\bar{n})}(j\omega_1, j\omega_2, \dots, j\omega_{\bar{n}}) &= \Lambda_{(i,p_1=1,p_2=1)}^{(2)}(\omega_1, j\omega_2) \\ &= 2(r_{(i,2)} - \omega_1\omega_2 w_{(i,2)}) \left( H_{(i,p_1=1,p_2=0)}^{(1)}(j\omega_1) H_{(i,p_1=0,p_2=1)}^{(1)}(j\omega_2) \right. \\ &\quad - H_{(i,p_1=1,p_2=0)}^{(1)}(j\omega_1) H_{(i+1,p_1=0,p_2=1)}^{(1)}(j\omega_2) \\ &\quad - H_{(i+1,p_1=1,p_2=0)}^{(1)}(j\omega_1) H_{(i,p_1=0,p_2=1)}^{(1)}(j\omega_2) \\ &\quad \left. + H_{(i+1,p_1=1,p_2=0)}^{(1)}(j\omega_1) H_{(i+1,p_1=0,p_2=1)}^{(1)}(j\omega_2) \right) \end{aligned} \quad (D.24)$$

Obviously,  $NF_{(i,p_1=n_1,p_2=n_2,\dots,p_m=n_m)}^{(\bar{n})}(j\omega)$  depends not only linear parameters but also nonlinear parameters. According to the definition of NOFRF of MIMO nonlinear system in Eq. (5.7), if mass  $i$  and mass  $i + 1$  are both within the range of the nonlinear components, namely,  $J_1 - 1 \leq i \leq J_j$ , then

$$\begin{aligned} & G_{(i,p_1=n_1,\dots,p_m=n_m)}^{(\bar{n})}(j\omega) \\ &= \frac{\int_{\omega_1+\omega_2+\dots+\omega_{\bar{n}}=\omega} Q_i(j\omega) H_{(i+1,p_1=n_1,\dots,p_m=n_m)}^{(\bar{n})}(j\omega_1, \dots, j\omega_{\bar{n}}) \prod_{q=1}^m \prod_{p=n_0+n_1+\dots+n_{q-1}+1}^{n_1+\dots+n_q} F_q(j\omega_p) d\sigma_{\bar{n}\omega}}{\int_{\omega_1+\omega_2+\dots+\omega_{\bar{n}}=\omega} \prod_{q=1}^m \prod_{p=n_0+n_1+\dots+n_{q-1}+1}^{n_1+\dots+n_q} F_q(j\omega_p) d\sigma_{\bar{n}\omega}} \\ &= Q_i(j\omega) \left( 1 + \frac{\Gamma_{(i,p_1=n_1,p_2=n_2,\dots,p_m=n_m)}^{(\bar{n})}(j\omega)}{(jc_{i+1}\omega + k_{i+1})H_{(i+1,p_1=n_1,p_2=n_2,\dots,p_m=n_m)}^{(\bar{n})}(j\omega)} \right) G_{(i+1,p_1=n_1,\dots,p_m=n_m)}^{(\bar{n})}(j\omega) \end{aligned} \quad (D.25)$$

where

$$\begin{aligned} & \Gamma_{(i,p_1=n_1,p_2=n_2,\dots,p_m=n_m)}^{(\bar{n})}(j\omega) \\ &= \frac{\int_{\omega_1+\omega_2+\dots+\omega_{\bar{n}}=\omega} NF_{(i,p_1=n_1,\dots,p_m=n_m)}^{(\bar{n})}(j\omega_1, \dots, j\omega_{\bar{n}}) \prod_{q=1}^m \prod_{p=n_0+n_1+\dots+n_{q-1}+1}^{n_1+\dots+n_q} F_q(j\omega_p) d\sigma_{\bar{n}\omega}}{\int_{\omega_1+\omega_2+\dots+\omega_{\bar{n}}=\omega} \prod_{q=1}^m \prod_{p=n_0+n_1+\dots+n_{q-1}+1}^{n_1+\dots+n_q} F_q(j\omega_p) d\sigma_{\bar{n}\omega}} \end{aligned}$$

Therefore,

$$\frac{G_{(i,p_1=n_1,\dots,p_m=n_m)}^{(\bar{n})}(j\omega)}{G_{(i+1,p_1=n_1,\dots,p_m=n_m)}^{(\bar{n})}(j\omega)} = Q_i(j\omega) \left( 1 + \frac{\Gamma_{(i,p_1=n_1,p_2=n_2,\dots,p_m=n_m)}^{(\bar{n})}(j\omega)}{(jc_{i+1}\omega + k_{i+1})H_{(i+1,p_1=n_1,p_2=n_2,\dots,p_m=n_m)}^{(\bar{n})}(j\omega)} \right) \quad (D.26)$$

but

$$\gamma_{(i,i+1,p_1=n_1,\dots,p_m=n_m)}^{(N)}(j\omega) \neq \frac{G_{(i,p_1=n_1,\bar{n},\dots,p_m=n_m,\bar{n})}^{(\bar{n})}(j\omega)}{G_{(i+1,p_1=n_1,\bar{n},\dots,p_m=n_m,\bar{n})}^{(\bar{n})}(j\omega)} \quad (D.27)$$

Because it always holds that

$$\begin{aligned} & \frac{G_{(i,p_1=n_1,\bar{n},\dots,p_m=n_m,\bar{n})}^{(\bar{n})}(j\omega)}{G_{(k,p_1=n_1,\bar{n},\dots,p_m=n_m,\bar{n})}^{(\bar{n})}(j\omega)} \\ &= \frac{G_{(i,p_1=n_1,\bar{n},\dots,p_m=n_m,\bar{n})}^{(\bar{n})}(j\omega)}{G_{(i+1,p_1=n_1,\bar{n},\dots,p_m=n_m,\bar{n})}^{(\bar{n})}(j\omega)} \frac{G_{(i+1,p_1=n_1,\bar{n},\dots,p_m=n_m,\bar{n})}^{(\bar{n})}(j\omega)}{G_{(i+2,p_1=n_1,\bar{n},\dots,p_m=n_m,\bar{n})}^{(\bar{n})}(j\omega)} \dots \frac{G_{(k-1,p_1=n_1,\bar{n},\dots,p_m=n_m,\bar{n})}^{(\bar{n})}(j\omega)}{G_{(k,p_1=n_1,\bar{n},\dots,p_m=n_m,\bar{n})}^{(\bar{n})}(j\omega)} \end{aligned} \quad (D.28)$$

If any of mass  $i$  and mass  $k$  is within the range of the nonlinear components, it can be concluded easily that

$$\gamma_{(i,k,p_1=n_1,\dots,p_m=n_m)}^{(N)}(j\omega) \neq \frac{G_{(i,p_1=n_1,\bar{n},\dots,p_m=n_m,\bar{n})}^{(\bar{n})}(j\omega)}{G_{(k,p_1=n_1,\bar{n},\dots,p_m=n_m,\bar{n})}^{(\bar{n})}(j\omega)} \quad (D.29)$$

Therefore, the second equation in Eq.(5.17) holds.

When there is only one nonlinear components in system (5.1), that is,  $\bar{J} = 1$ , it can be easily deduced according to Eqs. (D.20) and (D.29) that

$$\gamma_{(i,k,p_1=n_1,\dots,p_m=n_m)}^{(N)}(j\omega) = \frac{G_{(i,p_1=n_1,\bar{n},\dots,p_m=n_m,\bar{n})}^{(\bar{n})}(j\omega)}{G_{(k,p_1=n_1,\bar{n},\dots,p_m=n_m,\bar{n})}^{(\bar{n})}(j\omega)} = \bar{Q}_{i,k}(j\omega) \quad (D.30)$$

where

$$\bar{Q}_{i,k}(j\omega) \in \left\{ \frac{1}{Q'_{i+1}(j\omega)Q'_i(j\omega) \dots Q'_k(j\omega)}, Q_i(j\omega)Q_{i+1}(j\omega) \dots Q_{k-1}(j\omega) \right\} \quad (D.31)$$

Therefore, Eq.(5.18) holds.

When the inputs applied on the MIMO nonlinear system (5.1) are

$$\begin{cases} f_1(t) = e^{j\omega_1 t} \\ \vdots \\ f_l(t) = e^{j\omega_l t} \\ \vdots \\ f_m(t) = e^{j\omega_m t} \end{cases} \quad (D.32)$$

the corresponding  $i$ th output according to the Volterra series is

$$\begin{aligned} x_i = & H_{(i,p_1=1,p_2=0,\dots,p_m=0)}^{(1)}(j\omega_1)e^{j\omega_1 t} + \dots + H_{(i,p_1=0,\dots,p_l=1,\dots,p_m=0)}^{(1)}(j\omega_l)e^{j\omega_l t} + \dots \\ & + H_{(i,p_1=0,\dots,p_m=1)}^{(1)}(j\omega_m)e^{j\omega_m t} + \dots \\ & + \chi H_{(i,p_1=n_1,p_2=n_2,\dots,p_m=n_m)}^{(\bar{n})}(j\omega_1, j\omega_2, \dots, j\omega_{\bar{n}})e^{j(\omega_1+\omega_2+\dots+\omega_{\bar{n}})t} + \dots \end{aligned} \quad (D.33)$$

Substitute Eqs. (D.32) and (D.33) into Eq.(5.1), and then extract the coefficients of one driving frequency, say,  $e^{j\omega_{\bar{m}}t}$  in each row, the following relationship can be achieved.

For the first row,

$$\begin{aligned} & (-m_1\omega_{\bar{m}}^2 + j(c_1 + c_2)\omega_{\bar{m}} + k_1 + k_2)H_{(1,p_1=0,\dots,p_{\bar{m}}=1,\dots,p_m=0)}^{(1)}(j\omega_{\bar{m}}) \\ & - (jc_2\omega_{\bar{m}} + k_2)H_{(2,p_1=0,\dots,p_{\bar{m}}=1,\dots,p_m=0)}^{(1)}(j\omega_{\bar{m}}) = 0 \end{aligned} \quad (D.34)$$

Then, it can be obtained that

$$\frac{H_{(1,p_1=0,\dots,p_{\bar{m}}=1,\dots,p_m=0)}^{(1)}(j\omega_{\bar{m}})}{H_{(2,p_1=0,\dots,p_{\bar{m}}=1,\dots,p_m=0)}^{(1)}(j\omega_{\bar{m}})} = \frac{jc_2\omega_{\bar{m}} + k_2}{-m_1\omega_{\bar{m}}^2 + j(c_1 + c_2)\omega_{\bar{m}} + k_1 + k_2} = Q_1(j\omega_{\bar{m}}) \quad (D.35)$$

According to the definition of NOFRF of MIMO nonlinear system in Eq. (5.7), then

$$\begin{aligned}
 G_{(1,p_1=0,\dots,p_{\bar{m}}=1,\dots,p_m=0)}^{(1)}(j\omega_{\bar{m}}) &= \frac{\int_{\omega_{\bar{m}}=\omega} Q_1(j\omega_{\bar{m}}) H_{(2,p_1=0,\dots,p_{\bar{m}}=1,\dots,p_m=0)}^{(1)}(j\omega_{\bar{m}}) F_{\bar{m}}(j\omega_{\bar{m}}) d\sigma_{\bar{n}\omega}}{\int_{\omega_1+\omega_2+\dots+\omega_{\bar{n}}=\omega} F_{\bar{m}}(j\omega_{\bar{m}}) d\sigma_{\bar{n}\omega}} \\
 &= Q_1(j\omega_{\bar{m}}) G_{(2,p_1=0,\dots,p_{\bar{m}}=1,\dots,p_m=0)}^{(1)}(j\omega_{\bar{m}})
 \end{aligned} \tag{D.36}$$

Therefore,

$$\frac{G_{(1,p_1=0,\dots,p_{\bar{m}}=1,\dots,p_m=0)}^{(1)}(j\omega_{\bar{m}})}{G_{(2,p_1=0,\dots,p_{\bar{m}}=1,\dots,p_m=0)}^{(1)}(j\omega_{\bar{m}})} = Q_1(j\omega_{\bar{m}}) \tag{D.37}$$

For the last mass, the GFRFs satisfy the following relationships:

$$\begin{aligned}
 (-m_n \omega_{\bar{m}}^2 + j c_n \omega_{\bar{m}} + k_n) H_{(n,p_1=0,\dots,p_{\bar{m}}=1,\dots,p_m=0)}^{(1)}(j\omega_{\bar{m}}) \\
 - (j c_n \omega + k_n) H_{(n-1,p_1=0,\dots,p_{\bar{m}}=1,\dots,p_m=0)}^{(1)}(j\omega_{\bar{m}}) = 0
 \end{aligned} \tag{D.38}$$

Then,

$$\frac{H_{(n,p_1=0,\dots,p_{\bar{m}}=1,\dots,p_m=0)}^{(1)}(j\omega_{\bar{m}})}{H_{(n-1,p_1=0,\dots,p_{\bar{m}}=1,\dots,p_m=0)}^{(1)}(j\omega_{\bar{m}})} = \frac{j c_n \omega_{\bar{m}} + k_n}{-m_n \omega_{\bar{m}}^2 + j c_n \omega_{\bar{m}} + k_n} = Q'_n(j\omega_{\bar{m}}) \tag{D.39}$$

According to the definition of NOFRF of MIMO nonlinear system in Eq. (5.7), then,

$$\begin{aligned}
 G_{(n,p_1=0,\dots,p_{\bar{m}}=1,\dots,p_m=0)}^{(1)}(j\omega_{\bar{m}}) &= \frac{\int_{\omega_{\bar{m}}=\omega} Q'_n(j\omega_{\bar{m}}) H_{(n-1,p_1=0,\dots,p_{\bar{m}}=1,\dots,p_m=0)}^{(1)}(j\omega_{\bar{m}}) F_{\bar{m}}(j\omega_{\bar{m}}) d\sigma_{\bar{n}\omega}}{\int_{\omega_1+\omega_2+\dots+\omega_{\bar{n}}=\omega} F_{\bar{m}}(j\omega_{\bar{m}}) d\sigma_{\bar{n}\omega}} \\
 &= Q'_n(j\omega_{\bar{m}}) G_{(n-1,p_1=0,\dots,p_{\bar{m}}=1,\dots,p_m=0)}^{(1)}(j\omega_{\bar{m}})
 \end{aligned} \tag{D.40}$$

Therefore,

$$\frac{G_{(n,p_1=0,\dots,p_{\bar{m}}=1,\dots,p_m=0)}^{(1)}(j\omega_{\bar{m}})}{G_{(n-1,p_1=0,\dots,p_{\bar{m}}=1,\dots,p_m=0)}^{(1)}(j\omega_{\bar{m}})} = Q'_n(j\omega_{\bar{m}}) \tag{D.41}$$

for the masses that not connected to the  $J_i$ th ( $i = 1, \dots, J_J$ ) spring and is not  $S_{\bar{m}}$ th mass, the GFRFs satisfy the following relationships:



$$\begin{aligned}
 & (-m_i \omega_{\tilde{m}}^2 + j(c_i + c_{i+1})\omega_{\tilde{m}} + k_i + k_{i+1})H_{(i,p_1=0,\dots,p_{\tilde{m}}=1,\dots,p_m=0)}^{(1)}(j\omega_{\tilde{m}}) \\
 & - (jc_i \omega_{\tilde{m}} + k_i)H_{(i-1,p_1=0,\dots,p_{\tilde{m}}=1,\dots,p_m=0)}^{(1)}(j\omega_{\tilde{m}}) \\
 & - (jc_{i+1} \omega_{\tilde{m}} + k_{i+1})H_{(i+1,p_1=0,\dots,p_{\tilde{m}}=1,\dots,p_m=0)}^{(1)}(j\omega_{\tilde{m}}) = 0
 \end{aligned} \tag{D.42}$$

Then,

$$\begin{aligned}
 & \frac{H_{(i,p_1=0,\dots,p_{\tilde{m}}=1,\dots,p_m=0)}^{(1)}(j\omega_{\tilde{m}})}{H_{(i+1,p_1=0,\dots,p_{\tilde{m}}=1,\dots,p_m=0)}^{(1)}(j\omega_{\tilde{m}})} \\
 & = \frac{jc_{i+1} \omega + k_{i+1}}{\left( -m_i \omega_{\tilde{m}}^2 + j(c_i + c_{i+1})\omega_{\tilde{m}} + k_i + k_{i+1} - (jc_i \omega_{\tilde{m}} + k_i) \frac{H_{(i-1,p_1=0,\dots,p_{\tilde{m}}=1,\dots,p_m=0)}^{(1)}(j\omega_{\tilde{m}})}{H_{(i,p_1=0,\dots,p_{\tilde{m}}=1,\dots,p_m=0)}^{(1)}(j\omega_{\tilde{m}})} \right)}
 \end{aligned} \tag{D.43}$$

if mass  $i$  is on the left side of all nonlinear components and  $S_{\tilde{m}}$ th mass, namely,  $1 < i \leq J_1 - 2$ , and  $i < S_{\tilde{m}}$  then

$$\begin{aligned}
 & G_{(i,p_1=0,\dots,p_{\tilde{m}}=1,\dots,p_m=0)}^{(1)}(j\omega_{\tilde{m}}) \\
 & = \frac{\int_{\omega_{\tilde{m}}=\omega} Q_i(j\omega_{\tilde{m}})H_{(i+1,p_1=0,\dots,p_{\tilde{m}}=1,\dots,p_m=0)}^{(1)}(j\omega_{\tilde{m}})F_{\tilde{m}}(j\omega_{\tilde{m}})d\sigma_{\bar{n}\omega}}{\int_{\omega_1+\omega_2+\dots+\omega_{\bar{n}}=\omega} F_{\tilde{m}}(j\omega_{\tilde{m}})d\sigma_{\bar{n}\omega}} \\
 & = Q_i(j\omega_{\tilde{m}})G_{(i+1,p_1=0,\dots,p_{\tilde{m}}=1,\dots,p_m=0)}^{(1)}(j\omega_{\tilde{m}})
 \end{aligned} \tag{D.44}$$

Therefore,

$$\frac{G_{(i,p_1=0,\dots,p_{\tilde{m}}=1,\dots,p_m=0)}^{(1)}(j\omega_{\tilde{m}})}{G_{(i+1,p_1=0,\dots,p_{\tilde{m}}=1,\dots,p_m=0)}^{(1)}(j\omega_{\tilde{m}})} = Q_i(j\omega_{\tilde{m}}) \tag{D.45}$$

If the  $\tilde{m}$ th input is on the right side of the nonlinear component, that is  $S_{\tilde{m}} \geq J_1$ , and masses  $i$  and  $k$  are both on the left side of all nonlinear components and  $S_{\tilde{m}}$ th mass, that is  $1 \leq i < k \leq J_1 - 1$ , then

$$\gamma_{(i,k,p_1=0,\dots,p_{\tilde{m}}=1,\dots,p_m=0)}^{(1)}(j\omega_{\tilde{m}}) = \frac{G_{(i,p_1=0,\dots,p_{\tilde{m}}=1,\dots,p_m=0)}^{(1)}(j\omega_{\tilde{m}})}{G_{(k,p_1=0,\dots,p_{\tilde{m}}=1,\dots,p_m=0)}^{(1)}(j\omega_{\tilde{m}})} = Q_i(j\omega_{\tilde{m}})Q_{i+1}(j\omega_{\tilde{m}}) \dots Q_{k-1}(j\omega_{\tilde{m}}) \tag{D.46}$$

If the  $\tilde{m}$ th input is on the right side of the nonlinear component, that is  $S_{\tilde{m}} \geq J_1$ , and masses  $i$  and  $k$  are both on the right side of all nonlinear components and  $S_{\tilde{m}}$ th mass, that is  $S_{\tilde{m}} \leq i < k \leq n$ , then

$$\begin{aligned}
 Y_{(i,k,p_1=0,\dots,p_{\bar{m}}=1,\dots,p_m=0)}^{(1)}(j\omega_{f\bar{m}}) &= \frac{G_{(i,p_1=0,\dots,p_{\bar{m}}=1,\dots,p_m=0)}^{(1)}(j\omega_{f\bar{m}})}{G_{(k,p_1=0,\dots,p_{\bar{m}}=1,\dots,p_m=0)}^{(1)}(j\omega_{f\bar{m}})} \\
 &= \frac{1}{Q'_i(j\omega_{f\bar{m}})Q'_{i+1}(j\omega_{f\bar{m}}) \dots Q'_{k-1}(j\omega_{f\bar{m}})}
 \end{aligned} \tag{D.47}$$

According to Eqs.(D.46) and (D.47), it can be concluded that if  $S_{\bar{m}} \geq J_1$ ,  $1 \leq i < k \leq J_1 - 1$  or  $S_{\bar{m}} \leq i < k \leq n$ , then

$$Y_{(i,k,p_1=0,\dots,p_{\bar{m}}=1,\dots,p_m=0)}^{(1)}(j\omega_{f\bar{m}}) = \frac{G_{(i,p_1=n_1,\bar{n},\dots,p_m=n_m,\bar{n})}^{(\bar{n})}(j\omega_{f\bar{m}})}{G_{(k,p_1=n_1,\bar{n},\dots,p_m=n_m,\bar{n})}^{(\bar{n})}(j\omega_{f\bar{m}})} = Q_{i,k}(j\omega_{f\bar{m}}) = Y_{(i,k,p_1=n_1,\dots,p_m=n_m)}^{(N)}(j\omega_{f\bar{m}}) \tag{D.48}$$

where

$$Q_{i,k}(j\omega_{f\bar{m}}) \in \left\{ \frac{1}{Q'_i(j\omega_{f\bar{m}})Q'_{i+1}(j\omega_{f\bar{m}}) \dots Q'_{k-1}(j\omega_{f\bar{m}})}, Q_i(j\omega_{f\bar{m}})Q_{i+1}(j\omega_{f\bar{m}}) \dots Q_{k-1}(j\omega_{f\bar{m}}) \right\} \tag{D.49}$$

Therefore, the first equation in Eq.(5.19) holds.

For the  $S_{\bar{m}}$ th mass, namely,  $i = S_{\bar{m}}$ , the GFRFs satisfy the following relationships:

$$\begin{aligned}
 &(-m_i\omega_{\bar{m}}^2 + j(c_i + c_{i+1})\omega_{\bar{m}} + k_i + k_{i+1})H_{(i,p_1=0,\dots,p_{\bar{m}}=1,\dots,p_m=0)}^{(1)}(j\omega_{f\bar{m}}) \\
 &- (jc_i\omega_{\bar{m}} + k_i)H_{(i-1,p_1=0,\dots,p_{\bar{m}}=1,\dots,p_m=0)}^{(1)}(j\omega_{f\bar{m}}) \\
 &- (jc_{i+1}\omega_{\bar{m}} + k_{i+1})H_{(i+1,p_1=0,\dots,p_{\bar{m}}=1,\dots,p_m=0)}^{(1)}(j\omega_{f\bar{m}}) - 1 = 0
 \end{aligned} \tag{D.50}$$

Then,

$$\frac{H_{(i,p_1=0,\dots,p_{\bar{m}}=1,\dots,p_m=0)}^{(1)}(j\omega_{f\bar{m}})}{H_{(i+1,p_1=0,\dots,p_{\bar{m}}=1,\dots,p_m=0)}^{(1)}(j\omega_{f\bar{m}})} = Q_i(j\omega_{f\bar{m}}) \left( 1 + \frac{1}{(jc_{i+1}\omega_{\bar{m}} + k_{i+1})H_{(i+1,p_1=0,\dots,p_{\bar{m}}=1,\dots,p_m=0)}^{(1)}(j\omega_{f\bar{m}})} \right) \tag{D.51}$$

According to the definition of NOFRF of MIMO nonlinear system in Eq. (5.7), if mass  $i$  connect with the nonlinear component, namely,  $i = J_1 - 1$  or  $J_1$ , then

$$G_{(i,p_1=0,\dots,p_{\bar{m}}=1,\dots,p_m=0)}^{(1)}(j\omega_{f\bar{m}}) = \frac{\int_{\omega_1+\omega_2+\dots+\omega_{\bar{n}}=\omega} Q_i(j\omega_{f\bar{m}})H_{(i-1,p_1=0,\dots,p_{\bar{m}}=1,\dots,p_m=0)}^{(1)}(j\omega_{f\bar{m}})F_{\bar{m}}(j\omega_{f\bar{m}})d\sigma_{\bar{n}\omega}}{\int_{\omega_1+\omega_2+\dots+\omega_{\bar{n}}=\omega} F_{\bar{m}}(j\omega_{f\bar{m}})d\sigma_{\bar{n}\omega}} \tag{D.52}$$

$$= Q_i(j\omega_{\tilde{m}}) \left( 1 + \frac{1}{(jc_{i+1}\omega + k_{i+1})H_{(i+1,p_1=0,\dots,p_{\tilde{m}}=1,\dots,p_m=0)}^{(1)}(j\omega_{\tilde{m}})} \right) G_{(i+1,p_1=0,\dots,p_{\tilde{m}}=1,\dots,p_m=0)}^{(1)}(j\omega_{\tilde{m}})$$

Therefore,

$$\frac{G_{(i,p_1=0,\dots,p_{\tilde{m}}=1,\dots,p_m=0)}^{(1)}(j\omega_{\tilde{m}})}{G_{(i+1,p_1=0,\dots,p_{\tilde{m}}=1,\dots,p_m=0)}^{(1)}(j\omega_{\tilde{m}})} = Q_i(j\omega_{\tilde{m}}) \left( 1 + \frac{1}{(jc_{i+1}\omega + k_{i+1})H_{(i+1,p_1=0,\dots,p_{\tilde{m}}=1,\dots,p_m=0)}^{(1)}(j\omega_{\tilde{m}})} \right) \quad (D.53)$$

but

$$\gamma_{(i,k,p_1=0,\dots,p_{\tilde{m}}=1,\dots,p_m=0)}^{(1)}(j\omega_{f\tilde{m}}) \neq \frac{G_{(i,p_1=n_{1,\tilde{n}},\dots,p_m=n_{m,\tilde{n}})}^{(\tilde{n})}(j\omega)}{G_{(i+1,p_1=n_{1,\tilde{n}},\dots,p_m=n_{m,\tilde{n}})}^{(\tilde{n})}(j\omega)} \quad (D.54)$$

For the masses that are connected to nonlinear springs, the GFRFs satisfy the following relationships:

$$\begin{aligned} & (-m_i\omega_{\tilde{m}}^2 + j(c_i + c_{i+1})\omega_{\tilde{m}} + k_i + k_{i+1})H_{(i,p_1=0,\dots,p_{\tilde{m}}=1,\dots,p_m=0)}^{(1)}(j\omega_{\tilde{m}}) \\ & - (jc_i\omega_{\tilde{m}} + k_i)H_{(i-1,p_1=0,\dots,p_{\tilde{m}}=1,\dots,p_m=0)}^{(1)}(j\omega_{\tilde{m}}) \\ & - (j\omega_{\tilde{m}} + k_{i+1})H_{(i+1,p_1=0,\dots,p_{\tilde{m}}=1,\dots,p_m=0)}^{(1)}(j\omega_{\tilde{m}}) \\ & - NF_{(i,p_1=0,\dots,p_{\tilde{m}}=1,\dots,p_m=0)}^{(1)}(j\omega_{\tilde{m}}) = 0 \end{aligned} \quad (D.55)$$

Then,

$$\frac{H_{(i,p_1=0,\dots,p_{\tilde{m}}=1,\dots,p_m=0)}^{(1)}(j\omega_{\tilde{m}})}{H_{(i+1,p_1=0,\dots,p_{\tilde{m}}=1,\dots,p_m=0)}^{(1)}(j\omega_{\tilde{m}})} = Q_i(j\omega_{\tilde{m}}) \left( 1 + \frac{NF_{(i,p_1=0,\dots,p_{\tilde{m}}=1,\dots,p_m=0)}^{(1)}(j\omega_{\tilde{m}})}{(jc_{i+1}\omega_{\tilde{m}} + k_{i+1})H_{(i+1,p_1=0,\dots,p_{\tilde{m}}=1,\dots,p_m=0)}^{(1)}(j\omega_{\tilde{m}})} \right) \quad (D.56)$$

According to the definition of NOFRF of MIMO nonlinear system in Eq. (5.7), if mass  $i$  connect with the nonlinear component, namely,  $i = J_1 - 1$  or  $J_1$ , then

$$G_{(i,p_1=0,\dots,p_{\bar{m}}=1,\dots,p_m=0)}^{(1)}(j\omega_{\bar{m}}) = \frac{\int_{\omega_1+\omega_2+\dots+\omega_{\bar{m}}=\omega} Q_i(j\omega_{\bar{m}})H_{(i-1,p_1=0,\dots,p_{\bar{m}}=1,\dots,p_m=0)}^{(1)}(j\omega_{\bar{m}})F_{\bar{m}}(j\omega_{\bar{m}})d\sigma_{\bar{n}\omega}}{\int_{\omega_1+\omega_2+\dots+\omega_{\bar{m}}=\omega} F_{\bar{m}}(j\omega_{\bar{m}})d\sigma_{\bar{n}\omega}} \quad (D.57)$$

$$= Q_i(j\omega_{\bar{m}}) \left( 1 + \frac{\Gamma_{(i,p_1=0,\dots,p_{\bar{m}}=1,\dots,p_m=0)}^{(1)}(j\omega_{\bar{m}})}{(jc_{i+1}\omega + k_{i+1})H_{(i+1,p_1=0,\dots,p_{\bar{m}}=1,\dots,p_m=0)}^{(1)}(j\omega_{\bar{m}})} \right) G_{(i+1,p_1=0,\dots,p_{\bar{m}}=1,\dots,p_m=0)}^{(1)}(j\omega_{\bar{m}})$$

Obviously,  $\Gamma_{(i,p_1=0,\dots,p_{\bar{m}}=1,\dots,p_m=0)}^{(1)}(j\omega_{\bar{m}})$  depends not only linear parameters but also nonlinear parameters.

Therefore,

$$\frac{G_{(i,p_1=0,\dots,p_{\bar{m}}=1,\dots,p_m=0)}^{(1)}(j\omega_{\bar{m}})}{G_{(i+1,p_1=0,\dots,p_{\bar{m}}=1,\dots,p_m=0)}^{(1)}(j\omega_{\bar{m}})} = Q_i(j\omega_{\bar{m}}) \left( 1 + \frac{\Gamma_{(i,p_1=0,\dots,p_{\bar{m}}=1,\dots,p_m=0)}^{(1)}(j\omega_{\bar{m}})}{(jc_{i+1}\omega + k_{i+1})H_{(i+1,p_1=0,\dots,p_{\bar{m}}=1,\dots,p_m=0)}^{(1)}(j\omega_{\bar{m}})} \right) \quad (D.58)$$

but

$$\gamma_{(i,k,p_1=0,\dots,p_{\bar{m}}=1,\dots,p_m=0)}^{(1)}(j\omega_{f\bar{m}}) \neq \frac{G_{(i,p_1=n_{1,\bar{n}},\dots,p_m=n_{m,\bar{n}})}^{(\bar{n})}(j\omega)}{G_{(i+1,p_1=n_{1,\bar{n}},\dots,p_m=n_{m,\bar{n}})}^{(\bar{n})}(j\omega)} \quad (D.59)$$

Because it always holds that

$$\begin{aligned} & \frac{G_{(i,p_1=0,\dots,p_{\bar{m}}=1,\dots,p_m=0)}^{(1)}(j\omega_{\bar{m}})}{G_{(k,p_1=0,\dots,p_{\bar{m}}=1,\dots,p_m=0)}^{(1)}(j\omega_{\bar{m}})} \\ &= \frac{G_{(i,p_1=0,\dots,p_{\bar{m}}=1,\dots,p_m=0)}^{(1)}(j\omega_{\bar{m}})}{G_{(i+1,p_1=0,\dots,p_{\bar{m}}=1,\dots,p_m=0)}^{(1)}(j\omega_{\bar{m}})} \frac{G_{(i+1,p_1=0,\dots,p_{\bar{m}}=1,\dots,p_m=0)}^{(1)}(j\omega_{\bar{m}})}{G_{(i+2,p_1=0,\dots,p_{\bar{m}}=1,\dots,p_m=0)}^{(1)}(j\omega_{\bar{m}})} \cdots \frac{G_{(k-1,p_1=0,\dots,p_{\bar{m}}=1,\dots,p_m=0)}^{(1)}(j\omega_{\bar{m}})}{G_{(k,p_1=0,\dots,p_{\bar{m}}=1,\dots,p_m=0)}^{(1)}(j\omega_{\bar{m}})} \end{aligned} \quad (D.60)$$

if any of mass  $i$  and mass  $k$  is within the range of the nonlinear components and the  $S_{\bar{m}}$ th mass, there is only one nonlinear components in system (5.1), according to Eqs.(D.30), (D.54) and (D.59), it can be concluded easily that

$$\gamma_{(i,k,p_1=0,\dots,p_{\bar{m}}=1,\dots,p_m=0)}^{(1)}(j\omega_{f\bar{m}}) \neq \frac{G_{(i,p_1=n_{1,\bar{n}},\dots,p_m=n_{m,\bar{n}})}^{(\bar{n})}(j\omega_{f\bar{m}})}{G_{(k,p_1=n_{1,\bar{n}},\dots,p_m=n_{m,\bar{n}})}^{(\bar{n})}(j\omega_{f\bar{m}})} = Q_{i,k}(j\omega_{f\bar{m}}) = \gamma_{(i,k,p_1=n_{1,\dots,p_m=n_m})}^{(N)}(j\omega_{f\bar{m}}) \quad (D.61)$$

Therefore, the second equation in Eq.(5.19) holds.

Similarly, the first and second equations in Eq.(5.20) can be proved by following the same approach above. Thus, the proof of Proposition 5.1 is completed.

## Appendix E

### Proof of Proposition 5.3

Proposition 5.3 can be proved by using similar method in the proof of proposition 4.3. Because nonlinearity generated frequency  $\omega_{NL}$  is different from any one of driving frequencies, it can only be produced by the combination of different driving frequencies. Consequently, only higher order NOFRFs contribute to nonlinearity generated frequency components, that is  $\bar{n} \geq 2$ . Therefore, the system response at one nonlinearity generated frequency  $\omega_{NL}$  can be determined by using Proposition 5.2 as

$$X_i(j\omega_{NL}) = \sum_{\bar{n}=2}^N \sum_{n_1+\dots+n_m=\bar{n}} G_{(i,p_1=n'_1,\dots,p_m=n'_m)}^{(\bar{n})}(j\omega_{NL}) F_{(i,p_1=n'_1,\dots,p_m=n'_m)}^{(\bar{n})}(j\omega_{NL}) \quad (E.1)$$

where  $\bar{n}, n'_1, n'_2, \dots, n'_m$  should satisfy the following relationships

$$\left\{ \begin{array}{l} n_1^+ + n_1^- = n'_1 \\ n_2^+ + n_2^- = n'_2 \\ \vdots \\ n_m^+ + n_m^- = n'_m \\ n'_1 + n'_2 + \dots + n'_m = \bar{n} \\ \bar{n} = 2, 3, \dots, N \end{array} \right. \quad (E.2)$$

and

$$\omega_{NL} = (n_1^+ - n_1^-)\omega_{f1} + (n_2^+ - n_2^-)\omega_{f2} + \dots + (n_m^+ - n_m^-)\omega_{fm} \quad (E.3)$$

It is known from Property (i) of the NOFRF transmissibility of MIMO nonlinear system given by Eq.(5.17) that if  $\bar{J} > 1$ , for  $1 \leq i \leq J_1 - 2$  or  $J_j \leq i \leq n - 1$

$$\begin{aligned}
 & \mathcal{Y}_{(i,i+1,p_1=n'_1,\dots,p_m=n'_m)}^{(N)}(j\omega_{NL}) \\
 &= \frac{G_{(i,p_1=n'_1,\dots,p_m=n'_m)}^{(\bar{n})}(j\omega_{NL})F_{(i,p_1=n'_1,\dots,p_m=n'_m)}^{(\bar{n})}(j\omega_{NL})}{G_{(i+1,p_1=n'_1,\dots,p_m=n'_m)}^{(\bar{n})}(j\omega_{NL})F_{(i+1,p_1=n'_1,\dots,p_m=n'_m)}^{(\bar{n})}(j\omega_{NL})} \\
 &= \bar{Q}_{i,i+1}(j\omega_{NL})
 \end{aligned} \tag{E.4}$$

Eqs.(E.1)-(E.4) imply that

$$\begin{aligned}
 ST_{i,i+1}^{NL}(j\omega_{NL}) &= \frac{X_i(j\omega_{NL})}{X_{i+1}(j\omega_{NL})} \\
 &= \frac{\sum_{\bar{n}=2}^N \sum_{n'_1+\dots+n'_m=\bar{n}} G_{(i,p_1=n'_1,\dots,p_m=n'_m)}^{(\bar{n})}(j\omega_{NL})F_{(i,p_1=n'_1,\dots,p_m=n'_m)}^{(\bar{n})}(j\omega_{NL})}{\sum_{\bar{n}=2}^N \sum_{n'_1+\dots+n'_m=\bar{n}} G_{(i+1,p_1=n'_1,\dots,p_m=n'_m)}^{(\bar{n})}(j\omega_{NL})F_{(i+1,p_1=n'_1,\dots,p_m=n'_m)}^{(\bar{n})}(j\omega_{NL})} \\
 &= \mathcal{Y}_{(i,i+1,p_1=n'_1,\dots,p_m=n'_m)}^{(N)}(j\omega_{NL}) = \bar{Q}_{i,i+1}(j\omega_{NL})
 \end{aligned} \tag{E.5}$$

Therefore, Eq.(5.28) holds.

Similarly, according to Property (i) of the NOFRF transmissibility of MIMO nonlinear system given by Eq.(5.17) that if  $\bar{J} > 1$ , for  $J_1 - 1 \leq i \leq J_J - 1$ ,

$$\begin{aligned}
 & \mathcal{Y}_{(i,i+1,p_1=n'_1,\dots,p_m=n'_m)}^{(N)}(j\omega_{NL}) \\
 & \neq \frac{G_{(i,p_1=n'_1,\dots,p_m=n'_m)}^{(\bar{n})}(j\omega_{NL})F_{(i,p_1=n'_1,\dots,p_m=n'_m)}^{(\bar{n})}(j\omega_{NL})}{G_{(i+1,p_1=n'_1,\dots,p_m=n'_m)}^{(\bar{n})}(j\omega_{NL})F_{(i+1,p_1=n'_1,\dots,p_m=n'_m)}^{(\bar{n})}(j\omega_{NL})} \\
 & \neq \bar{Q}_{i,i+1}(j\omega_{NL})
 \end{aligned} \tag{E.6}$$

Eqs.(E.1)-(E.3) and (E.6) imply that

$$\begin{aligned}
 ST_{i,i+1}^{NL}(j\omega_{NL}) &= \frac{X_i(j\omega_{NL})}{X_{i+1}(j\omega_{NL})} \\
 &= \frac{\sum_{\bar{n}=2}^N \sum_{n'_1+\dots+n'_m=\bar{n}} G_{(i,p_1=n'_1,\dots,p_m=n'_m)}^{(\bar{n})}(j\omega_{NL})F_{(i,p_1=n'_1,\dots,p_m=n'_m)}^{(\bar{n})}(j\omega_{NL})}{\sum_{\bar{n}=2}^N \sum_{n'_1+\dots+n'_m=\bar{n}} G_{(i+1,p_1=n'_1,\dots,p_m=n'_m)}^{(\bar{n})}(j\omega_{NL})F_{(i+1,p_1=n'_1,\dots,p_m=n'_m)}^{(\bar{n})}(j\omega_{NL})} \\
 &\neq \mathcal{Y}_{(i,i+1,p_1=n'_1,\dots,p_m=n'_m)}^{(N)}(j\omega_{NL}) \neq \bar{Q}_{i,i+1}(j\omega_{NL})
 \end{aligned} \tag{E.7}$$

Therefore, Eq.(5.29) holds.

According to Property (ii) of the NOFRF transmissibility of MIMO nonlinear system

given by Eq.(5.18) that if  $\bar{J} = 1$ , for  $i = 1, 2, \dots, n - 1$

$$\begin{aligned}
 & \mathcal{Y}_{(i,i+1,p_1=n'_1,\dots,p_m=n'_m)}^{(N)}(j\omega_{NL}) \\
 &= \frac{G_{(i,p_1=n'_1,\dots,p_m=n'_m)}^{(\bar{n})}(j\omega_{NL})F_{(i,p_1=n'_1,\dots,p_m=n'_m)}^{(\bar{n})}(j\omega_{NL})}{G_{(i+1,p_1=n'_1,\dots,p_m=n'_m)}^{(\bar{n})}(j\omega_{NL})F_{(i+1,p_1=n'_1,\dots,p_m=n'_m)}^{(\bar{n})}(j\omega_{NL})} \\
 &= \bar{Q}_{i,i+1}(j\omega_{NL})
 \end{aligned} \tag{E.8}$$

Eqs.(E.1)-(E.3) and (E.8) imply that

$$\begin{aligned}
 ST_{i,i+1}^{NL}(j\omega_{NL}) &= \frac{X_i(j\omega_{NL})}{X_{i+1}(j\omega_{NL})} \\
 &= \frac{\sum_{\bar{n}=2}^N \sum_{n'_1+\dots+n'_m=\bar{n}} G_{(i,p_1=n'_1,\dots,p_m=n'_m)}^{(\bar{n})}(j\omega_{NL})F_{(i,p_1=n'_1,\dots,p_m=n'_m)}^{(\bar{n})}(j\omega_{NL})}{\sum_{\bar{n}=2}^N \sum_{n'_1+\dots+n'_m=\bar{n}} G_{(i+1,p_1=n'_1,\dots,p_m=n'_m)}^{(\bar{n})}(j\omega_{NL})F_{(i+1,p_1=n'_1,\dots,p_m=n'_m)}^{(\bar{n})}(j\omega_{NL})} \\
 &= \mathcal{Y}_{(i,i+1,p_1=n'_1,\dots,p_m=n'_m)}^{(N)}(j\omega_{NL}) = \bar{Q}_{i,i+1}(j\omega_{NL})
 \end{aligned} \tag{E.9}$$

Therefore, Eq.(5.30) holds.

The system response at the driving frequency of  $\tilde{m}$ th input  $\omega_{f\tilde{m}}$  can also be determined by using Proposition 5.2 as

$$X_i(j\omega_{f\tilde{m}}) = \sum_{\bar{n}=1}^N \sum_{n_1+\dots+n_m=\bar{n}} G_{(i,p_1=n''_1,\dots,p_m=n''_m)}^{(\bar{n})}(j\omega_{f\tilde{m}})F_{(i,p_1=n''_1,\dots,p_m=n''_m)}^{(\bar{n})}(j\omega_{f\tilde{m}}) \tag{E.10}$$

where  $\bar{n}, n''_1, n''_2, \dots, n''_m$  should satisfy the following relationship

$$\left\{ \begin{array}{l} n_1^+ + n_1^- = n''_1 \\ n_2^+ + n_2^- = n''_2 \\ \vdots \\ n_m^+ + n_m^- = n''_m \\ n''_1 + n''_2 + \dots + n''_m = \bar{n} \\ \bar{n} = 1, 2, 3, \dots, N \end{array} \right. \tag{E.11}$$

and

$$\omega_{f\tilde{m}} = (n_1^+ - n_1^-)\omega_{f1} + (n_2^+ - n_2^-)\omega_{f2} + \dots + (n_m^+ - n_m^-)\omega_{fm} \tag{E.12}$$

It is know from the Property (ii) of the NOFRF transmissibility of MIMO nonlinear system given by the first equation in Eqs.(5.19) and (5.20) and Eqs.(E.10)-(E.12) that for  $\bar{J} = 1$ , when  $S_{\tilde{m}} < J_1$ , if  $1 \leq i \leq S_{\tilde{m}} - 1$  or  $J_1 \leq i < n$ , or when  $S_{\tilde{m}} \geq J_1$ , if  $1 \leq i \leq J_1 - 2$  or  $S_{\tilde{m}} \leq i < n$

$$\begin{aligned}
 ST_{i,i+1}^{NL}(j\omega_{f\tilde{m}}) &= \frac{X_i(j\omega_{f\tilde{m}})}{X_{i+1}(j\omega_{f\tilde{m}})} \\
 &= \frac{\sum_{\bar{n}=1}^N \sum_{n_1''+\dots+n_m''=\bar{n}} G_{(i,p_1=n_1'',\dots,p_m=n_m'')}^{(\bar{n})}(j\omega_{f\tilde{m}}) F_{(i,p_1=n_1'',\dots,p_m=n_m'')}^{(\bar{n})}(j\omega_{f\tilde{m}})}{\sum_{\bar{n}=1}^N \sum_{n_1''+\dots+n_m''=\bar{n}} G_{(i+1,p_1=n_1'',\dots,p_m=n_m'')}^{(\bar{n})}(j\omega_{f\tilde{m}}) F_{(i+1,p_1=n_1'',\dots,p_m=n_m'')}^{(\bar{n})}(j\omega_{f\tilde{m}})} \quad (E.13) \\
 &= \gamma_{(i,i+1,p_1=n_1'',\dots,p_m=n_m'')}^{(N)}(j\omega_{f\tilde{m}}) = Q_{i,i+1}(j\omega_{f\tilde{m}})
 \end{aligned}$$

Therefore, the first equation in Eq.(5.31) holds. Otherwise, it is know from the second equation in Eqs.(5.19) and (5.20) and Eqs.(E.10)-(E.12) that

$$\begin{aligned}
 ST_{i,i+1}^{NL}(j\omega_{f\tilde{m}}) &= \frac{X_i(j\omega_{f\tilde{m}})}{X_{i+1}(j\omega_{f\tilde{m}})} \\
 &= \frac{\sum_{\bar{n}=1}^N \sum_{n_1''+\dots+n_m''=\bar{n}} G_{(i,p_1=n_1'',\dots,p_m=n_m'')}^{(\bar{n})}(j\omega_{f\tilde{m}}) F_{(i,p_1=n_1'',\dots,p_m=n_m'')}^{(\bar{n})}(j\omega_{f\tilde{m}})}{\sum_{\bar{n}=1}^N \sum_{n_1''+\dots+n_m''=\bar{n}} G_{(i+1,p_1=n_1'',\dots,p_m=n_m'')}^{(\bar{n})}(j\omega_{f\tilde{m}}) F_{(i+1,p_1=n_1'',\dots,p_m=n_m'')}^{(\bar{n})}(j\omega_{f\tilde{m}})} \quad (E.14) \\
 &\neq \gamma_{(i,i+1,p_1=n_1'',\dots,p_m=n_m'')}^{(N)}(j\omega_{f\tilde{m}}) = Q_{i,i+1}(j\omega_{f\tilde{m}})
 \end{aligned}$$

Therefore, the first equation in Eq.(5.31) holds. Thus, the proof of Proposition 5.3 is completed.



## Appendix F

### Mathematical model of the power cable system

Applying Kirchhoff's voltage laws and current laws to the first section, it can be obtained that:

$$\begin{cases} L_1 \frac{di_1(t)}{dt} + R_1 i_1(t) = u_{s1}(t) - u_1(t) \\ i_1(t) = i_2(t) + C_1 \frac{du_1(t)}{dt} + G_1 u_1(t) \end{cases} \quad (\text{F.1})$$

Taking Laplace transform for equation (F.1) and assuming all initial conditions are zero yields:

$$\begin{cases} L_1 s i_1(s) + R_1 i_1(s) = u_{s1}(s) - u_1(s) \\ i_1(s) = i_2(s) + C_1 s u_1(s) + G_1 u_1(s) \end{cases} \quad (\text{F.2})$$

Then it can be obtained that

$$u_1(s) = \frac{i_1(s) - i_2(s)}{C_1 s + G_1} \quad (\text{F.3})$$

and

$$L_1 s i_1(s) + R_1 i_1(s) = u_{s1}(s) - u_1(s) = u_s(s) - \frac{i_1(s) - i_2(s)}{C_1 s + G_1} \quad (\text{F.4})$$

Equation (F.4) can be further written as:

$$\begin{aligned} L_1 C_1 s^2 i_1(s) + (R_1 C_1 + L_1 G_1) s i_1(s) + (R_1 G_1 + 1) i_1(s) - i_2(s) \\ = u_{s1}(s) C_1 s + u_{s1}(s) G_1 \end{aligned} \quad (\text{F.5})$$

Applying Kirchhoff's voltage laws and current laws to the  $p$ th section, it can be obtained that:

$$\begin{cases} i_{p-1} = i_p(t) - C_{p-1} \frac{du_{p-1}(t)}{dt} + G_{p-1}u_{p-1}(t) \\ L_p \frac{di_p(t)}{dt} + R_p i_p(t) = u_{p-1}(t) - u_p(t) \\ i_p(t) = i_{p+1}(t) + C_p \frac{du_p(t)}{dt} + G_p u_p(t) \end{cases} \quad (\text{F.6})$$

Taking Laplace transform for equation (F.6) and assuming all initial conditions are zero yields:

$$\begin{cases} i_{p-1}(s) = i_p(s) + C_{p-1}s u_{p-1}(s) + G_{p-1}u_{p-1}(s) \\ L_p s i_p(s) + R_p i_p(s) = u_{p-1}(s) - u_p(s) \\ i_p(s) = i_{p+1}(s) + C_p s u_p(s) + G_p u_p(s) \end{cases} \quad (\text{F.7})$$

Then it can be obtained that

$$u_{p-1}(s) = \frac{i_{p-1}(s) - i_p(s)}{C_{p-1}s + G_{p-1}} \quad \text{and} \quad u_p(s) = \frac{i_p(s) - i_{p+1}(s)}{C_p s + G_p} \quad (\text{F.8})$$

and

$$L_p s i_p(s) + R_p i_p(s) = \frac{i_{p-1}(s) - i_p(s)}{C_{p-1}s + G_{p-1}} - \frac{i_p(s) - i_{p+1}(s)}{C_p s + G_p} \quad (\text{F.9})$$

Equation (F.9) can be further written as:

$$\begin{aligned} & L_p C_{p-1} C_p s^3 i_p(s) + (R_p C_{p-1} C_p + L_p G_{p-1} C_p + L_p C_{p-1} G_p) s^2 i_p(s) \\ & + (R_p C_p G_{p-1} + R_p C_{p-1} G_p + L_p G_{p-1} G_p + C_{p-1} \\ & + C_p) s i_p(s) + (R_p G_{p-1} G_p + G_{p-1} + G_p) i_p(s) \\ & - C_p s i_{p-1}(s) - G_p i_{p-1}(s) - C_{p-1} i_{p+1}(s) s - G_{p-1} i_{p+1}(s) \end{aligned} \quad (\text{F.10})$$

Applying Kirchhoff's voltage laws and current laws to the last section, it can be obtained that:

$$\begin{cases} L_n \frac{di_n(t)}{dt} + R_n i_n(t) = u_{n-1}(t) - u_n(t) \\ i_n(t) = i_{n+1}(t) + C_n \frac{du_n(t)}{dt} + G_n u_n(t) \\ i_{n-1}(t) = i_n(t) + C_{n-1} \frac{du_{n-1}(t)}{dt} + G_{n-1} u_{n-1}(t) \\ L_{n+1} \frac{di_{n+1}(t)}{dt} + R_{n+1} i_{n+1} + Z_{load} i_{n+1}(t) = u_n(t) - u_{s2}(t) \end{cases} \quad (\text{F.11})$$

Taking Laplace transform for equation (F.11) and assuming all initial conditions are zero yields:

$$\begin{cases} i_{n-1}(s) = i_n(s) + C_{n-1}s u_{n-1}(s) + G_{n-1}u_{n-1}(s) \\ L_n s i_n(s) + R_n i_n(s) = u_{n-1}(s) - u_n(s) \\ i_n(s) = i_{n+1}(s) + C_n s u_n(s) + G_n u_n(s) \\ (L_{n+1}s + R_{n+1} + z_{load})i_{n+1}(s) = u_n(s) - u_{s2}(s) \end{cases} \quad (F.12)$$

Then it can be obtained that

$$\begin{cases} u_{n-1}(s) = \frac{i_{n-1}(s) - i_n(s)}{C_{n-1}s + G_{n-1}} \\ u_n(s) = \frac{i_{n-1}(s) - i_n(s)}{C_{n-1}s + G_{n-1}} - L_n s i_n(s) - R_n i_n(s) \\ i_{n+1}(s) = \frac{u_n(s)}{L_{n+1}s + R_{n+1} + z_{load}} - \frac{u_{s2}(s)}{L_{n+1}s + R_{n+1} + z_{load}} \end{cases} \quad (F.13)$$

Then,

$$\begin{aligned} i_n(s) &= i_{n+1}(s) + C_n s u_n(s) + G_n u_n(s) \\ &= \left( \frac{1}{L_{n+1}s + R_{n+1} + z_{load}} + C_n s + G_n \right) \frac{i_{n-1}(s) - i_n(s)}{C_{n-1}s + G_{n-1}} \\ &\quad - \frac{u_{s2}(s)}{L_{n+1}s + R_{n+1} + z_{load}} \end{aligned} \quad (F.14)$$

Equation (F.14) can be further written as:

$$\begin{aligned} &L_{n+1}C_{n-1}ss i_n(s) - C_n L_{n+1}ss i_{n-1}(s) + C_n L_{n+1}ss i_n(s) \\ &+ (R_{n+1}C_{n-1} + z_{load}C_{n-1} + L_{n+1}G_{n-1} + G_n L_{n+1} \\ &+ C_n R_{n+1} + C_n z_{load})s i_n(s) \\ &+ (R_{n+1}G_{n-1} + z_{load}G_{n-1} + 1 + G_n R_{n+1} + G_n z_{load})i_n(s) \\ &- (C_n R_{n+1} + C_n z_{load} + G_n L_{n+1})s i_{n-1}(s) \\ &- (G_n R_{n+1} + G_n z_{load} - 1)i_{n-1}(s) \\ &= C_{n-1}s u_{s2}(s) + G_{n-1}u_{s2}(s) \end{aligned} \quad (F.5)$$

Eqs. (F.5), (F.10) and (F.15) can be written with the form of Eq. (5.48) where

$$\mathbf{F}(t) = [f_1(t) \ 0 \ \dots \ f_2(t)]^T$$

$$\mathbf{A}_3 = \begin{bmatrix} 0 & 0 & 0 & \cdots & 0 \\ 0 & L_2 C_2 C_1 & 0 & \ddots & 0 \\ \vdots & \ddots & \ddots & \ddots & \vdots \\ 0 & \ddots & \ddots & L_{n-1} C_{n-1} C_{n-2} & 0 \\ 0 & 0 & 0 & \cdots & 0 \end{bmatrix}$$

$$\mathbf{A}_2 = \begin{bmatrix} A_2(1,1) & 0 & 0 & \cdots & 0 \\ 0 & A_2(2,2) & 0 & \ddots & 0 \\ \vdots & \ddots & \ddots & \ddots & \vdots \\ 0 & \ddots & 0 & A_2(n-1, n-1) & 0 \\ 0 & 0 & 0 & -L_{n+1} C_n & A_2(n, n) \end{bmatrix}$$

$$\mathbf{A}_1 = \begin{bmatrix} A_1(1,1) & 0 & 0 & \cdots & 0 \\ -G_2 & A_1(2,2) & -G_1 & \ddots & \vdots \\ \vdots & \ddots & \ddots & \ddots & 0 \\ 0 & \ddots & -G_{n-1} & A_1(n-1, n-1) & -G_{n-2} \\ 0 & 0 & 0 & A_1(n, n-1) & A_1(n, n) \end{bmatrix}$$

$$\mathbf{A}_0 = \begin{bmatrix} A_0(1,1) & -1 & 0 & \cdots & 0 \\ -C_2 & A_0(2,2) & -C_1 & \ddots & 0 \\ \vdots & \ddots & \ddots & \ddots & \vdots \\ 0 & \ddots & -C_{n-1} & A_0(n-1, n-1) & -C_{n-2} \\ 0 & 0 & 0 & A_0(n, n-1) & A_0(n, n) \end{bmatrix}$$

$$f_1(t) = \dot{u}_{s1}(s)C_1 + u_{s1}(s)G_1$$

$$f_2(t) = C_{n-1}\dot{u}_{s2}(t) + G_{n-1}u_{s2}(t)$$

$$A_2(1,1) = L_1 C_1$$

$$A_2(p, p) = R_p C_{p-1} C_p + L_p G_{p-1} C_p + L_p C_{p-1} G_p, \quad p = 2, 3, \dots, n-1$$

$$A_2(n, n) = L_{n+1} C_{n-1} + C_n L_{n+1}$$

$$A_1(1,1) = R_1 C_1 + L_1 G_1$$

$$A_1(p, p) = R_p C_p G_{p-1} + R_p C_{p-1} G_p + L_p G_{p-1} G_p + C_{p-1} + C_p \quad p = 2, 3, \dots, n-1$$

$$A_1(n, n) = R_{n+1} C_{n-1} + z_{load} C_{n-1} + L_{n+1} G_{n-1} + G_n L_{n+1} + C_n R_{n+1} + C_n z_{load}$$

$$A_1(n, n-1) = C_n R_{n+1} + C_n z_{load} + G_n L_{n+1}$$

$$A_0(1,1) = R_1 G_1 + 1$$

$$A_0(p, p) = R_p G_{p-1} G_p + G_{p-1} + G_p$$

$$A_0(n, n) = R_{n+1} G_{n-1} + z_{load} G_{n-1} + 1 + G_n R_{n+1} + G_n z_{load}$$

$$A_0(n, n - 1) G_n R_{n+1} + G_n z_{load} - 1$$

## References

1. Farrar, C.R. and K. Worden, *An introduction to structural health monitoring*. Philosophical Transactions of the Royal Society a-Mathematical Physical and Engineering Sciences, 2007. **365**(1851): p. 303-315.
2. Catbas, F.N., M. Gul, and J.L. Burkett, *Conceptual damage-sensitive features for structural health monitoring: Laboratory and field demonstrations*. Mechanical Systems and Signal Processing, 2008. **22**(7): p. 1650-1669.
3. Farrar, C.R. and K. Worden, *Structural health monitoring: a machine learning perspective*. 2013, U.K.: Wiley.
4. Sedding, H. and A. Brown, *Review of Effective Diagnostic and Condition Monitoring Methods for Rotating Machines*. 2008 IEEE Power & Energy Society General Meeting, Vols 1-11, 2008: p. 3025-3027.
5. Caselitz P, G.J., Mevenkamp M, *On-line fault detection and prediction in wind energy converters*.
6. Hameed, Z., et al., *Condition monitoring and fault detection of wind turbines and related algorithms: A review*. Renewable & Sustainable Energy Reviews, 2009. **13**(1): p. 1-39.
7. Farrar, C.R., S.W. Doebling, and D.A. Nix, *Vibration-based structural damage identification*. Philosophical Transactions of the Royal Society of London Series a-Mathematical Physical and Engineering Sciences, 2001. **359**(1778): p. 131-149.
8. Rytter, A., *Vibrational based inspection of civil engineering structures*, in *Department of Building Technology and Structural Engineering*1993, Aalborg University: Denmark.
9. Worden, K. and J.M. Dulieu-Barton, *An overview of intelligent fault detection in systems and structures*. Structural Health Monitoring, 2004. **3**(1): p. 85-98.
10. Isermann, R., *Fault-diagnosis systems, an introduction from fault detection to fault tolerance*. 2006, Germany: Springer.
11. Kulkarni, S.S. and J.D. Achenbach, *Structural health monitoring and damage prognosis in fatigue*. Structural Health Monitoring-an International Journal, 2008. **7**(1): p. 37-49.
12. Salawu, O.S., *Detection of structural damage through changes in frequency: A review*. Engineering Structures, 1997. **19**(9): p. 718-723.

## References

---

13. Qiao, P.Z. and W. Fan, *Vibration-based damage identification methods: a review and comparative study*. Structural Health Monitoring-an International Journal, 2011. **10**(1): p. 83-111.
14. Fanning, P. and E.P. Carden, *Vibration based condition monitoring: A review*. Structural Health Monitoring, 2004. **3**(4): p. 355-377.
15. Mechefske, C.K., *Machine Condition Monitoring and Fault Diagnosis*, . Vibration and Shock Handbook, ed. C.W.d. Silva. Vol. Chapter 25. 2005, Florida: CRC Press, Taylor and Francis Group, Boca Raton, Florida, USA.
16. Peng, Z.K. and F.L. Chu, *Application of the wavelet transform in machine condition monitoring and fault diagnostics: a review with bibliography*. Mechanical Systems and Signal Processing, 2004. **18**(2): p. 199-221.
17. C.R. Farrar, W.E.B., T.M. Bell, K.M. Colle, T.W. Darling, T.A. Duffey, A. Eklund, A.Migliori, *Dynamic characterization and damage detection in the I-40 bridge over the Rio Grande*. Los Alamos National Laboratory Report: LA-12762-MS, 1994.
18. Farrar, C.R., et al., *Variability of modal parameters measured on the Alamosa Canyon bridge*. Proceedings of the 15th International Modal Analysis Conference - Imac, Vols I and II, 1997. **3089**: p. 257-263.
19. Askegaard, V.M., P, *Long term observation of RC-bridge using changes in natural frequencies*. Nordic Concrete Research, 1988. **7**: p. 20-27.
20. Zhang, Q.W., L.C. Fan, and W.C. Yuan, *Traffic-induced variability in dynamic properties of cable-stayed bridge*. Earthquake Engineering & Structural Dynamics, 2002. **31**(11): p. 2015-2021.
21. M. Metwally, M.A., Y. Fujino. *Analysis of suspension bridge by ambient vibration measurement using the time domain method and its application to health monitoring*. in *2001 IMAC XIX - 19th International Modal Analysis Conference*. 2001. Kissimmee, Florida.
22. Han, Q.K., et al., *Periodic Motion Stability of a Dual-Disk Rotor System with Rub-Impact at Fixed Limiter*. Vibro-Impact Dynamics of Ocean Systems and Related Problems, 2009. **44**: p. 105-119.
23. Ma, H., et al., *Fixed-point rubbing fault characteristic analysis of a rotor system based on contact theory*. Mechanical Systems and Signal Processing, 2013. **38**(1): p. 137-153.
24. Sohn, H., *Effects of environmental and operational variability on structural health monitoring*. Philosophical Transactions of the Royal Society a-Mathematical Physical and Engineering Sciences, 2007. **365**(1851): p.

- 539-560.
25. Maia, N.M.M., et al., *Damage detection and quantification using transmissibility*. Mechanical Systems and Signal Processing, 2011. **25**(7): p. 2475-2483.
  26. Johnson, T., D.E. Adams, and M. Schiefer, *An analytical and experimental study to assess structural damage and integrity using dynamic transmissibility*. Proceedings of Imac-Xx: Structural Dynamics Vols I and II, 2002. **4753**: p. 472-476.
  27. Sampaio, R.P.C., et al., *Transmissibility techniques for damage detection*. Proceedings of Imac-Xix: A Conference on Structural Dynamics, Vols 1 and 2, 2001. **4359**: p. 1524-1527.
  28. Lang, Z.Q., et al., *Transmissibility of non-linear output frequency response functions with application in detection and location of damage in MDOF structural systems*. International Journal of Non-Linear Mechanics, 2011. **46**(6): p. 841-853.
  29. Johnson, T.J. and D.E. Adams, *Transmissibility as a differential indicator of structural damage*. Journal of Vibration and Acoustics-Transactions of the Asme, 2002. **124**(4): p. 634-641.
  30. Chanpheng T, Y.H., Katsuchi H, *Nonlinear features for damage detection on large civil structures due to earthquakes*. Structural Health Monitoring-an International Journal, 2012. **11**(4): p. 482-488
  31. Lang, Z.Q. and S.A. Billings, *Energy transfer properties of non-linear systems in the frequency domain*. International Journal of Control, 2005. **78**(5): p. 345-362.
  32. Isermann, R., *Fault-diagnosis systems : an introduction from fault detection to fault tolerance*. 2006: Berlin ; London : Springer.
  33. Luo, H., *Dynamic Study of Single and Dual Rotor with Rub-impact Fault*, in *Department of Mechanical Engineering and Automation 2009*, Northeastern University: Shenyang.
  34. Sreejith, B., A.K. Verma, and A. Srividya, *Fault diagnosis of rolling element bearing using time-domain features and neural networks*. Ieee Region 10 Colloquium and Third International Conference on Industrial and Information Systems, Vols 1 and 2, 2008: p. 619-624.
  35. Tandon, N., *A comparison of some vibration parameters for the condition monitoring of rolling element bearings*. Measurement, 1994. **12**: p. 285-289.
  36. Williams, T., et al., *Rolling element bearing diagnostics in run-to-failure lifetime*



## References

---

- testing*. Mechanical Systems and Signal Processing, 2001. **15**(5): p. 979-993.
37. Ma, H., et al., *Time-frequency features of two types of coupled rub-impact faults in rotor systems*. Journal of Sound and Vibration, 2009. **321**(3-5): p. 1109-1128.
38. Han, O.K., et al., *Experiment of oil-film whirl in rotor system and wavelet fractal analyses*. Proceedings of the ASME International Design Engineering Technical Conferences and Computers and Information in Engineering Conference, Vol 6, Pts A-C, 2005: p. 1149-1154.
39. [http://en.wikipedia.org/wiki/Probability\\_density\\_function](http://en.wikipedia.org/wiki/Probability_density_function).
40. Dyer, D. and R.M. Stewart, *Detection of Rolling Element Bearing Damage by Statistical Vibration Analysis*. Journal of Mechanical Design-Transactions of the Asme, 1978. **100**(2): p. 229-235.
41. Martins L.G., G.S.N.Y., *Comparison between signal analysis for detecting incipient bearing damage*. Proceedings of the International Condition Monitoring Conference, Swansea, UK,, 1984: p. 191-204.
42. Stronach AF, C.C., Johnston AB., *Condition monitoring of rolling element bearings*. Proceedings of the International Condition Monitoring Conference, Swansea, UK,, 1984: p. 162-177.
43. Tandon, N. and A. Choudhury, *A review of vibration and acoustic measurement methods for the detection of defects in rolling element bearings*. Tribology International, 1999. **32**(8): p. 469-480.
44. Mathew, J. and R.J. Alfredson, *The Condition Monitoring of Rolling Element Bearings Using Vibration Analysis*. Journal of Vibration Acoustics Stress and Reliability in Design-Transactions of the Asme, 1984. **106**(3): p. 447-453.
45. P.Y., K., *A review of rolling element bearing health monitoring (II): preliminary test results on current technologies*. Proceedings of Machinery Vibration Monitoring and Analysis Meeting, New Orleans, LA, 1984. **127-137**.
46. Guo, L., J. Chen, and X.L. Li, *Rolling Bearing Fault Classification Based on Envelope Spectrum and Support Vector Machine*. Journal of Vibration and Control, 2009. **15**(9): p. 1349-1363.
47. Ho, D. and R.B. Randall, *Optimisation of bearing diagnostic techniques using simulated and actual bearing fault signals*. Mechanical Systems and Signal Processing, 2000. **14**(5): p. 763-788.
48. Spectra Quest, I., *Rotating Machinery Fault Diagnosis Techniques Envelope and Cepstrum Analyses*. 2006.

## References

---

49. Konstantin-Hansen, H. and H. Herlufsen, *Envelope and Cepstrum Analyses for Machinery Fault Identification*. Sound and Vibration, 2010. **44**(5): p. 10-12.
50. Liang, B., S.D. Iwnicki, and Y. Zhao, *Application of power spectrum, cepstrum, higher order spectrum and neural network analyses for induction motor fault diagnosis*. Mechanical Systems and Signal Processing, 2013. **39**(1-2): p. 342-360.
51. Sinha, J.K., *Higher order spectra for crack and misalignment identification in the shaft of a rotating machine*. Structural Health Monitoring-an International Journal, 2007. **6**(4): p. 325-334.
52. L. Xiong, T.S., S. Yang, R.B.K.N. Rao,, *A novel application of wavelet-based bispectrum analysis to diagnose faults in gears*. International Journal of COMADEM, 2002. **5**(3): p. 31-38.
53. Yang, D.M., et al., *Third-order spectral techniques for the diagnosis of motor bearing condition using artificial neural networks*. Mechanical Systems and Signal Processing, 2002. **16**(2-3): p. 391-411.
54. B.E. Parker, H.A.W., D.P. Wipf, W.R. Tompkins, B.R. Clark, E.C. Larson, H.V. Poor, *Fault diagnostics using statistical change detection in the bispectral domain*. Mechanical Systems and Signal Processing, 2000. **14**(4): p. 561-570.
55. McCormick, A.C. and A.K. Nandi, *Bispectral and trispectral features for machine condition diagnosis*. Ieee Proceedings-Vision Image and Signal Processing, 1999. **146**(5): p. 229-234.
56. Li, Z.X., et al., *Time-varying system identification using a newly improved HHT algorithm*. Computers & Structures, 2009. **87**(23-24): p. 1611-1623.
57. Fassois, S.D. and M.D. Spiridonakos, *Parametric identification of a time-varying structure based on vector vibration response measurements*. Mechanical Systems and Signal Processing, 2009. **23**(6): p. 2029-2048.
58. Allen, J.B., *Short-Term Spectral Analysis, Synthesis, and Modification by Discrete Fourier-Transform*. Ieee Transactions on Acoustics Speech and Signal Processing, 1977. **25**(3): p. 235-238.
59. Allan, J.B.a.R., L.R., *A Unified Approach to Short Time Fourier Analysis and Synthesis*. Proc. IEEE, 1977. **65**: p. 1558-1564
60. Melhem, H. and H.S. Kim, *Damage detection of structures by wavelet analysis*. Engineering Structures, 2004. **26**(3): p. 347-362.
61. Yang, J.N., et al., *Hilbert-Huang based approach for structural damage detection*. Journal of Engineering Mechanics-Asce, 2004. **130**(1): p. 85-95.

## References

---

62. Huang, N.E.Z.S.e.a., *The empirical mode decomposition and hilbert spectrum for nonlinear and nonstationary time series analysis*. Proc. R. Soc. London, Ser. A, 1998: p. 454, 903–995.
63. Satish, L., *Short-time Fourier and wavelet transforms for fault detection in power transformers during impulse tests*. Ieee Proceedings-Science Measurement and Technology, 1998. **145**(2): p. 77-84.
64. Arabaci, H. and O. Bilgin, *Neural Network Classification and Diagnosis of Broken Rotor Bar Faults by Means of Short Time Fourier Transform*. Imecs 2009: International Multi-Conference of Engineers and Computer Scientists, Vols I and Ii, 2009: p. 219-223.
65. Arabaci, H. and O. Bilgin, *The detection of rotor faults by using Short Time Fourier Transform*. 2007 Ieee 15th Signal Processing and Communications Applications, Vols 1-3, 2007: p. 648-651.
66. Chu, F.L. and Z.K. Peng, *Application of the wavelet transform in machine condition monitoring and fault diagnostics: a review with bibliography*. Mechanical Systems and Signal Processing, 2004. **18**(2): p. 199-221.
67. Peng, Z., et al., *Feature extraction of the rub-impact rotor system by means of wavelet analysis*. Journal of Sound and Vibration, 2003. **259**(4): p. 1000-1010.
68. Lim, G.H., H. Chen, and P.S.K. Chua, *Adaptive wavelet transform for vibration signal modelling and application in fault diagnosis of water hydraulic motor*. Mechanical Systems and Signal Processing, 2006. **20**(8): p. 2022-2045.
69. Wu, J.D. and J.C. Chen, *Continuous wavelet transform technique for fault signal diagnosis of internal combustion engines*. Ndt & E International, 2006. **39**(4): p. 304-311.
70. Ren, X.P., et al., *Extraction of gearbox fault features from vibration signal using wavelet transform*. 4th International Symposium on Instrumentation Science and Technology (ISIST' 2006), 2006. **48**: p. 490-494.
71. Harsha, S.P., P.K. Kankar, and S.C. Sharma, *Fault diagnosis of ball bearings using continuous wavelet transform*. Applied Soft Computing, 2011. **11**(2): p. 2300-2312.
72. Park, C.W., et al., *Generator Fault Detection Technique using Detailed Coefficients Ratio by Daubechies Wavelet Transform*. 2009 Ieee Power & Energy Society General Meeting, Vols 1-8, 2009: p. 1176-1182.
73. Singh, G.K. and S.A.S. Al Kazzaz, *Isolation and identification of dry bearing faults in induction machine using wavelet transform*. Tribology International, 2009. **42**(6): p. 849-861.

## References

---

74. Harsha, S.P., P.K. Kankar, and S.C. Sharma, *Rolling element bearing fault diagnosis using wavelet transform*. Neurocomputing, 2011. **74**(10): p. 1638-1645.
75. Seker, S., et al., *Stationary wavelet transform for fault detection in rotating machinery - art. no. 67630A*. Wavelet Applications in Industrial Processing V, 2007. **6763**: p. A7630-A7630.
76. Wu, J.D. and C.C. Hsu, *Fault gear identification using vibration signal with discrete wavelet transform technique and fuzzy-logic inference*. Expert Systems with Applications, 2009. **36**(2): p. 3785-3794.
77. Xiong, G., et al., *Fault diagnosis based on optimized node entropy using lifting wavelet packet transform and genetic algorithms*. Proceedings of the Institution of Mechanical Engineers Part I-Journal of Systems and Control Engineering, 2010. **224**(15): p. 557-573.
78. Vahidi, B., et al., *An Approach to Detection of High Impedance Fault Using Discrete Wavelet Transform and Artificial Neural Networks*. Simulation-Transactions of the Society for Modeling and Simulation International, 2010. **86**(4): p. 203-215.
79. Vanamadevi, N., M. Arivamudhan, and S. Santhi, *Detection and Classification of Impulse faults in transformer using Wavelet Transform and Artificial Neural Network*. 2008 IEEE International Conference on Sustainable Energy Technologies (Icset), Vols 1 and 2, 2008: p. 72-76.
80. Zervakis, M.E., Z.E. Gketsis, and G. Stavrakakis, *Detection and classification of winding faults in windmill generators using Wavelet Transform and ANN*. Electric Power Systems Research, 2009. **79**(11): p. 1483-1494.
81. Gketsis, Z., M. Zervakis, and G. Stavrakakis, *Early detection of winding faults in windmill generators using wavelet transform and ANN classification*. Artificial Neural Networks - Icnan 2006, Pt 2, 2006. **4132**: p. 746-756.
82. Wu, J.D. and C.H. Liu, *Investigation of engine fault diagnosis using discrete wavelet transform and neural network*. Expert Systems with Applications, 2008. **35**(3): p. 1200-1213.
83. Mallat, S.G., *A theory for multiresolution signal decomposition: the wavelet representation*. IEEE Transactions on Pattern Analysis and Machine Intelligence, 1989. **11**(7): p. 674 - 693.
84. Staszewski, W.J., *Wavelet based compression and feature selection for vibration analysis*. Journal of Sound and Vibration, 1998. **211**(5): p. 735-760.
85. Paya, B.A., I.I. Esat, and M.N.M. Badi, *Artificial neural network based fault*

## References

---

- diagnostics of rotating machinery using wavelet transforms as a preprocessor*. Mechanical Systems and Signal Processing, 1997. **11**(5): p. 751-765.
86. Yang, Y., et al., *Rub-impact fault vibration analysis of rotor system with the different parameters using Hilbert-Huang transform*. Icmmit 2009: Mechatronics and Information Technology, 2010. **7500**.
87. Yang, J.N. and Y. Lei, *System identification of linear structures using Hilbert transform and empirical mode decomposition*. Imac-Xviii: A Conference on Structural Dynamics, Vols 1 and 2, Proceedings, 2000. **4062**: p. 213-219.
88. Wu, T.Y., Y.L. Chung, and C.H. Liu, *Looseness Diagnosis of Rotating Machinery Via Vibration Analysis Through Hilbert-Huang Transform Approach*. Journal of Vibration and Acoustics-Transactions of the Asme, 2010. **132**(3).
89. Su, Z.Y., et al., *Gear fault identification and classification of singular value decomposition based on Hilbert-Huang transform*. Journal of Mechanical Science and Technology, 2011. **25**(2): p. 267-272.
90. Chen, C.W., et al., *A case study of damage detection in benchmark buildings using a Hilbert-Huang Transform-based method*. Journal of Vibration and Control, 2011. **17**(4): p. 623-636.
91. Chen, C.W., et al., *Applications of Hilbert-Huang transform to structural damage detection*. Structural Engineering and Mechanics, 2011. **39**(1): p. 1-20.
92. Yang, J.N., S.L. Lin, and S.W. Pan, *Damage detection of a health monitoring benchmark building using Hilbert-Huang spectral analysis*. Advances in Building Technology, Vols I and II, Proceedings, 2002: p. 1017-1024.
93. Yu, D.J., J.S. Cheng, and Y. Yang, *Application of EMD method and Hilbert spectrum to the fault diagnosis of roller bearings*. Mechanical Systems and Signal Processing, 2005. **19**(2): p. 259-270.
94. Strangas, E.G., S. Aviyente, and S.S.H. Zaidi, *Time-Frequency Analysis for Efficient Fault Diagnosis and Failure Prognosis for Interior Permanent-Magnet AC Motors*. Ieee Transactions on Industrial Electronics, 2008. **55**(12): p. 4191-4199.
95. Sun, M.Z., C. Wang, and Y.L. Xu, *Fault Diagnosis of Grinding Machine Using Choi-Williams Distribution Based on COM Module Technology*. Vibration, Structural Engineering and Measurement II, Pts 1-3, 2012. **226-228**: p. 572-575.
96. Staszewski, W.J., K. Worden, and G.R. Tomlinson, *Time-frequency analysis in gearbox fault detection using the Wigner-Ville distribution and pattern recognition*. Mechanical Systems and Signal Processing, 1997. **11**(5): p. 673-692.

## References

---

97. Li, H., H.Q. Zheng, and L.W. Tang, *Wigner-Ville distribution based on EMD for faults diagnosis of bearing*. Fuzzy Systems and Knowledge Discovery, Proceedings, 2006. **4223**: p. 803-812.
98. Gomes, A.J.M.A.a.S., J.M.M.E, *On the use of modal analysis for crack identification*. Proceedings , 8th International Modal Analysis Conference, Florida, 1990: p. 1108-1115.
99. Ju, F.D.a.M., *Modal frequency method in diagnosis of fracture damage in structure*. Proceedings , 4th International Modal Analysis Conference, Los Angeles, 1986: p. 1168-1174.
100. Chen, H.L., C.C. Spyrakos, and G. Venkatesh, *Evaluating Structural Deterioration by Dynamic-Response*. Journal of Structural Engineering-Asce, 1995. **121**(8): p. 1197-1204.
101. Allemang, R.J., *The modal assurance criterion - Twenty years of use and abuse*. Sound and Vibration, 2003. **37**(8): p. 14-23.
102. Fryba, L. and M. Pirner, *Load tests and modal analysis of bridges*. Engineering Structures, 2001. **23**(1): p. 102-109.
103. M. M. Abdel Wahab, G.D.R., *Damage Detection in Bridges Using Modal Curvatures: Application To a Real Damage Scenario*. Journal of Sound and Vibration, 1999 **226**(2): p. 217-235.
104. 2001, *Effect of modal curvatures on damage detection using model updating*. Mechanical Systems and Signal Processing, 2001. **15**(2): p. 439-445.
105. Williams, O.S.S.a.C., *Bridge Assessment Using Forced-Vibration Testing*. Journal of Structural Engineering, 1995. **121**(2): p. 161-173.
106. Ratcliffe, C.P.a.B., William J., *Vibration Technique for Locating Delamination in a Composite Beam*. AIAA Journal, 1998. **36**(6): p. 1074-1077.
107. Oyadiji, S.O. and S.C. Zhong, *Crack detection in simply supported beams without baseline modal parameters by stationary wavelet transform*. Mechanical Systems and Signal Processing, 2007. **21**(4): p. 1853-1884.
108. Poudel, U.P., G.K. Fu, and H. Ye, *Wavelet transformation of mode shape difference function for structural damage location identification*. Earthquake Engineering & Structural Dynamics, 2007. **36**(8): p. 1089-1107.
109. Farrar, C.R. and G.H. James, *System identification from ambient vibration measurements on a bridge*. Journal of Sound and Vibration, 1997. **205**(1): p. 1-18.
110. N, K.J.T.S., *Model-uncertainty impact and damage-detection accuracy in plate*

## References

---

- girder*. Journal of Structural Engineering, 1995. **121**(10): p. 1409-17.
111. S. S. Law, Z.Y.S.a.L.M.Z., *Structural Damage Detection from Incomplete and Noisy Modal Test Data*. Journal of Engineering Mechanics, 1998. **124**(11): p. 1280-1288.
112. Kim, J.T., et al., *Damage identification in beam-type structures: frequency-based method vs mode-shape-based method*. Engineering Structures, 2003. **25**(1): p. 57-67.
113. Bejger, A., *An application of the coherence function in diagnosis marine engine injection pumps*. Archives of Mechanical Technology and Automation, 2012. **32**(4): p. 15-22.
114. K.Shashidhar Reddy, M.P.V.V.R.K., B.P.Singh, M.Suryakalavathi, *Coherence Function Method of Detection of Fault in a Power Transformer during Impulse Test*. 2011 International Conference on Power and Energy Systems 2011: p. 1-6.
115. Sandberg, I.W., *A Perspective on System-Theory*. Ieee Transactions on Circuits and Systems, 1984. **31**(1): p. 88-103.
116. M.Schetzen, ed. *The Volterra and Wiener theories of nonlinear systems*. 1980, Wiley: New York.
117. Rugh, W.J., ed. *Nonlinear system theory : the Volterra/Weiner approach*. 1981, Johns Hopkins University Press: Baltimore.
118. Billings, S.A., *Identification of Non-Linear Systems - a Survey*. Iee Proceedings-D Control Theory and Applications, 1980. **127**(6): p. 272-285.
119. Korenberg, M.J. and I.W. Hunter, *The Identification of Nonlinear Biological-Systems - Wiener Kernel Approaches*. Annals of Biomedical Engineering, 1990. **18**(6): p. 629-654.
120. Hunter, I.W. and M.J. Korenberg, *The Identification of Nonlinear Biological-Systems - Wiener and Hammerstein Cascade Models*. Biological Cybernetics, 1986. **55**(2-3): p. 135-144.
121. Kotsios, S., *Finite input/output representative of a class of Volterra polynomial systems*. Automatica, 1997. **33**(2): p. 257-262.
122. GEORGE, D.A., ed. *Continuous nonlinear systems*. TECHNICAL REPORT. 1959: MASSACHUSETTS INSTITUTE OF TECHNOLOGY.
123. Lang, Z.Q. and S.A. Billings, *Output frequency characteristics of nonlinear systems*. International Journal of Control, 1996. **64**(6): p. 1049-1067.
124. Billings, S.A. and J.C.P. Jones, *Mapping Nonlinear Integrodifferential Equations into the Frequency-Domain*. International Journal of Control, 1990. **52**(4): p.

- 863-879.
125. Jones, J.C.P. and S.A. Billings, *Recursive Algorithm for Computing the Frequency-Response of a Class of Non-Linear Difference Equation Models*. International Journal of Control, 1989. **50**(5): p. 1925-1940.
  126. Worden, K., G. Manson, and G.R. Tomlinson, *A harmonic probing algorithm for the multi-input Volterra series*. Journal of Sound and Vibration, 1997. **201**(1): p. 67-84.
  127. Worden, K., ed. *Nonlinearity in structural dynamics : detection, identification, and modelling*. 2000, Institute of Physics: Bristol.
  128. Bedrosian, E. and S.O. Rice, *Output Properties of Volterra Systems (Nonlinear Systems with Memory) Driven by Harmonic and Gaussian Inputs*. Proceedings of the Institute of Electrical and Electronics Engineers, 1971. **59**(12): p. 1688-&.
  129. Jing, X.J., Z.Q. Lang, and S.A. Billings, *Mapping from parametric characteristics to generalized frequency response functions of non-linear systems*. International Journal of Control, 2008. **81**(7): p. 1071-1088.
  130. Rijlaarsdam, D., et al., *Uniquely connecting frequency domain representations of given order polynomial Wiener-Hammerstein systems*. Automatica, 2012. **48**(9): p. 2381-2384.
  131. Rijlaarsdam, D., et al., *Spectral analysis of block structured nonlinear systems and higher order sinusoidal input describing functions*. Automatica, 2011. **47**(12): p. 2684-2688.
  132. Ma, H.G., et al., *A chaos-GFRF based fault diagnosis method*. 2004 IEEE Conference on Cybernetics and Intelligent Systems, Vols 1 and 2, 2004: p. 1314-1317.
  133. Gao, Y.S., L.W. Tang, and H.W. Jin, *Application of generalized frequency response function in gearbox nonlinear diagnosis*. Icemi 2007: Proceedings of 2007 8th International Conference on Electronic Measurement & Instruments, Vol Iii, 2007: p. 347-350.
  134. Wei, R.X., et al., *Fault diagnosis based on the multiple preset GFRF models*. Proceedings of the Fifth International Conference on Information Fusion, Vol Ii, 2002: p. 1506-1510.
  135. Nataraj, P.S.V., P. Date, and A. Umrani, *Robust feedback synthesis for nonlinear integrodifferential equation models using generalized describing functions*. Automatica, 1997. **33**(5): p. 959-962.
  136. Peng, Z.K., Z.Q. Lang, and S.A. Billings, *Resonances and resonant frequencies for a class of nonlinear systems*. Journal of Sound and Vibration, 2007. **300**(3-5): p.



## References

---

- 993-1014.
137. Peng, Z.K., Z.Q. Lang, and F.L. Chu, *Numerical analysis of cracked beams using nonlinear output frequency response functions*. Computers & Structures, 2008. **86**(17-18): p. 1809-1818.
138. Peng, Z.K., Z.Q. Lang, and S.A. Billings, *Crack detection using nonlinear output frequency response functions*. Journal of Sound and Vibration, 2007. **301**(3-5): p. 777-788.
139. Peng, Z.K., Z.Q. Lang, and S.A. Billings, *Non-linear output frequency response functions of MDOF systems with multiple non-linear components*. International Journal of Non-Linear Mechanics, 2007. **42**(7): p. 941-958.
140. Peng, Z.K. and Z.Q. Lang, *The Nonlinear Output Frequency Response Functions of One-Dimensional Chain Type Structures*. Journal of Applied Mechanics-Transactions of the Asme, 2010. **77**(1).
141. Peng, Z.K., Z.Q. Lang, and S.A. Billings, *Analysis of Locally Nonlinear MDOF Systems Using Nonlinear Output Frequency Response Functions*. Journal of Vibration and Acoustics-Transactions of the Asme, 2009. **131**(5).
142. Lang, Z.Q. and L. Zhao, *Detection and location of nonlinearities in MDOF structural systems*. Acta Montanistica Slovaca, 2010. **15**(1): p. 28-32.
143. Lang, Z.Q. and Z.K. Peng, *A novel approach for nonlinearity detection in vibrating systems*. Journal of Sound and Vibration, 2008. **314**(3-5): p. 603-615.
144. Peng, Z.K. and Z.Q. Lang, *Detecting the position of non-linear component in periodic structures from the system responses to dual sinusoidal excitations*. International Journal of Non-Linear Mechanics, 2007. **42**(9): p. 1074-1083.
145. Peng, Z.K., et al., *Locating Nonlinear Components in Periodic Structures using Nonlinear Effects*. Structural Health Monitoring-an International Journal, 2010. **9**(5): p. 401-411.
146. Cao, M.S., Q.W. Ren, and P.Z. Qiao, *Novel structural damage indices: Vibration transmissibility and its curvatures*. Fracture and Damage Mechanics V, Pts 1 and 2, 2006. **324-325**: p. 343-346.
147. Maia, N.M.M., et al., *Using the detection and relative damage quantification indicator (DRQ) with transmissibility*. Damage Assessment of Structures Vii, 2007. **347**: p. 455-460.
148. Zhang, H., et al., *Structural health monitoring using transmittance functions*. Mechanical Systems and Signal Processing, 1999. **13**(5): p. 765-787.
149. Johnson, T.J., *Analysis of dynamic transmissibility as a feature for structural*

## References

---

- damage detection*, in *Mechanical Engineering*2002, Purdue University: Purdue.
150. Devriendt, C., et al., *Structural health monitoring in changing operational conditions using transmissibility measurements*. Shock and Vibration, 2010. **17**(4-5): p. 651-675.
151. Chesne, S. and A. Deraemaeker, *Damage localization using transmissibility functions: A critical review*. Mechanical Systems and Signal Processing, 2013. **38**(2): p. 569-584.
152. B.R. Brenner, M.S., E.S. Bell, P.L. Rosenstrauch, *The Influence of Temperature Changes on Bridge Structural Behavior*. [http://www.geocomp.com/files/technical\\_papers/TheInfluenceofTemperatureChangesonBridgeStructuralBehavior\\_WEB.pdf](http://www.geocomp.com/files/technical_papers/TheInfluenceofTemperatureChangesonBridgeStructuralBehavior_WEB.pdf).
153. T.H. Loutas, J.K., G. Sotiriades and V. Kostopoulos, *The combined use of vibration acoustic emission and oil debris sensor monitored data coming from rotating machinery for the development of a robust health monitoring system*.
154. Alampalli, S., *Influence of in-service environment on modal parameters*. Imac - Proceedings of the 16th International Modal Analysis Conference, Vols 1 and 2, 1998. **3243**: p. 111-116.
155. Kim, C.Y., et al., *Effect of vehicle mass on the measured dynamic characteristics of bridges from traffic-induced vibration test*. Proceedings of Imac-Xix: A Conference on Structural Dynamics, Vols 1 and 2, 2001. **4359**: p. 1106-1111.
156. Sohn, H., et al. *Online Damage Detection for Theme Park Rides*. in *Proceedings of 22nd International Modal Analysis Conferenc*. 2004. Dearborn, MI.
157. Hikami, Y. and N. Shiraishi, *Rain-Wind Induced Vibrations of Cables in Cable Stayed Bridges*. Journal of Wind Engineering and Industrial Aerodynamics, 1988. **29**(1-3): p. 409-418.
158. Matsumoto, M., et al., *Response Characteristics of Rain-Wind Induced Vibration of Stay-Cables of Cable-Stayed Bridges*. Journal of Wind Engineering and Industrial Aerodynamics, 1995. **57**(2-3): p. 323-333.
159. Pirner, M.F., O. *Monitoring stresses in GRP extension of the Prague TV tower*. in *DAMAS 97: structural damage assessment using advanced signal processing procedures*. 1997. University of Sheffield, UK.
160. G. De Roeck, B.P.a.J.M. *Dynamic monitoring of civil engineering structures*. in *Computational Methods for Shell and Spatial Structures, IASS-IACM 2000*. 2000. Chania, Crete, Greece.
161. Peeters, B. and G. De Roeck, *One-year monitoring of the Z24-Bridge: environmental effects versus damage events*. Earthquake Engineering &

## References

---

- Structural Dynamics, 2001. **30**(2): p. 149-171.
162. Makis, V. and M. Yang, *ARX model-based gearbox fault detection and localization under varying load conditions*. Journal of Sound and Vibration, 2010. **329**(24): p. 5209-5221.
163. Sohn, H. and C.R. Farrar, *Damage diagnosis using time series analysis of vibration signals*. Smart Materials & Structures, 2001. **10**(3): p. 446-451.
164. Sohn, H., et al., *Structural health monitoring using statistical pattern recognition techniques*. Journal of Dynamic Systems Measurement and Control-Transactions of the Asme, 2001. **123**(4): p. 706-711.
165. Worden, K., H. Sohn, and C.R. Farrar, *Novelty detection in a changing environment: Regression and interpolation approaches*. Journal of Sound and Vibration, 2002. **258**(4): p. 741-761.
166. Zhou, H.F., Y.Q. Ni, and J.M. Ko, *Eliminating Temperature Effect in Vibration-Based Structural Damage Detection*. Journal of Engineering Mechanics-Asce, 2011. **137**(12): p. 785-796.
167. Sohn, H., K. Worden, and C.R. Farrar, *Statistical damage classification under changing environmental and operational conditions*. Journal of Intelligent Material Systems and Structures, 2002. **13**(9): p. 561-574.
168. Sohn, H., et al., *Adaptive modeling of environmental effects in modal parameters for damage detection in civil structures*. Smart Systems for Bridges, Structures, and Highways, 1998. **3325**: p. 127-138.
169. Ruotolo, R. and C. Surace, *Using SVD to detect damage in structures with different operational conditions*. Journal of Sound and Vibration, 1999. **226**(3): p. 425-439.
170. Shane, C. and R. Jha, *Proper orthogonal decomposition based algorithm for detecting damage location and severity in composite beams*. Mechanical Systems and Signal Processing, 2011. **25**(3): p. 1062-1072.
171. Surace, C. and K. Worden, *A negative selection approach to novelty detection in a changing environment*. Proceedings of the Third European Workshop Structural Health Monitoring 2006, 2006: p. 571-577.
172. Surace, C. and K. Worden, *Novelty detection in a changing environment: A negative selection approach*. Mechanical Systems and Signal Processing, 2010. **24**(4): p. 1114-1128.
173. Kullaa, J., *Vibration-Based Structural Health Monitoring Under Variable Environmental or Operational Conditions*. New Trends in Vibration Based Structural Health Monitoring, 2010(530): p. 107-181.

## References

---

174. Cross, E.J., K. Worden, and Q. Chen, *Cointegration: a novel approach for the removal of environmental trends in structural health monitoring data*. Proceedings of the Royal Society a-Mathematical Physical and Engineering Sciences, 2011. **467**(2133): p. 2712-2732.
175. Cross, E.J., et al., *Features for damage detection with insensitivity to environmental and operational variations*. Proceedings of the Royal Society a-Mathematical Physical and Engineering Sciences, 2012. **468**(2148): p. 4098-4122.
176. Figueiredo, E., et al., *Machine Learning Algorithms for Damage Detection under Operational and Environmental Variability*. Health Monitoring of Structural and Biological Systems 2010, Pts 1 and 2, 2010. **7650**.
177. Khatkhate, A., et al., *Symbolic time-series analysis for anomaly detection in mechanical systems*. Ieee-Asme Transactions on Mechatronics, 2006. **11**(4): p. 439-447.
178. Abraham, O.N.L. and J.A. Brandon, *The Modeling of the Opening and Closure of a Crack*. Journal of Vibration and Acoustics-Transactions of the Asme, 1995. **117**(3): p. 370-377.
179. Andraeus, U., P. Casini, and F. Vestroni, *Non-linear dynamics of a cracked cantilever beam under harmonic excitation*. International Journal of Non-Linear Mechanics, 2007. **42**(3): p. 566-575.
180. Bovsunovsky, A. and C. Surace, *Considerations regarding superharmonic vibrations of a cracked beam and the variation in damping caused by the presence of the crack*. Journal of Sound and Vibration, 2005. **288**(4-5): p. 865-886.
181. Saavedra, P.N. and L.A. Cuitino, *Crack detection and vibration behavior of cracked beams*. Computers & Structures, 2001. **79**(16): p. 1451-1459.
182. Sundermeyer, J.N. and R.L. Weaver, *On Crack Identification and Characterization in a Beam by Nonlinear Vibration Analysis*. Journal of Sound and Vibration, 1995. **183**(5): p. 857-871.
183. Pun, D., S.L. Lau, and Y.B. Liu, *Internal resonance of an L-shaped beam with a limit stop .2. Forced vibration*. Journal of Sound and Vibration, 1996. **193**(5): p. 1037-1047.
184. Pun, D., S.L. Lau, and Y.B. Liu, *Internal resonance of an L-shaped beam with a limit stop .1. Free vibration*. Journal of Sound and Vibration, 1996. **193**(5): p. 1023-1035.
185. Ma, H., et al., *Analysis of dynamic characteristics for a rotor system with*

## References

---

- pedestal looseness*. Shock and Vibration, 2011. **18**(1-2): p. 13-27.
186. Han, Q.K., H.T. Luo, and B.C. Wen, *Simulations of a Dual-Rotor System with Local Rub-Impacts Based on Rigid-Flexible Multi-body Model*. Damage Assessment of Structures Viii, 2009. **413-414**: p. 677-682.
187. Han, Q., Z. Zhang, and B. Wen, *Periodic motions of a dual-disc rotor system with rub-impact at fixed limiter*. Proceedings of the Institution of Mechanical Engineers Part C-Journal of Mechanical Engineering Science, 2008. **222**(10): p. 1935-1946.
188. Chu, F. and W. Lu, *Determination of the rubbing location in a multi-disk rotor system by means of dynamic stiffness identification*. Journal of Sound and Vibration, 2001. **248**(2): p. 235-246.
189. Jalan, A.K. and A.R. Mohanty, *Model based fault diagnosis of a rotor-bearing system for misalignment and unbalance under steady-state condition*. Journal of Sound and Vibration, 2009. **327**(3-5): p. 604-622.
190. Pennacchi, P., A. Vania, and S. Chatterton, *Nonlinear effects caused by coupling misalignment in rotors equipped with journal bearings*. Mechanical Systems and Signal Processing, 2012. **30**: p. 306-322.
191. Wan, Z., et al., *Theoretical and experimental study on the dynamic response of multi-disk rotor system with flexible coupling misalignment*. Proceedings of the Institution of Mechanical Engineers Part C-Journal of Mechanical Engineering Science, 2012. **226**(C12): p. 2874-2886.
192. Schweizer, B., *Oil whirl, oil whip and whirl/whip synchronization occurring in rotor systems with full-floating ring bearings*. Nonlinear Dynamics, 2009. **57**(4): p. 509-532.
193. Chen, M.Y., et al., *A nonlinear frequency analysis based approach for power cable insulation fault detection*. Compel-the International Journal for Computation and Mathematics in Electrical and Electronic Engineering, 2012. **31**(2): p. 369-386.
194. Yagi, Y., H. Tanaka, and H. Kimura, *Study on diagnostic method for water treed XLPE cable by loss current measurement*. 1998 Annual Report Conference on Electrical Insulation and Dielectric Phenomena, Vols 1 and 2, 1998: p. 653-656.
195. Chen, M.Y., et al., *High Impedance Fault Location in Transmission Line Using Nonlinear Frequency Analysis*. Life System Modeling and Intelligent Computing, Pt I, 2010. **6328**: p. 104-111.
196. Ibrahim, D.K., et al., *Unsynchronized Fault-Location Scheme for Nonlinear HIF in Transmission Lines*. Ieee Transactions on Power Delivery, 2010. **25**(2): p.

- 631-637.
197. Peng, Z.K., Z.Q. Lang, and S.A. Billings, *Non-linear output frequency response functions for multi-input non-linear Volterra systems*. International Journal of Control, 2007. **80**(6): p. 843-855.
  198. H., P., B. W., and P. M., *Bezier and B-Spline Techniques*. 2010, Berlin: Springer.
  199. Billings, S.A., S. Chen, and M.J. Korenberg, *Identification of MIMO Non-Linear Systems Using a Forward-Regression Orthogonal Estimator*. International Journal of Control, 1989. **49**(6): p. 2157-2189.
  200. Hills, A.F., et al., *A novel baseline model-based technique for condition monitoring of wind turbine components*. The British Institute of Non-Destructive Testing, 2011. **53**(8): p. 434-438.
  201. Souza, S., et al., *Determination of the combined vibrational and acoustic emission signature of a wind turbine gearbox and generator shaft in service as a pre-requisite for effective condition monitoring*. Renewable Energy, 2013. **51**: p. 175-181.
  202. Cade, I.S., P.S. Keogh, and M.N. Sahinkaya, *Fault identification in rotor/magnetic bearing systems using discrete time wavelet coefficients*. IEEE-Asme Transactions on Mechatronics, 2005. **10**(6): p. 648-657.
  203. Quinn, D.D., et al., *Damage detection of a rotating cracked shaft using an active magnetic bearing as a force actuator - Analysis and experimental verification*. IEEE-Asme Transactions on Mechatronics, 2005. **10**(6): p. 640-647.
  204. Sahinkaya, M.N., et al., *Multiple sliding and rolling contact dynamics for a flexible rotor/magnetic bearing system*. IEEE-Asme Transactions on Mechatronics, 2007. **12**(2): p. 179-189.
  205. Sakellariou, J.S. and S.D. Fassois, *Stochastic output error vibration-based damage detection and assessment in structures under earthquake excitation*. Journal of Sound and Vibration, 2006. **297**(3-5): p. 1048-1067.
  206. Loh, C.H. and C.H. Chao, *Effectiveness of active tuned mass damper and seismic isolation on vibration control of multi-storey building*. Journal of Sound and Vibration, 1996. **193**(4): p. 773-792.
  207. Law, S.S. and X.Q. Zhu, *Dynamic behavior of damaged concrete bridge structures under moving vehicular loads*. Engineering Structures, 2004. **26**(9): p. 1279-1293.
  208. Marchesiello, S., et al., *Dynamics of multi-span continuous straight bridges subject to multi-degrees of freedom moving vehicle excitation*. Journal of Sound and Vibration, 1999. **224**(3): p. 541-561.

## References

---

209. Mead, D.J., *Wave propagation in continuous periodic structures: Research contributions from Southampton, 1964-1995*. Journal of Sound and Vibration, 1996. **190**(3): p. 495-524.
210. E., F., et al., *Structural health monitoring algorithm comparisons using standard data sets*. Los Alamos National Laboratory Report: LA-14393, 2009.
211. Yao, H.L., et al., *Detection of rubbing location in rotor system by super-harmonic responses*. Journal of Mechanical Science and Technology, 2012. **26**(8): p. 2431-2437.
212. Bharadwaj, R.M. and A.G. Parlos, *Neural speed filtering for induction motors with anomalies and incipient faults*. Ieee-Asme Transactions on Mechatronics, 2004. **9**(4): p. 679-688.
213. Jing, X., *Nonlinear Characteristic Output Spectrum for Nonlinear Analysis and Design*. Ieee-Asme Transactions on Mechatronics (accepted).
214. Takewaki, I. and H. Tsujimoto, *Scaling of design earthquake ground motions for tall buildings based on drift and input energy demands*. Earthquakes and Structures, 2011. **2**(2): p. 171-187.
215. Mitsuru Murase, M.T.a.I.T., *Smart passive control of buildings with higher redundancy and robustness using base-isolation and inter-connection*. Earthquake and Structures, 2013. **4**(6): p. 649-670.
216. Lang, Z.Q. and S.A. Billings, *Output frequencies of nonlinear systems*. International Journal of Control, 1997. **67**(5): p. 713-730.
217. Yagi, Y., H. Tanaka, and H. Kimura, *Study on diagnostic method for water treed XLPE cable by loss current measurement*, in *Annual Report Conference on Electrical Insulation and Dielectric Phenomena*1998: Atlanta, GA. p. 653 - 656.
218. Hvidsten, S. and E. Ildstad, *Criteria for diagnostic evaluation of water treed XLPE cables*, in *IEEE 7th International Conference on Solid Dielectrics*2001: Eindhoven. p. 385 - 389.
219. Adejumobi, I.A., *Carrier frequency and bandwidth requirements for data transmission in power distribution automation system*. The Pacific Journal of Science and Technology, 2010. **11**(2): p. 315-326.
220. Devriendt, C. and P. Guillaume, *The use of transmissibility measurements in output-only modal analysis*. Mechanical Systems and Signal Processing, 2007. **21**(7): p. 2689-2696.
221. Devriendt, C. and P. Guillaume, *Identification of modal parameters from transmissibility measurements*. Journal of Sound and Vibration, 2008. **314**(1-2): p. 343-356.

222. Weijtjens, W., et al., *Operational modal parameter estimation of MIMO systems using transmissibility functions*. Automatica, 2014. **50**(2): p. 559-564.